Modulation of Excited State Photophysics of Drugs and Biologically Important Molecules inside the Bio-mimetic Nano-cavities

A Thesis

Submitted in partial fulfillment of the requirements

for the degree of

Doctor of Philosophy

by

Krishna Gavvala

ID: 20113105

Indian Institute of Science Education and Research (IISER), Pune

2015

Dedicated

to

My Parents

Indian Institute of Science Education and Research (IISER), Pune

Certificate

Certified that the work incorporated in this thesis entitled "**Modulation of Excited State Photophysics of Drugs and Biologically Important Molecules inside the Bio-mimetic Nano-cavities**" submitted by **Mr. Krishna Gavvala** was carried out by the candidate, under my supervision. The work presented here or any part of it has not been included in any other thesis submitted previously for the award of any degree or diploma from any other university or institution.

Date: 28th December 2015

Dr. Partha Hazra
Research Supervisor

Email: p.hazra@iiserpune.ac.in | Contact no: +91 (20) 25908077

Declaration

I declare that this written submission represents my ideas in my own words and wherever other's ideas have been included; I have adequately cited and referenced the original sources. I also declare that I have adhered to all principles of academic honesty and integrity and have not misrepresented or fabricated or falsified any idea/data/fact/source in my submission. I understand that violation of the above will cause for disciplinary action by the Institute and can also evoke penal action from the sources which have thus not been properly cited or from whom proper permission has not been taken when needed.

Date: 28th December 2015

Krishna Gavvala

ID: 20113105

Acknowledgement

First and foremost, I would like to express my deeply felt thanks to my thesis advisor, Dr. **Partha Hazra** for his unflinching encouragement, support, and guidance throughout my research. His expertise in fluorescence spectroscopy improved my research skills and prepared me for future challenges. His diligent effort and training was the reason behind every success I achieved and undoubtedly is the asset for my future research. This thesis would not have been possible without his valuable support. I acknowledge Indian Institute of Science Education and Research (IISER), Pune for providing excellent research facilities and an outstanding research environment.

I am grateful to the Research Advisory Committee (RAC) members Dr. Pankaj Mandal and Dr. G. V. Pavan Kumar for their suggestions and comments during RAC meetings. The critical examination of my research work and valuable comments by all of the RAC members were always very useful. I am very thankful to Prof. Yves Mély and his team members at University of Strasbourg for allowing me to work with his group. I specially thank Prof. B. S. M. Rao and Dr. V. G. Anand, past and present deans of doctoral studies at IISER-Pune for their generous support and encouragement.

I am thankful to every faculty of IISER-Pune who was always ready to share their knowledge and experience with me. It was indeed a pleasure to work in such an ambiance. I thank IISER Pune librarians, IT staff and administrative staff especially Mayuresh, Suvarna, Nayana, Tushar, Snehal and Prabhas for their kind support.

It's my pleasure to thank all the members of the team, I belong to; Dr. Abhigyan, Rajkumar, Sagar and Bibhisan as they always maintained a very lively environment in lab. An all time running discussion and sharing of experiences helped me to expand the horizon of knowledge.

I thank all my friends, seniors and juniors for their help and support during my research travel.

No words can ever convey my sense of gratitude for my parents. It is due to their unconditional trust, timely encouragement, endless patience and unstinting sacrifice; I am able to reach this position. I dedicate this thesis to my parents who unremittingly supported me during my years of study.

IISER Pune **Krishna Gavvala**

Table of Contents

List of Abbreviations

Abs	Absorbance
ACN	Acetonitrile
ADC	Analog to digital converter
ADT	Auto dock tools
AOM	Acousto-optic modulator
av	Average
BP(OH)2	Bipyridine diol
CBn	Cucurbit[n]uril
CD	Circular dichroism
CFD	Constant fraction discriminator
CMC	Critical micellar concentration
CPT	Camptothecin
CTAB	Cetyl trimethylammonium bromide
DFT	Density functional theory
DIOX	Dioxane
DMF	Dimethyl formamide
DMSO	Dimethyl sulfoxide
DNA	Deoxyribonucleic acid
Em	Emission
Ex	Excitation
FA	Formamide
fs	Femtosecond
FWHM	Full width at half maximum
EPT	Ellipticine
EtOH	Ethanol
GFP	Green fluorescent protein
IC	Internal conversion
ISC	Inter system crossing
LBO	Lithium triborate
LED	Light emitting diode
MEOH	Methanol
MIR	Milrinone
mM	Milli molar
ns	Nanosecond
OBG	Octyl β-glucoside
PDB	Protein data bank
ps	Picosecond

Sam	Sample
SDS	Sodium dodecylsulphate
Ref	Reference
TAC	Time to amplitude converter
TCSPC	Time correlated single photon counting
TPT	Topotecan
TRES	Time-resolved emission spectra
TRANES	Time resolved area normalized emission spectra
TX-100	Triton X-100
μL	Micro liter
μM	Micro molar
UV-Vis	Ultraviolet-visible

Synopsis

Fluorescence spectroscopy, the most popular technique in scientific community, is widely used in many research fields because of its high sensitivity and selectivity towards surrounding environment. The sensitivity of fluorescence spectroscopy is mainly governed by modulation of the photophysics of given fluorophore in its surrounding environments. Hence, it is fundamental importance to understand the basic photophysics of fluorescent probes before using them in fluorescence based techniques. Moreover, owing to the importance of fluorescent probes and sensors for environmental and biological applications, it is usually desirable to "tune" fluorescent dyes in aqueous solution. Especially for fluorescent drugs it is very essential to establish a relationship between their fluorescence properties and surrounding environment for designing novel drug carriers and bio-imaging purposes. Motivation of my thesis is to understand the basic photophysical properties of important drugs and probes inside bio-mimetic confined environments. For understanding and tuning photophysical properties, we have chosen molecular containers and micelles because of their bio-mimetic nature, tunable nano-confined environments and importantly their applications in various fields ranging from chemistry to biology. We have noticed that the photophysical properties of molecules have been drastically modulated inside the above mentioned nano-cavities. We have also found very interesting fluorescence switch and pKa shifts of many fluorescent molecules when they are encapsulated in bio-mimetic cavities. The reasons for this kind of modulation of excited state photophysics have been unraveled using steady-state and time-resolved fluorescence techniques. Excited state processes like excited state proton transfer dynamics are being modulated significantly inside the above confined environments. These noteworthy observations with detailed descriptions are provided in the present thesis. The present thesis has been organized in five main chapters as described below.

Chapter 1 (**Introduction**) gives a brief introduction to fluorescence spectroscopy, fluorescence parameters (like fluorescence quenching, lifetime and anisotropy), different working systems (molecular containers and micelles) and motivation behind this thesis work.

Chapter 2 (**Experimental: Materials and Methods**) describes the chemicals, probes and biological molecules that we used in this thesis. This chapter also explains the

sample preparation protocols and experimental methods detailing about different techniques (absorption, steady state fluorescence, time correlated single photon counting (TCSPC), fluorescence up-conversion and circular dichroism (CD)).

Chapter 3 (**Modulation of Excited State Photophysics and pKa Shifts of Fluorescent Molecules inside the Nano-cavities of Molecular Containers**) explains the excited state photophysics of important drugs, one is anticancer drug camptothecin and a cardiotonic drug milrinone inside the molecular containers. A profound pKa shift was found inside the nanocavities of cucurbituril. A detailed spectroscopic and theoretical investigation is done to unravel the reasons for the modulation of above mentioned two drugs. This chapter is divided in to two sections, one is devoted for understanding the photophysics of camptothecon and second section deals with the cardiotonic drug, milrinone. Both the sections are discussed one by one as follows;

3a. Modulation of Photophysics and pK_a Shift of an Anticancer Drug, Camptothecin, inside the Nanocavities of Supramolecular Hosts: In this section, the interaction behaviour between an anticancer drug, camptothecin (CPT) and cucurbit[7]uril (CB7) has been demonstrated with the help of absorption, steady state emission, time-resolved emission techniques. Our experimental results indicate the formation of 1:1 inclusion complex at lower concentration of CB7 (<50 μM). Interestingly, CPT gets protonated when it is encased by two CB7 macrocycles at higher concentration of host (>50 μM), and, consequently, pK_a shifts from 1.2 to 6.2. The protonation of CPT inside CB7 nanocavity results in a fluorescence switch from blue to green emission (**Figure 3.1**) due to the pKa shift from 1.2 to 6.2. However, when CPT forms inclusion complex with β-CD, which has almost similar cavity size as that of CB7, no protonation of CPT takes place. Therefore, we believe that carbonyl portals of CB7 has important role for the observed pK_a shift in case of CB7. Not only formation of inclusion complex we have also studied release of the drug from CB7 cavity by introducing NaCl salt in to the system as an external stimulus. The molecular picture obtained from docking as well as quantum chemical calculation indicates that quinoline nitrogen of CPT is situated in between two high electron rich portals of CB7 in 2:1 inclusion complex, and as a result the basicity of quinoline nitrogen increases which causes the pK_a shift.

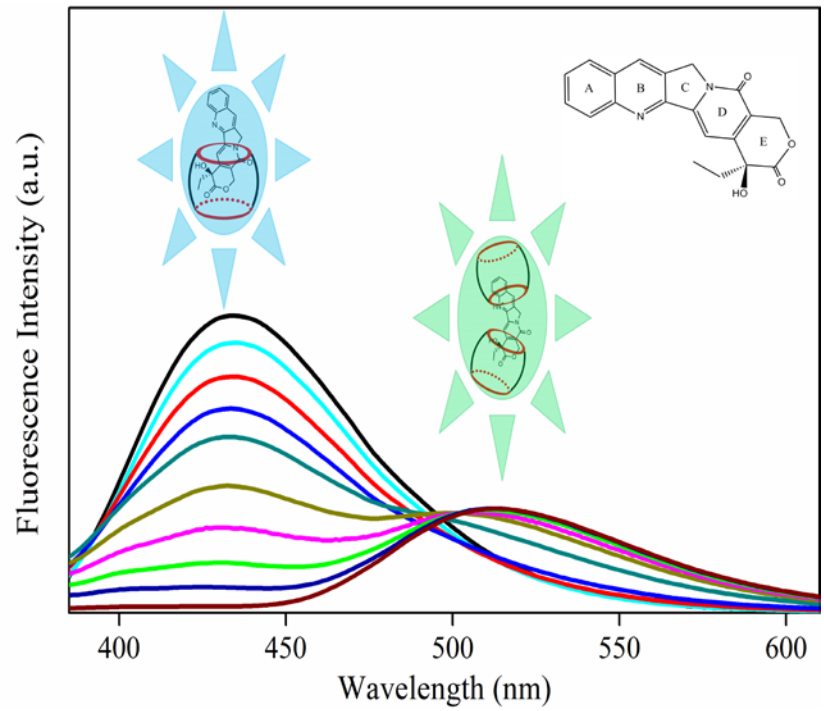

Figure 3.1. Modulation of photophysical properties of camptothecin inside the nano-cavity of cucurbit[7]uril.

3b. Cucurbit[7]uril Assisted Ultraviolet to Visible Fluorescence Switch of a Heart Medicine: In this section, the interaction behavior between an heart medicine, milrinone and cucurbit[7]uril has been demonstrated with the help of absorption, steady state and time-resolved emission measurements. Amazingly, fluorescence of MIR switches from UV to visible (cyan color) as a result of complexation (**Figure 3.2**), and we attribute this fluorescence switch to the increased pKa of protonation of pyridine nitrogen. However, visible fluorescence (cyan color) switches back to UV with increasing pH of the solution. The molecular picture obtained from docking and quantum chemical calculation depicts that pyridine nitrogen of MIR is situated at the electron rich portal of CB7 in inclusion complex, and as a result the basicity of pyridine nitrogen increases significantly. We believe that this kind of fluorescence switch is rarely observed with drug molecules, and therefore, it can be exploited to monitor the delivery process of the drug.

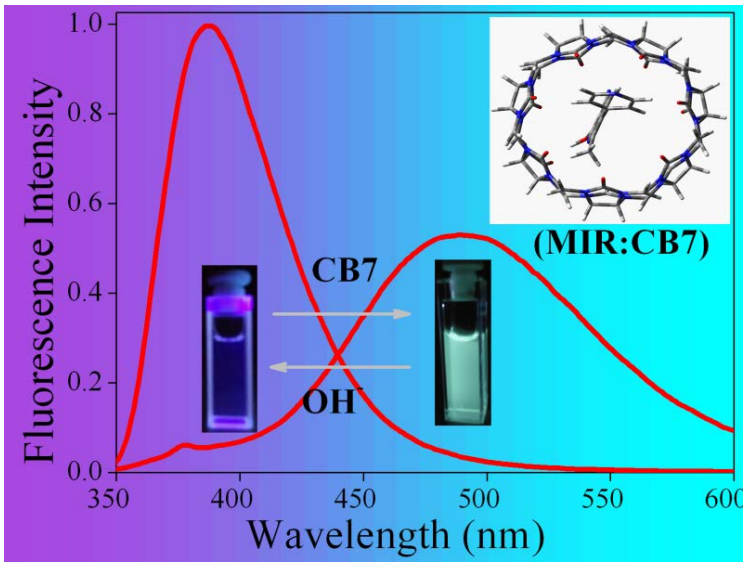

Figure 3.2. Fluorescence switching of milrinone inside the nanocavity of cucurbit[7]uril.

Chapter 4 (**Modulation of Excited State Proton Transfer Dynamics in Bio-mimetic Confined Environments**) deals with understanding an important excited state phenomenon excited state proton transfer (ESPT) process, of biologically important molecules in various bio-mimetic confined environments such as cyclodextrins, cucurbiturils and micelles. We have noticed very intriguing observations in ESPT modulations for topotecan, bipyridine diol and ellipticine when they are encapsulated in confined nano-environments. The reasons and discussions explained with proper evidences are discussed in this chapter. Depending over the type of proton transfer process, molecule and confined environment this chapter is further divided into three sections which are discussed one by one in detailed manner as follows;

4a. Supramolecular Host Inhibits Excited State Proton Transfer of an Anti-cancer Drug, Topotecan: This section describes the interaction and modulation of photophysical properties of an important anticancer drug, topotecane (TPT) with CB7 by several spectroscopic techniques like absorption, fluorescence and time resolved measurements. We found CB7 has a selective affinity to cationic form (C) of TPT and forms a 1:1 inclusion complex (CB7:TPT(C)) with CB7. Thereby, the excited state transformation of C to zwitterion (Z) form through excited state proton transfer (ESPT) process is restricted inside the CB7 cavity, and it is reflected by the appearance of a new peak at 425 nm at the cost of 530 nm peak (responsible for Z form of TPT) in presence of CB7 (**Figure 4.1**). Appearance of ~2 ns component in the decay profile monitored at 425 nm also confirms the

encapsulation of C form of drug by the CB7 host. Moreover, the retarded rotational motion of C form of TPT fortifies our claim that C form is encased by the macrocyclic host. On the other hand the rotational motion of Z* does not hinder in presence of CB7 indicating TPT (Z) is not encased by CB7, rather it interacts with the C=O portal of CB7 through the hydrogen bond formation. The process of complexation and molecular orientation of the drug inside cavity has been conceptualized using computational studies, which show that the quinoline moiety of TPT lies partly inside the cavity of CB7, thereby, restricts ESPT and lowers the population of Z*. Finally, controlled release of the drug has been achieved through the introduction of NaCl, which is rich in cell, as an external stimulus. We hope this recognition mediated binding as well as release mechanism can be useful for activation of the drug and controlled release of the drug in the therapeutic applications.

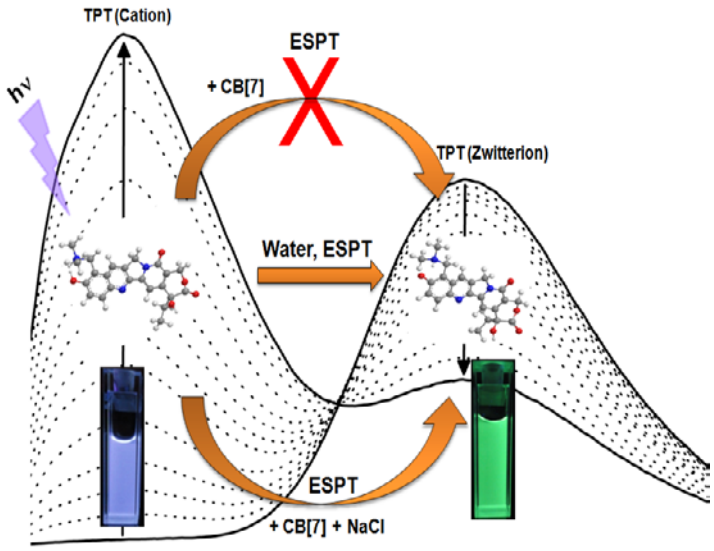

Figure 4.1. Modulation of ESPT process of topotecane inside the nanocavity of CB7.

4b. Ultrafast Dynamics of 2,2′-Bipyridine-3,3′-diol inside the Nano-cavities of Molecular Containers: In this work, host-guest interactions between the molecular containers cucurbit[7]uril (CB7) and β-cyclodextrin (β-CD)) and a biological probe 2,2′-Bipyridine-3,3′-diol (BP(OH)2) are investigated with the help of steady state and time-resolved fluorescence measurements. Ground state absorption study indicates that the conversion of diketo (DK) to dienol (DE) form in BP(OH)2 takes place in presence of CB7. Steady state and time-resolved fluorescence studies confirm that the main emissive species is DK form of BP(OH)2 inside the CB7 nano-cavity. Femtosecond fluorescence upconversion

measurements are employed to elucidate the mechanism of ultrafast proton transfer dynamics of BP(OH)2 inside nano-containers (CB7 and β-CD). Femtosecond up-conversion study of BP(OH)2 in water reveals that the two step sequential proton transfer process via MK to DK form appears as a growth component (~35 ps) in the up-converted signal. Astonishingly, the fluorescence up-converted signal of BP(OH)2 is devoid of any growth component in presence of CB7, and it supports that concerted mechanism of proton transfer (takes place in <100 fs time scale) is present inside the nano-cavity of CB7 instead of two step-sequential process of PT dynamics (**Figure 4.2**). Interestingly, two step sequential process is feasible mechanism in case of β-CD, as inside the nano-cavity of β-CD the growth component of ~28 ps is detected. The reason for this observation is the presence of surrounding water solvation network of BP(OH)2 inside the cavity of β-CD, which is absent in case of CB7 nano-cavity. Finally, docking and DFT quantum chemical calculations have been employed in deciphering the molecular orientation of BP(OH)2 in inclusion complex with the macrocyclic host. Theoretical calculations confirm that BP(OH)2 molecule resides at the centre of the hydrophobic nano-cavity of CB7, and thereby it is believed to be affected the double proton transfer dynamics significantly.

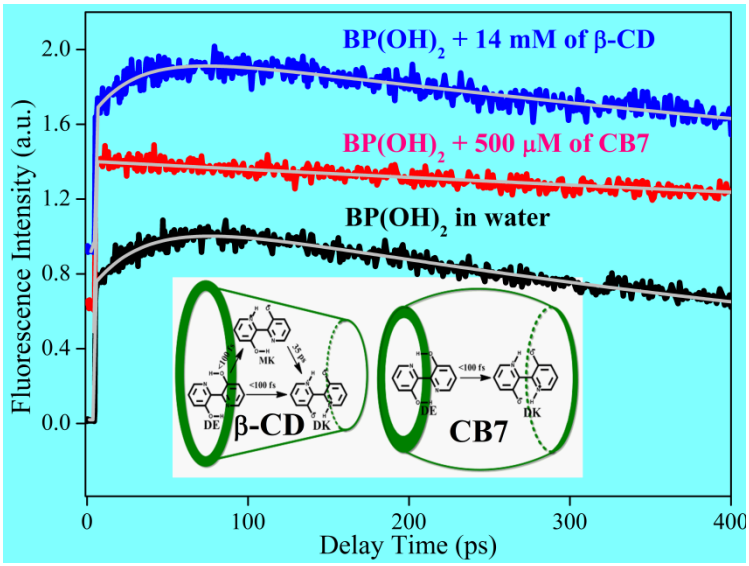

Figure 4.2. ESIDPT dynamics and mechanism of BP(OH)2 inside CB7 and β-CD.

4c. Excited State Proton Transfer Dynamics of an Eminent Anticancer Drug, Ellipticine in Octyl Glucoside Micelle: In this work, we have studied the photophysical and proton transfer dynamics of an eminent anticancer drug, ellipticine (EPT) inside a biocompatible octyl-β-D-glucoside (OBG) micellar medium using steady state as well as

time resolved spectroscopic techniques. UV-visible absorption study reveals the conversion of protonated to neutral form of EPT, when OBG concentration reaches above critical micellar concentration. Interestingly, the emission at 530 nm (attributed to the protonated form of the drug) is also observed along with neutral form (emits at 440 nm), even when we selectively excite the neutral molecules. The above observation clearly demonstrates that excited state proton transfer process inside the OBG micelle is responsible for the conversion of neutral to protonated form of the drug. Time resolved emission measurements depict a pronounced enhancement in the average lifetime of both neutral and protonated species collected at 440 nm and 530 nm, respectively, when EPT is encapsulated inside OBG micelles. Astonishingly, a rise component of ~4 ns is observed in the time-resolved emission decays collected at 530 nm above CMC of OBG, and it is attributed to the excited state proton transfer dynamics of EPT inside OBG micellar confinement. Time-resolved area normalized emission spectra confirm the existence of two species in the excited state, where neutral form transforms to the protonated form (**Figure 4.3**). This kind of proton transfer dynamics is absent in conventional micelles, like SDS, Triton X and CTAB, and therefore, indicates that the glucose molecules residing in the palisade layer of OBG micelle may have some role in the excited state proton transfer. Based on all the above observations, we conclude that the observed ESPT dynamics is a combined effect of local dielectric constant as well as presence of glucose moieties at the palisade layer of the OBG micelle.

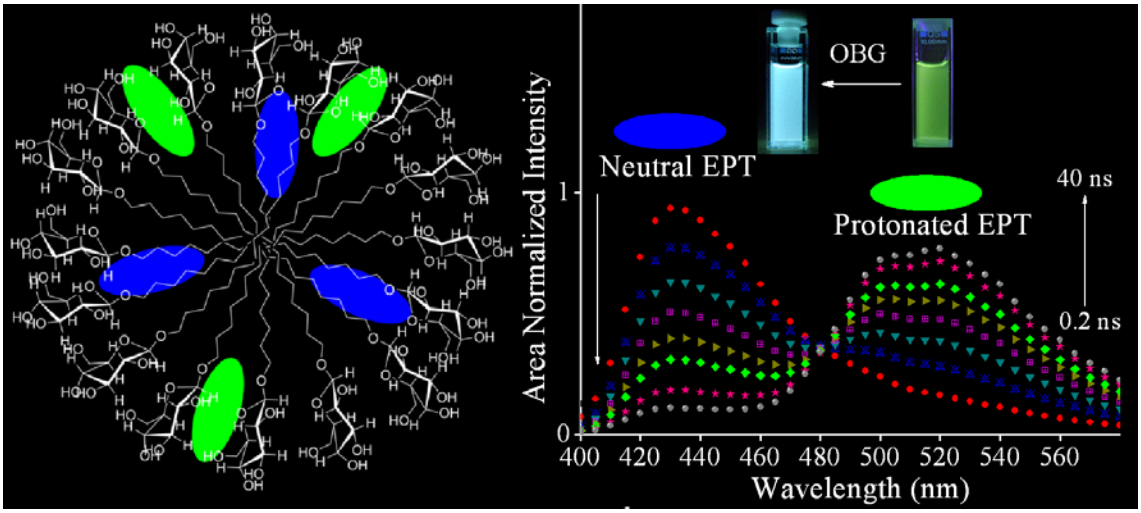

Figure 4.3. Schematic representation of modulation in fluorescence and ESPT of EPT in OBG micelles.

Chapter 5 (**Prototropical and Photophysical Properties of Ellipticine inside Molecular Containers and DNA**) interrogates the prototropical and photophysical properties of an important anticancer drug, ellipticine inside various molecular containers. When the drug is encapsulated in molecular containers the photophysics have been modulated depending over type and size of the nanocavity of molecular container. Using photophysical properties of the drug, it is released from the nanocavity to an important biomolecule DNA by altering pH of the medium as external stimuli. This chapter is divided in to two sections; in first section we explain the photophysical properties of ellipticine in molecular containers and in second section we cover the pH responsive release of the drug to DNA. These two sections are explained in detailed manner one by one as follows;

5a. Prototropical and Photophysical Properties of Ellipticine inside the Nano-cavities of Molecular Containers: In this section, the interaction behavior between an anticancer drug EPT and cucurbitruils has been demonstrated with the help of absorption, steady state fluorescence and time-resolved fluorescence techniques. For comparison, we have done similar experiments using conventional hosts, cyclodextrins. Our experimental results indicate the formation of 1:1 inclusion complexation of EPT with CB7 and CB8, and protonated form of EPT gets stabilized mainly through the ion-dipole interaction between host and positively charged drug. On the other hand, drug does not from inclusion complex with CB6. Among cyclodextrins, α-CD does not form inclusion complex with the drug, whereas β-CD forms 1:1 inclusion complex with the protonated form of the drug. Notably, binding affinity for β-CD is less compared to CB7/CB8. Interestingly, in case of γ-CD, drug forms stable 1:1 inclusion complex in its protonated form at lower concentration of host, whereas drug is encapsulated by two γ-CD molecules at higher concentration of host, and thereby drug exists in neutral form at higher concentration of γ-CD. Molecular docking as well as quantum chemical calculations were employed to get insight into the orientation of EPT drug inside the nano-cavities of these macrocycles. The molecular pictures indicate that pyridine nitrogen of EPT is situated at the electron rich portal in the inclusion complexes with CBn, and as a result the basicity of quinoline nitrogen increases significantly. But in case of 2:1 inclusion complex (γ-CD:EPT) with γ-CD, the EPT is completely buried inside hydrophobic cavity of the capsule formed by two γ-CD molecules, and this hydrophobic environment stabilizes the neutral form of EPT which is not observed in other 1:1 inclusion complexes with CBn and β-CD (**Figure 5.1**).

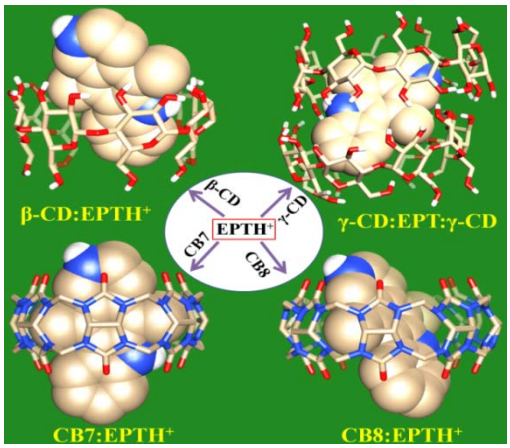

Figure 5.1. Schematic representation of inclusion complex formation between EPT and CDs.

5b. pH Induced Translocation of Ellipticine between Supramolecular Host and DNA: In this section, we have investigated the pH triggered interplay of EPT inside the nano-cavities of β-CD and DNA using photophysical properties of the drug by means of fluorescence based techniques. When EPT resides in β-CD nano-cavity its fluorescence increases with a large hypsochromic shift whereas the fluorescence is enhanced several folds without such blue shift in presence of DNA. Based on these fluorescence changes, the transportation of drug between β-CD and DNA is successfully monitored by simple change of pH of the medium (**Figure 5.2**). Steady state and time resolved studies confirm that at higher pH (8.5) the drug stays inside the nano-cavity of β-CD and at lower pH (5.0) it resides in DNA. Circular dichroism results further confirm the translocation of EPT between above mentioned host molecules. Hence, by using the simple fluorescence switch one can monitor the location of drug, and this kind of pH driven translocation of drug might find possible applications in emergent controlled drug delivery process.

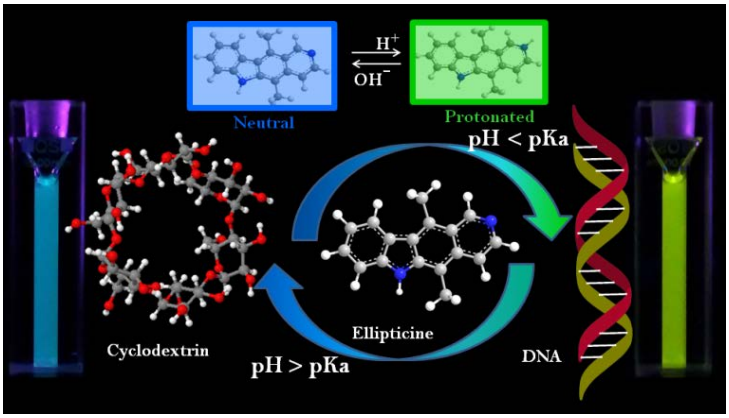

Figure 5.2. Different prototropic forms of ellipticine and its pH induced translocation between β-CD and DNA.

List of Publications

No.	Publications (Included in Thesis)	Year
01.	pH responsive translocation of an anticancer drug between cyclodextrin and DNA. **K. Gavvala**, S. Satpathi, P. Hazra*. ***RSC Advances***, 5, 98080-98086.	**2015**
02.	Excited state proton transfer dynamics of an eminent anticancer drug, ellipticine, in octyl glucoside (OBG) micelle. **K. Gavvala**, Raj K. Koninti, A. Sengupta, Partha Hazra*. ***Physical Chemistry Chemical Physics***, 16, 14953-14960.	**2014**
03.	Cucurbit[7]uril assisted ultraviolet to visible fluorescence switch of a heart medicine. **K. Gavvala**, R. K. Koninti, A. Sengupta, P. Hazra*. ***Physical Chemistry Chemical Physics (Communication)***, 16, 2823-2826.	**2014**
04.	Prototropical and photophysical properties of ellipticine inside the nanocavities of molecular containers. **K. Gavvala**, A. Sengupta, R. K. Koninti, P. Hazra*. ***The Journal of Physical Chemistry B***, 117, 14099-14107.	**2013**
05.	Femtosecond to nanosecond dynamics of 2, 2′-bipyridine-3, 3′-diol inside the nano-cavities of molecular containers. **K. Gavvala**, A. Sengupta, R. K. Koninti, P. Hazra*. ***Physical Chemistry Chemical Physics***, 16, 933-939.	**2013**
06.	Supramolecular host-inhibited excited state proton transfer and fluorescence switching of the anti-cancer drug, topotecan. **K. Gavvala**, A. Sengupta, R. K. Koninti, P. Hazra*. ***ChemPhysChem***, 14, 3375-3383.	**2013**
07.	Modulation of photophysics and pKa shift of the anti-cancer drug camptothecin in the nanocavities of supramolecular hosts. **K. Gavvala**, A. Sengupta, P. Hazra*. ***ChemPhysChem***, 14, 532-542.	**2013**

No.	Publications (Not Included in Thesis)	Year
08.	Acetylcholine induced interplay of an anticancer drug between cucurbit[7]uril and DNA. **K. Gavvala**,* S. Satpathi. ***Journal of Luminescence***, 171, 234-237.	**2016**
09.	Fluorescence up-conversion studies of [2,2′-Bipyridyl]-3,3′-diol in octyl-β-D-glucoside and other micellar aggregates S. Satpathi, **K. Gavvala**, P. Hazra*. ***The Journal of Physical Chemistry A***, **DOI:** 10.1021/acs.jpca.5b09832	**2016**
10.	Spectroscopy and dynamics of cryptolepine in the nano-cavity of cucurbit[7]uril and DNA. R. K. Koninti, S. Satpathi, **K. Gavvala**, P. Hazra*. ***ChemPhysChem***, **DOI:** 10.1002/cphc.201501011R1.	**2016**
11.	Ultrafast dynamics of a molecular rotor in chemical and biological nanocavities. **K. Gavvala**, S. Satpathi, P. Hazra*. ***RSC Advances***, 5, 72793-72800.	**2015**
12.	Solvation dynamics in different phases of the lyotropic liquid crystalline system B. Roy, S. Satpathi, **K. Gavvala**, R. K. Koninti, P. Hazra*. ***The Journal of Physical Chemistry B***, 119, 11721-11731.	**2015**
13.	Excited state proton transfer dynamics of topotecan, a potential anti-cancer drug, inside bio-mimicking nano-cavity. R. K. Koninti, **K. Gavvala**, A. Sengupta, P. Hazra*. ***The Journal of Physical Chemistry B***, 119, 2363-2371.	**2015**
14.	Fluorescence switching of sanguinarine in micellar environments S. Satpathi, **K. Gavvala**, P. Hazra*. ***Physical Chemistry Chemical Physics***, 17, 20725-20732.	**2015**
15.	A green solvent induced DNA package. S. Satpathi, A. Sengupta, V. M. Hridya, **K. Gavvala**, R. K. Koninti, B. Roy, P. Hazra *. ***Scientific Reports***, 5:09137.	**2015**
16.	Proflavine stabilizes human telomeric G-quadruplex DNA: An additional mode of action for anticancer agent. V. Kumar, A. Sengupta, R. K. Koninti, **K. Gavvala**, P. Hazra*. ***The Journal of Physical Chemistry B***, 118, 11090-11099.	**2014**
17.	An anticancer drug to probe non-specific protein-DNA interactions A. Sengupta, R. Koninti, **K. Gavvala**, N. Ballav, P. Hazra*. ***Physical Chemistry Chemical Physics (Communication)***, 16, 3914-3917.	**2014**

18. Folding dynamics of flavin adenine dinucleotide (FAD) inside non-aqueous and aqueous reverse micelles. **2014**
A. Sengupta*, **K. Gavvala**, R. K. Koninti, H. Chaudhuri, P. Hazra*.
Chemical Physics Letters, 584, 67-70.

19. Influence of Mg^{+2} ions over flavin recognition by RNA aptamer: A spectroscopic and thermodynamic glimpse. **2014**
A Sengupta, **K. Gavvala**, R. K. Koninti, P. Hazra*.
Journal of Photochemistry and Photobiology B: Biology, 140, 240-248.

20. Loading of an anti-cancer drug onto graphene oxide and subsequent release to DNA/RNA: a direct optical detection. **2014**
R. K. Koninti, A. Sengupta, **K. Gavvala**, N. Ballav, P. Hazra*.
Nanoscale, 6, 2937-2944.

21. Urea induced unfolding dynamics of flavin adenine dinucleotide (FAD): Spectroscopic and molecular dynamics simulation studies from femto-second to nano-second regime. **2014**
A. Sengupta, R. K. Singh, **K. Gavvala**, R. K. Koninti, A. Mukherjee*, P. Hazra*.
The Journal of Physical Chemistry B, 118, 1881–1890.

22. Unraveling the mode of binding of the anticancer drug topotecan with ds-DNA. **2014**
H. Joshi, A. Sengupta, **K. Gavvala**, P. Hazra*.
RSC Advances, 4, 1015-1024.

23. Modulation of excimer formation of 9-(dicyano-vinyl) julolidine by the macrocyclic hosts. **2013**
K. Gavvala, W. D. Sasikala, A. Sengupta, S. A. Dalvi, A. Mukherjee, P. Hazra*.
Physical Chemistry Chemical Physics, 15, 330-340.

Chapter 1

Introduction

The present chapter describes a brief introduction to fluorescence spectroscopy and its parameters. The working systems used in the present thesis molecular containers (cyclodextrins and cucurbiturils) and micelles are also introduced in this chapter. Motivation behind this thesis work has also been discussed in this chapter.

1a. Introduction to Fluorescence Spectroscopy:

Fluorescence spectroscopy is one of the most widely used molecular spectroscopy in chemistry and biology.[1, 2] In earlier days, this technique had been used just as an analytical tool for identifying various molecular species and determining its concentration based on the fluorescence intensity profile of the fluorophore (analyte). Later advancements in laser systems, optical detection methods and data analysis have been rapidly enhancing and adding significant contribution for advancing the fluorescence based techniques. These advanced fluorescence tools are in turn increasing our capability of gaining deeper understanding of the complex systems in all the fields ranging from chemistry, biology to physics, and hence, it is now a dominant technique used extensively everywhere.

1a.1. Fluorescence:

Fluorescence is one of the photoluminescence phenomena defined as the process in which a substance absorbs electromagnetic radiation of certain energy, and subsequently, emits radiation with lower energy. The other type of luminescence is phosphorescence. In either of these cases the molecule is excited to a higher energy state and then returns to a lower energy state accompanied by the emission of a photon. However, the processes by which the molecule emits the photon differ. To understand these two processes of photoluminescence, first the energy levels in a molecule must be defined. It is known that molecules have discrete energy levels depending on the structure of the molecule in accordance with quantum theory. The energy levels can be classified based on energy in the following order, rotational < vibrational < electronic. Various energy levels of a molecule and the transitions involved between them are classically presented by a Jablonski energy diagram (**Figure 1a.1**), named in honor of the Polish physicist Professor Alexander Jablonski. Energetic levels with spin multiplicity of 1 are called singlet states and are indicated by the letter “S”. Energetic levels with spin multiplicity of 3 are called triplet states and are indicated by the letter “T”. When a molecule absorbs a photon with energy equal to, or greater than, the energy difference between the ground state and the excited state, its energy can be transferred to the valance electron. And this electron will subsequently be promoted to a higher electronic orbit, thus putting the molecule into the excited state. This

transition period between ground and excited state is very fast, of the order of 10^{-15} s. This time scale is apparently too fast for significant displacement of the nuclei. This concept is referred to as the Franck-Condon Principle. Immediately following the absorption of a photon, several processes will occur with varying probabilities, but the most probable process will be relaxation to the lowest vibrational energy level of the first excited state (**Figure 1a.1**). This non-radiative process is known as internal conversion (IC) or vibrational relaxation, and generally, occurs in a picoseconds timescale or less. On other hand, the radiative pathway involves photon emission called photoluminescence (fluorescence and phosphorescence). The return of excited state electron to ground state is spin allowed and results in emission of light called, fluorescence. The fluorescence intensity of any fluorophore is characterized by a measure known as quantum yield. Quantum yield (Φ) is defined as the number of emitted photons relative to the number of absorbed photons.

Quantum yield = Number of photons emitted / Number of photons absorbed

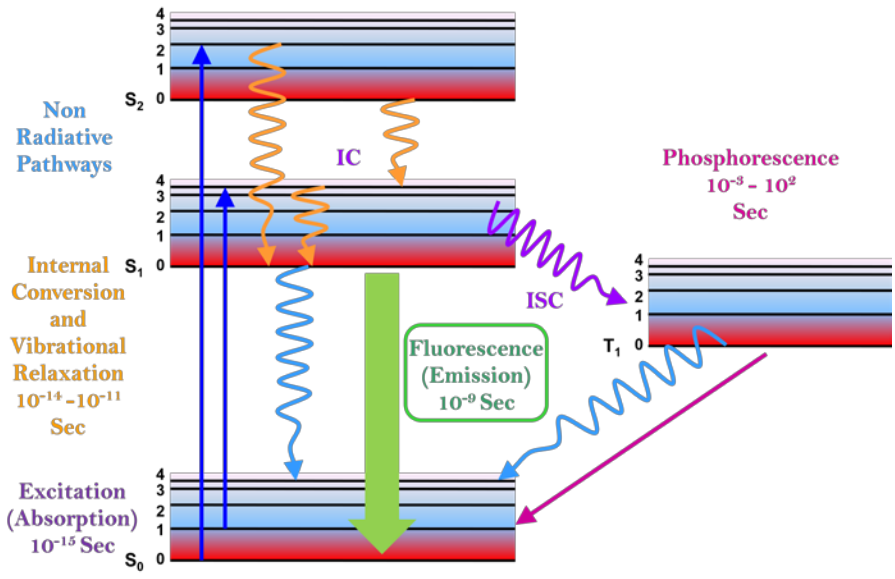

Figure 1a.1. Jablonski diagram of various radiative and non-radiative processes

The maximum value of quantum yield can be close to unity only when number of photons emitted is equal to the number of absorbed photons. In practical, this is not at all possible due to the Stokes losses. Fluorophores with the largest quantum yield, approaching unity, such as rhodamine, display the brightest emission. The quantum yield can also be defined in terms of radiative and non-radiative decay rate constants as given below;

$$\Phi = k_r/(k_r+k_{nr}) \qquad (1a.1)$$

Where k_r is the rate constant for fluorescence emission and k_{nr} is the sum of non-radiative decay rate constants. The relative quantum yield is determined by using the following equation.

$$\Phi_{sam} = \Phi_{ref} \times \frac{A_{sam}}{A_{ref}} \times \frac{Abs_{ref}}{Abs_{sam}} \times \frac{\eta_{sam}^2}{\eta_{ref}^2} \qquad (1a.2)$$

Where, Φ is the quantum yield, A represents the integration of emission spectrum, Abs is the absorbance at the excitation wavelength and η is the refractive index of the solvent. The subscripts sam and ref stands for the sample and reference, respectively.

1a.2. Fluorescence Lifetime:

Fluorescence lifetime is another important parameter in fluorescence spectroscopy and is the time-resolved characteristic of fluorescence. Time-resolved fluorescence spectroscopy is a well-established technique for studying the emission dynamics of fluorescent molecules with respect to its surroundings and confirmations. Fluorescence lifetime is a parameter that is mostly unaffected by inner filter effects, static quenching and variations in the fluorophore concentration. For this reason, it can be considered as one of the most robust fluorescence parameters, and therefore, it is advantageous in clinical and high throughput screening (HTS) applications, where it is necessary to discriminate against the high background fluorescence from biological samples. Unlike emission spectrum, lifetime of fluorophores is largely independent on fluorescence intensity and concentration of the sample. Steady state fluorescence spectrum is an

average emission profile of all excited fluorophores present in the sample. Hence, this technique has some limitations differentiating between individual fluorophores found in a heterogeneous population, such as those associated with different conformational states. Thus, fluorescence lifetime measurement can be used to distinguish individual fluorophores present in the multi-component mixture based on their fluorescence lifetime. The excited state lifetimes provide insight into the excited state dynamics and the decay pathways of the excited fluorophore. In this regard, it is possible, to extract information on different excited species in a heterogeneous medium based on differences in their fluorescence lifetime. The combination of environmental sensitivity and parametric independence mentioned above renders fluorescence lifetime a separate yet complementary method to conventional fluorescence intensity measurements. As previously explained when any molecule absorbs a photon of appropriate energy, a chain of photophysical events ensues, such as internal conversion or vibrational relaxation, fluorescence, intersystem crossing, and phosphorescence. Each of these processes occurs with a certain probability, and is characterized by respective decay rate constants (k). It can be shown that the average time duration τ for the set of molecules to decay from one state to another is reciprocally proportional to the rate of decay: $\tau = 1/k$. This τ is called lifetime of that particular process and for fluorescence it is fluorescence lifetime. The fluorescence lifetime is defined as the time a fluorophore spends in the excited state before returning to the ground state by emitting a photon. The lifetimes of fluorophores generally range from picoseconds to hundreds of nanoseconds.

If a population of fluorophores is excited, the lifetime is mathematically the time it takes for the number of excited molecules to decay to 1/e or 36.8% of the original population.

$$I(t) = I_0 e^{-t/\tau} \qquad (1a.3)$$

Where I(t) is the fluorescence intensity at time t, I_0 the fluorescence intensity at time t=0 and τ is the fluorescence lifetime of the fluorophore.

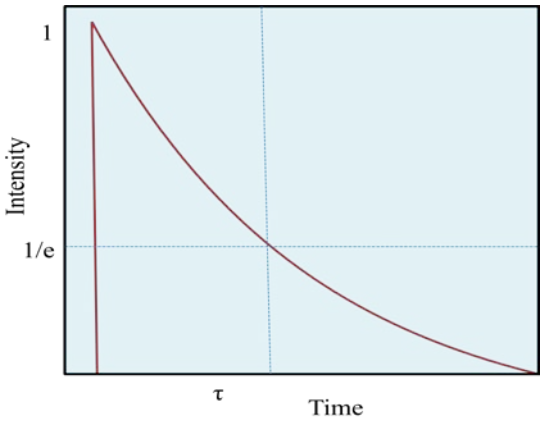

Figure 1a.2. Fluorescence decay profile with time

As shown in above Figure the plot of I(t) versus time gives an exponential decay. The fitting of this decay results in the fluorescence lifetime and its contribution. If more than one lifetime component then the fluorescence decay will be fitted with more than one lifetime component as stated below.

$$I(t) = \Sigma\, \alpha_i\, e^{-t/\tau i} \qquad (1a.4)$$

Where τ_i and α_i is the fluorescence lifetime and its contribution of *i* th component.

As fluorescence lifetime depends upon radiative and non-radiative decay channels it can be related to radiative and non-radiative decay rate constants;

$$\tau_f = 1/(k_r + k_{nr}) \qquad (1a.5)$$

where k_r and k_{nr} are radiative and non-radiative decay rate constants.

The fluorescence lifetime can be measured by using two methods; temporal domain and frequency domain. The details of the instrumentation, data acquisition and analysis methods are explained in 2nd chapter of this thesis.

1a.3. Fluorescence Anisotropy:

Fluorescence anisotropy measurement is one of the powerful tools in biochemical research and medical testing. When the sample is excited by polarized incident light, only those whose transition moments are aligned in a direction close to that of the electric vector of the incident beam are preferentially excited. This phenomenon is called as photoselection. Because the random distribution of excited fluorophores is anisotropic, the emitted fluorescence is also anisotropic. Thus, any change in the direction of the transition moment during the lifetime of the excited state will change this anisotropy. At the same time molecules with transition moments oriented perpendicular to the excitation polarization plane are not excited and remain in their ground state. This eventually induces a partial or total depolarization of fluorescence. There are many causes for the depolarization of fluorescence emission. One of them could be presence of nonparallel absorption and emission transition moments due to the random molecular motion, e.g. Brownian rotation or conformational flexibility that tends to randomize the initially well aligned and photoselected fluorophore population. This angular displacement of the fluorophore that occurs between absorption and emission depends upon rate and extent of rotational diffusion during lifetime of the excited state. The rotational diffusion of the fluorophore depends upon viscosity of the medium, size and shape of the rotating molecule. Fluorescence polarization measurements can thus provide valuable information about molecular mobility, size, shape conformational changes, flexibility of molecules and fluidity of the medium.

Fluorescence anisotropy can be measure by detecting polarized light at perpendicular and parallel to the excited incident beam as given below.

$$r = (I_{\parallel} - I_{\perp})/(I_{\parallel} + 2I_{\perp}) \qquad (1a.6)$$

Where $I_{\parallel}$ is the fluorescence intensity collected along the direction of incident beam and $I_{\perp}$ is the fluorescence intensity perpendicular to the direction of incident beam.

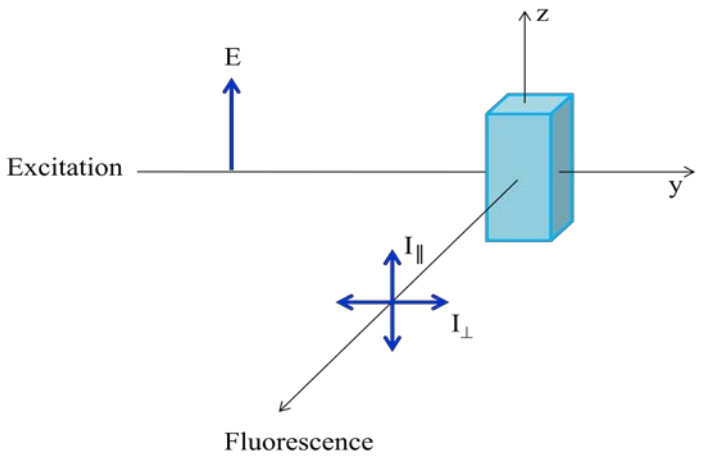

Figure 1a.3. Fluorescence measurements at parallel and perpendicular directions of incident light

Time dependent anisotropy decays offer excellent information about the diffusive motion of the fluorophore, which can reveal whether a fluorophore rotates freely or the surrounding environment of the fluorophore restricts its rotational motion.[1-5] Therefore, the time-resolved fluorescence anisotropy measurement has been extensively utilized to study the rotational dynamics of fluorophore in various bio-mimetic nanocavities. During anisotropy measurement, the sample is excited with a polarized light pulses and the time dependent parallel [$I_{\parallel}$(t)] and perpendicular [$I_{\perp}$(t)] components of the fluorescence are used to form the time-resolved fluorescence anisotropy, r(t), which is governed by the following equation;

$$r(t) = \frac{I_{\parallel_{\parallel}}(t) - I_{\perp}(t)}{I_{\parallel_{\parallel}}(t) + 2I_{\perp}(t)} \qquad (1a.7)$$

To compensate the polarization biased of the detection system and monochromator efficiency, the above equation is modified to;

$$r(t) = \frac{I_{\parallel}(t) - GI_{\perp}(t)}{I_{\parallel}(t) + 2GI_{\perp}(t)} \qquad (1a.8)$$

where, *G* is the instrumental correction factor introduced for the polarization sensitivity of the detection system and monochromator.

For a simple isotropic rotor, *r*(t) decays with a single rotational correlation time (τ_r) represented by the following equation;

$$r(t) = r_0 exp^{-(\frac{t}{\tau_r})} \qquad (1a.9)$$

For more complicated systems, *r*(t) takes the form of a sum of exponentials;

$$r(t) = r_0 \sum \beta_i \, exp^{-(\frac{t}{\tau_{ri}})} \qquad (1a.10)$$

where, β and τ_{ri} are the fractional contribution of total depolarization and rotational correlation times of the i^{th} component, respectively. r_0 represents fundamental anisotropy. In terms of Stokes-Einstein theory, τ_r is related to the medium viscosity by;

$$\tau_r = \frac{\eta V}{kT} = \frac{1}{6D} \qquad (1a.11)$$

where, η is the viscosity coefficient of the medium, *V* is the molecular volume, *k* is the Boltzmann's constant, *T* is the absolute temperature, and *D* is the rotational diffusion coefficient.

1b. Molecular Containers:

The macrocyclic molecules with void cavities inside their walls are called molecular containers. The inner cavities are known as nano-cavities and these are responsible for encapsulating guest molecules which are then isolated from the bulk outside the container. The volume of the nano-cavity can be tuned according to the size of incoming guest molecule. The formation of host-guest inclusion complexes in solution can result in significant changes in chemical and physical properties of the included guest. The scientific insights gained from these host-guest interactions have been of practical value in a wide range of applications including drug delivery,[6, 7] chromatography,[8] trace analysis,[9] sensors,[10] food industry[11] and for designing molecular architectures.[12]

There are numerous examples of large-sized ring compounds existing in nature. In some instances for example, many cyclic peptides, proteins, oligonucleotides, cyclic oligosaccharides lipids and their multimolecular complexes, have been the major source of inspiration for supramolecular chemists. Inspired by these natural molecules, many supramolecular scientists have dreamed of design and synthesis of novel supramolecular hosts with better structure and functionality. Research work on the synthesis of macrocyclic host molecules has blossomed over the last few decades in the wake of the discovery of crown ethers by Pedersen in 1967.[13] Since then, a whole range of large-sized ring macrocyclic compounds have appeared in the literature: some of the best known include the calixarenes,[14-17] cyclodextrins,[18-20] cucurbiturils,[21-23] cyclophanes,[24-26] octa acid,[27-29] cavitands[30-32] and many others.[33-36] Among these supramolecular hosts cyclodextrins and cucurbiturils have been received much interest owing to their unique tunable size and versatile guest binding properties as discussed below.

1b.1. Cyclodextrin:

The history of cyclodextrins (CDs) started in France in the late 19th century when the pharmacist and chemist Antoine Villiers have found some anomalous organic compounds upon reaction of enzymes on various carbohydrates.[37] CDs are cyclic oligomers of α-D-glucose obtained from enzymatic action on starch. Mainly three cyclodextrins are readily available known as the native CDs (**Figure 1b.1**): α-CD, having six glucose units; β-CD with seven units; and γ-CD with eight units. The CD molecule is often described as a torus, but it actually is somewhat more realistically pictured as a shallow truncated cone, with the primary hydroxyl rim of the cavity having a somewhat reduced diameter compared with the secondary hydroxy rim which results in container cup shape (**Figure 1b.1** and **1b.3**). The CD exterior, coated with hydroxyl groups, is polar in nature, whereas the interior of the cavity is nonpolar relative to the exterior and also external environments, water in particular. The core of their structure, composed of a dimensionally stable hydrophobic cavity is majorly responsible for trapping or encapsulating neutral molecules whereas the hydroxyl groups present at portals are responsible for stabilizing charged guest molecules to be included inside CD cavity. These remarkable encapsulation properties lead to a "host−guest" type relationship that can modify and/or improve the physical, chemical, and/or biological characteristics of the guest molecule.[37] In most of the cases, the host-guest complexation stoichiometry is 1:1, but there may be occasionally interferences from the formation of 1:2 and 2:2 host-guest complexes.[38-42] The binding constants of CDs range typically from 10 to 10^5 M^{-1},[43-45] which requires milli molar concentrations of macrocycle in order to achieve significant complexation of any guest molecule in aqueous solution.

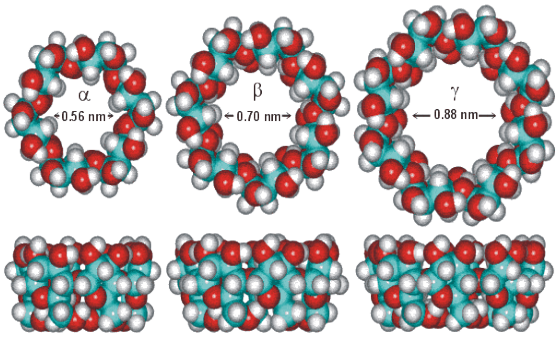

Figure 1b.1. Chemical structures of cyclodextrins with various cavity sizes
(Source: http://www1.lsbu.ac.uk/water/cyclodextrin.html)

The inclusion of guest molecules into these macrocycles can affect their physical and chemical properties and potentially guide to unprecedented effects which ultimately lead to versatile applications. The chemistry of CDs is very rich, and many applications at the laboratory as well as at the industrial level have been evaluated so far. Natural and modified CDs are widely used in chemistry and macromolecular chemistry,[46, 47] supramolecular chemistry,[48-50] catalysis,[51, 52] membranes,[53] aromas,[11] foods,[54, 55] agrochemistry,[56] biotechnology,[57] enzyme technology,[58] cosmetics,[59-63] pharmacy and medicine,[64-68] textiles,[63, 69] chromatography,[70, 71] microencapsulation,[72] nanotechnologies,[73-75] click chemistry,[76] analytical chemistry,[77] remediation,[78] and decontamination.[72] Besides, CDs have proved to be the most enduringly popular enzyme mimics, catalyzing various reactions.[79-83] Their negligible toxicity and tendency to improve the solubility and stability of drugs led them to use in pharmacy and biomedical applications as novel pharmaceutical excipients and drug delivery carriers.[18, 84-87] Many studies with fluorescent guest molecules are also endeavored to unravel the photophysical effects accompanying host-guest complexation.[19, 88-94] In many instances the fluorescence properties of guests are severely modulated upon complex formation with CDs, and these complex induced fluorescence properties are utilized for many applications, such as, for sensing, imaging, lasing, stabilizing, and other purposes.[37, 46, 88]

1b.2. Cucurbituril:

Cucurbit[n]urils (CBn) are a recently emerged another family of macrocyclic hosts synthesized by an acid-catalyzed condensation reaction between glycoluril and formaldehyde. The "n" represents the number of glycoluril monomers per cucurbituril macrocycle.

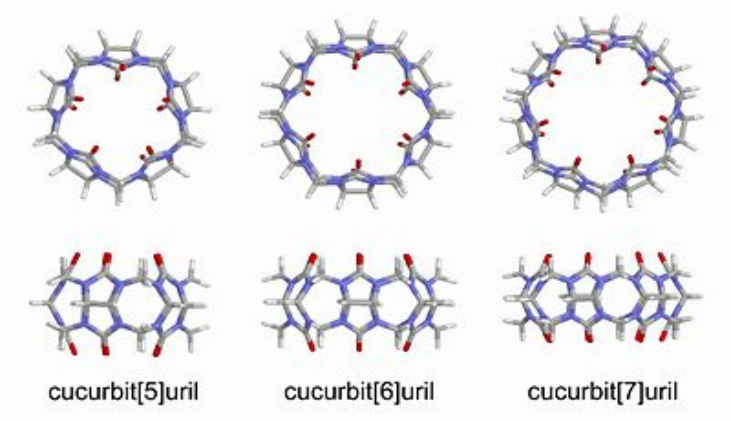

Figure 1b.2. Chemical structures of different cavity sized cucurbiturils
(Source: https://en.wikipedia.org/wiki/Cucurbituril)

Cucurbit[n]urils are highly symmetrical and rigid macrocycles with a hydrophobic cavity at centre and two identical carbonyl-laced portals projected outwards (**Figure 1b.2**). The hydrophobic interior is a potential inclusion site for several nonpolar and neutral guest molecules, whereas the polar ureido carbonyl groups at the portals allow the binding of charged molecules through charge-dipole and/or hydrogen bonding interactions. All CBn have a depth of 9.1 Å, whereas the outer diameter, internal cavity, volume, and the molecular weight increases progressively depending on the number of glycoluril units of the CBn homologues, on going from CB5 to CB10.[95-97] One of the outstanding features of the CBn family is their high thermal stability; they are stable even up to 370 ºC.[97, 98] The solubility of CBn is limited in common solvents constitutes. Particularly, CB6 and CB8 are less soluble ($<10^{-5}$ M) in water, whereas CB5 and CB7 have good solubility (~ 20-30 mM) in water. Apart from physical properties its cytotoxicity studies revealed that CBn are non-toxic in nature which boosts their applications in pharmaceutical field.[99-101]

CBn have both a hydrogen-bonding and ion-dipole interaction ability at the portals and a hydrophobic interior, which lead to remarkable molecular recognition properties. These distinct binding and restriction environments have profound implications in the formation of highly stable host-guest complexes than other well-known host molecules such as cyclodextrins and crown ethers.[101-103] The studies related to stabilization of charge-transfer complexes inside their cavity,[104] inclusion of two guest molecules,[105] encapsulation of macrocyclic guests,[106] inclusion of drug molecules,[97] formation of controllable vesicles,[107] control of chemical reactions inside the cavity,[108] CB7 as an hydrogel,[109] and so on, allowed numerous applications but not limited to, recognition and separation of wanted/unwanted guest molecules,[110, 111] improvement of dye properties,[112, 113] catalysis,[103, 114, 115] DNA binding and gene transfection,[116, 117] controlled drug delivery,[97, 118, 119] molecular switches,[120-122] logic devices,[123, 124] and photoswitchable molecular machines.[43] Photophysical properties of many guest molecules under CBn confinement have been extensively studied by W. Nau, H. Pal and few other research groups.[92, 118, 125-131] The fluorescence properties of guest molecules are severely modulated when they are encapsulated inside the molecular containers.[125-131] Few drug molecules are also incorporated to validate their applications towards pharmaceutical fields as drug delivery cargos.[130, 131] In the present chapter we have studied inclusion complex formation of many biologically important molecules and drugs with molecular containers. We have also tried to release them by different

external stimuli. All these important observations are discussed with deep insights are provided in the later chapters of this thesis.

The cucurbiturils are closest relatives of cyclodextrins in terms of size and shape (**Figure 1b.3**). Whilst CDs have the shape of a tapered cylinder, with one opening being wider than the other, CBn are symmetrical, with both of their portals being the same size. Compared with CD, the electrostatic potential of the portals of CBn are more negative, hence CBn hosts bind more readily and strongly with cationic guests, while CD favors binding to neutral and anionic guests.[122] These high electrostatic potential of the portals of CBn causes upward pKa shifts of included guest molecules.[92, 118, 122, 126, 132]

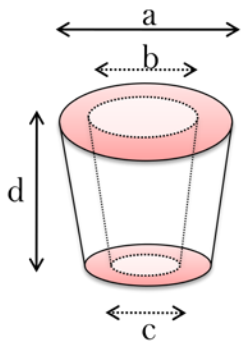

Cavity	a(A^0)	b(A^0)	c(A^0)	d(A^0)	Volume ((A^0)^3)
CB[6]	14.4	5.8	3.9	9.1	164
α-CD	14.6	5.6	4.7	8.0	174
CB[7]	16.0	7.3	5.4	9.1	279
β-CD	15.4	6.8	6.0	8.0	262
CB[8]	17.5	8.8	6.9	9.1	479
γ-CD	17.4	8.7	7.5	8.0	472

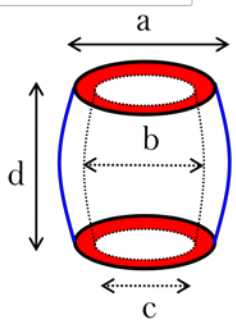

Figure 1b.3. Structure and cavity size comparison between cyclodextrins and cucurbiturils

1c. Micelles:

Micelles are supramolecular assemblies of surfactant molecules. Surfactants, commonly known as detergents, are amphipathic molecules having hydrophobic and hydrophilic regions at both the ends. The aggregation process depends on the nature of the surfactant, concentration and the condition of the system such as temperature of the system.[133, 134] Surfactants are divided into neutral, cationic, anionic or zwitterionic depending on the chemical structure of their polar head groups.[133-135] Whereas the hydrophobic or nonpolar moiety can be of different lengths, contain unsaturated bonds and/or consist of two or more chains. In aqueous solution the surfactants aggregate in such a way that these hydrophobic moieties are away from water and form a 'dry' core at middle of the micelles (**Figure 1c.1**). The hydrophilic part remains intact with water. The concentration of surfactants above which they form micelles is called 'critical micellar concentration (CMC)' and the temperature is called 'krafft temperature'.[133-135] The core of the micelles is surrounded by a polar 'Stern' layer for ionic micelles and 'palisade' layer for neutral micelles.[133, 136, 137] The polar headgroups, counterions and water molecules are present in this layer. But most of the counter ions are located in the Gouy-Chapman (GC) electrical double layer which separates Stern (or palisade) layer from bulk water.[119] Among various surfactants the anionic surfactant sodium dodecylsulphate (SDS), cationic surfactant cetyltrimethylammonium bromide (CTAB), and neutral surfactant triton X-100 (TX-100) are well studied.[138-146] Few polymer based surfactants also synthesized and evaluated for biological applications.[147] Unfortunately, many of these surfactant micelles have found major drawbacks particularly while using in pharmaceutical sector due to their in vivo toxicity and biocompatibility.[148, 149] To circumvent this problem researchers have been looking for biocompatible surfactants. To this context Alkyl glucoside surfactants have become popular owing to their non-toxic and bio-compatible activities.[150-153]

Alkyl glucosides belong to the class of non-ionic surfactants which are widely used in food, cosmetic and pharmacy products.[153-155] These surfactants contain a hydrophilic part comprised of glucose moiety, and a hydrophobic part consisting of hydrocarbon chain.[156] These sugar based surfactants are non-toxic and can be synthesized from renewable resources. Another important aspect of these surfactants is that they are biodegradable in nature.[150] The main reason for the biodegradability is the presence of glucoside linkage, which is widely occur in nature, and

its formation and breakage are controlled by different glucosidases.[150] These biocompatible sugar surfactants have frequently been used to study the dissolution and formation of biological membranes as well as the stabilization of proteins.[153-155] Considering the bio-compatible behavior of the alkyl glucoside, in the present thesis we have used octyl-β-D-glucoside (OBG), one of the familiar alkyl glucosides. The reason we chose OBG among alkyl glucosides is that many properties such as phase diagram, structural behavior of the OBG have been extensively studied by various techniques. In the present thesis, we have probed fluorescence properties of an anticancer drug, ellipticine in these micellar structures. We have found intriguing results which are discussed in detailed manner in chapter 4.

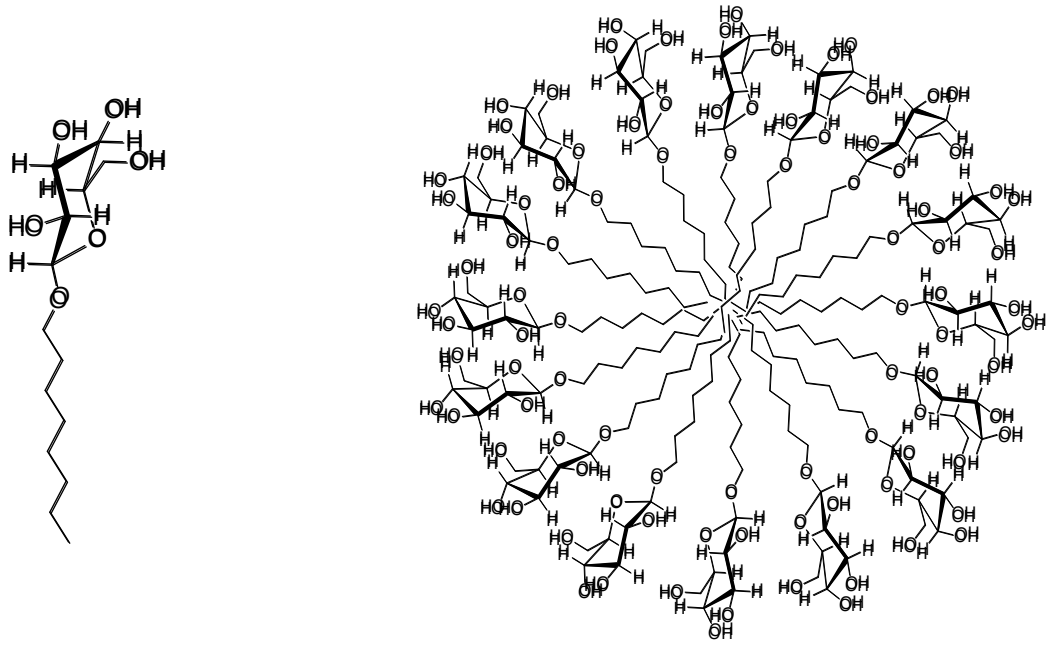

Figure 1c.1. Structure of octyl glucoside surfactant and its micelle

1d. Motivation of the Thesis:

Fluorescence spectroscopy, the most popular technique in scientific community, is widely used in many research fields as mentioned in the earlier section of this chapter because of its high sensitivity and selectivity towards surrounding environment. The sensitivity of fluorescence spectroscopy is mainly governed by modulation of the photophysics of given fluorophore in its surrounding environments. Hence, it is fundamental importance to understand the basic photophysics of fluorescent probes before using them in fluorescence based techniques. Owing to the importance of fluorescent probes and sensors for environmental and biological applications, it is usually desirable to "tune" fluorescent dyes in aqueous solution. Especially for fluorescent drugs it is very essential to establish a relationship between their fluorescence properties and surrounding environment for designing novel drug carriers and bio-imaging purposes. Motivation of my thesis is to understand the basic photophysical properties of important drugs and probes inside bio-mimetic confined environments. For understanding and tuning photophysical properties, we have chosen molecular containers and micelles because of their bio-mimetic nature, tunable nano-confined environments and importantly their applications in various fields as mentioned in the earlier sections of this chapter. The photophysical properties of molecules have been drastically modulated inside the above mentioned nano-cavities. We have found very interesting fluorescence switch and pKa shifts of many drug/fluorescent molecules, when they are encapsulated in bio-mimetic nano-cavities. The reasons for this kind of modulation of excited state photophysics have been unraveled using steady-state and time-resolved fluorescence techniques. We also observed that excited state proton transfer dynamics are being significantly modulated inside the above confined environments. All these observations are deep insights are provided in the later three chapters.

1e. Reference:

1. J. R. Lakowicz, *Principles of Fluorescence Spectroscopy*, Springer Science, New York, 3rd ed. edn., 2006.
2. B. Valeur, *Molecular fluorescence: principles and applications*, Wiley-VCH, 2002.
3. M. Maroncelli, *J. Mol. Liq.*, 1993, **57**, 1-37.
4. I. B. Berlman, *Handbook of fluorescence spectra of aromatic molecules*, Academic Press, 1965.
5. S. Udenfriend, *Protein Sci.*, 1995, **4**, 542-551.
6. J. Li and X. J. Loh, *Adv. Drug Delivery Rev.*, 2008, **60**, 1000-1017.
7. J. Li, *NPG Asia Mater*, 2010, **2**, 112-118.
8. A. Bogdanski, D. Wistuba, K. L. Larsen, U. Hartnagel, A. Hirsch and V. Schurig, *New J. Chem.*, 2010, **34**, 693-698.
9. O. F. Sayo, L. Mark, A. F. Kristin, H. Xiaodong, M. P. Aleeta and M. W. Isiah, *Curr. Anal. Chem.*, 2007, **3**, 171-181.
10. S. Karuppannan and J.-C. Chambron, *Chem Asian J*, 2011, **6**, 964-984.
11. H. M. C. Marques, *Flavour and Fragrance Journal*, 2010, **25**, 313-326.
12. A. Harada, *Acc. Chem. Res.*, 2001, **34**, 456-464.
13. D. Phlip, *Adv. Mater.*, 1996, **8**, 866-868.
14. F. Perret and A. W. Coleman, *Chem. Commun.*, 2011, **47**, 7303-7319.
15. V. Lau and B. Heyne, *Chem. Commun.*, 2010, **46**, 3595-3597.
16. D.-S. Guo, K. Wang, Y.-X. Wang and Y. Liu, *J. Am. Chem. Soc*, 2012, **134**, 10244-10250.
17. K. Wang, D.-S. Guo, X. Wang and Y. Liu, *ACS Nano*, 2011, **5**, 2880-2894.
18. K. Uekama, F. Hirayama and T. Irie, *Chem. Rev.*, 1998, **98**, 2045-2076.
19. A. Douhal, *Chem. Rev.*, 2004, **104**, 1955-1976.
20. T. Kida, T. Iwamoto, H. Asahara, T. Hinoue and M. Akashi, *J. Am. Chem. Soc*, 2013, **135**, 3371-3374.
21. E. Masson, Y. M. Shaker, J.-P. Masson, M. E. Kordesch and C. Yuwono, *Org. Lett.*, 2011, **13**, 3872-3875.

22. H. Tang, D. Fuentealba, Y. H. Ko, N. Selvapalam, K. Kim and C. Bohne, *J. Am. Chem. Soc*, 2011, **133**, 20623-20633.
23. X. Wang and Z. Guo, *Chem. Soc. Rev.*, 2013, **42**, 202-224.
24. P. L. Anelli, N. Spencer and J. F. Stoddart, *J. Am. Chem. Soc*, 1991, **113**, 5131-5133.
25. A. C. Fahrenbach, S. Sampath, D. J. Late, J. C. Barnes, S. L. Kleinman, N. Valley, K. J. Hartlieb, Z. Liu, V. P. Dravid, G. C. Schatz, R. P. Van Duyne and J. F. Stoddart, *ACS Nano*, 2012, **6**, 9964-9971.
26. B. Shirinfar, N. Ahmed, Y. S. Park, G.-S. Cho, I. S. Youn, J.-K. Han, H. G. Nam and K. S. Kim, *J. Am. Chem. Soc*, 2013, **135**, 90-93.
27. C. L. D. Gibb and B. C. Gibb, *J. Am. Chem. Soc*, 2004, **126**, 11408-11409.
28. S. Jockusch, M. Porel, V. Ramamurthy and N. J. Turro, *J. Phys. Chem. Lett.*, 2011, **2**, 2877-2880.
29. H. Tang, C. S. de Oliveira, G. Sonntag, C. L. D. Gibb, B. C. Gibb and C. Bohne, *J. Am. Chem. Soc*, 2012, **134**, 5544-5547.
30. R. Pinalli, M. Suman and E. Dalcanale, *Eur. J. Org. Chem.*, 2004, **2004**, 451-462.
31. B. W. Purse and J. Rebek, *Proc. Natl. Acad. Sci. U.S.A.*, 2005, **102**, 10777-10782.
32. S. M. Biros and J. J. Rebek, *Chem. Soc. Rev.*, 2007, **36**, 93-104.
33. J.-M. Lehn, *Angew. Chem., Int. Ed.*, 1988, **27**, 89-112.
34. A. E. Rowan, J. A. A. W. Elemans and R. J. M. Nolte, *Acc. Chem. Res.*, 1999, **32**, 995-1006.
35. M. D. Pluth and K. N. Raymond, *Chem. Soc. Rev.*, 2007, **36**, 161-171.
36. Z. Laughrey and B. C. Gibb, *Chem. Soc. Rev.*, 2011, **40**, 363-386.
37. G. Crini, *Chem. Rev.*, 2014, **114**, 10940-10975.
38. A. Nakamura and Y. Inoue, *J. Am. Chem. Soc*, 2005, **127**, 5338-5339.
39. A. Nakamura and Y. Inoue, *J. Am. Chem. Soc*, 2003, **125**, 966-972.
40. R. S. Murphy, T. C. Barros, J. Barnes, B. Mayer, G. Marconi and C. Bohne, *J. Phys. Chem. A*, 1999, **103**, 137-146.
41. A. S. M. Dyck, U. Kisiel and C. Bohne, *J. Phys. Chem. B*, 2003, **107**, 11652-11659.
42. S. Monti, P. Bortolus, F. Manoli, G. Marconi, G. Grabner, G. Kohler, B. Mayer, W. Boszczyk and K. Rotkiewicz, *Photochem. Photobiol. Sci.*, 2003, **2**, 203-211.

43. K. N. Houk, A. G. Leach, S. P. Kim and X. Zhang, *Angew. Chem., Int. Ed.*, 2003, **42**, 4872-4897.
44. M. V. Rekharsky and Y. Inoue, *Chem. Rev.*, 1998, **98**, 1875-1918.
45. B. Zhang and R. Breslow, *J. Am. Chem. Soc*, 1993, **115**, 9353-9354.
46. J. Szejtli, *Chem. Rev.*, 1998, **98**, 1743-1754.
47. A. Tonelli, *J. Inclusion Phenom. Mol. Recognit. Chem.*, 2008, **60**, 197-202.
48. F. Hapiot, S. Tilloy and E. Monflier, *Chem. Rev.*, 2006, **106**, 767-781.
49. G. Wenz, B.-H. Han and A. Müller, *Chem. Rev.*, 2006, **106**, 782-817.
50. A. Harada, Y. Takashima and H. Yamaguchi, *Chem. Soc. Rev.*, 2009, **38**, 875-882.
51. E. A. Karakhanov and A. L. Maximov, *Curr. Org. Chem.*, 2010, **14**, 1284-1295.
52. M. Komiyama and E. Monflier, in *Cyclodextrins and Their Complexes*, Wiley-VCH Verlag GmbH & Co. KGaA, 2006, DOI: 10.1002/3527608982.ch4, pp. 93-105.
53. C. A. Kozlowski and W. Sliwa, *Carbohydr. Polym.*, 2008, **74**, 1-9.
54. G. Astray, C. Gonzalez-Barreiro, J. C. Mejuto, R. Rial-Otero and J. Simal-Gándara, *Food Hydrocolloids*, 2009, **23**, 1631-1640.
55. J. M. López-Nicolás, P. Rodríguez-Bonilla and F. García-Carmona, *Crit. Rev. Food Sci. Nutri.*, 2014, **54**, 251-276.
56. H. Dodziuk, in *Cyclodextrins and Their Complexes*, Wiley-VCH Verlag GmbH & Co. KGaA, 2006, DOI: 10.1002/3527608982.ch1, pp. 1-30.
57. J. Li, F. Zhao and J. Li, *Appl Microbiol Biotechnol*, 2011, **90**, 427-443.
58. R. Villalonga, R. Cao and A. Fragoso, *Chem. Rev.*, 2007, **107**, 3088-3116.
59. U. Numanoğlu, T. Şen, N. Tarimci, M. Kartal, O. M. Y. Koo and H. Önyüksel, *AAPS PharmSciTech*, 2007, **8**, 34-42.
60. C. d. G. Venturini, J. Nicolini, C. Machado and V. G. Machado, *Química Nova*, 2008, **31**, 360-368.
61. N. Tarimci, in *Cyclodextrins in Pharmaceutics, Cosmetics, and Biomedicine*, John Wiley & Sons, Inc., 2011, DOI: 10.1002/9780470926819.ch7, pp. 131-144.
62. H.-J. Buschmann, D. Knittel, K. Beermann and E. Schollmeyer, *Nachrichten aus der Chemie*, 2001, **49**, 620-622.
63. H. J. Buschmann, D. Knittel and E. Schollmeyer, *J. Inclusion Phenom. Mol. Recognit. Chem.*, 2001, **40**, 169-172.

64. F. van de Manakker, T. Vermonden, C. F. van Nostrum and W. E. Hennink, *Biomacromolecules*, 2009, **10**, 3157-3175.
65. J. R. Kanwar, B. M. Long and R. K. Kanwar, *Curr. Med. Chem.*, 2011, **18**, 2079-2085.
66. M. Fliur, B. Veaceslav, G. Athina and S. Natalia, *Curr. Top. Med. Chem.*, 2013, **13**, 2677-2683.
67. A. Concheiro and C. Alvarez-Lorenzo, *Adv. Drug Delivery Rev.*, 2013, **65**, 1188-1203.
68. J. Zhang and P. X. Ma, *Adv. Drug Delivery Rev.*, 2013, **65**, 1215-1233.
69. H. J. Buschmann, U. Denter, D. Knittel and E. Schollmeyer, *J. Text. Inst.*, 1998, **89**, 554-561.
70. W. Caroline, *Curr. Anal. Chem.*, 2014, **10**, 99-120.
71. Y. Xiao, S.-C. Ng, T. T. Y. Tan and Y. Wang, *J. Chromatogr. A*, 2012, **1269**, 52-68.
72. G. Rui and D. W. Lee, *Curr. Org. Chem.*, 2013, **17**, 14-21.
73. G. Tejashri, B. Amrita and J. Darshana, in *Acta Pharmaceutica*, 2013, vol. 63, p. 335.
74. S. V. Chilajwar, P. P. Pednekar, K. R. Jadhav, G. J. C. Gupta and V. J. Kadam, *Expert Opinion on Drug Delivery*, 2014, **11**, 111-120.
75. K. G. Amit, E. S. Johal and G. Rath, *Curr. Nanosci.*, 2011, **7**, 640-654.
76. K. Divya, D. Pratibha, K. K. Saroj and K. T. Vinod, *Curr. Org. Synth.*, 2013, **10**, 90-135.
77. J. Tong and L. Chen, *Anal. Lett.*, 2013, **46**, 2635-2656.
78. O. Atteia, E. Del Campo Estrada and H. Bertin, *Rev Environ Sci Biotechnol*, 2013, **12**, 379-389.
79. A. J. Kirby, *Angew. Chem., Int. Ed.*, 1996, **35**, 706-724.
80. O. S. Tee and X. X. Du, *J. Am. Chem. Soc*, 1992, **114**, 620-627.
81. T. A. Gadosy and O. S. Tee, *J. Chem. Soc., Perkin Trans. 2*, 1994, DOI: 10.1039/P29940000715, 715-721.
82. T. A. Gadosy and O. S. Tee, *J. Chem. Soc., Perkin Trans. 2*, 1995, DOI: 10.1039/P29950000071, 71-76.
83. D. M. Davies, G. A. Garner and J. R. Savage, *J. Chem. Soc., Perkin Trans. 2*, 1994, DOI: 10.1039/P29940001531, 1531-1537.
84. K. A. Connors, *Chem. Rev.*, 1997, **97**, 1325-1358.
85. M. E. Brewster, K. S. Estes, T. Loftsson, R. Perchalski, H. Derendorf, G. Mullersman and N. Bodor, *Journal of Pharmaceutical Sciences*, 1988, **77**, 981-985.

86. T. Loftsson and M. E. Brewster, *Journal of Pharmaceutical Sciences*, 1996, **85**, 1017-1025.
87. V. Stella and R. Rajewski, *Pharm Res*, 1997, **14**, 556-567.
88. R. N. Dsouza, U. Pischel and W. M. Nau, *Chem. Rev.*, 2011, **111**, 7941-7980.
89. J. Mohanty, A. C. Bhasikuttan, W. M. Nau and H. Pal, *J. Phys. Chem. B*, 2006, **110**, 5132-5138.
90. A. Chatterjee, B. Maity and D. Seth, *J. Phys. Chem. B*, 2014, **118**, 9768-9781.
91. M. Marchena, M. Gil, C. Martín, J. A. Organero, F. Sanchez and A. Douhal, *J. Phys. Chem. B*, 2011, **115**, 2424-2435.
92. M. Shaikh, J. Mohanty, P. K. Singh, W. M. Nau and H. Pal, *Photochem. Photobiol. Sci.*, 2008, **7**, 408-414.
93. P. K. Singh, S. Murudkar, A. K. Mora and S. Nath, *J. Photochem. Photobiol., A*, 2015, **298**, 40-48.
94. Y. Liu, C.-J. Li, D.-S. Guo, Z.-H. Pan and Z. Li, *Supramol. Chem.*, 2007, **19**, 517-523.
95. R. Behrend, E. Meyer and F. Rusche, *Justus Liebigs Annalen der Chemie*, 1905, **339**, 1-37.
96. W. A. Freeman, W. L. Mock and N. Y. Shih, *J. Am. Chem. Soc*, 1981, **103**, 7367-7368.
97. J. W. Lee, S. Samal, N. Selvapalam, H.-J. Kim and K. Kim, *Acc. Chem. Res.*, 2003, **36**, 621-630.
98. A. Day, A. P. Arnold, R. J. Blanch and B. Snushall, *J. Org. Chem.*, 2001, **66**, 8094-8100.
99. K. Kim, N. Selvapalam, Y. H. Ko, K. M. Park, D. Kim and J. Kim, *Chem. Soc. Rev.*, 2007, **36**, 267-279.
100. A. I. Day, R. J. Blanch, A. P. Arnold, S. Lorenzo, G. R. Lewis and I. Dance, *Angew. Chem., Int. Ed.*, 2002, **41**, 275-277.
101. J. Lagona, P. Mukhopadhyay, S. Chakrabarti and L. Isaacs, *Angew. Chem., Int. Ed.*, 2005, **44**, 4844-4870.
102. C. Márquez, R. R. Hudgins and W. M. Nau, *J. Am. Chem. Soc*, 2004, **126**, 5806-5816.
103. W. L. Mock and N. Y. Shih, *J. Am. Chem. Soc*, 1989, **111**, 2697-2699.
104. J. Kim, I.-S. Jung, S.-Y. Kim, E. Lee, J.-K. Kang, S. Sakamoto, K. Yamaguchi and K. Kim, *J. Am. Chem. Soc*, 2000, **122**, 540-541.

105. S. Liu, C. Ruspic, P. Mukhopadhyay, S. Chakrabarti, P. Y. Zavalij and L. Isaacs, *J. Am. Chem. Soc*, 2005, **127**, 15959-15967.

106. S.-Y. Kim, I.-S. Jung, E. Lee, J. Kim, S. Sakamoto, K. Yamaguchi and K. Kim, *Angew. Chem., Int. Ed.*, 2001, **40**, 2119-2121.

107. Y. J. Jeon, P. K. Bharadwaj, S. Choi, J. W. Lee and K. Kim, *Angew. Chem., Int. Ed.*, 2002, **41**, 4474-4476.

108. S. Y. Jon, Y. H. Ko, S. H. Park, H.-J. Kim and K. Kim, *Chem. Commun.*, 2001, DOI: 10.1039/B105153A, 1938-1939.

109. I. Hwang, W. S. Jeon, H.-J. Kim, D. Kim, H. Kim, N. Selvapalam, N. Fujita, S. Shinkai and K. Kim, *Angew. Chem., Int. Ed.*, 2007, **46**, 210-213.

110. T. Robinson, G. McMullan, R. Marchant and P. Nigam, *Biores. Tech.*, 2001, **77**, 247-255.

111. A. Kornmüller, S. Karcher and M. Jekel, *Water Res.*, 2001, **35**, 3317-3324.

112. A. L. Koner and W. M. Nau, *Supramol. Chem.*, 2007, **19**, 55-66.

113. R. W. Clarke, S. S. White, D. Zhou, L. Ying and D. Klenerman, *Angew. Chem., Int. Ed.*, 2005, **44**, 3747-3750.

114. H. C. Kolb, M. G. Finn and K. B. Sharpless, *Angew. Chem., Int. Ed.*, 2001, **40**, 2004-2021.

115. W. L. Mock and N. Y. Shih, *J. Org. Chem.*, 1983, **48**, 3618-3619.

116. E. Nakamura, H. Isobe, N. Tomita, M. Sawamura, S. Jinno and H. Okayama, *Angew. Chem., Int. Ed.*, 2000, **39**, 4254-4257.

117. Y.-b. Lim, T. Kim, J. W. Lee, S.-m. Kim, H.-J. Kim, K. Kim and J.-s. Park, *Bioconjugate Chem.*, 2002, **13**, 1181-1185.

118. N. i. Saleh, A. L. Koner and W. M. Nau, *Angew. Chem., Int. Ed.*, 2008, **47**, 5398-5401.

119. Y. Jin Jeon, S.-Y. Kim, Y. Ho Ko, S. Sakamoto, K. Yamaguchi and K. Kim, *Org. Biomol. Chem.*, 2005, **3**, 2122-2125.

120. K. Kim, *Chem. Soc. Rev.*, 2002, **31**, 96-107.

121. D. M. Bailey, A. Hennig, V. D. Uzunova and W. M. Nau, *Chem.Eur. J.*, 2008, **14**, 6069-6077.

122. A. Praetorius, D. M. Bailey, T. Schwarzlose and W. M. Nau, *Org. Lett.*, 2008, **10**, 4089-4092.

123. U. Pischel, *Angew. Chem., Int. Ed.*, 2007, **46**, 4026-4040.

124. U. Pischel, V. D. Uzunova, P. Remon and W. M. Nau, *Chem. Commun.*, 2010, **46**, 2635-2637.
125. A. C. Bhasikuttan, J. Mohanty, W. M. Nau and H. Pal, *Angew. Chem., Int. Ed.*, 2007, **46**, 4120-4122.
126. T. Fukaminato, E. Tateyama and N. Tamaoki, *Chem. Commun.*, 2012, **48**, 10874-10876.
127. M. Shaikh, S. Dutta Choudhury, J. Mohanty, A. C. Bhasikuttan, W. M. Nau and H. Pal, *Chem.Eur. J.*, 2009, **15**, 12362-12370.
128. J. Mohanty, H. Pal, A. K. Ray, S. Kumar and W. M. Nau, *ChemPhysChem*, 2007, **8**, 54-56.
129. A. C. Bhasikuttan, H. Pal and J. Mohanty, *Chem. Commun.*, 2011, **47**, 9959-9971.
130. A. Goyanes, G. B. Hatton, H. A. Merchant and A. W. Basit, *Int. J. Pharm.*, 2015, **484**, 103-108.
131. S. D. Choudhury, J. Mohanty, H. Pal and A. C. Bhasikuttan, *J. Am. Chem. Soc*, 2010, **132**, 1395-1401.
132. I. Ghosh and W. M. Nau, *Adv. Drug Delivery Rev.*, 2012, **64**, 764-783.
133. F. M. Menger, *Acc. Chem. Res.*, 1979, **12**, 111-117.
134. H. Wennerström and B. Lindman, *Physics Reports*, 1979, **52**, 1-86.
135. B. Lindman and H. Wennerström, in *Micelles*, Springer Berlin Heidelberg, 1980, vol. 87, ch. 1, pp. 1-83.
136. B. Bagchi, *Chem. Rev.*, 2005, **105**, 3197-3219.
137. L. J. C. Love, J. G. Habarta and J. G. Dorsey, *Anal. Chem.*, 1984, **56**, 1132A-1148A.
138. J. L. Anderson, V. Pino, E. C. Hagberg, V. V. Sheares and D. W. Armstrong, *Chem. Commun.*, 2003, DOI: 10.1039/B307516H, 2444-2445.
139. N. J. Turro, M. Grätzel and A. M. Braun, *Angew. Chem., Int. Ed.*, 1980, **19**, 675-696.
140. M. H. Gehlen and F. C. De Schryver, *Chem. Rev.*, 1993, **93**, 199-221.
141. N. Nandi, K. Bhattacharyya and B. Bagchi, *Chem. Rev.*, 2000, **100**, 2013-2046.
142. A. Sorrenti, O. Illa and R. M. Ortuno, *Chem. Soc. Rev.*, 2013, **42**, 8200-8219.
143. B. Maity, A. Chatterjee, S. A. Ahmed and D. Seth, *J. Phys. Chem. B*, 2015, **119**, 3776-3785.
144. B. Maity, A. Chatterjee and D. Seth, *RSC Adv.*, 2015, **5**, 3814-3824.

145. T. K. Mukherjee, P. Ahuja, A. L. Koner and A. Datta, *J. Phys. Chem. B*, 2005, **109**, 12567-12573.

146. S. Satpathi, K. Gavvala and P. Hazra, *Phys. Chem. Chem. Phys.*, 2015, **17**, 20725-20732.

147. K. Letchford and H. Burt, *European Journal of Pharmaceutics and Biopharmaceutics*, 2007, **65**, 259-269.

148. V. P. Torchilin, *Pharm Res*, 2007, **24**, 1-16.

149. D. Sutton, N. Nasongkla, E. Blanco and J. Gao, *Pharm Res*, 2007, **24**, 1029-1046.

150. H. Luders, *Nonionic Surfactants: Alkylpolyglucosides*, Dekker, New York, 2000.

151. B. J. n. K. Holmberg, B. Kronberg and B. Lindman, *Surfactants and Polymers in Aqueous Solution*, Wiley, New York, 2nd edn edn., 2002.

152. M. Kasahara and P. C. Hinkle, *Proc. Natl. Acad. Sci. U.S.A.*, 1976, **73**, 396-400.

153. M. Ollivon, O. Eidelman, R. Blumenthal and A. Walter, *Biochemistry*, 1988, **27**, 1695-1703.

154. L. T. Mimms, G. Zampighi, Y. Nozaki, C. Tanford and J. A. Reynolds, *Biochemistry*, 1981, **20**, 833-840.

155. S. Nakamura and M. Rodbell, *Proc. Natl. Acad. Sci. U.S.A.*, 1990, **87**, 6413-6417.

156. R. Zhang, P. A. Marone, P. Thiyagarajan and D. M. Tiede, *Langmuir*, 1999, **15**, 7510-7519.

Chapter 2

Experimental: Materials and Methods

"In the present chapter we discuss the experimental details of materials, sample preparations and various methods that are used for different studies in this thesis. This chapter is divided in to two main sections. The procedure of sample preparation and different instruments that used for various experiments are discussed briefly in these two sections of the current chapter. In first section the full list materials and sample preparations are discussed where as in second section we discuss about different technical methods. These sections are discussed one by one in detailed manner as follows."

2a. Materials:

2a.1. Different Fluorescent Drugs and Probes:

In the present section we have tabulated several fluorescent drugs, molecules, organic solvents and salts that are being used for different experiments mentioned in this thesis.

Table 2a.1. Different materials, its source and purity along with the chapter number it has been used are mentioned in the table.

Name	Source	Grade (Purity)	Ch.
Camptothecin	Sigma Aldrich	Purity ≥ 99%	3
Milrinone	Sigma Aldrich	Purity ≥ 99%	3
Topotecan	Sigma Aldrich	Purity ≥ 99%	4
Ellipticine	Sigma Aldrich	Purity ≥ 99%	4,5
Bipyridine diol	Sigma Aldrich	Purity ≥ 99%	4
Octyl β-glucoside	Sigma Aldrich	Purity ≥ 99%	4
Calf thymus DNA Na salt (10000 bp long)	Sigma Aldrich	Molecular Biology	5
Cucurbit[n]uril (n=6, 7 and 8)	Sigma Aldrich	Purity ≥ 99%	3,4
Cyclodextrins (α, β and γ)	Sigma Aldrich	Purity ≥ 99%	3,4,5
Sodium phosphate dibasic (NaH_2PO_4)	SRL, India,	Purity 99.5%	3,4,5
Sodium phosphate dibasic (Na_2HPO_4)	SRL, India,	Purity 99.5%	3,4,5
Sodium chloride (NaCl)	Sigma Aldrich	BioXtra ≥ 99.5%	3,4,5
Hydrochloric acid	Merck, India	Purity 90%	3,4,5
Sodium hydroxide (NaOH)	SRL, India	Purity 98%	3,4,5
SDS	Sigma Aldrich	Purity ≥ 99%	4
CTAB	Sigma Aldrich	Purity ≥ 99%	4
Triton-X	Sigma Aldrich	Purity ≥ 99%	4
Glucose	Sigma Aldrich	Purity ≥ 99%	4
Methanol	Merck, India	Spectroscopy	4
DMSO	Merck, India	Spectroscopy	3,4,5
Dioxane	Merck, India	Spectroscopy	4
Acetonitrile	Merck, India	Spectroscopy	4
Formamide	Merck, India	Spectroscopy	4
Acetone	Merck, India	Spectroscopy	4

2a.2. Sample Preparations:

All the chemicals brought from as mentioned earlier (**Table 2a.1**) and were used without any further purification. As few drug molecules (CPT and EPT) are not soluble in water we have used DMSO stock solution of for all experiments. For spectroscopic measurements a 2-5 μL stock of probe was dissolved in 2.5 ml of PBS (10 mM), and then the solution was strongly sonicated in a thermostat for ~1 hr (avoiding heating effect) to obtain a homogeneous solution in water/buffer. This solution is found to be stable enough for long duration even for few days, without any separation or precipitation. The working concentrations for all the measurements were kept fixed at 10-20 μM for most of the studies. For host-guest complexation studies an increasing concentration of different host molecules (CBn or CDs) were added to the guest solutions with micro-molar/milli-molar interval additions. For micelles formation increasing amounts of OBG surfactant was gradually added directly to EPT solution. After each addition ~10 minutes of equilibration time was given before proceeding for further measurements. Calf Thymus DNA Na Salt (**Table 2a.1)** was used as purchased. The concentration of DNA stock solution was calculated using molar extinction coefficient 6600 $M^{-1}.cm^{-1}$/base for DNA at 260 nm. From absorption ratio value (<1.8) at 260 nm/280 nm we have confirmed that DNA samples are free of any protein contamination. The individual solutions with different concentration were prepared by adding respective amount from stock to the buffer. The samples were annealed at 90ºC for 3 minutes and allowed to come back at room temperature normally to ensure the maximum extent of hybridization. For pH dependent experiments the pH is varied by adding dilute HCl or NaOH solution to the PBS solution. pH of the solution was measured by using pH-1500 (Eutech Instruments) and it was further cross checked by silicon micro sensor pocket sized pH meter (ISFETCOM Co. Ltd., Japan). Detailed description of preparation of solutions in each chapter is given below.

Chapter 3a: Camptothecin (CPT) and CB7 were obtained from Sigma Aldrich and used without further purification. As CPT is sparingly soluble in water, we have prepared a concentrated stock solution of CPT in DMSO. ~2 μL of CPT stock solution was added in 2 ml of Millipore water having pH = 6.2, and the solution was sonicated for few minutes in order to achieve homogeneous solution of CPT. Then, CB7 was gradually added to the solution containing CPT. The solution was gently shaken after each addition of CB7 until complete

solubilisation of CB7 took place. Moreover, we have given 10 minutes equilibration time for each addition of CB7.

Chapter 3b: Milrinone (MIR), CB7 were purchased from Sigma Aldrich, and used without further purification. Millipore water was used for sample preparation. CB7 was gradually added to the solution containing MIR, and the solution was gently shaken after each addition of CB7 until complete solubilization took place. Moreover, we have given 20 minutes equilibration time for each addition of CB7. Fine adjustment of pH was done by drop wise addition of diluted hydrochloric acid for lower pH range and 0.1 M sodium hydroxide solution for the higher pH range. pH of the solution was measured by using pH-1500 (Eutech Instruments) and it was further cross checked by silicon micro sensor pocket sized pH meter (ISFETCOM Co. Ltd., Japan).

Chapter 4a: TPT and CB7 were purchased from Sigma Aldrich, and used without further purification. Acetonitrile (ACN), dimethylsulfoxide (DMSO), acetone, formamide, methanol, ethanol, and dioxane are of high purity (HPLC Grade, >99%) and obtained from Merck, India. Millipore water was used for sample preparation. Concentration of TPT in water was adjusted using reported value of molar extinction coefficient (ε381 = 25580 M-1 cm-1).[28] CB7 was gradually added to the solution containing TPT, and the solution was gently shaken after each addition of CB7 until complete solubilisation of CB7 took place. Moreover, we have given 20 minutes equilibration time for each addition of CB7.

Chapter 4b: CB7, β-CD and [2,2′-bipyridyl]-3,3′-diol (BP(OH)2) are purchased from Sigma-Aldrich and used as received. All the samples are prepared in Millipore water. CB7/β-CD was gradually added to the solution containing BP(OH)2, and the solution was gently shaken after each addition of CB7/β-CD until complete solubilization of CB7/β-CD took place. Moreover, we have given 20 minutes equilibration time for each addition of host.

Chapter 4c: Ellipticine (EPT), octyl-β-D-glucopyranoside (OBG), glucose, sodium dodecyl sulfate (SDS), cetyltrimethylammonium bromide (CTAB) and Triton X-100 were purchased from Sigma Aldrich, and used without further purification. All the samples were prepared in phosphate buffer (10 mM), unless otherwise mentioned. Concentration of EPT in water was adjusted to ~10-5 M using reported value of molar extinction coefficient (ε300 = 39000 M-1 cm-1).36

Chapter 5a: EPT, CBn and CDs were purchased from Sigma Aldrich, and used without further purification. Millipore water was used for sample preparation. Concentration of EPT in water was adjusted to ~10-5 M using reported value of molar extinction coefficient (ε300 = 39000 M-1 cm-1).33 CBn/CD was gradually added to the solution containing EPT, and the solution was gently shaken after each addition of CBn/CD until completely solubilized. Moreover, we have given 20 minutes equilibration time after each addition of CBn/CD.

Chapter 5b: EPT, β-CD and CT-DNA were purchased from Sigma Aldrich, and used without further purification. Millipore water was used for sample preparation. Fine adjustment of pH was done by drop wise addition of diluted hydrochloric acid for lower pH range and 0.1 M sodium hydroxide solution for the higher pH range. pH of the solution was measured by using pH-1500 (Eutech Instruments) and it was further cross checked by silicon micro sensor pocket sized pH meter (ISFETCOM Co. Ltd., Japan).

2b. Methods:

In this section we have provided detailed description of experimental and theoretical methods used for various experiments done in this thesis.

2b.1. Absorption Measurements:

The absorbance experiments are more trivial and common hence we are not providing the instrumental setup here. Briefly, All the absorption measurements were recorded on a double beam, ultraviolet-visible (UV-Vis) spectrophotometer (Shimadzu-2450). In all experimental conditions chromophore concentrations were kept very low (5 µM - 10 µM) to avoid molecular aggregations and any other artifacts. Path length of the cuvette was kept fixed at 1cm for all the measurements. Moreover, all the absorption measurements were carried out at room temperature (25 ºC) unless otherwise specified.

2b.2. Steady State Fluorescence Measurements:

Steady state fluorescence spectra, quantum yield measurements and resonance light scattering spectra were carried out on a Jobin Yvon Fluoromax-4 spectrofluorimeter. The schematic diagram of spectrofluorometer is shown in **Figure 2b.1**. The excitation source was a Xe-lamp (power 150 Watt), which emits a continuous emission from ~250 nm to ~800 nm. Monochromator (MC1) is used to select a particular excitation wavelength. Fluorescence is collected at right angle to the incident light beam to avoid transmitted light coming from the light source and detected through a monochromator (MC2) and a photomultiplier tube (PMT).[3, 4] PMT is the detection device which works based on principle of photoelectric current generation. When a photon emitted from sample falls over metal array kept in vacuum and high voltage (950 V), it immediately generates electrons. The flow of electron along the voltage bias generates the signal. This method minimizes the inherent background noise (dark count ~1000 counts/sec) in detector (compared to traditional voltage detection module) and results much sensitive detection. Polarizers (P1 and P2) on both excitation and emission sides are used to filter the light for specific polarized light which will be used to calculate anisotropy. Monochromators (MC1 and MC2) and polarizers (P1 and P2) controlling the direction and wavelengths of excitation and emission light are automated and computer controlled.

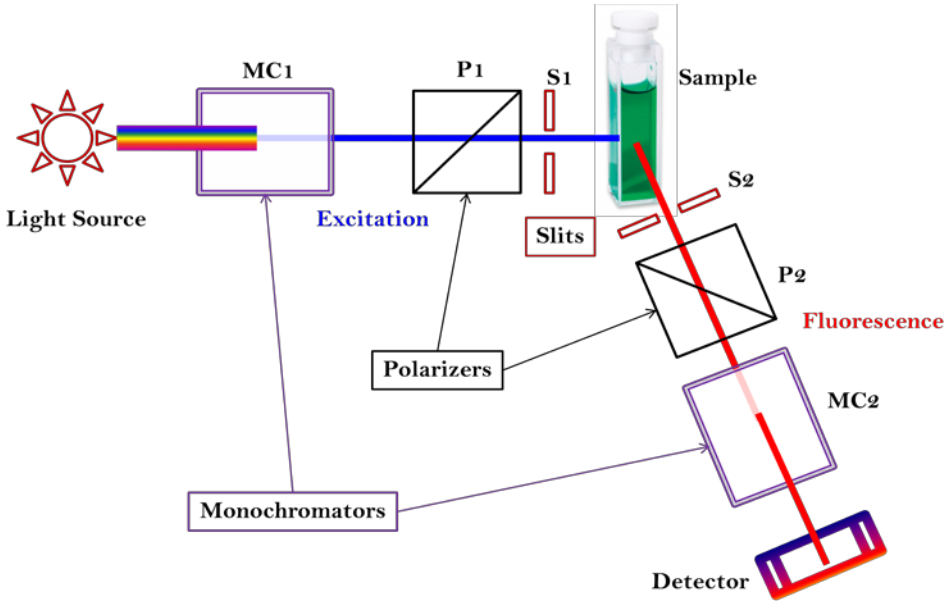

Figure 2b.1. Schematic diagram of fluorescence spectrophotometer

2b.3. Time Resolved Fluorescence Measurements:

2b.3a. Time Correlated Single Photon Counting (TCSPC) Technique:

Time-correlated single photon counting (TCSPC) is the most popular technique for the determination of fluorescence lifetime (or decay parameters). The basic principle of TCSPC is the probability of detecting a single photon at time t after an exciting pulse is proportional directly to the fluorescence intensity at that time.[1,2] **Figure 2b.2** shows the schematic outline of a conventional single-photon counting instrument set-up. The excitation source can be a flash lamp, nano-LED or a mode-locked laser. An electrical pulse associated with optical pulse is generated and it excites the sample. This pulse also sends a signal to another electronics constant fraction discriminator (CFD) through synchronizer (SYNC) (it synchronizes the optical and electrical pulses). Then, CFD accurately records the arrival time of the photons. After passing through CFD, the excitation pulse reaches to TAC (time to amplitude converter) and immediately starts charging the capacitor inside TAC. Charging of the TAC capacitor generates a voltage ramp. TCSPC instrument is set in such a way that after the excitation only one stop photon from the sample is detected for every 100-200 excitations. An emission photon resulting from the sample excitation meanwhile reaches to TAC and stops the charging of TAC capacitor. TAC is the main component of the TCSPC system. It acts as a stopwatch and measures the time

gap between the start (excitation) and stop (fluorescence) pulses. The amplitude of this pulse is proportional to the charge in the capacitor, and hence to the time difference between the start and stop pulses. The TAC output pulse is given a numerical value within the analog-to-digital converter (ADC) and a count is stored in the data storage corresponding to that number. This process is repeated several times to generate a histogram corresponding to the lifetime decay of the sample. The so called decay result from TCSPC instrument can be either deconvoluted considering the effect of the pulse or can be analyzed by graph plotting software by neglecting the effect of the excitation pulse.

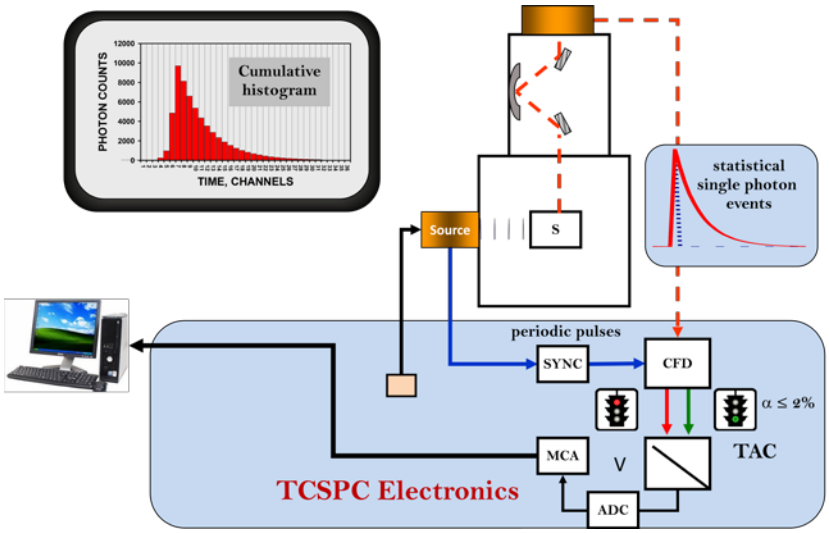

Figure 2b.2. Schematic diagram of TCSPC technique

It is pertinent to mention that the our TCSPC instrument runs in the reverse mode i.e. emission photon resulting from the sample excitation acts as starts pulse for the TAC and an excitation pulse resulting from the laser/LED acts as stop pulse. The reason for such reverse orientation is a high repetition rate of excitation LEDs. When TCSPC operates in forward mode due to a high repetition rate of the excitation lasers and LEDs, start pulse reaches prior to reset time of the electronics. To overcome such problem from the electronic response time, modern days TCSPC set up operate in reverse mode. We have used majorly two LEDs for sample excitation, namely, 375 nm (FWHM < 100 ps) and 402 nm (FWHM < 100 ps). Instrument response of our TCSPC set-up using the above mentioned diode lasers is ~100 ps, and with the

help of deconvolution method (discussed next section) we could able to detect the lifetime of ~40 ps. The detector used in this TCSPC set-up is micro-channel plate PMT (MCP-PMT). In comparison to simple dynode chains in PMT, MCP-PMT consists of numerous small holes. The holes in these plates are micro-channels, and the generated photoelectrons are proximity focused into the MCP. As here electrons travel short distances, this type of PMT shows fastest time response compare to conventional PMT, and is used in most of the time-resolved measurements.

2b.3a.1. Analysis of Fluorescence Decays:

The measured decay function is a convolution of the measured instrumental prompt response *P*(t) and the theoretical fluorescence response function *F*(t), the net result (*R*(t)) obtained for δ function excitation will be;[1-3]

$$R(t) = \int_0^t P(t') \times F(t - t') dt' \qquad (2b.1)$$

Where, *t*′ is the variable time delays (in practice, channel numbers) of the infinitesimally small widths dt′ (i.e, channel widths) of which *P*(t′) is composed. By measuring *P*(t) experimentally over '*i*' channels of data, the convoluted form of *R*(t) can be obtained from equation 2b.1. Here one has to assume a functional form of *F*(t), for example one, two or three exponentials. By iterating the values of the decay components until good agreement is obtained, the best fit values are determined.

$$F(t) = \sum_i a_i e^{-t/\tau_i} \qquad (2b.2)$$

The standard statistical procedure to confirm goodness of fit is by χ^2 test. The χ^2 is given by;

$$\chi^2 = \sum_{i=1}^{n} \omega_i [R(t) - R_c(t)]^2 \qquad (2b.3)$$

where, R_c(t) is calculated by assuming functional form of *F*(t) and $\omega_i = 1/R(t)$. The χ^2 value ~1 indicates good fit.

The analysis of fluorescence decays were performed using the commercially available global lifetime analysis software (DAS6) of IBH (UK). Error in all lifetime measurements is ~10%.

2b.3b. Time Resolved Fluorescence Anisotropy Measurements:

During anisotropy measurement, the sample is excited with a polarized light pulses and the time dependent parallel [$I_{\parallel}$(t)] and perpendicular [$I_{\perp}$(t)] components of the fluorescence are used to calculate the time-resolved fluorescence anisotropy, r(t), by following equation;[1,2]

$$r(t) = \frac{I_{\parallel_{\parallel}}(t) - I_{\perp}(t)}{I_{\parallel_{\parallel}}(t) + 2I_{\perp}(t)} \qquad (2b.4)$$

To compensate the polarization biased of the detection system and monochromator efficiency, the above equation is modified to;

$$r(t) = \frac{I_{\square}(t) - GI_{\perp}(t)}{I_{\square}(t) + 2GI_{\perp}(t)} \qquad (2b.5)$$

where, G is the instrumental correction factor introduced for the polarization sensitivity of the detection system and monochromator.

The time-resolved anisotropy measurements were done by automated toggling method using time-correlated single photon counting set-up and exciting the sample by different diode lasers (375 nm (IBH, UK, Nano LED, FWHM ~100 ps) and 405 nm (IBH, UK, FWHM ~100 ps)) for different systems. In toggling method, a movable polarizer was used in the emission side, whereas the excitation polarizer was kept fixed at vertical position. This polarizer rotates between parallel and perpendicular orientations and the emission intensities at parallel [$I_{\parallel}$(t)] and perpendicular [$I_{\perp}$(t)] polarization were collected alternatively for 60 seconds until a certain peak difference between parallel [$I_{\parallel}$(t)] and perpendicular [$I_{\perp}$(t)] decay is reached. For typical anisotropy decay the difference between the peak counts at parallel and perpendicular polarization were kept at 5000. The G factor was measured by taking two additional decay measurements [I_{HV}(t) and I_{HH}(t)] of the same sample with the excitation polarizer toggling

between perpendicular or horizontal positions. Value of G factor is given by, G = $I_{HV}(t)/I_{HH}(t)$, where $I_{HV}(t)$ and $I_{HH}(t)$ denotes the fluorescence decay profiles of the sample measured using horizontally or perpendicularly (H) polarized excitation light and detecting the emission components polarized vertically (V) and horizontally (H), respectively. For a simple isotropic rotor, $r(t)$ decays with a single rotational correlation time[1,2] (τ_r) represented by the following equation;

$$r(t) = r_0 exp^{-(\frac{t}{\tau_r})} \qquad (2b.6)$$

For more complicated systems, $r(t)$ takes the form of a sum of exponentials;

$$r(t) = r_0 \sum \beta_i \, exp^{-(\frac{t}{\tau_{ri}})} \qquad (2b.7)$$

where, β and τ_{ri} are the fractional contribution of total depolarization and rotational correlation times of the ith component, respectively. r_0 represents the fundamental anisotropy.

2b.3c. Femtosecond Time Resolved Fluorescence Upconversion:

Fluorescence decays of few fluorophores occur within tens of picosecond, which appears impossible to be resolved by TCSPC set-up. In such cases, we have used the femtosecond fluorescence up-conversion set-up to unravel the fast dynamics taking place within ~ 10 picoseconds or even lesser time-scale. Here a tunable Mai Tai HP (Spectra Physics, USA) is used as excitation source. Mai-Tai laser provides beams with <100 fs pulse width, and therefore, helps to resolve lifetime components of picoseconds to sub picoseconds time-scale. The high tunability (690-1040 nm) of Mai-Tai oscillator is also appropriate to excite different kinds of samples. Furthermore, high quality, stable, horizontally polarized (>500:1 horizontal), Gaussian pulses (TEM_{00}, M^2<1.1) with stable power (>2.5 W) and very high peak power (>300 kW) offers minimum fluctuation of the laser pulse. Mai Tai uses the output from the high power fiber coupled diode laser module(s) to end-pump Nd^{+3} ion doped Yttrium Vanadate crystalline matrix ($Nd:YVO_4$). The triply ionized neodymium act as an active medium for this four-level solid state pump laser, which has principle absorption bands in the red and near infra-red region. While

excited with a diode laser, the strongest lasing form Nd:YVO_4 results in a wavelength ~1064 nm. The resulting 1064 nm emission is converted to a visible wavelength (532 nm) via frequency doubling (also known as second harmonic generation or SHG) in a nonlinear crystal. Lithium triborate (LBO) nonlinear crystal is used as a frequency doubling (or SHG) medium inside Mai-Tai one box oscillator. A dichroic output coupler allows the 532 nm light to exit from the pump cavity, and it reflects the 1064 nm light back to the cavity. This 532 nm continues wave (CW) from a frequency doubled output of the Nd:YVO_4 pump laser is used to pump Ti-Sapphire laser, which in turn produces the Mai Tai output. Ti-Sapphire is a crystalline material produced by doping Ti_2O_3 into a melt of Sapphire (Al_2O_3). The Ti^{+3} ion is responsible for the lasing action of Ti-Sapphire. Although the fluorescence band of Ti^{+3} extends from wavelengths as short as 600 nm to wavelength greater than 1000 nm, the lasing action is possible at greater than 670 nm (most strong emission band ~795 nm). Mai Tai uses an acousto-optic modulator (AOM) (constitutes a high quality optical material like quartz) to ensure the mode locked output from Ti-Sapphire. The Mai Tai reliability is maintained using the ultra-stable regenerative modelocking technique proven with the Spectra-Physics Tsunami® oscillator. A schematic diagram of a femtosecond up-conversion system is shown in Figure 2b.3. The sample (Bipyridine diol) was excited at 380 nm using the second harmonic of a mode-locked Ti-sapphire laser (Mai-Tai, Spectra Physics). The emitted fluorescence from sample was up-converted in another nonlinear crystal using the gated pulse of the fundamental beam (**Figure 2b.3**). The sum frequency of fluorescence and the gate pulse was detected as a function of the time delay between excitation and gate pulses. The angle between the polarization of the pump and gate pulses was kept at magic angle (54.7^o) to eliminate effects from rotational diffusion. The up-converted signal is dispersed into a monochromator and detected using photon counting electronics. A cross-correlation function obtained using the Raman scattering from ethanol displayed a full-width at half-maximum (FWHM) of ~350 fs. Error in all the up-conversion measurements is ~10%. The data was analyzed using Igor software using cross correlation function obtained from Raman scattering. During data fitting, the long component appeared decay profile is usually guessed from the average lifetime value obtained from the TCSPC setup.

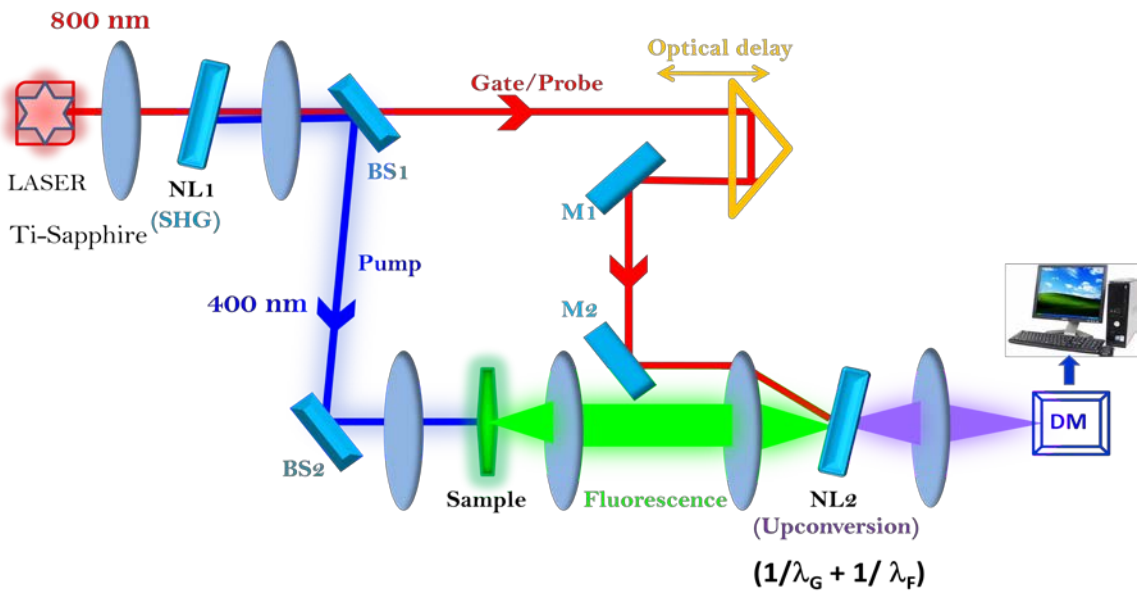

Figure 2b.3. Schematic diagram of femtosecond fluorescence upconversion technique

2b.4. Circular Dichroism (CD):

Asymmetric chromophores or symmetric chromophores in asymmetric environments interact in different ways with right- and left-circularly polarized light ensuing two related phenomena.[4-6] Circularly-polarized light travels through an optically active medium with diverse velocities due to the different refraction indices for right- and left-circularly polarized light called optical rotation or circular birefringence. The deviation of optical rotation as a function of wavelength is called optical rotary dispersion (ORD). Right- and left-circularly polarized light is absorbed to various extents at any particular wavelengths due to differences in extinction coefficients for the two polarized light rays called circular dichroism (CD). ORD enables any chiral molecule to rotate the plane of incident polarized light. ORD spectra are dispersive (called a Cotton effect[4-6] for a single band) whereas CD spectra are absorptive. The two phenomena are connected by the so-called Kramers–Kronig transformation. All CD spectra were recorded on a JASCO-800 automatic recording circular dichroism spectrophotometer. Quartz cuvette with 1.0 cm path length was used for CD measurements. CD spectra were accumulated at 25ºC at a scan rate of 100 nm/min. A fixed concentration of macromolecules (DNA) was titrated with increasing concentration of ligand and/or host molecule. Final CD spectrum was corrected by taking the blank of the individual ligand/host concentrations and buffer solution.

2b.5. Computational Methods:

Chapter 3a: The computational study comprised of docking followed by semi-empirical quantum chemical calculation. The crystal structure of CB7 was obtained from Cambridge Structural Database (CSD).[7] Molecular docking study was performed by AutoDock 4.2 software package using Auto Dock Tools 1.5.4 (ADT).[8] Polar hydrogens and Kollman charges were added to the input files. The binding site on the macromolecule was defined using Auto Grid with 60 × 60 × 60 grid points and grid space of 0.375 Å. Lamarckian Genetic Algorithm (LGA) with local search was used as search method.[9] On the basis of LGA, total of 100 runs for each ligand were performed with population size of 150. Maximum number of energy evaluations and generations were set to 250000 and 27000, respectively. Docking analysis was performed using the cluster of root mean square deviation (rmsd) of 2.0 Å. During docking, the host (CB7) was kept rigid and the guest (CPT) was flexible. The docking results were analyzed and visualized using ADT. After 100 runs, the best conformer was ranked according to the docking energy and geometry matching. All the docked structures were fully optimized on MOPAC2012 software package[10] using PM6-DH2 method (solvent effect is included by using COSMO method and EPS=78.4 as keyword).

Chapter 3b: The computational study comprised of docking followed by semi-empirical quantum chemical (PM3MM) calculations. Initially, all the chemical structures (host and guest) were geometry optimized using density functional theory (DFT) using B3LYP functional with 3-21G basis set on gaussian09 software.[11] The molecular docking study was performed by means of the AutoDock 4.2 software package using Auto Dock Tools 1.5.4 (ADT). Polar hydrogen atoms and Kollman charges were added to the input files. The Lamarckian Genetic Algorithm (LGA) with a local search was used as a search method. Docking analysis was performed by using the cluster of a root-mean-square deviation (rmsd) of 2.0 Å. During docking, the host (CB7) was kept rigid and the guest (milrinone) was flexible. Here it is pertinent to mention that we have used cationic form of the drug during docking, as inside the nano-cavity of CB7 the cationic form generates. The docking results were analyzed and visualized by using ADT. After 100 runs, the best conformer was ranked according to the docking energy and geometry matching. The final docked structure was fully optimized on the gaussian09 software package using PM3MM method.

Chapter 4a: Initially, all the chemical structures (host and guest) were geometry optimized using density functional theory (DFT) using B3LYP functional with 3-21G basis set on Gaussian 09 software. TPT:CB7 inclusion complex was built by bringing both TPT (cationic form) and CB7 close together. Geometry optimization of TPT:CB7 inclusion complex was performed at semi-empirical PM3 level using Gaussian 09. Here it is pertinent to mention that since the geometry optimization was done without consideration of any solvent and other medium parameters, this model provides only a qualitative picture of the complex in the ground state.

Chapter 4b: Initially, all the chemical structures (host and guest) were geometry optimized using density functional theory (DFT) using B3LYP functional with 3-21G basis set on Gaussian 09 software. During docking, the receptor was kept rigid and the ligand was flexible. Finally, the inclusion complex obtained from docking studies is further optimized using DFT with B3LYP functional and 3-21G basis set on Gaussian 09 software.

Chapter 5a: Initially, all the chemical structures (host and guest) were geometry optimized using density functional theory (DFT) using B3LYP functional with 3-21G basis set on Gaussian 09 software. The docking has been performed using AutoDock (4.2) software. Following the experimental findings, we have taken protonated form of EPT for all the docking studies, except in the case of γ-CD, in which neutral form of the drug has also been considered during docking study. In case of γ-CD we have docked EPT (protonated form) and γ-CD to get 1:1 (γ-CD:EPT) inclusion complex. In order to get 2:1 (γ-CD:EPT) inclusion complex, we have docked 1:1 (γ-CD:EPT) inclusion complex with neutral EPT to another γ-CD. Finally, all the inclusion complexes obtained from docking studies are further optimized using Gaussian 09 software at PM3MM level.

2c. References:

1. J. R. Lakowicz, *Principles of fluorescence spectroscopy.* Springer Verlay, 2007.
2. B. Valeur, *Molecular fluorescence: principles and applications.* Wiley-VCH, 2002.
3. Fleming, G.R. *Chemical applications of ultrafast spectroscopy.* Oxford University Press, New York, 1986.
4. N. Berova, K. Nakanishi & R. Woody, *Circular dichroism: Principles and applications.* John Wiley & Sons, 2000.
5. D. S. Rodgers, *Circular dichroism: Theory and spectroscopy.* Nova Science Publishers, 2012.
6. B. Nordén, A. Rodger & T. Dafforn, *Linear dichroism and circular dichroism: A textbook on polarized-light spectroscopy.* Royal Society of Chemistry, 2010.
7. F. Allen, *ActaCrystallogr. Sect. B* 2002, **58**,380.
8. G. M. Morris, R. Huey, W. Lindstrom, M. F. Sanner, R. K. Belew, D. S. Good-sell, A. J. Olson, *J. Comput. Chem.* 2009, **30**, 2785.
9. G. M. Morris, D. S. Goodsell, R. S. Halliday, R. Huey, W. E. Hart, R. K. Belew, A. J. Olson, *J. Comput. Chem.* 1998, **19**, 1639.
10. J. J. P. Stewart, *MOPAC2012*, *Stewart Computational Chemistry*, Colorado Springs, CO, USA, 2012.
11. M. J. Frisch, G. W. Trucks, H. B. Schlegel, G. E. Scuseria, M. A. Robb, J. R. Cheeseman, J. A. J. Montgomery, T. Vreven, K. N. Kudin, J. C. Burant, J. M. Millam, S. S. Iyengar, Tomasi, J., Barone, V., Mennucci, B., Cossi, M., Scalmani, G., Rega, N., Petersson,, N. G. A., H., Hada, M., Ehara, M., Toyota, K., Fukuda, R., Hasegawa, J., Ishida, M.,, T. Nakajima, Honda, Y., Kitao, O., Nakai, H., Klene, M., Li, X., Knox, J. E., Hratchian,, C. H. P., J. B., Bakken, V., Adamo, C., Jaramillo, J., Gomperts, R., Stratmann, R. E.,, O. Yazyev, Austin, A. J., Cammi, R., Pomelli, C., Ochterski, J.W., Ayala, P. Y.,Morokuma,, V. K., G. A., Salvador, P., Dannenberg, J. J., Zakrzewski, V. G., Dapprich, S., Daniels,, S. A. D., M. C., Farkas, O., Malick, D. K., Rabuck, A. D., Raghavachari, K., Foresman,, O. J. B., J. V., Cui, Q., Baboul, A. G., Clifford, S., Cioslowski, J., Stefanov, B. B., Liu,, L. G., A., Piskorz, P., Komaromi, I., Martin, R. L., Fox, D. J., Keith, T., Al-Laham,, P. M. A., C. Y., Nanayakkara, A., Challacombe, M., Gill, P. M. W., Johnson, B., Chen, and W. W., M. W., Gonzalez, C., Pople, J. A., *Gaussian Inc.*, 2004, **Revision C.02.**

Chapter 3

Modulation of Excited State Photophysics and pKa Shifts of Fluorescent Molecules inside the Nano-cavities of Molecular Containers

"In this chapter we explain the excited state photophysics of important drugs, one is anticancer drug camptothecin and a cardiotonic drug milrinone inside the molecular containers. A profound pK_a shift was found inside the nanocavities of cucurbituril. A detailed spectroscopic and theoretical investigation is done to unravel the reasons for the modulation of above mentioned two drugs. This chapter is divided in to two sections, one is devoted for understanding the photophysics of camptothecon and second section deals with the cardiotonic drug, milrinone. Both the sections are discussed one by one as follows."

3a. Modulation of Photophysics and pK_a Shift of an Anticancer Drug, Camptothecin, inside the Nanocavities of Supramolecular Hosts

3a.1. Introduction and Motivation of the Work:

20(S)-camptothecin (CPT), an anticancer drug, was first discovered by Wall *et al.* in 1966 from a Chinese tree known as *Camptotheca acuminate*.[1] It is a potent inhibitor of the growth of Leukemia cell by an unique mechanism: inhibition of DNA topoisomerase I[2,3] an enzyme responsible for DNA replication. CPT consists of five rings (**Scheme 3a.1**), of which A/B parts of CPT constitute the quinoline ring system, and pyridone D ring exerts electron withdrawing effect on quinoline ring. This reduces the pK_a value of quinoline from 4.87 to 1.18 for CPT.[4] CPT is weakly soluble in water, and known to undergo hydrolysis in aqueous medium even at physiological pH.[5] It exists in two forms in aqueous medium: one is biologically active lactone form which dominates at pH<5,[6] whereas carboxylate form dominating at pH>9 exhibits low activity against topoisomerase I.[6]

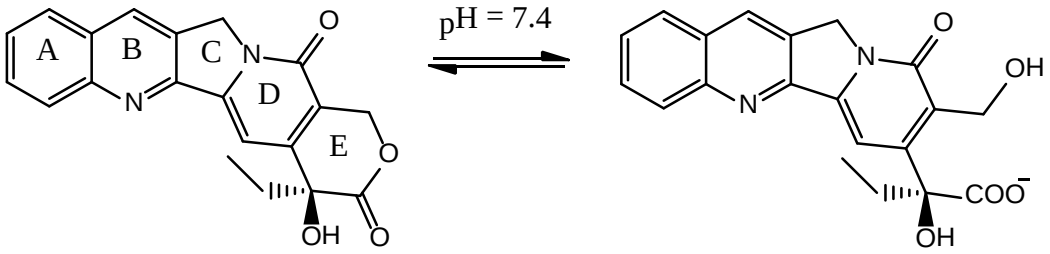

Scheme 3a.1. Chemical structure of CPT and its hydrolysis from lactone to carboxylate form.

In human plasma, the carboxylate form becomes the principal species which shows strong affinity to the human serum albumin.[7] Therefore, the main challenge of using CPT and its derivatives as anticancer drugs is the inhibition of their hydrolysis rate from active lactone to inactive and toxic carboxylate form. In continuation of this effort, several researchers found that binding of CPT to lipid bilayer,[8] liposome[9] and DNA[10] leads to the stabilization of the lactone form of the drug.

It has been already well established that macrocyclic host molecules have the ability to encase drugs, and act as drug carriers, drug solubilizers, and drug stabilizers. Therefore, hydrolysis of CPT may be prevented by encapsulating the drug inside the nano-cavity of macrocyclic host molecule, and thereby protecting the accessibility of solvent towards the drug. Dong *et al.* studied the complex formation between CPT and cucurbituril by using different spectroscopic techniques.[11,12] Although they have shown that the stability of the lactone form is increased in presence of cucurbituril, they haven't focused on the modulation of CPT photophysics upon encapsulation in CB7 cavity. Moreover, the dynamics aspect, which provides deep insight about the complex formation process, has not been addressed in their study. So, herein the present chapter we have extensively studied the interaction behaviour between CPT and CB7 with the help of steady state, time-resolved fluorescence techniques. Interestingly, the steady state fluorescence results resemble to that of pH dependent study of CPT reported by Douhal *et al.*[4] We have got enough evidence for the formation of protonated CPT molecule in presence of CB7 as a result of pK_a shift of quinoline nitrogen of CPT. However, in presence of β-CD, which has similar cavity size as that of CB7, CPT does not show any pK_a shift upon encapsulation by β-CD. Finally, the docking as well semi-empirical quantum chemical calculations have been employed to decipher the molecular pictures of the interactions between CPT and CB7. We believe that these results might provide a boost for using CPT as a potential antitumor drug with the help of CB7 as an efficient drug carrier.

3a.2. Results and Discussion:

3a.2a. Steady State Measurements:

Figure 3a.1 depicts the UV-visible absorption spectra of CPT in water (pH 6.2) and in presence of increasing concentration of CB7. The absorption spectrum of CPT in water consists of two bands at 355 nm and 369 nm corresponds to π-π^* character of ^1L_b transition.[13, 14] Although $^1\pi,\pi^*$ is the lowest excited singlet state in CPT, a small contribution from close lying $^1n,\pi^*$ state is also evident.[13, 14] Significant spectral changes were observed when macrocyclic host CB7 was added to the CPT (~8 μM) solution. On gradual addition of CB7, the absorbance bands at 355 nm and 369 nm gradually diminish and totally disappear at ~500 μM of host concentration, and the absorption peak retracts to ~410 nm along with another small peak around ~300 nm (**Figure**

3a.1). Astonishingly, these absorption spectral characteristics of CPT in presence of CB7 closely resembles to the pH dependent study recently reported by Douhal *et al*.[4] In their study, a long wavelength band appeared at 401 nm in very acidic solution (pH < 2.0), and it was attributed to the protonation of quinoline N atom in CPT.[4] Hence, the appearance of a new peak at 410 nm infers the formation of ground state protonated CPT in presence of CB7. The specific hydrogen bond interactions with CB7 leads to ~10 nm red shift in the absorption spectra of protonated CPT. The appearance of two isosbestic points at 310 nm and 377 nm (up to 500 μM concentration) indicates the presence of equilibrium between free CPT (either protonated or neutral) to CPT-CB7 complex, and there exists two different types of complexation equilibria in the presence of CB7. The disappearance of vibronic structure of CPT might be outcome of specific hydrogen bond interactions between protonated CPT and CB7. The appearance of new peak at 310 nm in presence of host might be attributed to the ^1L_a transition of protonated CPT, whereas 410 nm peak is attributed to the ^1L_b transition of protonated CPT. These noteworthy changes in absorption features infer a significant perturbation of electronic distributions of CPT on encapsulation into the CB7 cavity. CB7 induced changes in the absorption profiles of CPT were also substantiated by emission measurements. As shown in **Figure 3a.1b**, the emission spectrum of CPT in aqueous solution (pH 6.2) exhibits a maximum at 436 nm**,** when the excitation wavelength is at 377 nm (isosbestic point in **Figure 3a.1a**). By gradual addition of CB7, the emission peak intensity at 436 nm reduces down, and a new red shifted peak at ~500 nm developed progressively with further addition of CB7 (**Figure 3a.1b**). At highest concentration of host (~1 mM), the former peak totally vanishes and a sole peak appears at 512 nm. Moreover, like absorption spectra, two isoemissive points are observed in the emission profiles. One isoemissive point at 502 nm exists only at lower host concentration (≤50 μM), whereas another isoemissive point prevails at 490 nm after 50 μM of host concentration (**Figure 3a.1b**). The presence of isoemissive points in two different concentration regimes implies the existence of two different stoichiometric complexation equilibria in the system. These substantial changes in emission profiles (**Figure 3a.1b**) confirm that the strong interaction is going on between CPT and CB7. Astonishingly, the net effect of CB7 on emission spectral profiles of CPT closely resembles to that of changes observed during the pH dependent study of CPT by Douhal *et al.*[4]; where they observed a new peak appeared at 530 nm at the cost of 436 nm as pH of the medium decreases, and the latter peak completely disappears at very low pH (pH =0.9).[4]

The estimated excited state pK_a of quinoline nitrogen of CPT from fluorescence spectra was found to be 1.85; hence, 530 nm peak observed in lower pH range (<pH 2) was attributed to the cationic CPT, where quinoline nitrogen gets protonated.[4] On the other hand, 436 nm peak, which exist in between pH 6-3, was assigned to be due to the excited neutral form of CPT. In analogy to the pH dependent study, newly observed peak at ≥500 nm of CPT after a certain concentration of CB7 (50 μM) is likely to be the protonated form of CPT. However, the protonation of quinoline nitrogen is difficult at pH 6.2, as pK_a for the protonation of quinoline nitrogen is ~1.8. Hence, the appearance of a new peak at 512 nm in presence of CB7 indicates that encapsulation by CB7 enhances proton affinity of quinoline nitrogen of CPT.

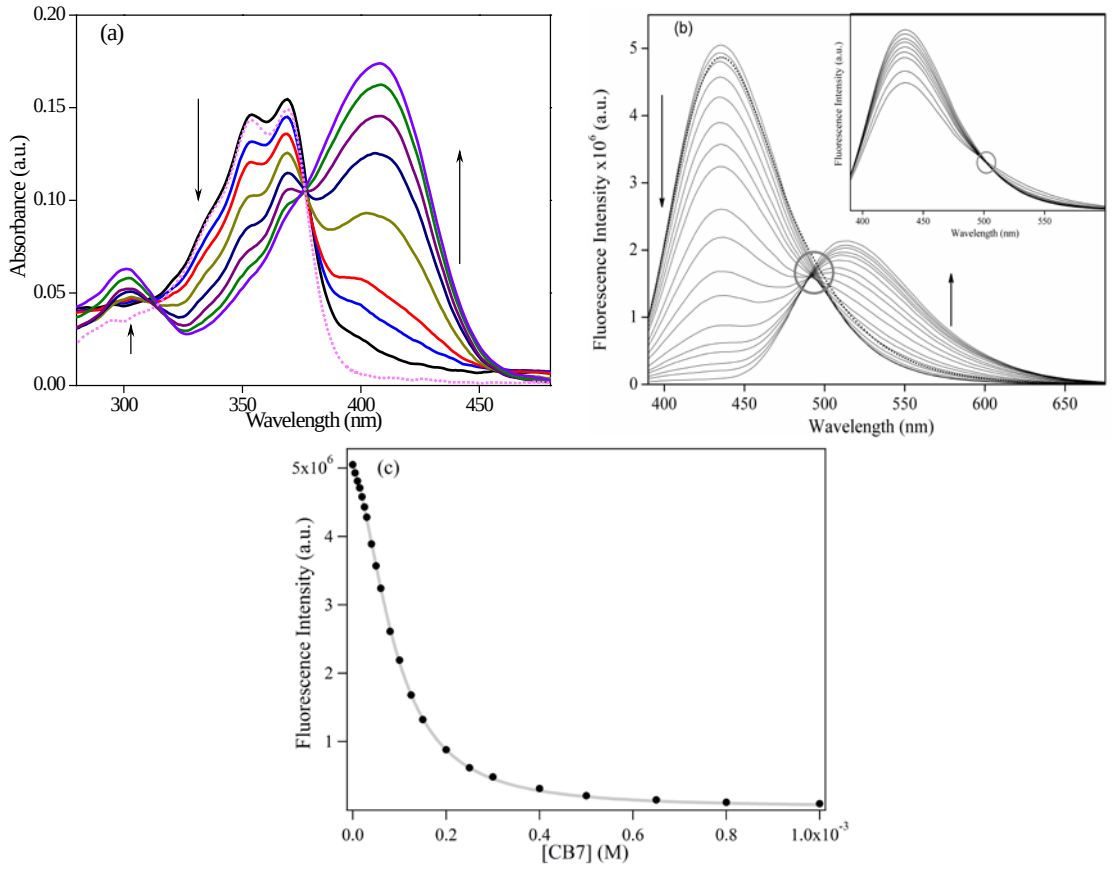

Figure 3a.1. (a) Absorption and (b) emission spectra (λ_{ex} = 377 nm) of CPT (8 μM) in presence of CB7 (0-1 mM) and with 1 M NaCl (dotted line) as an external stimulus. (c) The changes in the fluorescence intensity monitored at 436 nm were plotted against concentration of CB7. The solid line represents the best fitted line as per equation 3.

For further clarification of CPT protonation, we have collected the emission profiles exciting at 405 nm, which is responsible for the absorption of protonated CPT[4] (**Figure 3a.2**).

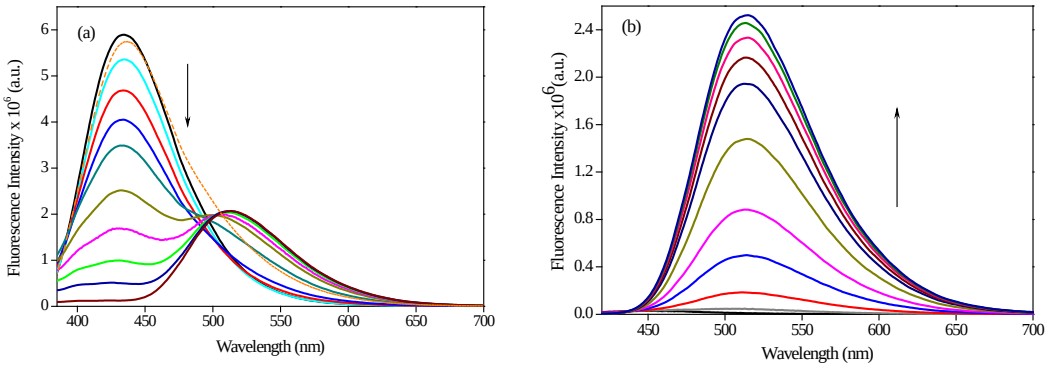

Figure 3a.2. Emission spectra of CPT (8 μM) exciting at (a) 370 nm, and (b) 405 nm, in presence of CB7 (0-1 mM) and with 1 M NaCl (dotted line) as an external stimulus.

Here, we have noticed that the peak at 436 nm in water has negligible fluorescence**,** as neutral CPT molecules have very minute absorption at 405 nm, and the 436 nm peak is totally absent in presence of CB7. However, a clear emission peak at ~512 nm starts appearing ~30 μM of CB7 concentration, and then the peak position remains same, but intensity increases tremendously with further addition of CB7. It is also noticeable that the peak at ~512 nm appears >50 μM of host concentration when the excitation wavelength is 377 nm, however, the 512 nm peak appears at 30 μM host concentration when the excitation wavelength is 405 nm. This is because when the excitation wavelength is at 377 nm, then we are exciting both neutral as well as protonated CPT molecules as both the species absorb at this isosbestic point. On the other hand when the excitation wavelength is at 405 nm (**Figure 3a.2**), only protonated CPT molecules are selectively getting excited. Therefore, even minute population of protonated CPT is detected at lower host concentration (~30 μM). Here it is pertinent to mention that when we monitor the emission spectra exciting at 370 nm (absorption peak maximum of neutral CPT) and 405 nm (absorption maximum of protonated CPT), the emission profiles devoid of isoemissive point (**Figure 3a.2**), because of the selective excitation of one kind of species (either neutral or protonated).

Fluorescence contour mapping is a very promising tool for the identification and characterization of fluorescent species, and the determination of several components in a complex system. Therefore, contour plots of CPT have been collected to get insight into the newly formed species in presence of CB7 (**Figure 3a.3**).

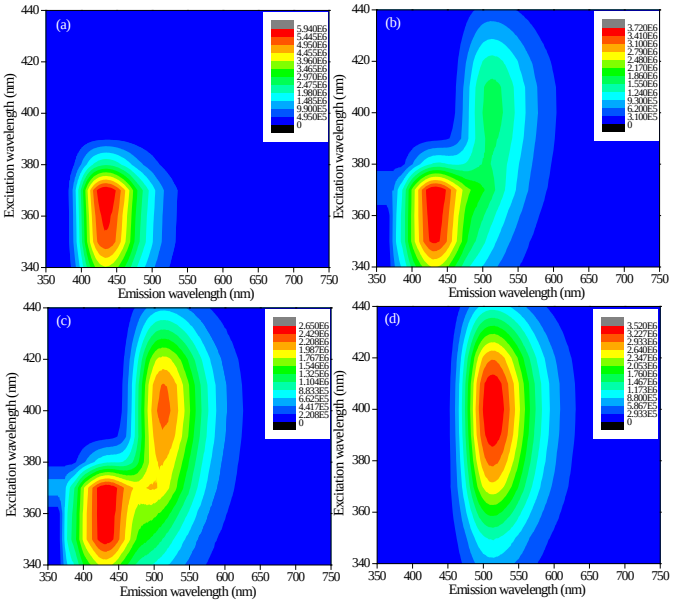

Figure 3a.3. Contour plots of CPT (8 μM) in absence (a), and presence of 70 μM (b), 200 μM (c) and 1 mM (d) of CB7.

As it is seen from the **Figure 3a.3**, the emission spectrum of CPT in waterconsists of a peak at 435 nm, and it is devoid of any peak around ~512 nm. However, the peak at ≥500 nm starts appearing at ~30 μM of CB7 concentration when the excitation wavelength is around 400 nm. As the concentration of host is hiked, the intensity at ~512 nm is getting intensified at the cost of 436 nm peak, and the 512 nm peak becomes the sole peak at very high concentration of CB7 (**Figure 3a.3**). These contour plots support our conjecture that 512 nm peak in presence of CB7 corresponds to a newly formed species, which is generated by the host assisted protonation of CPT.

The authenticity of the peaks at 436 nm and 512 nm, which are assigned for the neutral and protonated CPT, respectively, was also validated through the excitation spectrum monitored at 436 nm and 512 nm (**Figure 3a.4**). It is observed that when we monitored at 436 nm, then the excitation spectra devoid of peak at 410 nm, which the responsible for the cationic CPT, and the feature exactly resembles to that absorption spectrum of neutral CPT molecules. However, the excitation spectra monitored at 512 nm consist of 410 nm peak, and the peak at 410 nm becomes the sole peak at higher CB7 concentration. In a nutshell, the excitation spectra of CPT in presence of CB7 also confirm that 512 nm peak arises due to the protonation of CPT assisted by CB7.

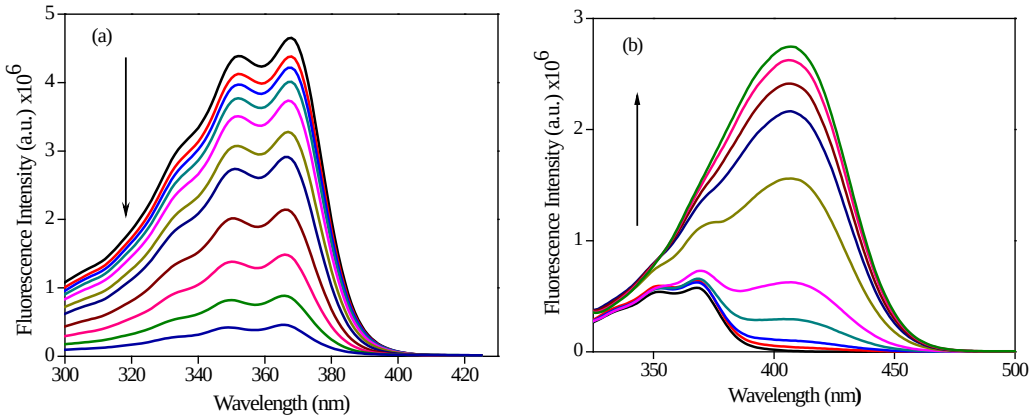

Figure 3a.4. Excitation spectra of CPT (8 μM), monitored at 435 nm (a) and 515 nm (b) in absence and presence of increasing concentration of CB7.

The presence of two isoemissive points in two different concentration regimes implies the existence of following step wise stoichiometric equilibia in the system.

$$CB7 + CPT \rightleftharpoons CB7{:}CPT \qquad (3a.1)$$

$$CB7{:}CPT + CB7 \rightleftharpoons CB7{:}CPTH^{+}{:}CB7 \qquad (3a.2)$$

The first equilibrium exists at lower concentration of host (≤50 uM), and responsible for exhibiting an isoemissive point at 502 nm; whereas the second equilibrium prevails at higher concentration of host, and accounable for the existence of iso-emissive point at 490 nm. The stoichiometry and association constants can be better understood from Benesi-Hildebrand (BH) plot[15]. The BH plot have been constructed considering the intensity changes at 435 nm, when λ_{ex} = 377 nm. The reason for monitoring intensity changes at 435 nm is that the intensity of 435 nm peak gradually diminishes as the host concentration increases, whereas 515 nm intensity almost remains constant after certain host concentration (>150 μM). The BH plot constructed in this way exhibits non-linear feature. However, double reciprocal plot is linear up to ~50 μM of CB7 concentration (**Figure 3a.5**), indicating stoichiometry is 1:1 up to ~50 μM of CB7. After 50 μM concentration, the plot deviates from linearity, and it indicates that the stoichiometry is more than 1:1 after that host concentration. It is also noticeable that the prominent protonated peak appears at 512 nm around ~50 μM host concentration (**Figure 3a.1b**). Therefore, we believe that the

protonation of CPT starts when two CB7 molecules partially encapsulate one CPT molecule. In order to fit all the data points, we have used following modified non-linear B-H equation[15].

$$I = \frac{I_0 + I_1 K_1 [CB7] + I_2 K_1 K_2 [CB7]^2}{1 + K_1 [CB7] + K_1 K_2 [CB7]^2} \qquad (3a.3)$$

Where I is the observed intensity at various host concentration, K_1 is the association constant for CB7:CPT, and K_2 is the association constant for CB7:CPTH$^+$:CB7. I_0, I_1 and I_2 denote the fluorescence intensities in pure water, 1:1 and 2:1 inclusion complexes, respectively. Using non-linear regression analysis, the estimated K_1 and K_2 are 2.8×10^3 (±100) and 3.4×10^4 (± 1890) M^{-1}, respectively (**Figure 3a.1c**). Here it is relevant to mention that initial guesses for I_1, I_2, K_1 and K_2 are considered from the double reciprocal B-H plots (**Figure 3a.5**).

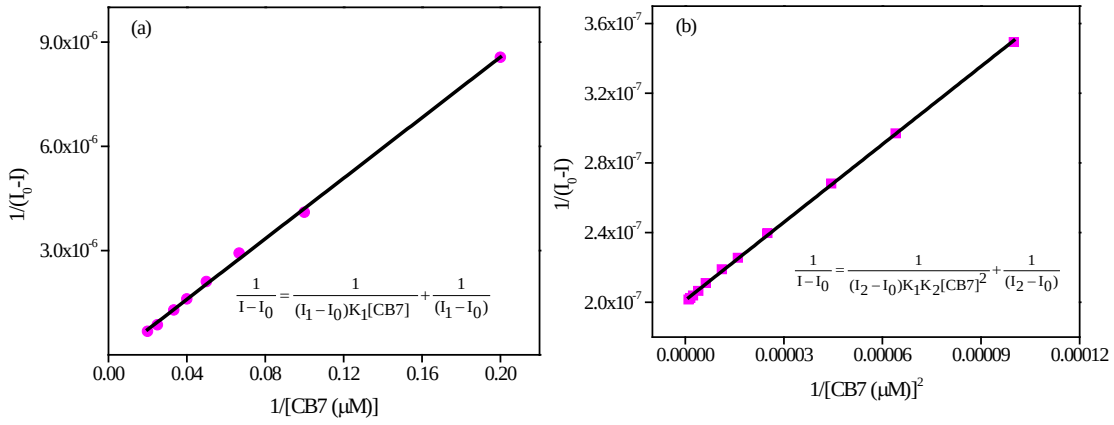

Figure 3a.5. (a) B-H plot for 1:1 (CB7:CPT) 2:1 inclusion complex using equation shown in the inset. (b) represents the B-H plot for 2:1 inclusion complex using equation shown in the inset. For both the cases intensity was monitored at 436 nm when λ_{ex}=377 nm.

Formation of 2:1 (CB7:CPT) complex has been further confirmed from Job's plot constructed by monitoring absorbance changes at 410 nm with continuous variation of mole fraction of CB7 (**Figure 3a.6**). The interaction free energies (ΔG^0) of drug in both 1:1 and 2:1 complexes are estimated to be -19.73 and -25.83 $kJ.mol^{-1}$, respectively. The higher negative free energy change for 2:1 inclusion complex implies that binding interaction between protonated

CPT is more favoured than the neutral one. This is reasonable as protonated CPT molecule in 2:1 complex is getting more stabilized by the electron rich carbonyl portals of CB7.

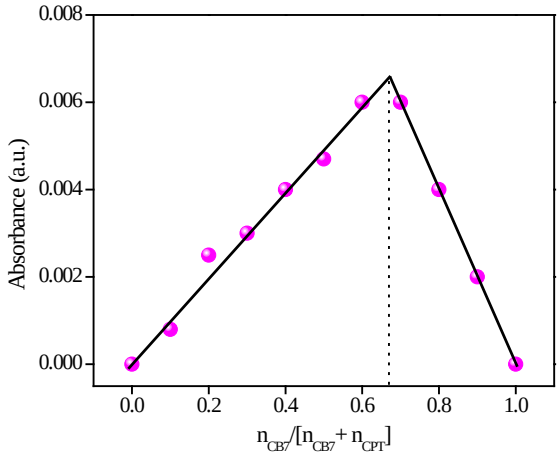

Figure 3a.6. Job's plot constructed monitoring the absorbance changes at 410 nm.

3a.2b. Effect of pK_a of CPT on the Formation of Inclusion Complex with CB7:

To get a quantitative idea about the pK_a shift, we have collected absorption as well as fluorescence profiles of CPT in the presence of 1 mM CB7 in dependence on pH. As it is shown in **Figure 3a.7**, the absorbance or fluorescence intensity is in saturation level below pH=5. However, after pH=5 the absorbance or fluorescence intensity drastically decreases, and after pH=6.5 the value almost remains constant. The point of inflexion of the sigmoidal plot has been determined by the derivative plot, and the ground state pK_a is estimated to be 6.2 from absorption spectra (**Figure 3a.7a**) and the excited state pK_a^* is estimated to be 6.8 from the fluorescence spectra (**Figure 3a.7b**). The ground and excited state pK_a of CPT in absence of CB7 are determined to be 1.2 and 1.6, respectively from absorption and fluorescence measurements, which are in close agreements with the reported ground state and excited state pK_a of CPT.[16] Therefore, we have observed almost 5 unit pK_a shift of CPT in the presence of CB7. Although the shifts of pK_a upon inclusion in cucurbituril cavity are documented in literature,[16-19] the pK_a shift of drugs inside CB7 cavity is rather limited.

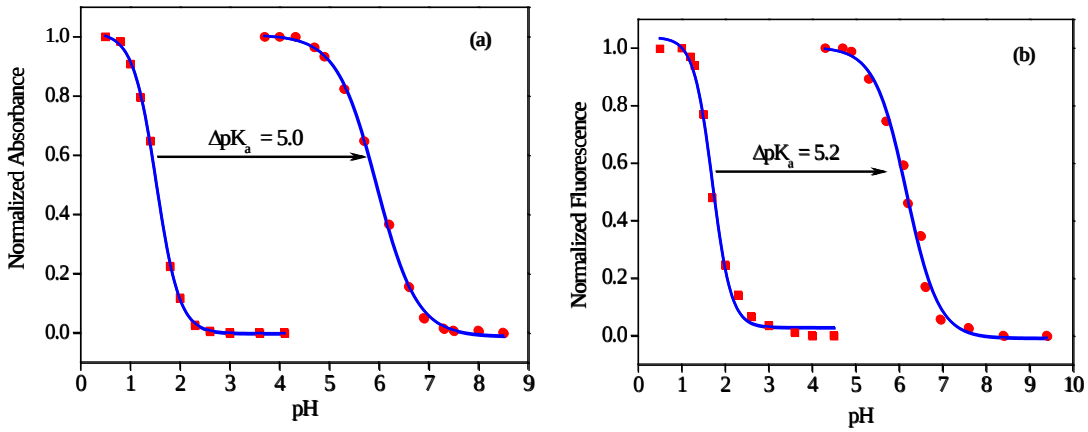

Figure 3a.7. pH titration of CPT (8 μM) in absence (filled square) and presence (filled circle) of 1mM of CB7 by (a) absorbance and (b) fluorescence measurements. The absorbance was collected at 405 nm and emission was collected at 515 nm.

Recently, Saleh *et al.* demonstrated how CB7 induced pK_a shift can be used to activate and stabilize proton pump inhibitor drugs, such as lansoprazole and omeprazole, which are being prescribed to cure diseases related to the secretion of gastric acid.[16] The histamine H2-receptor antagonist ranitidine shows a pK_a shift through encapsulation and is thereby stabilized.[20] Similarly, the local anaesthetics procaine, tetracaine, procainamide, dibucaine, and prilocaine also increase their pK_a values upon CB7 encapsulation.[21] This is the first report where an anti-cancer drug inside the CB7 cavity exhibits almost 5 units of pK_a shift. Although Dong *et al.* already shown that the stability of lactone form of CPT is increased in presence of CB7 or C8U due to the limited access of water towards the inclusion complex,[12] we believe that the pK_a shift of CPT by CB7 has some role on the stability of CPT inside the cavity of CB7.

3a.2c. Fluorescence Lifetime Measurements:

The modulation in the radiative properties of CPT on interaction with CB7 is also clarified by the fluorescence lifetime measurements at suitable solution conditions. It is observed from the **Table 3a.1** and **Figure 3a.8a** that the decay profile of CPT in water (pH = 6.2) monitored at 435 nm exhibits a single exponential decay consisting of fluorescence lifetime of almost 4.04 ns. Here it is pertinent to mention that lactone form of CPT has a lifetime of almost ~4.0 ns, whereas

carboxylate form has a longer lifetime of ~4.48ns.[22] Therefore, we believe the 4.04 ns fluorescence lifetime of CPT in water (at pH=6.2) reflects predominantly the lifetime of lactone form. In order to verify the percentage contribution of carboxylate form, the decay has been fitted with biexponential function by fixing the lifetime of carboxylate form of ~4.48 ns, and it was found that carboxylate form of CPT contributes only ~5% of the total decay. Hence, it is quite reasonable to assume that the lactone form of CPT is the dominating species at pH=6.2 in the stipulated period of our measurement. The addition of CB7 to the water containing CPT solution has almost negligible effect until 50 μM of host concentration (**Figure 3a.8a**). However, around 100 μM of CB7 concentration the decay cannot be fitted with single exponential, and it indicates another new species contributing to the profile (**Figure 3a.8a**, **Table 3a.1**). It is already observed from the steady state spectra that the protonation of CPT starts >50 μM of CB7 concentration. We anticipate the newly developed component appearing in the decay profile of CPT at ≥100 μM of host concentration (**Table 3a.1**) reflects the existence of protonated form of CPT. However, we do not have any clue about the fluorescence lifetime of protonated CPT, which generates when it is encapsulated in between two CB7 molecules. In order to get a clear perception about the lifetime of protonated CPT, we have collected the decay profile at 515 nm in presence of 1 mM of CB7 at λ_{ex}= 405 nm. This is because exciting at 405 nm, only the protonated CPT will be selectively excited. The selection of 1 mM CB7 based on the fact that at this concentration almost all CPT molecules will be encapsulated by two CB7 macrocycles, and thereby**,** CPT will exist predominantly as protonated one. The decay profile of CPT in presence of 1 mM CB7 concentration monitored at 515 nm can be fitted with single exponential function, and the estimated lifetime is to be 5.56 ns, which is the lifetime of protonated CPT molecule encapsulated by two CB7 molecules. So, from 100 μM onwards we have fitted all the data by bi-exponential function keeping one component fixed at 5.56 ns. It is clearly seen from the **Table 3a.1a** that contribution of 5.56 ns component increases as the concentration of CB7 is hiked, and at the same time lifetime of neutral CPT molecule progressively decreases. The reduced fluorescence lifetime of CPT in presence of CB7 might be attributed to the neutral CPT molecules, those are encapsulated by CB7. Although it is clear from steady state spectra that encapsulation by CB7 assists the protonation of CPT, we cannot rule out the possibility that few CPT molecules exist as neutral one even upon encapsulation inside the cavity of CB7. This is because protonation of CPT depends on the orientation of CPT molecules during the formation

of inclusion complex. It has already been demonstrated that fluorescence lifetime of neutral CPT molecule reduces as the polarity of the medium decreases.[23, 24] This is attributed to the fact that the energy gap between $^1\pi$-π^* and ^{1}n-π^* becomes smaller as the polarity decreases.[13, 14] In the inclusion complex (either 1:1 or 2:1), neutral CPT senses less polar environment than water, hence its lifetime reduces down. We have also monitored the fluorescence lifetime of protonated form of drug by collecting the decay profiles of CPT at 515 nm (**Figure 3a.8b**). It is seen form the **Table 3a.1b** that in absence of CB7 the fluorescence lifetime monitored at 515 nm consist of ~4.04 ns component, which is the fluorescence lifetime of lactone form of neutral CPT. As the concentration of CB7 increases, another component of 5.6 ns appears in the decay profile reflecting the appearance of protonated form of CPT. After 100 µM concentration of host, the decay profile becomes single exponential with a lifetime component of 5.6 ns, indicating that protonated CPT exclusively exists in the system at higher concentration of host. This is quite consistent with steady state results, where we have seen that after 100 µM of CB7 the protonated peak at 515 nm dominates over the neutral peak at 435 nm. Therefore, fluorescence lifetime results once again support our conjecture that CB7 assists the protonation of CPT even at neutral pH.

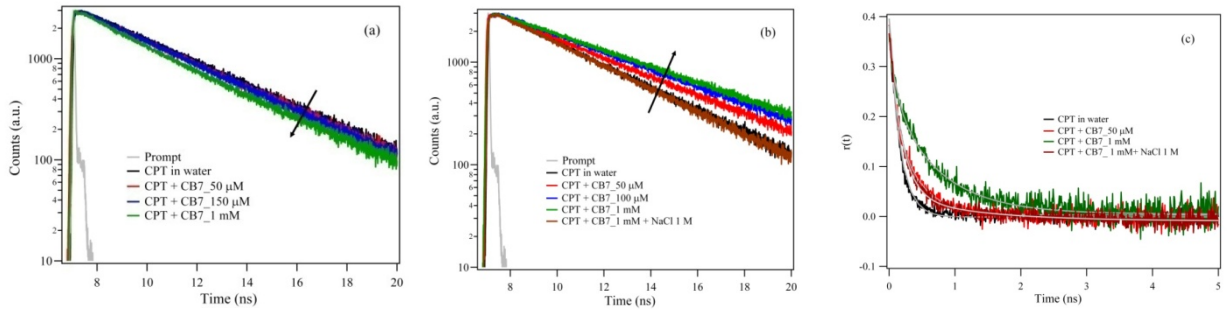

Figure 3a.8: Lifetime and time-resolved anisotropy of CPT (8 µM) in presence of CB7 (0-1 mM). (a) and (b) decay profiles monitored at 435 nm and 515 nm, respectively. (c) Anisotropy decay profiles of CPT in absence (monitored at 435 nm), presence of CB7 (monitored at 515 nm) as well as CB7 containing 1 M NaCl (monitored at 435 nm) as an external stimulus.

Table 3a.1. Fluorescence decay parameters of CPT (8 μM) in absence and presence of CB7 monitored at (a) 435 nm and (b) 515 nm. (λ_{ex}=375 nm).

(a)

Concentration (μM)	τ_1 (ns)	τ_2 (ns)	a_1	a_2	τ_{av}[c] (ns)	χ^2
0	4.048	-	1	-	4.048	1.02
50	3.97	-	1	-	3.97	1.09
100	3.82	5.56	0.95	0.04	3.9	1.03
150	3.7	5.56	0.92	0.08	3.84	0.99
300	3.49	5.56	0.91	0.09	3.67	1.08
500	3.17	5.56	0.82	0.18	3.58	1.04
800	2.92	5.56	0.75	0.25	3.58	1.08
1000	2.67	5.56	0.7	0.3	3.53	1.1

[c] $\tau_{av} = (a_1 \tau_1 + a_2 \tau_2)$

(b)

Concentration (μM)	τ_1 (ns)	τ_2 (ns)	a_1	a_2	τ_{av}[c] (ns)	χ^2
0	4.08	-	1	-	4.08	1.03
15	4.07	-	1	-	4.07	1.04
30	3.95	5.56	0.83	0.17	4.23	1.02
50	3.86	5.56	0.63	0.37	4.49	1.05
70	3.87	5.56	0.44	0.56	4.83	1.05
100	3.59	5.56	0.2	0.8	5.17	1.03
150	2.85	5.56	0.05	0.95	5.44	1.00
200	-	5.56	-	1	5.56	1.01
500	-	5.56	-	1	5.63	1.00
1000	-	5.56	-	1	5.56	1.01

[c] $\tau_{av} = (a_1 \tau_1 + a_2 a_2)$

3a.2d. Time Resolved Anisotropy Measurements:

It is well known that time resolved anisotropy measurements can provide valuable information regarding the rotational motion of a fluorophore, and hence, it can be used to probe the encapsulation process of CPT inside CB7. The rotational relaxation of CPT in water takes place in 150 ps time-scale (**Figure 3a.8c**). However, the anisotropy decay displays noteworthy changes in the rotational diffusion time with the variation in the concentration of CB7 (**Figure 3a.8c**). At low concentration of CB7 (50 μM), the anisotropy decay of CPT monitored at 435 nm (λ_{ex}=375 nm) displays rotational correlation time of ~350 ps, which corresponds to the rotational relaxation time ($\boldsymbol{\tau}_r$) of neutral CPT molecule encapsulated by one CB7 host. At higher CB7 concentration (1 mM)**,** the rotational correlation time monitored at 515 nm (λ_{ex}=405 nm) raised to 890 ps (**Figure 3a.8c**) due to the increased rigidity of 1:1 inclusion complex by another CB7 host. The variations of rotational relaxation times with respect to host concentration are clear indication in the change of complexation equilibrium from 1:1 to 2:1 (host:guest) complexes having different hydrodynamic volume. These $\boldsymbol{\tau}_r$ values are used to determine the hydrodynamic volumes of above mentioned stiochiometry from the Stokes-Einstein relationship[25]:

$$\tau_r = \frac{1}{6D_r} = \frac{\eta V}{kT} \qquad (3a.4)$$

D_r and η are the rotational diffusion coefficient and viscosity of the medium, respectively, V is the hydrodynamic molecular volume of the complex, and T is the absolute temperature. By using the above relation and assuming the viscosity of the medium is same as that of water, the evaluated effective hydrodynamic diameters of the complexes are 14.09 Å and 19.23 Å for 1:1 and 2:1 complexes, respectively, which directly reflects their hydrodynamic volume and hence taking account their structural differences.

3a.2e. Comparison of Binding Affinity and Stability of CPT between β-CD and CB7:

Macrocyclic host, particularly cyclodextrins have been frequently hired to stabilize and solubilize the drugs.[26] Significance of the CB7-CPT binding is better understood when the above results are compared with that of β-CD (**Figure 3a.9**), which has comparable size as that of CB7. In presence of β-CD, there is no evidence for the formation of protonated CPT in ground state**,** as no peak arises in absorption spectra at ~410 nm (**Figure 3a.9a**). Although time-resolved

anisotropy results give a clear hint that CPT forms inclusion complex with β-CD (**Figure 3a.9c**), emission spectral features of CPT in presence of β-CD devoid of a peak at ~510 nm (**Figure 3a.9b**), which is the signature for the excited state protonated form of CPT. Hence, hydrophobic cavities of both CB7 and β-CD are not responsible for the protonation of CPT, rather we believe that different topology of upper and lower rims of both the hosts is accountable for the modulation of photophysics of CPT in different extent. Owing to their carbonyl-lined portals and hydrophobic cavity, CB7 binds cation, positively charged alkyl amines and nitrogen containing neutral heterocyclic molecules mainly through ion-dipole along with the hydrophobic interactions.[27] On the other hand, cyclodextrin owing upper and lower rims with hydroxyl groups binds with the guest mainly by hydrogen bonds.[27] It is reported that electron withdrawing effect of pyridone ring is responsible for the observed low pk_a of quinoline nitrogen of CPT,[4] and this electron withdrawing effect develops partial positive charge on the quinoline part, and partial negative charge on the pyridone moiety. As the binding interaction with CB7 takes place mainly by ion-dipole intercation, it is quite likely that pyridone moiety of CPT is encapsulated in the hydrophobic pocket of CB7, and the quinoline moiety of CPT interacts with the electron rich carbonyl portal through the partial positive charge developed on the quinoline moiety. In the 1:1 inclusion complex, only the charge neutralization of quinoline nitrogen takes place by the electron rich carbonyl portals, but it cannot gain high electron density. However, in case of 2:1 (CB7:CPT) inclusion complex, probably the quinoline nitrogen is located in between two electron rich carbonyl portals and now quinoline nitrogen experiences high electron density, and hence, its basicity increases tremendously. The exact molecular picture of the orientation will be available through docking study followed by semi-empirical quantum chemical calculations, which will be discussed in the later part of the manuscript.

It has been demonstrated that the solubility as well as stability of CPT increases when it forms inclusion complexes with β-CD.[28] Although in the present work we have not focused on the stability of CPT in the inclusion complex with CB7, Dong *et al.* have already shown that the hydrolysis rate of CPT marginally has been reduced when it encapsulates inside the CB7 cavity.[12] The apparent association constant (K_c) for the CPT:β-CD inclusion complex is estimated to be 285 M^{-1} from B-H plot (inset in **Figure 3a.9b**), which is in good agreement with the previous report[28]; whereas the association constant between CPT and CB7 is varied from 2.8 $\times 10^3$ (± 100) M^{-1} to 3.4×10^4 ($\pm$ 1890) M^{-1}, indicating CB7 forms at least 10 times stronger

inclusion complexes with CPT than β-CD. Considering the fact that binding affinity has a critical role during transportation of a drug through blood, our results might provide another approach for effectively delivering CPT to the tumor cells.

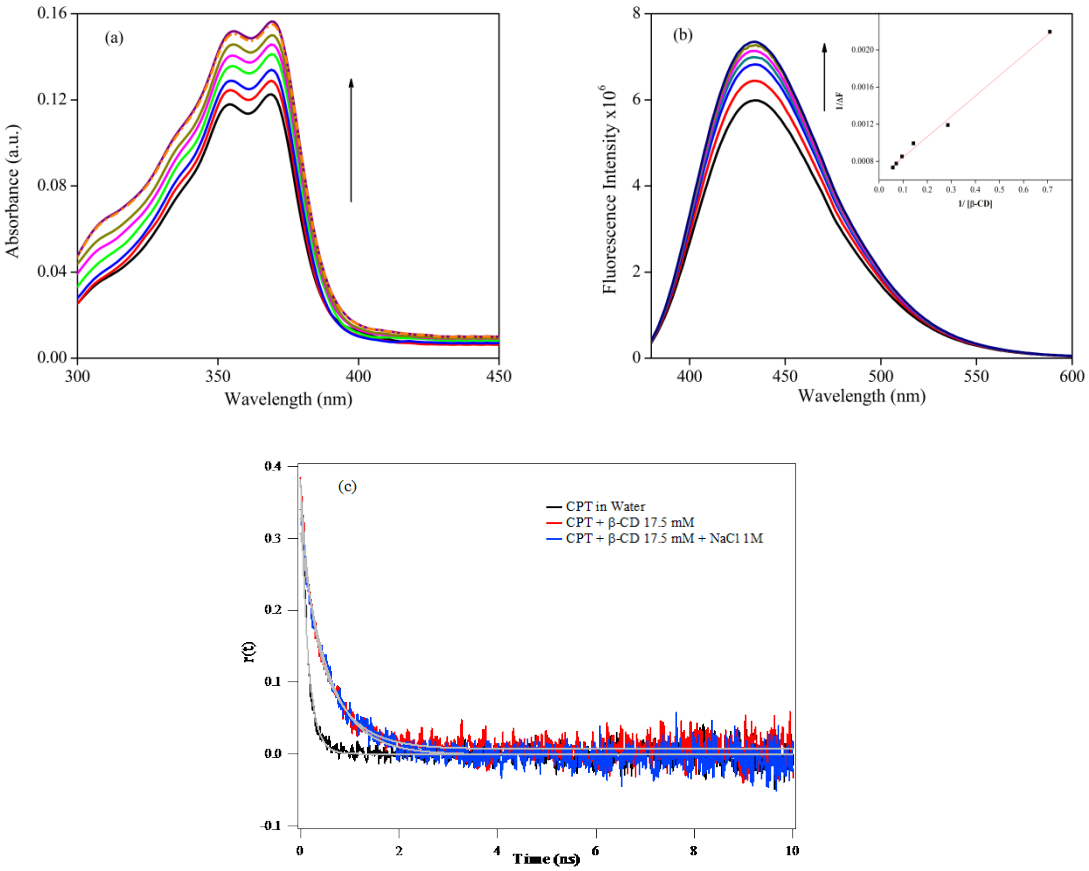

Figure 3a.9. Absorption (a), emission (b) and time-resolved anisotropy decay profiles (c) of CPT (8 μM) in presence of β-CD (0-17.5 mM) as well as β-CD containing 1 M NaCl as external stimulus.

3a.2f. Stimulus Assisted Release of the Drug:

Having demonstrated that CB7 can be used as a potential carrier of CPT, our next aim is to introduce a release mechanism of the drug. Drug can be effectively released from CB7 cavity using an external stimulus like salt or by varying the pH of solution.[29] Considering the facts that cell contains significant amount of Na^+ ions, and cucurbituril portals bind Na^+ with high affinity,[29] we have employed NaCl an external stimulus to release the drug from the cavity of CB7 host, and the release process has been monitored with the help of absorption, emission and time-resolved fluorescence studies. On addition of 1 M of NaCl to the drug containing 1mM of

CB7 solution, the absorption, emission spectra return to that of observed at pH 6.2 (**Figure 3a.1a**, **Figure 3a.1b** and **Figure 3a.8**). Moreover, the fluorescence lifetime and rotational motion of CPT in presence of 1 M of NaCl containing CB7 solution exactly matches with that of CPT in water at pH = 6.2. These results clearly demonstrate that drug can be easily released using very simple external stimulus like NaCl. For comparison, we have done similar experiment on the β-CD:CPT inclusion complex, and the experimental results indicate that the release of the drug does not take place by the Na^+ in case of inclusion complex between β-CD and CPT (**Figure 3a.9a** and **Figure 3a.9c**). Therefore, it can be concluded that cucurbituril is a better drug carrier for CPT than cyclodextrin considering binding affinity as well as release mechanism. Positively, considering the bio-compatibility of CB7[27], this methodology can evolve into a valuable protocol for the intracellular delivery and release of functional molecular components under simple chemical trigger control.

3a.2g. Docking and Quantum Chemical Calculations:

To obtain the molecular picture of orientation of CPT in the inclusion complexes as well as to gain insight into the stabilization achieved due to encapsulation, we have docked the drug (CPT) into the CB7, followed by a semi-empirical quantum chemical optimization. All the figures (**Figure 3a.10** and **Figures 3a.11**) are made in UCSF Chimera.[30] Since the docking as well geometry optimization were done without consideration of any solvent and other parameters, these geometries provide only qualitative picture of the structures in the ground states. All the docking results are displayed in the **Figure 3a.10**. Two conformers with small difference in the energy (~0.4 Kcal/mol) were observed in the cluster analysis of CPT, CB7 (1:1) docking (**Figure 3a.10**) study. The docked structure of 2:1 inclusion complex is obtained by docking 1:1 inclusion complex with another CB7 molecule. The structures obtained from docking studies are fully optimized on MOPAC2012 software using PM6-DH2 method (**Figure 3a.11**). Among all semi-empirical quantum mechanics methods, PM6-DH2 includes empirical corrections for dispersion (D) and hydrogen-bond (H) interactions, and therefore, it provides a good accuracy for calculating the interaction energy or binding energy (ΔE).[31, 32] So, binding energy (ΔE) was thus calculated by subtracting the heat of formation of individual molecules from each complex using a classical equation.[32]

ΔE for 1:1 complex= ΔH_f (CPT:CB7) - ΔH_f (CPT) - ΔH_f (CB7) (3a.5)

ΔE for 1:2 complex = ΔH_f (CPT:2CB7) - ΔH_f (CPT) - $2\Delta H_f$ (CB7) (3a.6)

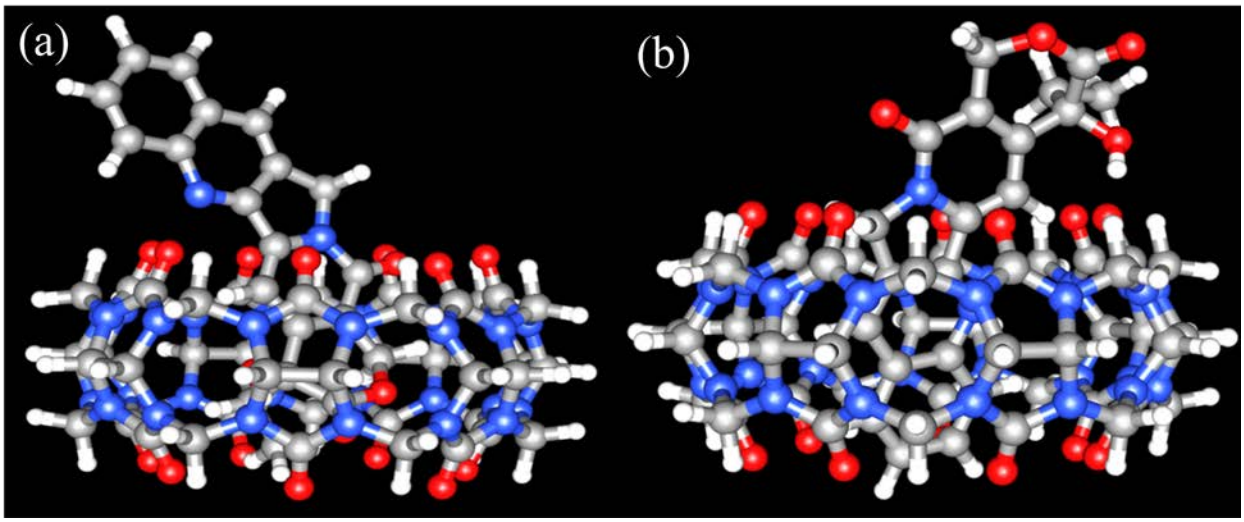

Figure 3a.10. Docked structures of 1:1 inclusion complexes between CPT and CB7. (a) and (b) represent two different types of 1:1 inclusion complexes between CPT and CB7.

The calculated interaction energies of 1:1 inclusion complexes are energetically feasible and exhibits binding energy (ΔE) of -42.5 kcal.mol^{-1} and -21.2 kcal.mol^{-1}. The interaction for the conformer with quinoline moiety completely resided inside the CB7 cavity (**Figure 3a.11a**) is more favored than the other in which lactone moiety resided inside the cavity. It is noteworthy to mention that in none of the above cases the N-atom in quinoline moiety could able to get protonated, as it lies away from the electron rich carbonyl portal ring of CB7, which is consistent with the experimental results where we have observed that 1:1 inclusion complex formation does not lead to protonation of CPT (**Figure 3a.1b**). 2:1 host-guest inclusion complex between CB7 and CPT exhibits energetically feasible negative binding energy (ΔE= -43.5 kcal/mol) obtained from the above mentioned equation. From the optimized structure of 2:1 inclusion complex obtained from semi-empirical quantum chemical calculation (**Figure 3a.11b**), it is clearly seen that the N-atom in quinoline moiety is very close to the electron rich carbonyl portals of both the CB7. Therefore, it supports our conjecture based on experimental results that these electron rich portals of two CB7 in 2:1 inclusion complex provides high electron density towards the

quinoline nitrogen of CPT, and as a results the protonation pK_a of quinoline nitrogen increases from ~1.2 to 6.2.

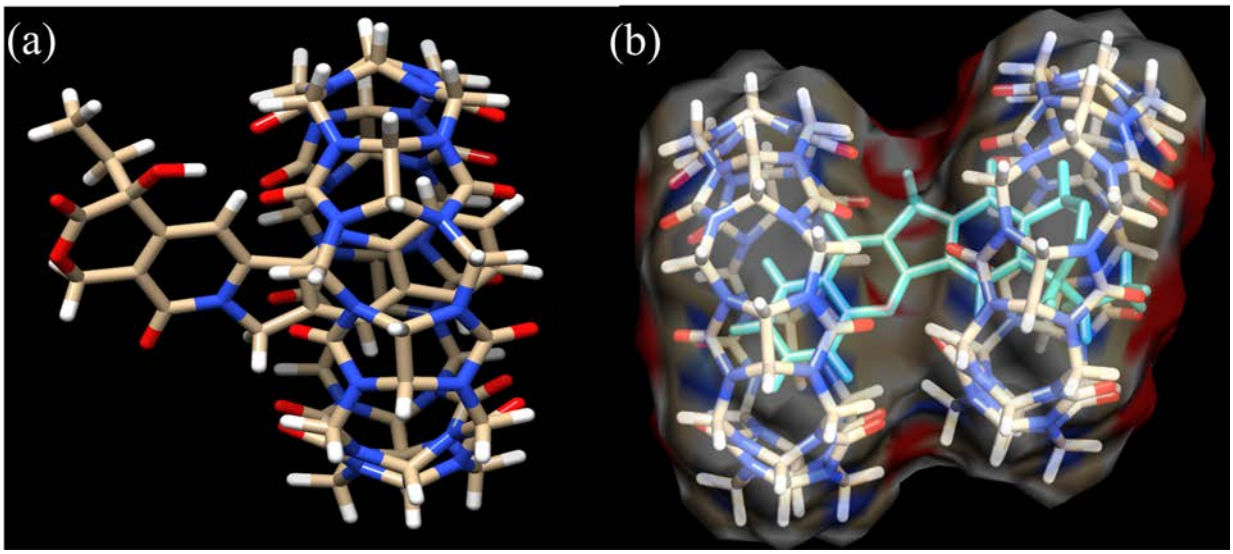

Figure 3a.11. Computationally optimized structures of inclusion complexes between CPT and CB7. (a) and (b) represent the 1:1 and 2:1 (CB7:CPT) inclusion complexes, respectively.

3a.3. Conclusion:

In this chapter, the interaction behaviour between an anticancer drug, CPT and CB7 has been demonstrated with the help of absorption, steady state emission, time-resolved emission techniques. Our experimental results indicate the formation of 1:1 inclusion complex at lower concentration of CB7 (<50 μM). Interestingly, CPT gets protonated when it is encased by two CB7 macrocycles at higher concentration of host (>50 μM), and, consequently, pK_a shifts from 1.2 to 6.2. However, when CPT forms inclusion complex with β-CD, which has almost similar cavity size as that of CB7, no protonation of CPT takes place. Therefore, we believe that carbonyl portals of CB7 has important role for the observed pK_a shift in case of CB7. Apart from prominent alteration of molecular properties of CPT, the inclusion complex responses to the Na^+ as an external stimulus.The molecular picture obtained from docking as well as quantum chemical calculation indicates that quinoline nitrogen of CPT is situated in between two high electron rich portals of CB7 in 2:1 inclusion complex, and as a result the basicity of quinoline nitrogen increases significantly.

3a.4. Reference:

1. M. E. Wall, M. C. Wani, C. E. Cook, K. H. Palmer, A. T. McPhail and G. A. Sim, *J. Am. Chem. Soc.*, 1966, **88**, 3888-3890.
2. M. Potmesil, Pinedo, H., *Camptothecins: New Anticancer Agents;* CRC Press: Boca Raton, FL, 1995.
3. R. Garcia-Carbonero and J. G. Supko, *Clin. Cancer Res.*, 2002, **8**, 641-661.
4. M. R. di Nunzio, B. Cohen and A. Douhal, *J. Phys. Chem. A*, 2011, **115**, 5094-5104.
5. J. Fassberg and V. J. Stella, *J. Pharm. Sci.*, 1992, **81**, 676-684.
6. R. P. Hertzberg, M. J. Caranfa, K. G. Holden, D. R. Jakas, G. Gallagher, M. R. Mattern, S. M. Mong, J. O. L. Bartus, R. K. Johnson and W. D. Kingsbury, *J. Med. Chem.*, 1989, **32**, 715-720.
7. T. G. Burke and Z. Mi, *J. Med. Chem.*, 1994, **37**, 40-46.
8. T. G. Burke, A. K. Mishra, M. C. Wani and M. E. Wall, *Biochemistry*, 1993, **32**, 5352-5364.
9. T. G. Burke, A. E. Staubus, A. K. Mishra and H. Malak, *J. Am. Chem. Soc.*, 1992, **114**, 8318-8319.
10. D. Yang, J. T. Strode, H. P. Spielmann, A. H. J. Wang and T. G. Burke, *J. Am. Chem. Soc.*, 1998, **120**, 2979-2980.
11. N. Dong, S.-F. Xue, Q.-J. Zhu, Z. Tao, Y. Zhao and L.-X. Yang, *Supramol. Chem.*, 2008, **20**, 663-671.
12. N. Dong, M. Dong, A. Zhao, Q. Zhu, Z. Tao and Y. Zhao, *Sci. China Chem.*, 2010, **53**, 2304-2310.
13. J. Dey and I. M. Warner, *J. Lumin.*, 1997, **71**, 105-114.
14. J. Dey and I. M. Warner, *J. Photochem. Photobiol., A*, 1998, **116**, 27-37.
15. S. Nigam and G. Durocher, *J. Phys. Chem.*, 1996, **100**, 7135-7142.
16. B. D. Wagner, N. Stojanovic, A. I. Day and R. J. Blanch, *J. Phys. Chem. B*, 2003, **107**, 10741-10746.
17. M. Freitag, L. Gundlach, P. Piotrowiak and E. Galoppini, *J. Am. Chem. Soc.*, 2012, **134**, 3358-3366.

18. N. Barooah, J. Mohanty, H. Pal and A. C. Bhasikuttan, *J. Phys. Chem. B*, 2012, **116**, 3683-3689.
19. N. i. Saleh, A. L. Koner and W. M. Nau, *Angew. Chem. Int. Ed.*, 2008, **47**, 5398-5401.
20. R. Wang and D. H. Macartney, *Org. Biomol. Chem.*, 2008, **6**, 1955-1960.
21. I. W. Wyman and D. H. Macartney, *Org. Biomol. Chem.*, 2010, **8**, 247-252.
22. J. Dey and I. M. Warner, *J. Photochem. Photobiol., A*, 1996, **101**, 21-27.
23. N. Schaschke, S. Fiori, E. Weyher, C. Escrieut, D. Fourmy, G. Müller and L. Moroder, *J. Am. Chem. Soc.*, 1998, **120**, 7030-7038.
24. K. Uekama, F. Hirayama and T. Irie, *Chem. Rev.*, 1998, **98**, 2045-2076.
25. G. R. Fleming, *Chemical applications of ultrafast spectroscopy.* 1986; p Medium: X; Size: Pages: 262.
26. M. E. Brewster and T. Loftsson, *Adv. Drug Delivery Rev.*, 2007, **59**, 645-666.
27. R. N. Dsouza, U. Pischel and W. M. Nau, *Chem. Rev.*, 2011, **111**, 7941-7980.
28. J. Kang, V. Kumar, D. Yang, P. R. Chowdhury and R. J. Hohl, *Eur. J. Pharm. Sci.*, 2002, **15**, 163-170.
29. H. Tang, D. Fuentealba, Y. H. Ko, N. Selvapalam, K. Kim and C. Bohne, *J. Am. Chem. Soc.*, 2011, **133**, 20623-20633.
30. E. F. Pettersen, T. D. Goddard, C. C. Huang, G. S. Couch, D. M. Greenblatt, E. C. Meng and T. E. Ferrin, *J. Comput. Chem.*, 2004, **25**, 1605-1612.
31. M. Korth, *J. Chem. Theory Comput.*, 2010, **6**, 3808-3816.
32. F. Avila-Salas, C. Sandoval, J. Caballero, S. Guiñez-Molinos, L. S. Santos, R. E. Cachau and F. D. González-Nilo, *J. Phys. Chem. B*, 2012, **116**, 2031-2039.

3b. Cucurbit[7]uril Assisted Ultraviolet to Visible Fluorescence Switch of a Heart Medicine

3b.1. Introduction:

Here in this section, we have studied the inclusion complexation of an important heart medicine, milrinone with cucurbit[7]uril (CB7). Milrinone (1,6-Dihydro-2-methyl-6-oxo-3,4′-bipyridine-5-carbonitrile) is a synthetic cardiotonic medicine widely used for the treatment of congestive heart failure.[1] The mechanism of the action of this drug is thought to be through the elevation of 3′,5′-cyclic adenosine monophosphate (cAMP) levels in the myocardial cell by inhibiting the cyclic nucleotide phosphodiesterase.[2, 3] Though milrinone (MIR) exists in different forms (keto, enol, cation and anion) depending upon the pH of the medium,[4,5] only cationic and keto forms (**Scheme 3b.1**) are believed to be medicinally active.[6,7] The drug has some limitations in oral usage due to its adverse side effects, like thrombocytopenia, fever, anorexia, abdominal pain, nausea and emesis.[8-11] Therefore the formulation of this drug with some less toxic materials may reduce some of these side effects. As CB7 acts as non-toxic drug delivery vehicle, we thought the interaction behavior between the drug and CB7 might provide a new insight towards the delivery aspect of the drug. Inspired by the fluorescence switching properties of CB7 in earlier section of this chapter we wanted to apply the same for MIR which generally exhibits fluorescence in the ultraviolet (UV) region which is not good for biological studies. But, when the drug is encapsulated within CB7 nano-cavity, astonishingly, a fluorescence switch from ultraviolet (UV) to visible (cyan) is observed as a result of increase in pK_a of MIR (**Figure 3b.1**). We have confirmed that the biologically active cationic form ($MIRH^+$) of the drug selectively exists within CB7 nano-cavity. Interestingly, cyan color of the drug in presence of CB7 switches back to violet color simply by increasing the pH of the medium due to release of the drug from the CB7 nano-cavity. We hope this kind of CB7 induced UV to visible fluorescence color switch can be utilized in the pharmaceutical sector for monitoring drug delivery process.

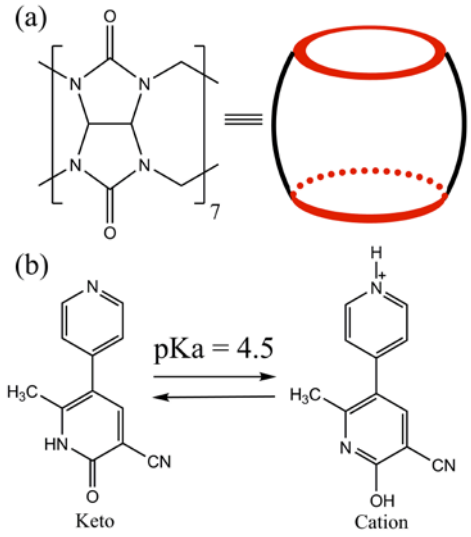

Scheme 3b.1. Chemical structures of CB7 (a) and milrinone (b).

3b.2. Results and Discussion:

3b.2a. Steady State Measurements:

Figure 3b.1a displays the UV-visible absorption spectrum of milrinone in water and with increasing concentrations of CB7. MIR exhibits two bands at ~336 nm and 266 nm corresponding to $S_0 \rightarrow S_1$ and $S_0 \rightarrow S_2$ transitions, respectively.[4] The higher energy band (266 nm) undergoes no significant shift, but absorbance decreases rapidly with increasing concentration of CB7. On the other hand for lower energy band the blue shift is observed in presence of CB7. These noteworthy changes in absorption profile confirm the interaction between MIR and CB7 in the ground state. To get more insight into the complexation process, we have collected emission spectra of MIR in water and in presence of CB7 (**Figure 3b.1b**). MIR exhibits a single fluorescence band with maximum at ~385 nm in water, and this band is believed to be originated from keto form.[4] On gradual addition of CB7, the fluorescence of drug at 385 nm rapidly decreases (**Figure 3b.1b**). Interestingly, a new emission peak is appeared at ~500 nm in addition to the decrement at 385 nm peak. At higher concentration of CB7, the higher energy emission band vanishes and a sole peak at 500 nm exists in the emission profile. Overall the fluorescence of MIR switches from violet to cyan color in presence of CB7 (**Figure 3b.1b**), and this dramatic change in emission spectra confirms the strong interaction between MIR and CB7.

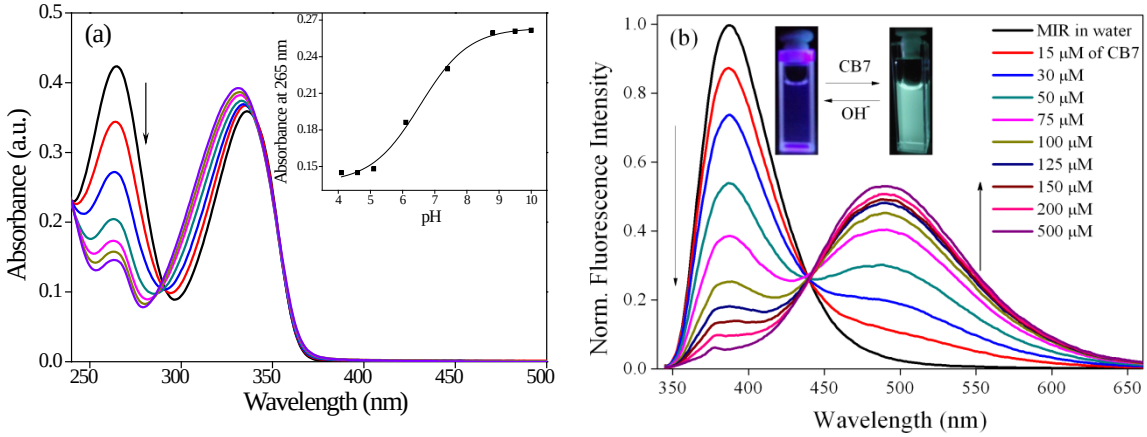

Figure 3b.1. Absorption (a) and emission spectra (b) of milrinone (18 uM) in water in presence of CB7 (0 to 500 uM), λ_{ex} = 340 nm. Inset of A shows the absorbance of MIR in presence of 500 uM at 265 nm versus pH.

Previously, this kind of color switch was observed with CB7 when one form of the drug/fluorophore gets converted to another form.[12-15] This suggests the keto form of MIR, which is the dominant species in water, is converted to some other form in presence of CB7 and gives fluorescence at around 500 nm. It has been reported that in acidic conditions, where the drug predominantly exists in cationic form, emits at ~475 nm.[4] Therefore, we reckon that the 500 nm peak, which is observed when MIR binds with CB7, might be attributed to the cation form ($MIRH^+$) of the drug. This infers that the pK_a for the conversion of keto to cation form of the drug is getting affected when MIR binds with CB7. It is well known that CB7 is prone to shift the pK_a value upward for many biological drugs.[12,13,16] To prove whether the increased pK_a is the cause for the appearance of cyan color in presence of CB7 or not, we have further measured pK_a of MIR in presence of CB7, and we found that the pK_a of MIR is increased to 7.1 in presence of 500 μM of CB7. Moreover, we have also noticed the cyan color of MIR in presence of CB7 switches back to violet in the solution of pH above 7.1. To ensure the formation of cationic MIR ($MIRH^+$) in presence of CB7, we have performed similar experiments at acidic pH (pH 4) and basic pH (pH 10). It is visible from the **Figure 3b.2** that the interaction pattern at pH 4 is quite similar to that of neutral aqueous solution. Whereas at pH 10, the drug does not exhibit any interaction with CB7, as MIR exists as anionic form at this pH, and anionic species generally does not interact with CB7 due to the presence of electron rich carbonyl portals.

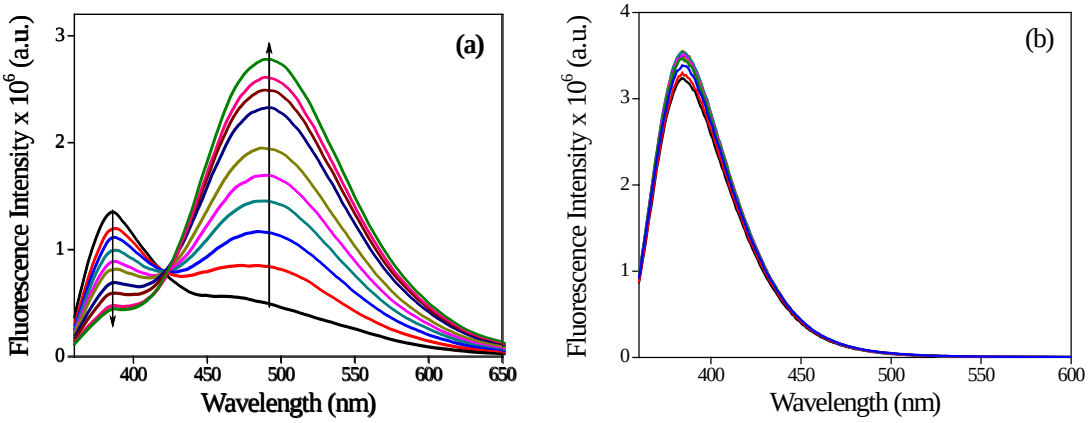

Figure 3b.2. Emission spectra of milrinone at pH 4 (a) and pH 10 (b) in presence of CB7 (0 to 500 uM), λ_{ex} = 340 nm.

All these observations lead us to conclude that there is a pronounced pK_a shift from 4.5[4] to 7.1, when MIR binds to CB7. It is well known that CB7 can increase the pK_a values of many drugs due to its high electron density carbonyl portals.[12, 13, 16] Therefore, we believe the observed upward pK_a shift is attributed to the residence of pyridyl nitrogen near to the electron rich carbonyl portals of CB7, and this will be further verified through docking followed by quantum chemical calculations. The stoichiometry and binding affinity are calculated by using following Benesi-Hildebrand (BH) plot.

$$\frac{1}{(I-I_0)} = \frac{1}{(I_1-I_0)} + \frac{1}{(I_1-I_0)K[CB7]} \qquad (3b.1)$$

where I_0, I and I_1 denote the fluorescence intensity of milrinone in pure water, in presence of CB7 and in the complex, respectively, and K is the binding constant for complexation. Linear BH analysis (**Figure 3b.3a**) confirms the 1:1 complexation between CB7 and MIR with a binding constant of 3.7×10^4 M^{-1}. The 1:1 stoichiometry is further confirmed from Job's method of continuous variation (**Figure 3b.3b**). The multiple equilibria of complexations between the drug and CB7 have been shown in Scheme 1. To see the effect of pH on binding affinity of MIR

with CB7, we have also calculated binding constants at pH 4 from the titration curve using BH plot. The binding constant calculated at pH =4 is found to be 4.0×10^4 M^{-1}, which is slightly higher compared to the value obtained at neutral condition. This is expected because at this acidic pH, cationic species predominantly exist in the solution, and thereby, they are easily attracted by the electron rich carbonyl portals of CB7. At pH 10, as the interaction between anionic form of the drug and CB7 is almost negligible (**Figure 3b.2b**), we could not able to determine the binding constant.

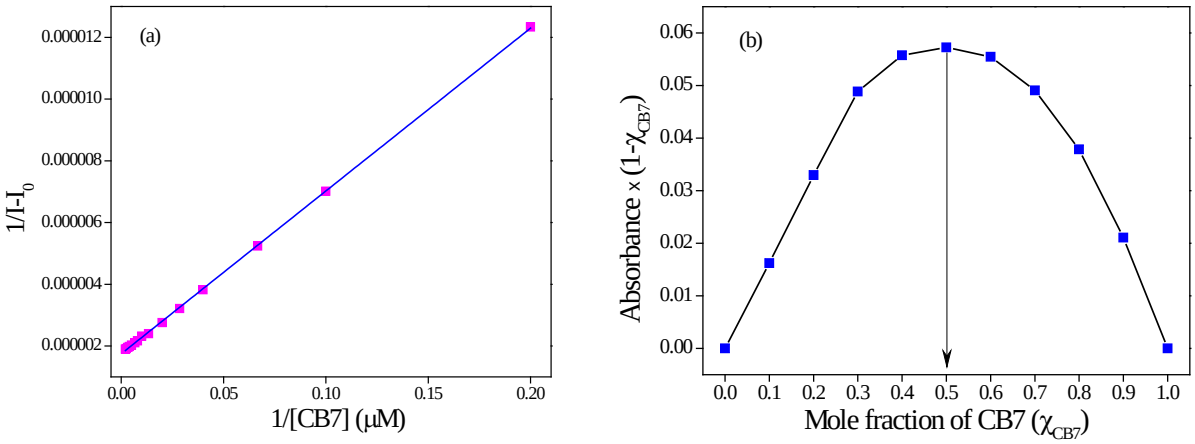

Figure 3b.3. (a) BH plot analysis for the complexation of milrinone with CB7 in water and (b) Job's method of continuous variation.

3b.2b. Time Resolved Measurements:

To explore the dynamics of MIR within CB7, we have employed picosecond time-resolved measurements. The fluorescence transients of MIR in aqueous solutions and in presence of CB7 are shown in **Figure 3b.4**, and the fitting results are summarized in **Table 3b.1**. In water, MIR exhibits double exponential decay (collected at 390 nm) with the time constants of ~90 ps and ~2.2 ns. The former component is believed to be originated from keto form, whereas the latter component is attributed to the relaxed state of keto due to an ICT character.[4] In presence of CB7, the decays collected at 500 nm (cation form) exhibit tri-exponential feature with two nanosecond components and a picosecond component (**Table 3b.1**, **Figure 3b.4**). Similar lifetime components of MIR also observed in presence of PMMA rigid matrix, and it was attributed to the restriction of free rotation of pyridine moiety, which is the major non-radiative decay channel

of MIR.[4] Therefore, we reckon the nanosecond components appeared in the decay profile is an outcome for the inhibition of free rotation of the drug inside the nano-cavity. The decay profile of MIR at 390 nm also consists of nano-second component (3.14 ns to 5.43 ns), and it is attributed to CB7 bound cationic species of the drug, as the emission of cationic species also contributes towards 390 nm. To prove the inclusion complexation between CB7 and MIR, we have employed rotational relaxation measurement of the drug in absence and presence of CB7 (**Figure 3b.4b**) with the help of time-resolved anisotropy measurements.

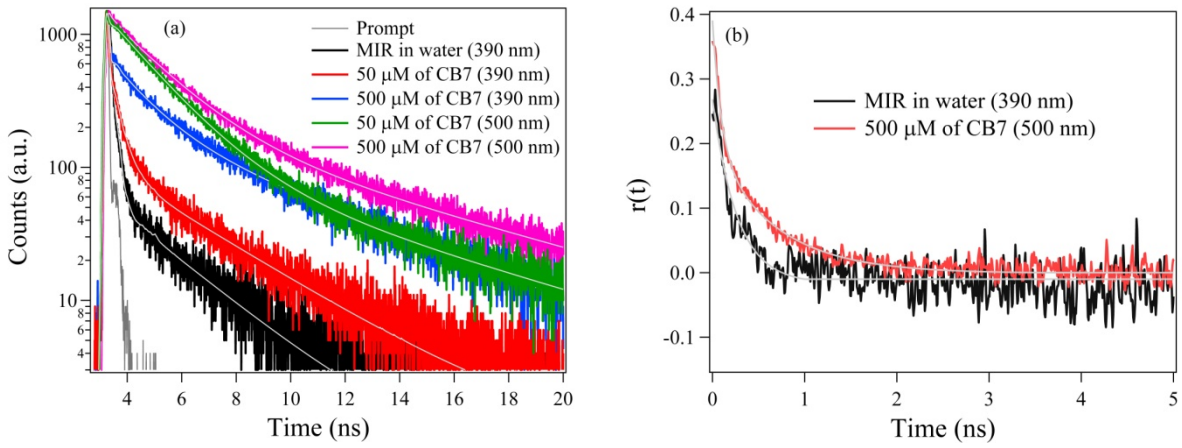

Figure 3b.4. Time resolved fluorescence (A) and anisotropy (B) decays of milrinone in water in presence of CB7 (λ_{ex}=375 nm).

The anisotropy decay of MIR in aqueous solution exhibits mono-exponential in nature with a rotational relaxation constant of 150 ps. A bi-exponential decay behavior is observed in anisotropy transient of MIR in presence of 500 µM of CB7 with time constants of 90 ps and 680 ps. Here the 90 ps is observed for MIR in aqueous solution can be assigned as unbound or free MIR and 680 ps is due to MIR bound with CB7. The increase in rotational relaxation time (τ_r) from 150 ps to 680 ps in presence of CB7 confirms the formation of inclusion complex where drug experiences more rigid environment inside the nano-cavity.

Table 3b.1a. Fluorescence decay transients of milrinone in presence of CB7 (0 to 500 µM) collected at 390 nm (λ_{ex} = 375 nm).

Name	τ_1	τ_2	τ_3	a_1	a_2	a_3	$\chi 2$	τ_{avg} [#]
MIR in water	0.097	2.61	-	0.99	0.01	-	0.99	0.131
16 µM of CB7	0.07	3.14	0.455	0.95	0.01	0.04	1.06	0.119
50 µM of CB7	0.052	3.43	0.373	0.87	0.02	0.11	1.18	0.158
100 µM of CB7	0.035	4.34	0.684	0.92	0.02	0.06	1.13	0.152
200 µM of CB7	0.027	5.11	1.139	0.94	0.02	0.04	1.16	0.156
300 µM of CB7	0.032	5.37	1.255	0.92	0.02	0.06	1.13	0.233
500 µM of CB7	0.031	5.43	1.333	0.9	0.03	0.07	1.17	0.289

[#] $\tau_{avg} = a_1\tau_1 + a_2\tau_2$

Table 3b.1b. Fluorescence decay transients of milrinone in presence of CB7 (50 to 500 µM) collected at 500 nm (λ_{ex} = 375 nm).

Name	τ_1	τ_2	τ_3	a_1	a_2	a_3	$\chi 2$	τ_{avg} [#]
50 µM of CB7	0.061	6.997	1.685	0.5	0.05	0.45	1.04	1.104
100 µM of CB7	0.099	7.129	1.691	0.36	0.05	0.59	1.1	1.428
500 µM of CB7	0.108	7.634	1.8	0.4	0.09	0.51	1.1	1.675

[#] $\tau_{avg} = a_1\tau_1 + a_2\tau_2$

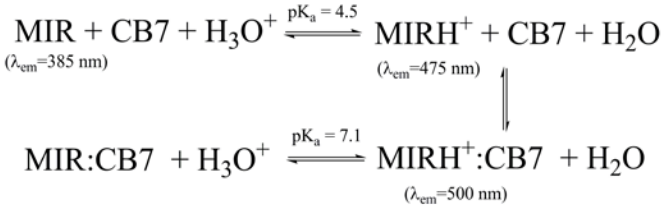

Scheme 3b.2. Representation of multiple equilibria of MIR:CB7 complexation in the solution.

Furthermore, docking and semi empirical methods (PM3MM) are employed to obtain the optimized structure of CB7:MIRH$^+$ inclusion complex. As shown in **Figure 3b.5** the drug is completely buried inside the CB7 nano-cavity. It can clearly be seen from the optimized structure that the pyridine nitrogen resides very close to the electron rich carbonyl portals of CB7, and thereby it experiences high electron density in the inclusion complex. As a result, the pK_a of pyridine nitrogen increases from 4.5 to ~7.1. Therefore, theoretical studies well corroborate the steady state and time-resolved experimental observations.

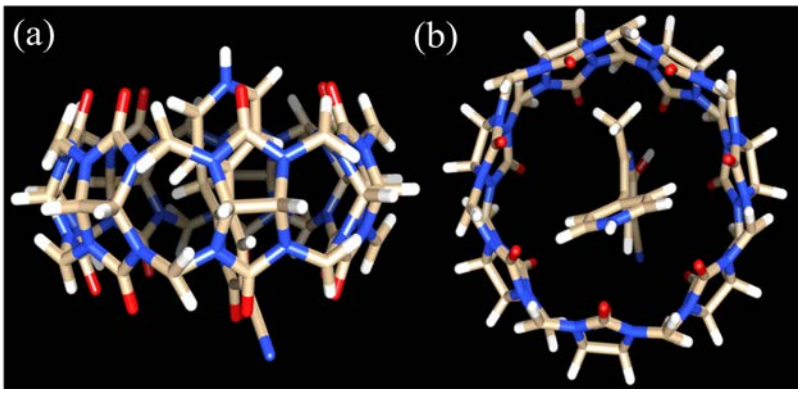

Figure 3b.5. Optimized structure of MIR:CB7 inclusion complex, (a) is from side view and (b) is top view.

3b.3. Conclusion:

In summary, the interaction behavior between an heart medicine, milrinone and cucurbit[7]uril has been demonstrated with the help of absorption, steady state and time-resolved emission measurements. Amazingly, fluorescence of MIR switches from UV to visible (cyan color) as a result of complexation, and we attribute this fluorescence switch to the increased pK_a of protonation of pyridine nitrogen. However, visible fluorescence (cyan color) switches back to UV with increasing pH of the solution.The molecular picture obtained from docking and quantum chemical calculation depicts that pyridine nitrogen of MIR is situated at the electron rich portal of CB7 in inclusion complex, and as a result the basicity of pyridine nitrogen increases significantly. We believe that this kind of fluorescence switch is rarely observed with drug molecules, and therefore, it can be exploited to monitor the delivery process of the drug.

3b.4. Reference:

1. A. A. Alousi, J. M. Canter, M. J. Montenaro, D. J. Fort and R. A. Ferrari, *J. Cardiovasc. Pharmacol.*, 1983, **5**.
2. W. H. Moos, C. C. Humblet, I. Sircar, C. Rithner, R. E. Weishaar, J. A. Bristol and A. T. McPhail, *J. Med. Chem.*, 1987, **30**, 1963-1972.
3. E. Butt, J. Beltman, D. E. Becker, G. S. Jensen, S. D. Rybalkin, B. Jastorff and J. A. Beavo, *Mol. Pharmacol.*, 1995, **47**, 340-347.
4. M. El-Kemary, J. A. Organero and A. Douhal, *J. Med. Chem.*, 2006, **49**, 3086-3091.
5. M. Gil and A. Douhal, *Chem. Phys. Lett.*, 2006, **432**, 106-109.
6. C. Altomare, S. Cellamare, L. Summo, P. Fossa, L. Mosti and A. Carotti, *Bioorg. Med. Chem.*, 2000, **8**, 909-916.
7. A. Krauze, R. Vītoliņa, V. Garaliene, L. Sīle, V. Kluša and G. Duburs, *Eur. J. Med. Chem.*, 2005, **40**, 1163-1167.
8. J. R. Benotti, W. Grossman, E. Braunwald and B. A. Carabello, *Circulation*, 1980, **62**, 28-34.
9. S. J. Siskind, E. H. Sonnenblick, R. Forman, J. Scheuer and T. H. LeJemtel, *Circulation*, 1981, **64**, 966-973.
10. K. T. Weber, V. Andrews, J. S. Janicki, J. R. Wilson and A. P. Fishman, *Am. J. Cardiol.*, 1981, **48**, 164-169.
11. J. Bayliss, M. Norell, R. Canepa-Anson, S. R. Reuben, P. A. Poole-Wilson and G. C. Sutton, *Brit. Heart J.*, 1983, **49**, 214-221.
12. T. Fukaminato, E. Tateyama and N. Tamaoki, *Chem. Commun.*, 2012, **48**, 10874-10876.
13. Z. Miskolczy, L. Biczók and H. Görner, *J. Photochem. Photobiol., A*, 2009, **207**, 47-51.
14. R. Wang, L. Yuan and D. H. Macartney, *Chem. Commun.*, 2005, 5867-5869.
15. U. Pischel, V. D. Uzunova, P. Remon and W. M. Nau, *Chem. Commun.*, 2010, **46**, 2635-2637.
16. I. Ghosh and W. M. Nau, *Adv. Drug Delivery Rev.*, 2012, **64**, 764-783.

Chapter 4

Modulation of Excited State Proton Transfer Dynamics in Bio-mimetic Confined Environments

"The present chapter deals with understanding an important excited state phenomenon excited state proton transfer (ESPT) process, of biologically important molecules in various bio-mimetic confined environments such as cyclodextrins, cucurbiturils and micelles. We have noticed very intriguing observations in ESPT modulations for topotecan, bipyridine diol and ellipticine when they are encapsulated in confined nano-environments. The reasons and discussions explained with proper evidences are discussed in this chapter. Depending over the type of proton transfer process, molecule and confined environment this chapter is further divided into three sections which are discussed one by one in detailed manner as follows."

4a. Supramolecular Host Inhibits Excited State Proton Transfer of an Anti-cancer Drug, Topotecan

4a.1. Introduction and Motivation of the Work:

Topotecan (TPT) is a water soluble analogue of Camptothecin (CPT), a pentacyclic alkaloid. It was first isolated by Wall et al. in 1966 from a Chinese tree Camptotheca acuminate.[1] It is clinically evaluated as an effective anti-cancer agent.[1] CPT and its water soluble derivatives inhibit the activity of topoisomerase I enzyme through the formation of a cleavable enzyme-drug-DNA ternary complex, and thereby, prevents important intracellular processes like replication, transcription and repair.[2-6] Compared to CPT, TPT has higher solubility in water and it also shows inhibitory activity against broad spectrum of animal and human tumors.[7-10] The basic structure of TPT consists of 5 fused rings; among them four are six membered and one is five membered (**Scheme 4a.1**). TPT contains an additional hydroxyl group at 9- and dimethylaminomethylene group at 10- position on quinoline moiety of CPT. Presence of these two functional groups causes this molecule to exhibit different photophysical properties in the excited state compared to CPT**,** and recently, this molecule emerged burgeoning interest to the researchers working in the photophysical field.[11-15] The photophysics of TPT in solution has been mainly studied by UV-Vis absorption and fluorescence spectroscopic techniques.[14, 15] It was observed that at physiological condition (pH 7), the drug exists in equilibrium between enol (E), cation (C) and zwitterionic forms (Z) in the ground state (**Scheme 4a.1**).[15] At lower pH, ground state equilibrium exists between three different cationic species; on the other hand at higher pH, only anionic (A) species prevail.[12] The presence of several protophilic and protophobic functional groups (10-hydroxyl group, quinoline nitrogen, 9-dimethylamino methylene etc.) is responsible for the existence of different forms of TPT at different pH. Although in the ground state drug exists in different forms (E, C and Z) at physiological pH, TPT exhibits a single fluorescence peak in aqueous solution responsible for the emission from Z^*, which is believed to be an outcome of excited state proton transfer.[14, 15] It is also found that the proton transfer process in TPT is very sensitive to polarity,[15] hence, the excited state photophysics of TPT can be modulated inside the nano-cavities of supramolecular host, like cyclodextrin, calixarene, cucurbituril etc. Although it has been shown that the stability of the drug could be improved by

encapsulating the drug molecule into liposomes, cyclodextrins and calixarene,[16-19] no focus has been made on modulating proton transfer process of TPT inside those nanocavities.

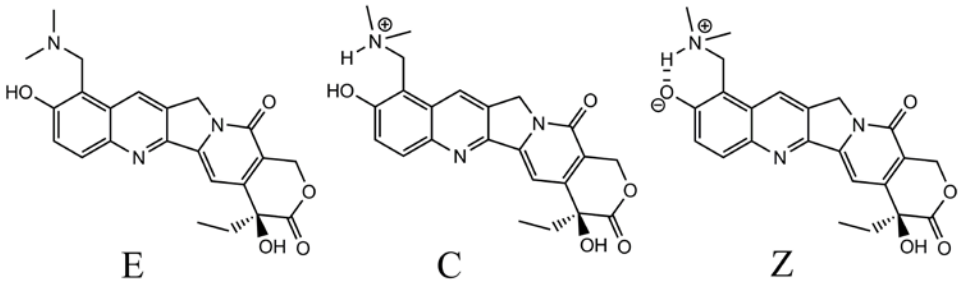

Scheme 4a.1. Different forms of TPT exist in aqueous solution.

Like CPT derivatives, antitumour activity of TPT is believed to be mainly dependent on the stability of α-hydroxy lactone moiety, which hydrolyses predominantly at physiological pH 7.4, and converts to inactive carboxylate form.[16] It was found that hydrolysis of active lactone part of CPT can be 200 times faster in the presence of human serum albumin (HSA), because of the high binding affinity of carboxylate form towards HSA.[20-22] On the other hand, TPT hydrolysis rate is almost unperturbed by the presence of serum albumin protein in blood, thereby favors anticancer activity of TPT compared to CPT.[23] Although the presence of HSA has no change on the cytotoxic activity of TPT,[23] its rate of hydrolysis from active lactone to inactive carboxylate form needs to be inhibited in order to use TPT as an effective anticancer drug. In continuation of this effort, researchers observed that stability of lactone moiety could be improved by encapsulating the drug molecule into liposomes and cyclodextrins.[16-19] The results suggest that the solubility, stability and bio-availability of drug are enhanced upon encapsulation compared to its free form.[16-19] The non-toxic behaviour of CBn provide a boost for the use of CBn as a potential drug delivery vehicle, hence it would be interesting to see whether CB7 forms any inclusion complex with TPT. Here in this section, we study the effect of confinement by CB7 on the photophysics of TPT with the help of steady state and time-resolved fluorescence spectroscopic techniques. The focus of this work is to characterize and compare the effect of nano-confinement on the excited state proton transfer reaction (ESPT) process, which is dominant photophysics observed in aqueous solution. Astonishingly, we have observed that

ESPT of TPT is inhibited inside the nano-cavity of CB7. Semi-empirical quantum chemical calculations have been employed in deciphering the molecular pictures of the interactions between TPT and CB7.

4a.2. Results and Discussion:

4a.2a. Steady State Measurements:

All the studies of TPT in absence and presence of CB7 were carried out in aqueous solution of pH 6 (**Figure 4a.1a**). The choice of pH 6 is based on the fact that lactone structure dominates at pH ≤ 6.[16] In order to avoid carboxylate form of TPT, which leads to toxicity, all the present work has been performed near neutral pH (pH 6). Absorption spectrum of topotecan (TPT) in water (pH 6) exhibits maxima between 350 and 400 nm, which are mainly coming from the π-π* type absorption of the quinoline moiety (A- and B- rings).[15] Considering the pK_a (6.5) of deprotonation of 10-hydroxyl group and the pK_a (10.7) of protonated 9-dimethylaminomethylene group,[24] we believe that the drug mainly exists as cationic (C) form in aqueous medium of pH 6. The very minute population of Z form of the drug is reflected by the slight absorption of the drug at ~410 nm, and it is attributed to the above mentioned pK_a values. On addition of CB7 to the TPT solution, absorption at 365 nm and 381 nm increases, whereas absorption at 410 nm drops down (**Figure 4a.1a**). The rise in absorbance of the former two peaks indicates increasing population of C species in presence of CB7, whereas the decrement of absorption at 410 nm infers that the population of Z form decreases compared to aqueous solution of pH 6. In summary, these substantial changes in absorption spectra provide preliminary notion of TPT-CB7 interaction. To elucidate the mechanism of interaction and stoichiometry, we have further employed steady state and time resolved emission measurements to divulge specific details of this interaction, and will be discussed afterwards.

The emission profiles of TPT in water (pH = 6) and presence of CB7 upon excitation at 375 nm are shown in **Figure 4a.1b**. In absence of CB7, the emission spectrum exhibits a single broad peak at 530 nm, which originates from excited state Z^* of TPT. This is because the excited state zwitterionic form (Z^*) of TPT is the main emitting species in water (pH 6.25), while the fluorescence from C^* is not detectable in water.[15] Here it is pertinent to mention that although the outcome fluorescence is from Z^*, C form of the drug is selectively getting excited at 375 nm. This can be attributed to the excited state proton transfer (ESPT) process by which water assisted

deprotonation of 10-hydroxyl group takes place, and leads to the formation of Z^* form of the drug from C^*. Therefore, we believe that the excited state conversion of $C^* \rightarrow Z^*$ is the dominating photophysics in aqueous solution of near neutral pH (pH 6).

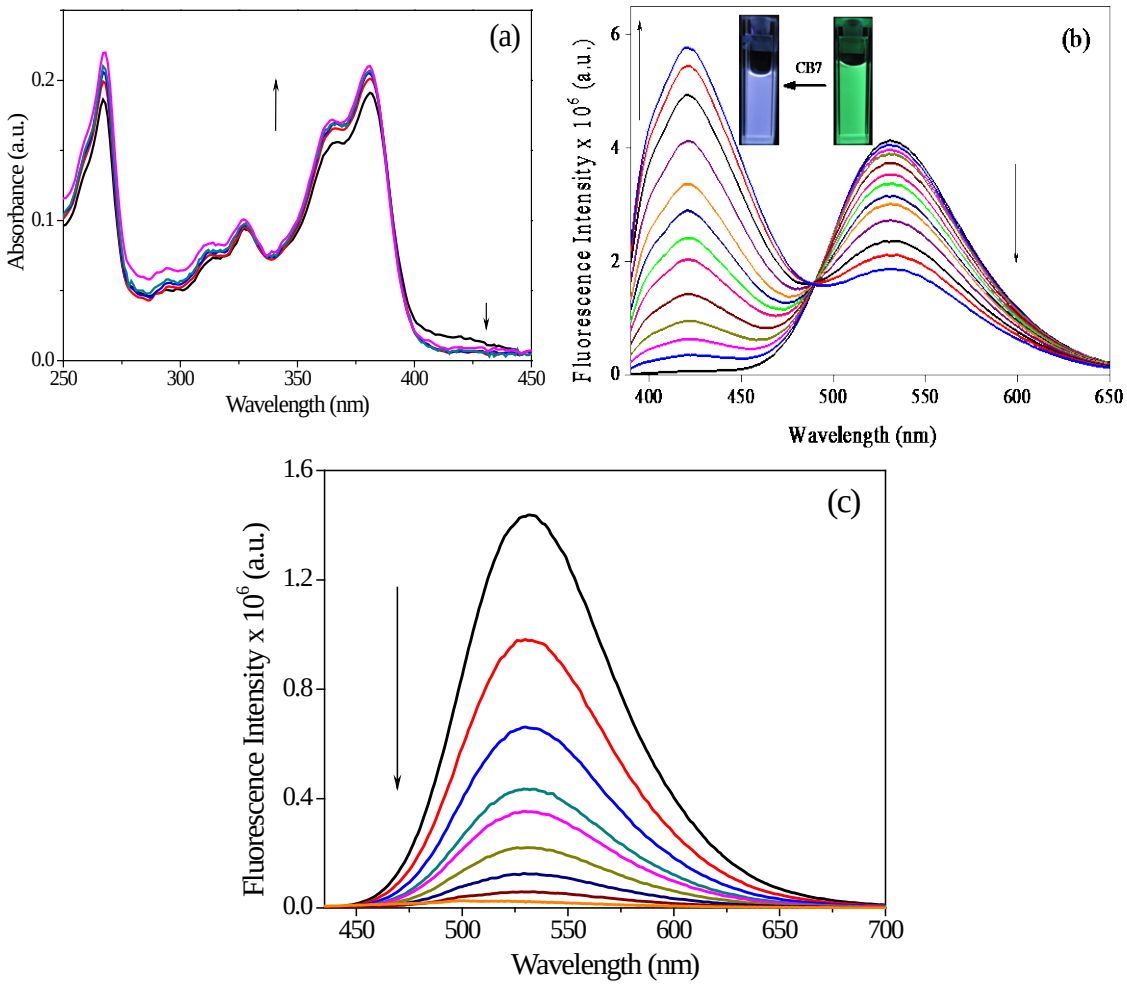

Figure 4a.1. Absorption (a) and Emission spectra of TPT (8 μM) in water and in presence of CB7 (0-1 mM, in the direction of arrow) exciting at (b) 380 nm and (c) 410 nm.

The fluorescence spectra of TPT in the presence of CB7 display a striking feature. By gradual addition of CB7, the emission peak intensity at 530 nm reduces, and a new blue shifted peak at 425 nm progressively develops (**Figure 4a.1b**). At higher CB7 concentration, the 425 nm peak almost gets saturated, whereas the intensity at 530 nm is drastically reduced. These substantial changes in the emission profiles (**Figure 4a.1b**) confirm the strong interaction between TPT and

CB7. As 530 nm peak originates from Z^*, decrease in peak intensity at 530 nm reflects that the formation of zwitterion is getting inhibited by the presence of CB7. The newly appeared peak at 425 in presence of CB7 may be attributed to either C^* or E^* form of the drug. However, at pH 6 the population of C form dominates over the E form. Moreover, if C form of the drug binds with CB7, then it will get additional binding strength through ion-dipole interaction.[25-30] On the other hand, binding of E form involves only weak hydrophobic interaction, and hence binding affinity of E form will be much weaker than that C form. Therefore, we believe that C form of the drug binds prudentially with CB7 and emits blue fluorescence at 425 nm. Inside the CB7 cavity excited state proton transfer (ESPT) from 10-hydroxyl group of TPT to water is ceased, and thereby, CB7 bound C forms of the drug are not able to transform to Z^* in the excited state. Another possibility is that pK_a of hydroxyl group of the drug undergoes an upward shift upon binding with CB7, and subsequently reduces the excited state transformation drift to Z^*. To verify the latter possibility, we have adopted pH titration methods to find out the pK_a value of phenol OH group in ground as well as excited states using absorption and fluorescence measurements, respectively (**Figure 4a.2**). Here it is relevance to mention that in absence of CB7, the reported pK_a value of phenol OH group in the ground and excited state are 6.5 and -2.62, respectively, and this large decrease in pK_a value ($\Delta pK_a = pK_a - pK_a^* = 9.12$) is solely responsible for exhibiting ESPT phenomenon in the excited state. It has been well documented in lietratures that pK_a values of guest molecule increases inside the CB7 cavity due to electron rich carbonyl portals of CB7.[30-32] Similarly, in present case both pK_a and pK_a^* values of TPT in presence of CB7 increases from 6.5 to 7.05 and -2.62 to 5.51, respectively (**Figure 4a.2**). Therefore, the decrease in ΔpK_a ($pK_a - pK_a^*$) from 9.12 to 1.54 in presence of CB7 may be one of the plausible reasons for inhibition of ESPT of TPT. In either of the cases, the excited state equilibrium between C^* and Z^*, which is the dominating excited state photophysics in normal aqueous medium, is inhibited by encapsulation of C form of the drug by CB7. With each addition of CB7, the equilibrium shifts more towards C^*, and therefore, the peak intensity corresponds to C^* progressively increases. In order to substantiate that ESPT process is getting inhibited by the presence of CB7, we have also monitored the emission profiles of TPT by selectively exciting the Z form of drug at 410 nm with increasing concentration of host (**Figure 4a.1c**). It has been observed that the peak intensity at 530 nm progressively decreases with

gradual addition of CB7. This observation further confirms that Z^* population of TPT is decreased by selective incorporation of the C form of drug inside the nano-cavity of CB7 host.

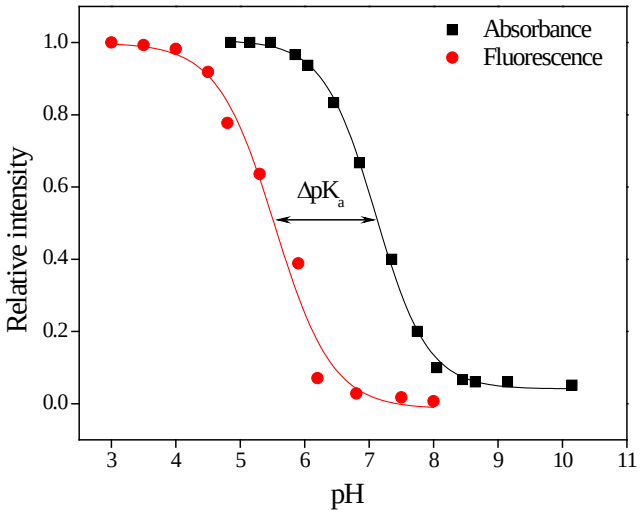

Figure 4a.2. Absorbance (at 410 nm) and fluorescence (at 425 nm, λ_{ex}=380 nm) of TPT in presence of 1 mM CB[7] monitored at different pH conditions.

Now, it is necessary to find out whether the reduced polarity and (or) lack of hydrogen-bonding network of water are (is) responsible for the existence of C^* instead of Z^* inside the CB7 nano-cavity. To verify the above mentioned effects on excited state photophysics of TPT, the emission profiles have been probed in both dioxane-water and ACN-water binary mixtures exciting at 375 nm (**Figure 4a.3**). ACN is chosen considering the fact that it is a polar aprotic solvent having $E_T(30)$ of 45.6. Dioxane is chosen because it is considered as non-polar solvent (having $E_T(30)$ of 36.0)[33] and at the same time it can act as Lewis base.[34, 35] Therefore, both ACN and dioxane can stabilize cationic species. It is observed that the emission from Z^* (at 530 nm) dominates at higher percentage of water, whereas the emission from C^* (at ~425 nm) dominates at higher percentage of acetonitrile or dioxane (**Figure 4a.3**). As the C^* is the main emitting species for both in acetonitrile and dioxane (although their polarity is hugely different), we believe that polarity of the solvent does not take part major role in stabilizing the Z^* form of TPT, rather hydrogen bonding network of the solvent is majorly contributing factor in stabilizing Z^* form of TPT. Our observation is also supported by the literature reports where it has been

reported that zwitterionic forms exist in hydrogen bonded solvents, like methanol, ethanol, and water.[36-38]

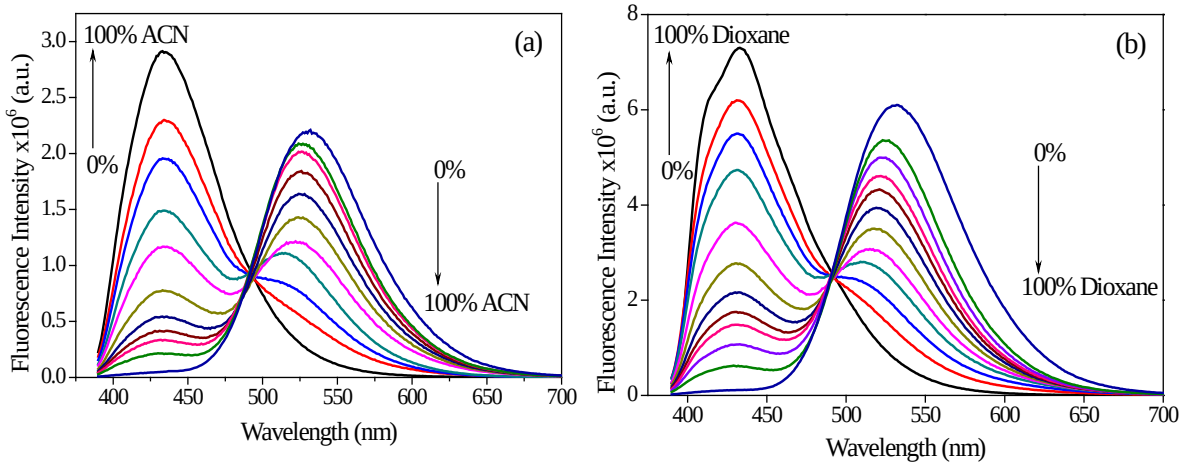

Figure 4a.3. Emission profiles of TPT in (a) ACN-water mixture, and (b) Dioxane-water mixure monitored at λ_{ex}= 380 nm.

The stoichiometry and apparent binding constant for the inclusion complexes are calculated using non-linear version of Benesi-Hildebrand (B-H) plot[39] (equation 4a.1),

$$F/F_0 = 1 + (F_1/F_0 - 1)\left(\frac{[CB7]K}{1+[CB7]K}\right) \qquad (4a.1)$$

where F_0 and F are fluorescence intensities of TPT in absence and presence of CB7, F_1 is the fluorescence intensity of TPT:CB7 inclusion complex. The non-linear fitting shows 1:1 inclusion complexation between TPT and CB7, and the association constant (K_1) is estimated to be 5000(±150) M^{-1} (**Figure 4a.4a**). The 1:1 stoichiometry of TPT:CB7 complex is further confirmed by Job's plot (**Figure 4a.4b**). Moreover, the value of free energy change (ΔG^0 = -21.25 kJ.mol^{-1} at 298 K) for the formation of inclusion complex infers that the complexation process is energetically feasible at the room temperature. Here it is necessary to mention that the population of Z^* does not completely disappear even at 1 mM of host concentration, as 530 nm peak still exists at the above mentioned host concentration. As there is no shift in emission maximum of Z^*, we can rule out the possibility that Z^* is getting encased by CB7. The value of binding constant also indicates that ~15% of TPT does not form inclusion complex with CB7.

However, there is a possibility that some Z* population might involve in the formation of exclusion complex with CB7, and this will be verified through time-resolved studies.

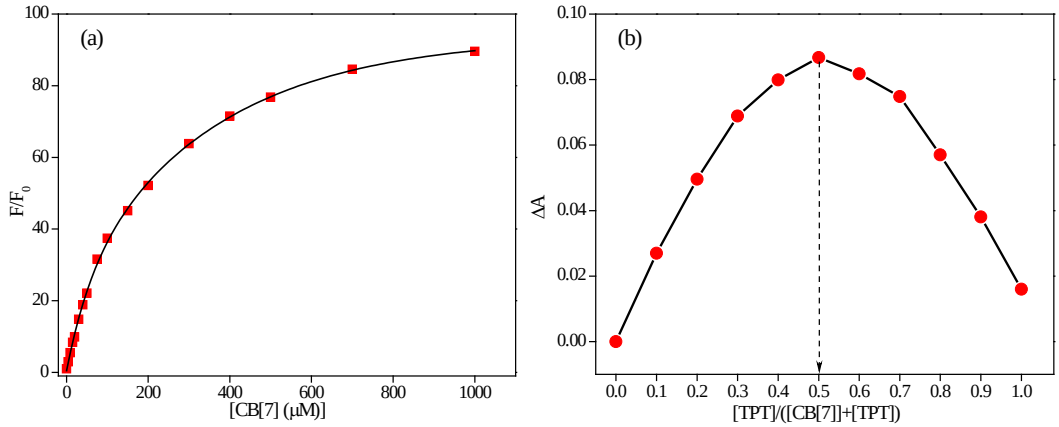

Figure 4a.4. (a) non-linear regression analysis using equation 1. (b) Job's plot constructed from the absorbance changes at 380 nm.

4a.2b. Time Resolved Fluorescence Measurements:

Decay profiles of TPT in absence and presence of CB7 have been collected at 425 nm and 530 nm (exciting at 375 nm) in order to monitor both excited state cationic species (C^*) and zwitterionic species (Z^*), respectively. Fluorescence transients are shown in **Figure 4a.5** and results are tabulated in **Table 4a.1**. The decay profile collected at 425 nm in aqueous solution of TPT is very fast, and very close to the response time of our TCSPC set-up. However, after deconvolution we were able to detect a fluorescence lifetime component of ~40 ps, which may be attributed to the fluorescence lifetime and/or deprotonation time of C form of TPT. In presence of CB7, a long component (~2 ns) appears in the decay profile along with ~40 ps component, and the contribution of long component progressively increases with the gradual addition of host (**Table 4a.1**). This newly appeared component is likely to be an outcome of interaction between C form of TPT and CB7. It is already evident from the emission spectra that the population of C^* is getting enhanced in presence of CB7 due to the suppression of transformation pathway from C^* to Z^* inside the nano-cavity of CB7. Moreover, it was found that cationic species has longer fluorescence lifetime in polar aprotic and non-polar solvents compared to water, which abstracts the proton from the 10-hydroxyl group and facilitates the

conversion to the Z^* form of TPT (**Table 4a.2**). Hence, the long lifetime of C^* is attributed to the absence of hydrogen bonding network inside the CB7 cavity, and infers that intermolecular hydrogen bond network with solvents has a pivotal role for the stability of C form of TPT. With the gradual addition of CB7, the contribution of long lifetime component enhances progressively, and becomes major component (~80%) at higher concentration of host (>300 μM). This observation suggests the dominating existence of encapsulated C form along with minute population of free C form of TPT at higher CB7 concentration. The average lifetime increases steadily with the concentration of CB7. We have also performed the same experiment in acidic solutions (pH 3). The fluorescence decay fitting parameters are summarized in **Table 4a.3**. The results are found to be same as that of pH 6. These observations clearly support our conjecture that CB7 mainly interacts with cationic TPT and the resulted complex stabilizes by ion dipole interaction. Therefore, the lifetime results validate our steady state observation, where we have found a strong rise of 425 nm emission corresponding to the formation of 1:1 inclusion complex between C form of TPT and CB7. We believe that the selective insertion of cationic form (C) of TPT inside the CB7 cavity keeps the molecule away from water and enhances the fluorescence intensity as well as lifetime of C form of the drug. To get insight into the dynamics of excited state zwitterion form (Z^*) of TPT in absence and presence of CB7, we have also monitored the decay profile of the drug at 530 nm, as the emission at 530 nm is mainly characterized by Z^* form of TPT. Zwitterionic species exhibit long lifetime of ~5.85 nm in aqueous solution of near neutral pH (pH 6). In presence of CB7, the fluorescence lifetime does not change drastically, however, a slight reduction of lifetime of Z^* observed at higher concentration of host, manifesting that Z form of TPT is not encaged by CB7. The slight reduction in lifetime might be attributed to the hydrogen bonding interaction between Z^* and carbonyl groups of CB7 portal, as it has been observed that hydrogen bonding interaction sometimes reduces the excited state lifetime of a fluorophore.[40, 41]

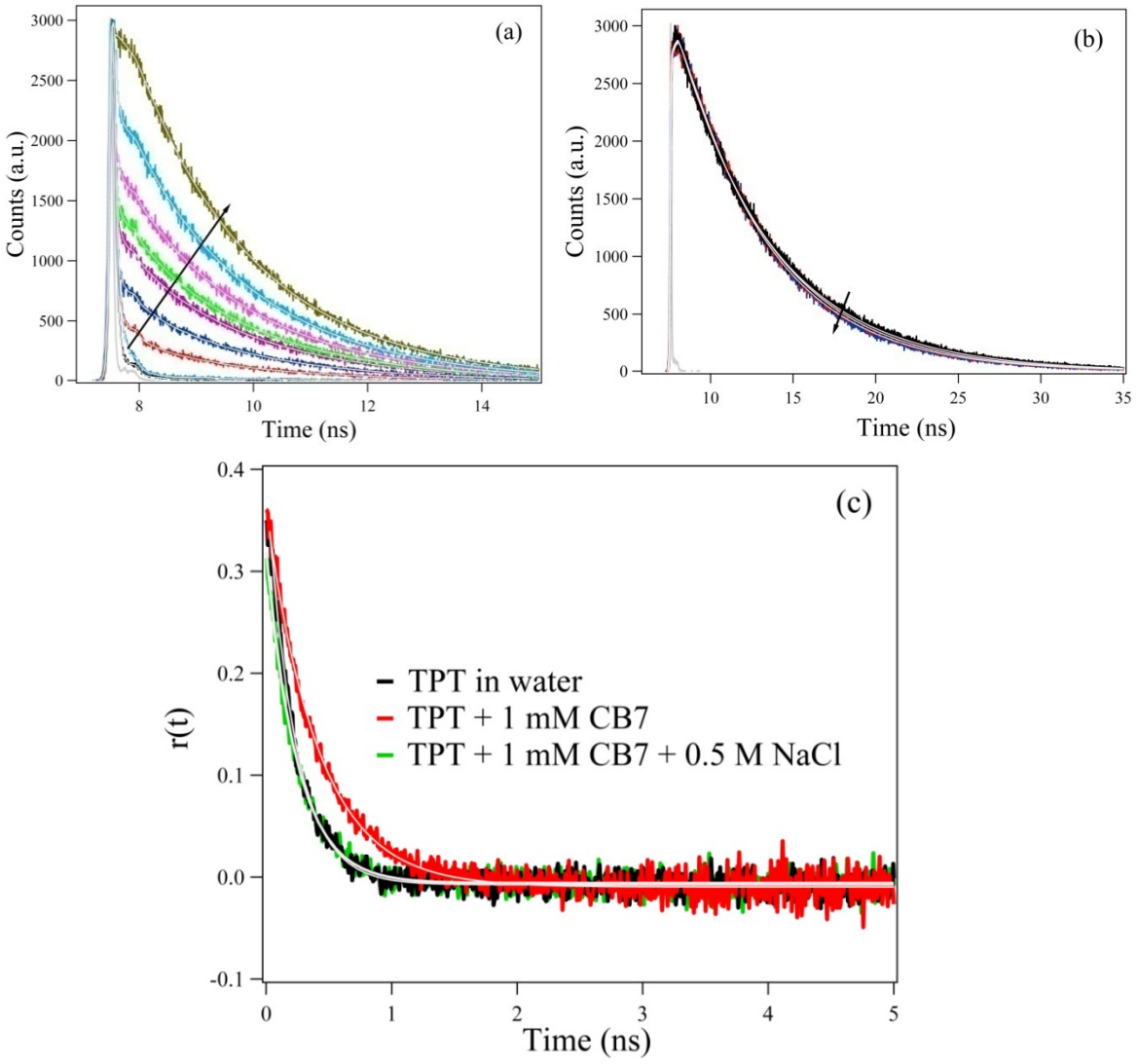

Figure 4a.5. Fluorescence and anisotropy decay transients of TPT (8 μM) in presence of CB7 (0-1 mM, in the direction of arrow). (a) and (b) fluorescence decay profiles monitored at 425 nm and 530 nm, respectively. Prompt is denoted by grey line in both (a) and (b). (c) Anisotropy decay profiles of TPT in absence (monitored at 530 nm), presence of CB7 (monitored at 425 nm) as well as CB7 containing 0.5 M NaCl (monitored at 530 nm) as an external stimulus.

Table 4a.1. Fluorescence decay transients of TPT (8 μM) in absence and presence of CB7 collected at (a) 425 nm and (b) 530 nm (λ_{ex}=375 nm).

(a)

Concentration of CB7 (μM)	τ_1	τ_2	a_1	a_2	τ_{avg} [#]	$\chi 2$
0	0.041	-	1	-	0.041	1.1
4	0.042	1.95	0.96	0.04	0.113	1.03
9	0.042	2.03	0.92	0.08	0.196	1.02
15	0.049	2.11	0.86	0.14	0.337	1.05
20	0.046	2.11	0.83	0.17	0.393	1.01
30	0.054	2.15	0.73	0.27	0.61	0.99
40	0.051	2.09	0.7	0.3	0.663	1.05
50	0.052	2.12	0.65	0.35	0.784	0.99
75	0.076	2.13	0.44	0.56	1.22	0.99
100	0.072	2.16	0.37	0.63	1.39	1.04
200	0.09	2.1	0.27	0.73	1.56	1.06
300	0.07	2.088	0.21	0.79	1.67	1.06
500	0.072	2.1	0.18	0.82	1.75	1.07
1000	0.07	2.12	0.12	0.88	1.87	0.99

[#] $\tau_{avg}=(a_1\tau_1 + a_2\tau_2)$

(b)

Concentration of CB7 (μM)	τ_1	$\chi 2$
0	5.85	1.05
100	5.81	1.09
200	5.79	1.06
300	5.73	0.99
500	5.64	1.02
700	5.56	1.02
1000	5.44	1.12

Table 4a.2. Fluorescence decay transients of TPT in organic solvents collected at 425 nm (λ_{ex}=375 nm).

Solvent	τ_1	τ_2	a_1	a_2	$\tau_{avg}^{\#}$	$\chi 2$
ACN	3.12	-	1	-	3.12	1.04
Dioxane	3.01	-	1	-	3.01	1.05
Formamide	2.09	-	1	-	2.09	1.02
Ethanol	2.29	0.087	0.80	0.20	1.86	1.01

$^{\#}$ $\tau_{avg}=(a_1\tau_1 + a_2\tau_2)$

Table 4a.3. Fluorescence decay transients of TPT (8 μM) at pH 3 in absence and presence of CB7 collected at 425 nm (λ_{ex}=375 nm).

Concentration of CB7 (μM)	τ_1	τ_2	a_1	a_2	$\tau_{avg}^{\#}$	$\chi 2$
0	0.042	-	1	-	0.042	1.1
15	0.045	1.99	0.94	0.06	0.167	1.00
50	0.049	2.07	0.81	0.19	0.424	0.99
100	0.062	2.06	0.66	0.34	0.739	1.05
200	0.086	2.04	0.46	0.54	1.148	1.06
300	0.086	2.04	0.36	0.64	1.33	1.03
500	0.086	2.05	0.28	0.72	1.495	1.06
850	0.086	2.02	0.23	0.77	1.577	1.07
1000	0.086	2.06	0.20	0.80	1.663	1.1

$^{\#}$ $\tau_{avg}=(a_1\tau_1 + a_2\tau_2)$

4a.2c. Time Resolved Anisotropy Measurements:

To get information about the rotational motion of the drug in solution and the restriction imposed by the microenvironment around the probe, we have performed time resolved anisotropy measurements. The anisotropy decays of TPT in absence and in presence of CB7 are shown in **Figure 4a.5c**. The rotational relaxation of TPT in aqueous solution of pH 6 collected at 530 nm, which is the emission signature of Z^* species, exhibits single exponential decay with a rotational relaxation time of 220 ps. It is already seen from steady state measurement that a new peak

appeared at 425 nm (which corresponds to cationic form of TPT) at the cost of 530 nm on addition of CB7. Therefore, we have collected anisotropy decays for TPT in presence of CB7 at both of 530 nm and 425 nm emission positions in order to get a notion about the rigidity of the surrounding environment sensed by both C^* and Z^* species, respectively. The anisotropy decay of TPT (C^*) bound to CB7 (collected at 425 nm) yields a retarded rotational relaxation with a relaxation time of ~450 ps at 1 mM of CB7 concentration. This retarded rotational motion of C^* in presence of CB7 is a further confirmation for the formation of inclusion complex between CB7 and cationic form of TPT. On the other hand, rotational correlation time of Z^* (obtained from collecting anisotropy decay profile at 530 nm) does not differ much from TPT in bulk water even at higher CB7 concentration (1mM), confirming our conjecture that Z^* does not involve in the inclusion complex formation with CB7. However, if Z^* interacts with CB7 by H-bonding interaction (through carbonyl portals), then it is very likely that rotational correlation time of the drug will be unaffected.

The estimated rotational relaxation times are used to determine the hydrodynamic volumes of inclusion complex formed between TPT and CB7 using the following Stokes-Einstein relationship. The hydrodynamic diameter calculated form anisotropy data (collected at 425 nm) are found to be 12 Å and 16 Å for TPT in water and in presence of 1 mM of CB7, respectively. Therefore, the increased hydrodynamic diameter of TPT is a proof for the TPT (C form) and CB7 inclusion complex, which supports our previous interpretations in steady state, time resolved studies.

4a.2d. Salt Triggered Controlled Release Mechanism of TPT:

In most of the drug encapsulation processes release of the drug is immensely important, as it is directly connected to the therapeutic importance of the drug.[42] Considering the facts that cell contains significant amount of Na^+ ions, and cucurbituril portals bind Na^+ with high affinity,[43, 44] we have employed NaCl an external stimulus to affect the non-covalent interaction between the drug and host. On addition of 0.5 M of NaCl to the drug containing 1mM of CB7 solution, the emission spectra return to that observed at pH 6.0 aqueous solution (**Figure 4a.6**). The most prominent feature of the release is obtained from the time resolved anisotropy measurements, where it is observed that NaCl induced anisotropy decay profile exactly overlays with that of TPT in water (**Figure 4a.5c**). These results clearly manifest that NaCl facilitates the release of C form of TPT from the CB7:TPT(C) inclusion complex. The dominating electrostatic interaction

between Na^+ ions and "C=O" groups at CB7 portal may be the responsible for the reduced interaction between TPT and CB7, and ultimately TPT comes out from the cavity.[45] The colour switch from green to blue (when TPT is embedded in CB7 nano cavity) and blue to green (when it is released from CB7 with the addition of NaCl) is much more interesting, and can be used to monitor the drug delivery process.

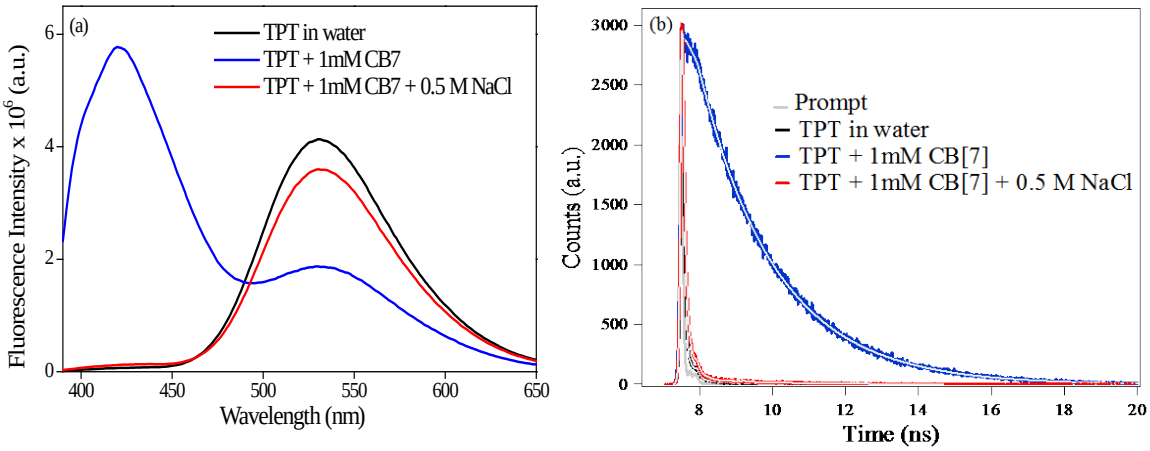

Figure 4a.6. (a) Emission spectra (λ_{ex}=380 nm) and (b) Fluorescence decay transients of TPT (8 μM) in water (black), in presence of 1 mM CB7 (blue) and with 0.5 M NaCl (Red) are collected at 425 nm by exciting with 375 nm diode. Prompt is denoted with the grey line.

4a.2e. Computational Study:

The above experimental findings are further examined with the help of computational studies, as it helps to realize the orientation as well as detailed understanding about the interactions. Optimized structure for CB7:TPT complex is shown in (**Figure 4a.7**), which clearly shows that quinoline part of TPT lies partly inside the cavity of CB7. Most importantly, dimethylamino methylene and hydroxyl groups of quinoline moiety responsible for zwitterion formation are found to be completely buried inside the CB7 cavity. As water molecules cannot access these two groups inside the cavity, thereby, excited state of cationic species (C^*) cannot transform to exited state zwitterion form (Z^*) of TPT in the CB7:TPT(C) inclusion complex. Moreover, in this orientation the hydroxyl group of TPT might experience high electron density of carbonyl portals. Therefore, its pK_a may increase when it is encased by CB7 nano-cavity. The optimized

structure undoubtedly supports the experimental observations and clearly implies that a strong 1:1 ground state complexation formed between C form of TPT and CB7.

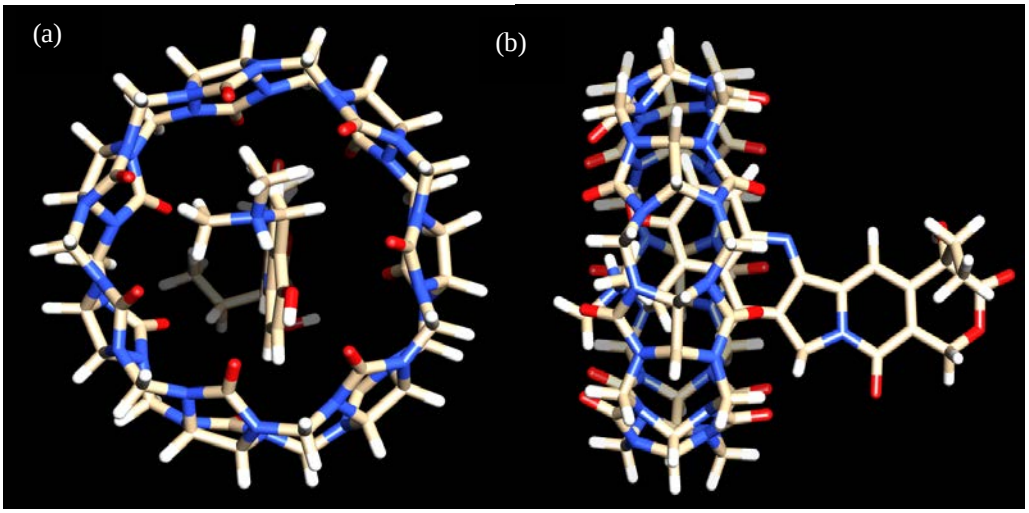

Figure 4a.7. Optimised structure of CB[7]:TPT (1:1) inclusion complex (a) top view and (b) side view.

4a.3. Conclusion:

Current chapter describes the interaction and modulation of photophysical properties of an important anticancer drug, TPT with CB7 by several spectroscopic techniques like absorption, fluorescence and time resolved measurements. We found CB7 has a selective affinity to cationic form (C) of TPT and forms a 1:1 inclusion complex (CB7:TPT(C)) with CB7. Thereby, the excited state transformation of C to zwitterion (Z) form through excited_state proton transfer (ESPT) process is restricted inside the CB7 cavity, and it is reflected by the appearance of a new peak at 425 nm at the cost of 530 nm peak (responsible for Z form of TPT) in presence of CB7. Appearance of ~2 ns component in the decay profile monitored at 425 nm also confirms the encapsulation of C form of drug by the CB7 host. Moreover, the retarded rotational motion of C form of TPT fortifies our claim that C form is encased by the macrocyclic host. On the other hand the rotational motion of Z^* does not hinder in presence of CB7 indicating TPT (Z) is not encased by CB7, rather it interacts with the C=O portal of CB7 through the hydrogen bond formation. The process of complexation and molecular orientation of the drug inside cavity has

been conceptualized using computational studies, which show that the quinoline moiety of TPT lies partly inside the cavity of CB7, thereby, restricts ESPT and lowers the population of Z^*. Finally, controlled release of the drug has been achieved through the introduction of NaCl, which is rich in cell, as an external stimulus. We hope this recognition mediated binding as well as release mechanism can be useful for activation of the drug and controlled release of the drug in the therapeutic uses.

4a.4. Reference:

1. M. E. Wall, M. C. Wani, C. E. Cook, K. H. Palmer, A. T. McPhail and G. A. Sim, *J. Am. Chem. Soc.*, 1966, **88**, 3888-3890.
2. P. D'Arpa and L. F. Liu, *Biochim. Biophysi. Acta, Rev. Cancer*, 1989, **989**, 163-177.
3. W. D. Kingsbury, J. C. Boehm, D. R. Jakas, K. G. Holden, S. M. Hecht, G. Gallagher, M. J. Caranfa, F. L. McCabe, L. F. Faucette, R. K. Johnson and R. P. Hertzberg, *J. Med. Chem.*, 1991, **34**, 98-107.
4. J. C. Wang, *Ann. Rev. Biochem.*, 1996, **65**, 635-692.
5. Y. Pommier, P. Pourquier, Y. Fan and D. Strumberg, *Biochim. Biophys. Acta, Gene Struct. Expression*, 1998, **1400**, 83-106.
6. Y. Pommier, *Nat. Rev. Cancer*, 2006, **6**, 789-802.
7. B. Anderson M.D, *Gynecol. Oncol.*, 1994, **55**, S143-S150.
8. E. K. Rowinsky, A. Adjei, R. C. Donehower, S. D. Gore, R. J. Jones, P. J. Burke, Y. C. Cheng, L. B. Grochow and S. H. Kaufmann, *J. Clin. Oncol.*, 1994, **12**, 2193-2203.
9. J. Sehouli and G. Oskay-Özcelik, *Curr. Med. Res. Opin.*, 2009, **25**, 639-651.
10. T. Idris, R. Winter, U. W. E. Lang and E. Petru, *Anticancer Res.*, 2009, **29**, 1761-1762.
11. E. Bardez, A. Chatelain, B. Larrey and B. Valeur, *J. Phys. Chem.*, 1994, **98**, 2357-2366.
12. S. A. Strel'tsov, S. L. Grokhovskii, I. A. Kudelina, V. A. Oleinikov and A. L. Zhuze, *Mol. Biol.*, 2001, **35**, 365-373.
13. N. Sanna, G. Chillemi, A. Grandi, S. Castelli, A. Desideri and V. Barone, *J. Am. Chem. Soc.*, 2005, **127**, 15429-15436.
14. M. R. di Nunzio, Y. Wang and A. Douhal, *J. Phys. Chem. B*, 2012, **116**, 8182-8190.
15. M. R. di Nunzio, Y. Wang and A. Douhal, *J. Phys. Chem. B*, 2012, **116**, 7522-7530.

16. W. J. M. Underberg, R. M. J. Goossen, B. R. Smith and J. H. Beijnen, *J. Pharm. Biomed. Anal.*, 1990, **8**, 681-683.
17. P. Tardi, E. Choice, D. Masin, T. Redelmeier, M. Bally and T. D. Madden, *Cancer Res.*, 2000, **60**, 3389-3393.
18. C. Foulon, J. Tedou, T. Queruau Lamerie, C. Vaccher, J. P. Bonte and J. F. Goossens, *Tetrahedron: Asymmetry*, 2009, **20**, 2482-2489.
19. G.-S. Wang, H.-Y. Zhang, F. Ding and Y. Liu, *J Incl Phenom Macrocycl Chem*, 2011, **69**, 85-89.
20. T. G. Burke and Z. H. Mi, *Anal. Biochem.*, 1993, **212**, 285-287.
21. Z. Mi and T. G. Burke, *Biochemistry*, 1994, **33**, 10325-10336.
22. Z. Mi and T. G. Burke, *Biochemistry*, 1994, **33**, 12540-12545.
23. Z. Mi, H. Malak and T. G. Burke, *Biochemistry*, 1995, **34**, 13722-13728.
24. J. Fassberg and V. J. Stella, *J. Pharm. Sci.*, 1992, **81**, 676-684.
25. J. Lagona, P. Mukhopadhyay, S. Chakrabarti and L. Isaacs, *Angew. Chem. Int. Ed.*, 2005, **44**, 4844-4870.
26. R. N. Dsouza, U. Pischel and W. M. Nau, *Chem. Rev.*, 2011, **111**, 7941-7980.
27. W. M. Nau, M. Florea and K. I. Assaf, *Isr. J. Chem.*, 2011, **51**, 559-577.
28. A. I. Day, R. J. Blanch, A. P. Arnold, S. Lorenzo, G. R. Lewis and I. Dance, *Angew. Chem. Int. Ed.*, 2002, **41**, 275-277.
29. J. W. Lee, S. Samal, N. Selvapalam, H.-J. Kim and K. Kim, *Acc. Chem. Res.*, 2003, **36**, 621-630.
30. Z. Miskolczy, L. Biczók and H. Görner, *J. Photochem. Photobiol. A*, 2009, **207**, 47-51.
31. I. Ghosh and W. M. Nau, *Adv. Drug Delivery Rev.*, 2012, **64**, 764-783.
32. R. Wang, L. Yuan and D. H. Macartney, *Chem. Commun.*, 2005, **0**, 5867-5869.
33. C. Reichardt, *Chem. Rev.*, 1994, **94**, 2319-2358.
34. J. V. B. Kanth and H. C. Brown, *J. Org. Chem.*, 2001, **66**, 5359-5365.
35. J. Garcia-Alvarez, E. Hevia, A. R. Kennedy, J. Klett and R. E. Mulvey, *Chem. Commun.*, 2007, **0**, 2402-2404.
36. J. P. Wignacourt, G. Mairesse, P. Barbier, A. Lorriaux-Rubbens and F. Wallart, *Can. J. Chem.*, 1982, **60**, 1747-1750.
37. M. Itoh, T. Adachi and K. Tokumura, *J. Am. Chem. Soc.*, 1984, **106**, 850-855.

38. N. Al-Lawatia, J. Husband, T. Steinbrecher and O. K. Abou-Zied, *J. Phys. Chem. A*, 2011, **115**, 4195-4201.

39. B. D. Wagner, N. Stojanovic, A. I. Day and R. J. Blanch, *J. Phys. Chem. B*, 2003, **107**, 10741-10746.

40. B. Reija, W. Al-Soufi, M. Novo and J. Vázquez Tato, *J. Phys. Chem. B*, 2005, **109**, 1364-1370.

41. M. Shaikh, J. Mohanty, M. Sundararajan, A. C. Bhasikuttan and H. Pal, *J. Phys. Chem. B*, 2012, **116**, 12450-12459.

42. B. Wang, T. J. Siahaan and R. A. Soltero, *Drug Delivery: Principles and Applications*, Wiley-VCH Publishers, Inc., 2005.

43. M. Shaikh, J. Mohanty, A. C. Bhasikuttan, V. D. Uzunova, W. M. Nau and H. Pal, *Chem. Commun.*, 2008, **0**, 3681-3683.

44. H. Tang, D. Fuentealba, Y. H. Ko, N. Selvapalam, K. Kim and C. Bohne, *J. Am. Chem. Soc.*, 2011, **133**, 20623-20633.

45. J. Mohanty, S. Dutta Choudhury, H. P. Upadhyaya, A. C. Bhasikuttan and H. Pal, *Chem. Eur. J.*, 2009, **15**, 5215-5219.

4b. Ultrafast Dynamics of 2,2′-Bipyridine-3,3′-diol inside the Nano-cavities of Molecular Containers

4b.1. Introduction and Motivation of the Work:

Molecules exhibiting excited state intramolecular proton transfer (ESIPT) have received lot of interest owing to their current cutting-edge applications in science, such as molecular probes, logic gates and light-emitting diodes.[1-5] Among the compounds exhibiting proton transfer process, [2,2′-bipyridyl]-3,3′-diol ($BP(OH)_2$) is of special interest, since it contains two protons, which can involve in double proton transfer process, and thereby, $BP(OH)_2$ serves as a model for natural base pairs to study tautomerization process in duplex DNA.[6] The $BP(OH)_2$ is known to undergo an ultrafast excited state intramolecular double proton transfer (ESIDPT) from dienol (DE) form (**Scheme 4b.1**), and this ESIDPT process results in displacement of two protons from hydroxyl groups towards the pyridyl-ring nitrogen atoms leading to the formation of diketo (DK) form (**Scheme 4b.1**). The proton transfer dynamics of $BP(OH)_2$ has been well explored using both experimental and theoretical studies.[7-15] Femtosecond fluorescence upconversion and transient absorption experiments report that intramolecular double proton transfer in $BP(OH)_2$ takes place via two channels, i.e., the process can be concerted (one-step) and/or sequential (two-step).[10-14] The concerted proton transfer process occurs in ultrafast time scale (<50 fs), whereas the sequential process takes place in an ultrafast first step (<50 fs) followed by a slow second step of ≥10 ps.[15] Considering its unique feature of proton transfer dynamics, photophysical properties of $BP(OH)_2$ have been investigated in various constrained environments like cyclodextrins, micelles, proteins, protein-SDS aggregates, bile salt aggregates, zeolites, sol-gel glasses, nafion membrane, binary solvent mixtures and ionic liquids.[16-25] However, in these confined environments proton transfer dynamics of $BP(OH)_2$, which takes place in ultrafast time regime (<20 ps), are rarely monitored.[22] Therefore, it would be very intriguing to probe proton transfer dynamics in confined environments with the help of fluorescence up-conversion technique. Here in this chapter, we study the effect of nano-confinement by cucurbit[7]uril (CB7) on the photophysics of $BP(OH)_2$ with the help of steady state and time-resolved fluorescence spectroscopic techniques and compared with that of β-cyclodextrin (β-CD), which has almost similar cavity size of CB7. To the best our knowledge,

we are reporting for the first time the dynamics of ESIDPT of $BP(OH)_2$ using femtosecond fluorescence up-conversion technique in above mentioned two macrocyclic hosts. Moreover, docking and DFT quantum chemical calculations have been employed in deciphering the molecular pictures of the interactions between $BP(OH)_2$ and macrocyclic hosts.

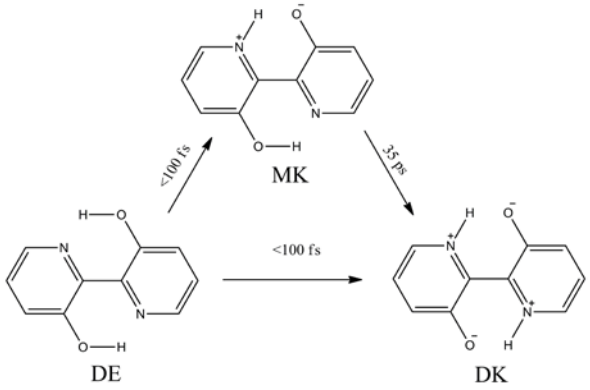

Scheme 4b.1. Different tautomeric forms of $BP(OH)_2$ after ESIDPT via concerted and sequential mechanisms.

4b.2. Results and Discussion:

4a.2a. Steady State Measurements:

Absorption spectra of $BP(OH)_2$ in water with varying concentrations of cucurbit[7]uril (CB7) are depicted in **Figure 4b.1a**. $BP(OH)_2$ in water exhibits a peak maximum at 345 nm and the double peak absorption band in the region of 400-450 nm. The 345 nm band is originated from π to π^* transition of dienol (DE) form and 400-450 nm band is appearing due to the water solvated diketo (DK) form.[16-18] The increase in absorbance at 345 nm along with bathochromic shift with the gradual addition of CB7 indicating the occurrence of interaction between DE form and CB7. In addition to the changes at 345 nm, the absorbance of water solvated DK band (400-450 nm) decreases in presence of CB7. The suppression of the low energy band in the region 400-450 nm clearly demonstrates that water solvation network around $BP(OH)_2$, which is believed to be responsible for the formation of DK form, is perturbed in presence of CB7. As a result, DK form of $BP(OH)_2$ is converted to DE form in presence of CB7. The presence of two isosbestic points in absorption spectra further confirms the existence of two equilibriums among DE, DK and CB7-DE complex.

To get clear insight about the complexation processes, we have monitored the emission profiles of $BP(OH)_2$ in absence and presence of CB7 (**Figure 4b.1b**). $BP(OH)_2$ in water exhibits an emission peak at 465 nm, when it is excited at 345 nm. The large Stokes-shifted emission of $BP(OH)_2$ is attributed to the DK form generated after ESIDPT process in the excited state, i.e., excitation of DE form results in the emission from DK form of $BP(OH)_2$.[16-18] With gradual addition of CB7, the intensity at peak maximum (465 nm) increases significantly with a ~5 nm red shift. Here it is relevant to mention that the caging effect generally reduces the water assisted non-radiative channels of $BP(OH)_2$.[16-19] Moreover, ~35 nm red shift is observed in going from water to non-polar solvent. Therefore, the hike in intensity as well as red shift in fluorescence spectra of $BP(OH)_2$ is a manifestation of caging effect by CB7 nano-cavity. We have also monitored the emission profiles by exciting the $BP(OH)_2$ molecules at 425 nm, where the DK form of $BP(OH)_2$ molecules are selectively getting excited, and the corresponding emission spectra are depicted in **Figure 4b.1c**. Increasing CB7 concentration leads to a decrease in the emission intensity of $BP(OH)_2$ at 465 nm and the observation is well corroborated with absorption studies. Similar observation was also reported previously when $BP(OH)_2$ is encapsulated in other hydrophobic constrained environments, like, cyclodextrins, micelles and protein.[16-19] Therefore, the decrease in emission intensity upon excitation at 425 nm further confirms the effect of hydrophobic environment of CB7 cavity on $BP(OH)_2$. In a nutshell, steady-state results clearly indicate that CB7 forms inclusion complex with $BP(OH)_2$. The interaction scenario between $BP(OH)_2$ and CB7 will be further verified through time-resolved fluorescence and computational studies.

In order to determine the stoichiometry as well as binding constant of the inclusion complex, the changes in fluorescence intensity were plotted against the concentration (Inset of **Figure 4b.1b**) of host using Benesi-Hildebrand (BH) equation[26] given below;

$$\frac{1}{F - F_0} = \frac{1}{K(F_1 - F_0)[host]} + \frac{1}{F_1 - F_0} \qquad (4b.1)$$

where F_0, F and F_1 are the fluorescence intensities of $BP(OH)_2$ in absence, presence of host, and in the inclusion complex, respectively. The double reciprocal plot monitored at 465 nm is observed clearly to be linear (R=0.997), indicating formation of 1:1 inclusion complex between $BP(OH)_2$ and CB7, and the association constant (K_1) is estimated to be ~3.1×10^3 M^{-1}.

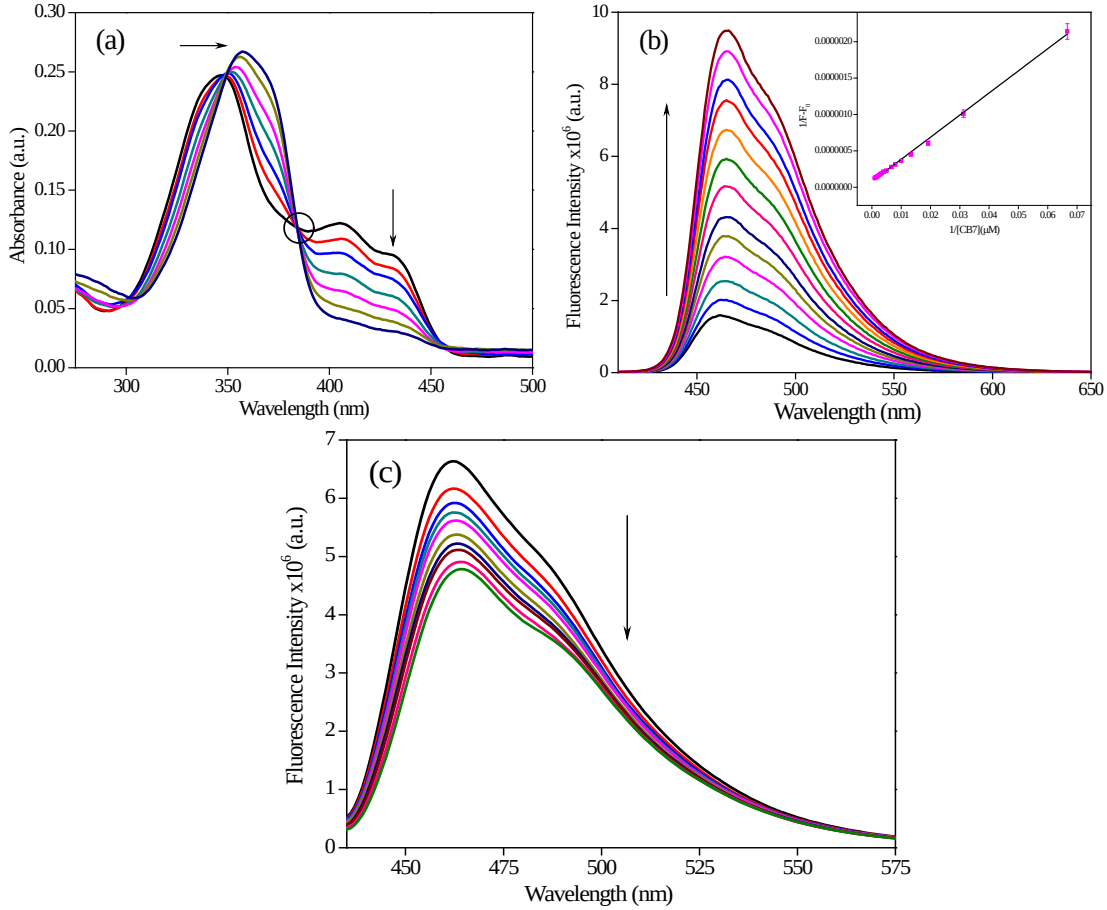

Figure 4b.1. Absorption (a) and Emission (b) (λ_{ex}=345 nm), (c) (λ_{ex}=425 nm) spectra of $BP(OH)_2$ in presence of 0 to 500 μM of cucurbit[7]uril (CB7). Inset of (b) shows BH plot. Arrow indicates the direction of increase in CB7 concentration.

4b.2b. Picosecond Time Resolved Fluorescence Study:

Modulation in radiative properties and excited state dynamics of $BP(OH)_2$ upon interaction with cucurbit[7]uril (CB7) can also be clarified by fluorescence lifetime measurements. Fluorescence decays of $BP(OH)_2$ in absence and presence of CB7 collected at respective emission maximum are shown in **Figure 4b.2** and corresponding fitting parameters are tabulated in **Table 4b.1**. $BP(OH)_2$ exhibits single exponential decay in water with a lifetime component of ~650 ps, which is in good accordance with the previous reported value.[18-20] In presence of CB7, a longer lifetime component (~8 ns) appears in the decay profile along with ~650 ps component (**Figure 4b.2b**).

With the gradual addition of CB7, the contribution of longer lifetime component enhances progressively (**Figure 4b.2b**), and becomes major component (~80%) at higher concentration of host (500 μM). This newly appeared component is likely to be an outcome of interaction between $BP(OH)_2$ and CB7. The increased lifetime of $BP(OH)_2$ on complexation with CB7 may be attributed to the decrease in non-radiative decay pathways of dye inside the molecular container. In addition to the non-radiative decay channels, polarity of surrounding environment may affect the lifetime of $BP(OH)_2$. It is already evident that emission of $BP(OH)_2$ is originating from DK form as result of ESIDPT process, and lifetime of this DK form is known to be sensitive to the polarity of the medium.[16-19] Recently, it was found that $BP(OH)_2$ shows longer fluorescence lifetime in hydrophobic pocket of cyclodextrin, protein and bile salt aggregates compared to water.[16-19] Therefore, the longer lifetime component of ~8 ns is originated from the $BP(OH)_2$ encapsulated inside hydrophobic nano-cavity of CB7. Apparently, this lifetime component of $BP(OH)_2$ in CB7 is much longer than any other observed nano-cavities having hydrophobic environments, and it may be attributed to the inaccessibility of water molecules inside the CB7 cavity.

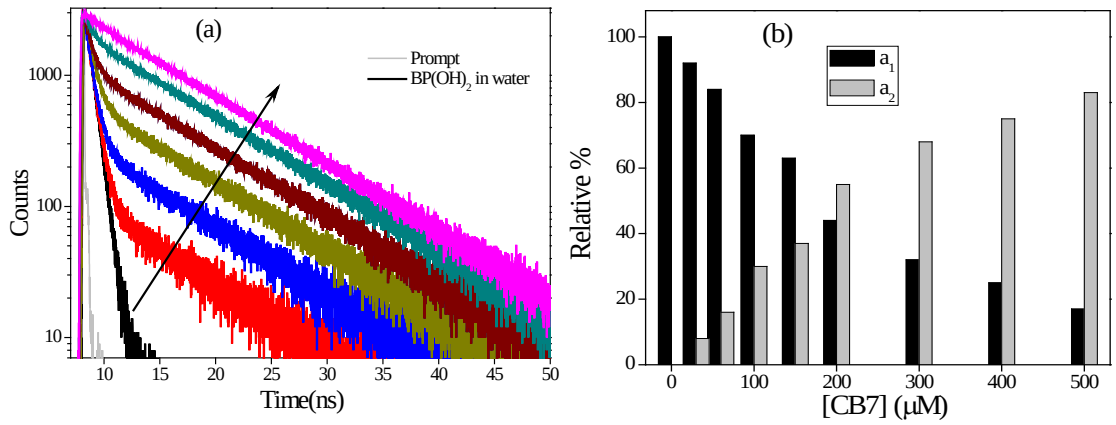

Figure 4b.2. (a) Fluorescence decays overlay of $BP(OH)_2$ in presence of cucurbit[7]uril ((CB7), from 0 to 500 μM) collected at 465 nm (λ_{ex}=375 nm). (b) Plot of relative contribution of lifetime components versus concentration of CB7. Arrow in (a) indicates the direction of increase in CB7 concentration.

Table 4b.1. Fluorescence decay transients (measured in TCSPC set-up) of $BP(OH)_2$ in absence and presence of cucurbit[7]uril (CB7) collected at 465 nm (λ_{ex}=375 nm).

[CB7] (μM)	τ_1(ns)	a_1	τ_2(ns)	a_2	τ_{avg} [#]	χ^2
0	0.63	1	-	-	0.63	1.09
30	0.64	0.92	8.43	0.08	1.26	1.01
60	0.67	0.84	8.56	0.16	1.93	1.08
100	0.68	0.7	8.65	0.3	3.07	1.00
150	0.68	0.63	8.65	0.37	3.63	0.99
200	0.69	0.44	8.73	0.55	5.15	1
300	0.69	0.32	8.71	0.68	6.16	1.03
400	0.69	0.25	8.74	0.75	6.69	1.03
500	0.69	0.17	8.73	0.83	7.37	1.04

[#] $\tau_{avg}=(a_1\tau_1 + a_2\tau_2)$

It is well known that time resolved fluorescence anisotropy measurements can provide valuable information regarding the rotational motion of a fluorophore, and hence, it can be used to probe the encapsulation process of $BP(OH)_2$ inside CB7. The rotational relaxation of $BP(OH)_2$ in water takes place in ~70 ps time scale (**Figure 4b.3**). The anisotropy decay displays noteworthy changes in the rotational relaxation time of $BP(OH)_2$ in presence of CB7. The rotational correlation time monitored at 465 nm (λ_{ex}=375 nm) raised to 350 ps (**Figure 4b.3**) in presence of CB7 due to the increased rigidity for $BP(OH)_2$ inside the cavity of CB7. By using the Stokes-Einstein relationship and assuming the viscosity of the medium is same as that of water, the calculated effective hydrodynamic diameter of $BP(OH)_2$ and the inclusion complex (CB7:$BP(OH)_2$) are 8.24 Å and 14.09 Å, respectively. Therefore, the increased hydrodynamic diameter of $BP(OH)_2$ is a proof for the formation of inclusion complex with CB7, which supports our previous interpretations in steady state and time resolved studies.

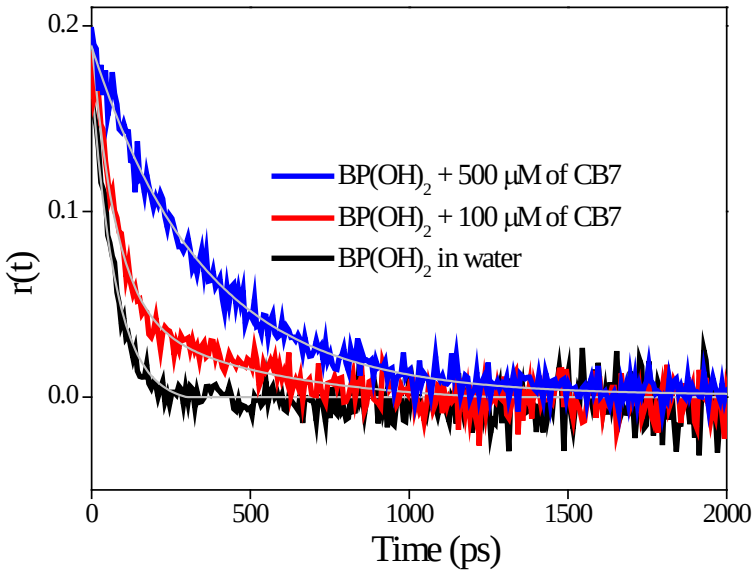

Figure 4b.3. Anisotropy decays overlay of $BP(OH)_2$ in absence and presence of cucurbit[7]uril (CB7) collected in TCSPC set-up at 465 nm (λ_{ex}=375 nm). Best fit is shown as grey coloured line.

4b.2c. Fluorescence Up-conversion Study:

To get insight into the ultrafast proton transfer dynamics of $BP(OH)_2$, which takes place within several tens of picosecond time scale, we have performed femtosecond fluorescence up-conversion measurements in water as well as in presence of CB7. For comparison, we have also probed the dynamics inside β-CD, having similar cavity size as that of CB7. The steady-state and TCSPC results obtained in presence of β-CD are shown in **Figure 4b.4**, match well with that of literature reports.[16, 27] $BP(OH)_2$ exhibits red shift in absorption spectra in presence of CB7, however, similar red shift is absent in case of β-cyclodextrin (β-CD), indicating CB7 forms more stable inclusion complex with $BP(OH)_2$ than that of β-CD. Observations from steady-state emission studies show that the enhancement in fluorescence of $BP(OH)_2$ in CB7 is much higher than that observed in case of β-CD. Though the stoichiometry is same for both the host molecules, binding affinity is 3 times more for CB7:$BP(OH)_2$ (3000 M^{-1}) compared to β-CD:$BP(OH)_2$ (900 M^{-1}). Pico-second time resolved study indicates that $BP(OH)_2$ exhibits bi-exponential fluorescence decay in both the hosts. But the lifetime of $BP(OH)_2$ in CB7 complex (~8.5 ns) is much higher than that of β-CD (~5 ns). This further confirms that stability of

$BP(OH)_2$ in $BP(OH)_2$:CB7 complex is higher than that in $BP(OH)_2$:β-CD. Therefore, all the above results conclude that the behaviour of nano-cavity is different for CB7 from β-CD.

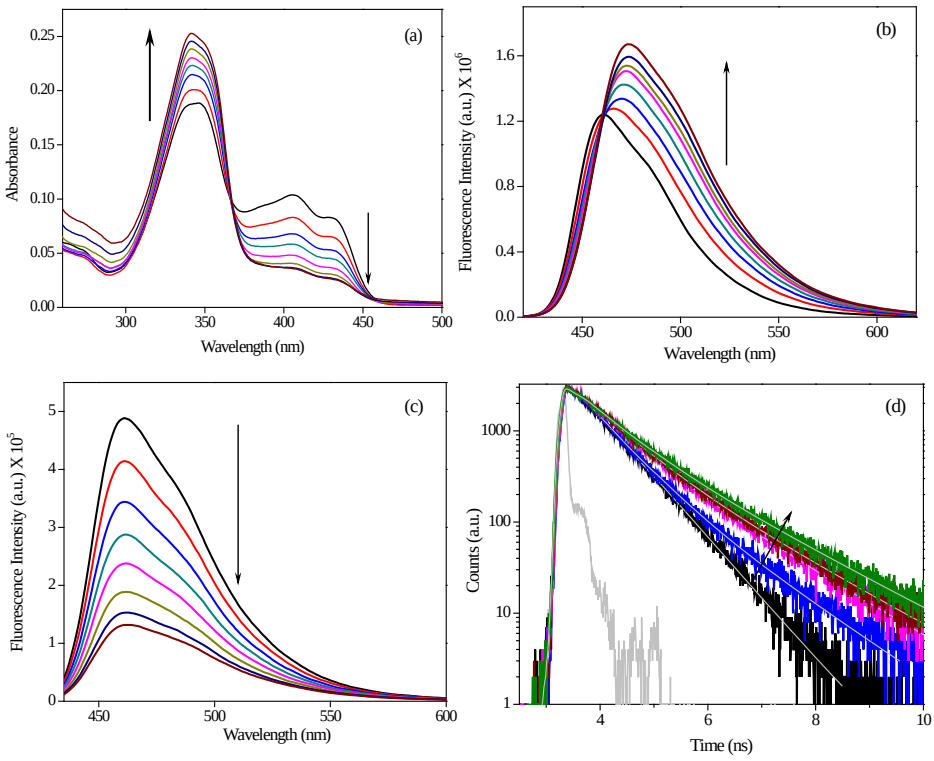

Figure 4b.4. Absorption (a), Emission (b) (λ_{ex}=345 nm), (c) (λ_{ex}=425 nm) spectra and (d) fluorescence decay transients (λ_{ex}=375 nm) of $BP(OH)_2$ in presence of 0 to 14 mM of β-CD.

Femtosecond transients of $BP(OH)_2$ in water and in presence of CB7/β-CD are shown in **Figure 4b.5**. The fluorescence up-converted decay profile of $BP(OH)_2$ in water exhibits growth and decay component having lifetime of ~30 ps and 650 ps, respectively. Notably, although there are reports about the fluorescence up-converted decay profiles of $BP(OH)_2$ in several aprotic and protic solvents.[28] The longer lifetime component of ~650 ps can be assigned to the lifetime of diketo (DK) form after ESIDPT process and is consistent with TCSPC results. We have already mentioned that ESIDPT process can take place via concerted or a two step sequential mechanism.[10-14] The concerted and first step of sequential process takes place in <50 fs time scale (**Scheme 4b.1**), which cannot be detected from the present setup (IRF = 350 fs); whereas the second step of sequential process (MK to DK conversion) takes place in several tens of

picosecond time scale (**Scheme 4b.1**).[15] Therefore, the ultrafast instantaneous rise component of ~35 ps reflects the proton transfer dynamics during conversion of mono (MK) to diketo (DK) form of $BP(OH)_2$. However, this proton transfer dynamics in water is slower than the reported time in hexane, which takes place in ~10 ps.[15] The sluggish PT dynamics in water may be attributed to the presence of hydrogen bonding network, which disturbs and competes with the proton transfer process from MK to DK form in the excited state. In presence of CB7, significant change in the fluorescence decay transient of $BP(OH)_2$ is observed (**Figure 4b.5**).

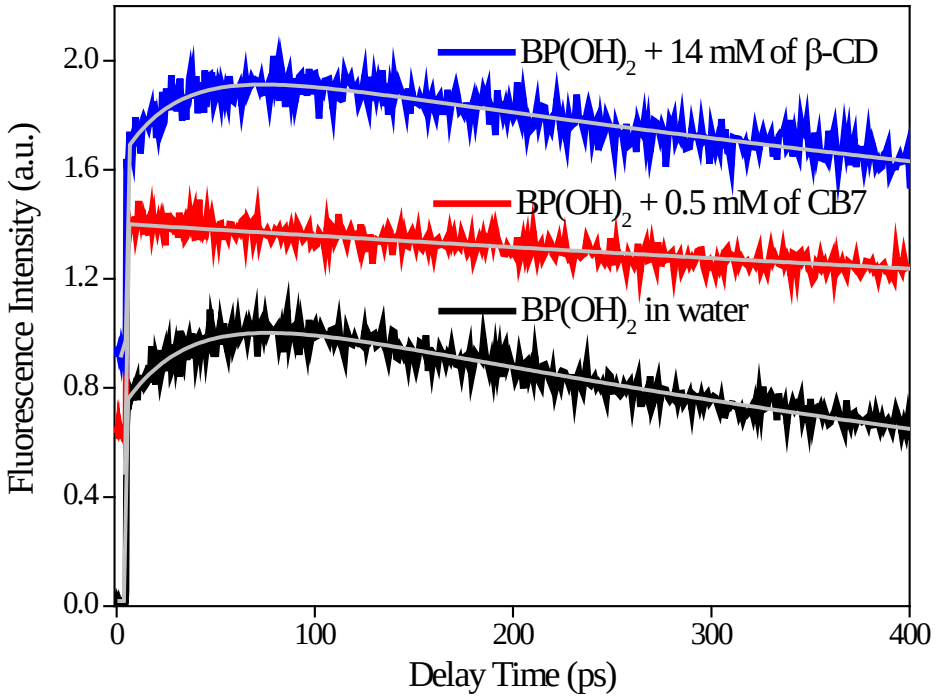

Figure 4b.5. Femtosecond fluorescence transients of $BP(OH)_2$ in water, in presence of 500 μM of cucurbit[7]uril (CB7), and in presence of 14 mM of β-cyclodextrin (β-CD), collected at 465 nm (λ_{ex}=380 nm). Best fit is shown as grey coloured line.

Astonishingly, fluorescence up-converted transient of $BP(OH)_2$ is devoid of any growth component in presence of CB7, and it exhibits single exponential fluorescence decay having lifetime of >3 ns, which may be ascribed to the lifetime of DK form inside the CB7 nano-cavity. This observation clearly indicates that MK→DK conversion process is getting inhibited inside CB7 nano-cavity. The steady state and TCSPC results suggest that even inside the CB7 cavity the final emission is coming from the DK form of $BP(OH)_2$. Therefore, absence of growth

component infers that the concerted mechanism, which occurs in <100 fs time scale, is favoured over two step sequential proton transfer process (takes place in several tens of picoseconds time scale) inside the CB7 nano-cavity. The reason of favoring concerted pathway over sequential pathway may be attributed to the absence of water molecules inside the cavity of CB7. Very recently, Biedermann et al. reported that the largest energy gain in the course of the complexation between neutral guests and CBn occurs due to the complete removal/displacement of water molecules from the nano-cavity of CB7.[29] The absence of intermolecular hydrogen bonding network with water molecules destabilize the MK form inside the CB7 cavity, and thereby, it blocks the proton transfer process via MK to DK form. As a result, $BP(OH)_2$ encaged with CB7 exhibits ESIDPT via concerted mechanism in which two protons move simultaneously from hydroxyl groups toward the pyridyl-ring nitrogen atoms. $BP(OH)_2$ shows biexponential transient (28 ps and 1 ns) feature inside the β-CD cavity, likewise in water (**Figure 4b.5**). Here it is relevant to mention that the features of steady state and TCSPC results of $BP(OH)_2$ with β-CD are very similar to that CB7. Hence, it is expected that the feature of PT dynamics of $BP(OH)_2$ in both the host systems would be very similar. However, the presence of ultrafast rise/growth component of ~28 ps clearly infers that proton transfer dynamics inside β-CD cavity is significantly different from that of CB7 nano-cavity. Moreover, the appearance of ultrafast rise/growth component of ~28 ps demonstrates sequential proton transfer pathway is feasible inside the β-CD host. Notably, in case of β-CD water molecules can access in the vicinity of included molecule,[30] so that $BP(OH)_2$ can form intermolecular hydrogen bonding network with water even inside the cavity, likewise in water. The presence of water shell around $BP(OH)_2$ inside the β-CD cavity is the main reason for the appearance of ultrafast growth component (~28 ps) corresponding to sequential two step proton transfer pathway, which is absent inside the CB7 cavity.

4b.2d. Docking and Quantum Chemical Calculations:

To obtain the molecular picture of orientation of $BP(OH)_2$ in the inclusion complexes as well as to gain insight into the stabilization achieved due to encapsulation, we have docked the DE form of $BP(OH)_2$ into cucurbit[7]uril (CB7), followed by DFT quantum chemical optimization. Since the docking and geometry optimization were done without consideration of any solvent and other parameters, these geometries provide only qualitative picture of the structures in the ground state. Optimized structure of the inclusion complex is shown in **Figure 4b.6**.

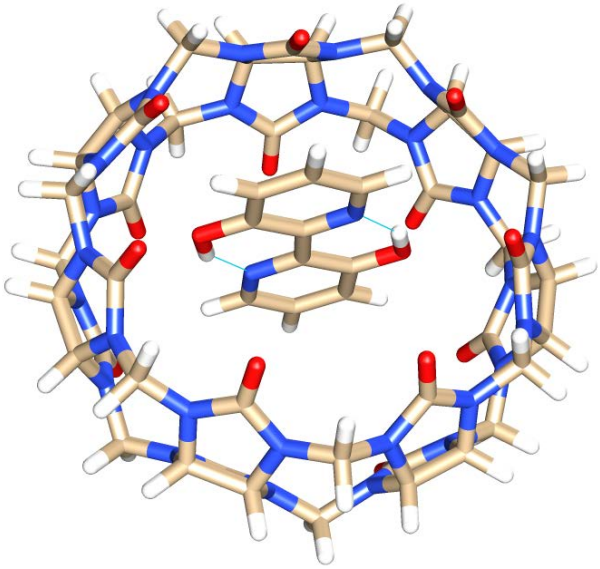

Figure 4b.6. Optimized structure of 1:1 docked CB7:$BP(OH)_2$ complex.

Further, we have evaluated the interaction energy for the inclusion complex by subtracting the energy of individual molecules from the complex.[31] The interaction energy obtained from quantum chemical optimization method is negative (-31.90 kcal mol^{-1}), suggesting that 1:1 inclusion complex formation between $BP(OH)_2$ and CB7 is energetically feasible. It is clear from the geometry optimized structure of inclusion complex that $BP(OH)_2$ molecule is completely sequestered in the centre of CB7 cavity (**Figure 4b.6**). Therefore, theoretical studies support the experimental evidences that the hydrophobic nano-cavity of CB7 is responsible for the complexation process which affects the photophysical properties of $BP(OH)_2$.

4b.3. Conclusion:

In this work, host-guest interactions between the molecular containers cucurbit[7]uril (CB7) and β-cyclodextrin (β-CD)) and $BP(OH)_2$ are investigated with the help of steady state and time-resolved fluorescence measurements. Ground state absorption study indicates that the conversion of diketo (DK) to dienol (DE) form in $BP(OH)_2$ takes place in presence of CB7. Steady state and time-resolved fluorescence studies confirm that the main emissive species is DK form of $BP(OH)_2$ inside the CB7 nano-cavity. Femtosecond fluorescence upconversion measurements are employed to elucidate the mechanism of ultrafast proton transfer dynamics of $BP(OH)_2$

inside nano-containers (CB7 and β-CD). Femtosecond up-conversion study of $BP(OH)_2$ in water reveals that the two step sequential proton transfer process via MK to DK form appears as a growth component (~35 ps) in the up-converted signal. Astonishingly, the fluorescence up-converted signal of $BP(OH)_2$ is devoid of any growth component in presence of CB7, and it supports that concerted mechanism of proton transfer (takes place in <100 fs time scale) is present inside the nano-cavity of CB7 instead of two step-sequential process of PT dynamics. Interestingly, two step sequential process is feasible mechanism in case of β-CD, as inside the nano-cavity of β-CD the growth component of ~28 ps is detected. The reason for this observation is the presence of surrounding water solvation network of $BP(OH)_2$ inside the cavity of β-CD, which is absent in case of CB7 nano-cavity. Finally, docking and DFT quantum chemical calculations have been employed in deciphering the molecular orientation of $BP(OH)_2$ in inclusion complex with the macrocyclic host. Theoretical calculations confirm that $BP(OH)_2$ molecule resides at the centre of the hydrophobic nano-cavity of CB7, and thereby it is believed to be affected the double proton transfer dynamics significantly.

4b.4. Reference:

1. D. Zhong, A. Douhal and A. H. Zewail, *Proc. Natl. Acad. Sci.U.S.A.*, 2000, **97**, 14056-14061.
2. C. Rodríguez-Rodríguez, N. Sánchez de Groot, A. Rimola, A. n. Álvarez-Larena, V. Lloveras, J. Vidal-Gancedo, S. Ventura, J. Vendrell, M. Sodupe and P. González-Duarte, *J. Am. Chem. Soc.*, 2009, **131**, 1436-1451.
3. M. Suresh, D. A. Jose and A. Das, *Organic Letters*, 2007, **9**, 441-444.
4. R. F. Service, *Science*, 2005, **310**, 1762-1763.
5. K.-C. Tang, M.-J. Chang, T.-Y. Lin, H.-A. Pan, T.-C. Fang, K.-Y. Chen, W.-Y. Hung, Y.-H. Hsu and P.-T. Chou, *J. Am. Chem. Soc.*, 2011, **133**, 17738-17745.
6. O. K. Abou-Zied, *J. Photochem. Photobiol., A*, 2006, **182**, 192-201.
7. H. Bulska, *Chem. Phys. Lett.*, 1983, **98**, 398-402.
8. H. Bulska, A. Grabowska and Z. R. Grabowski, *J. Lumin.*, 1986, **35**, 189-197.
9. R. Wortmann, K. Elich, S. Lebus, W. Liptay, P. Borowicz and A. Grabowska, *J. Phys. Chem.*, 1992, **96**, 9724-9730.
10. H. Zhang, P. van der Meulen and M. Glasbeek, *Chem. Phys. Lett.*, 1996, **253**, 97-102.

11. D. Marks, P. Prosposito, H. Zhang and M. Glasbeek, *Chem. Phys. Lett.*, 1998, **289**, 535-540.
12. P. Toele, H. Zhang and M. Glasbeek, *J. Phys. Chem. A*, 2002, **106**, 3651-3658.
13. V. Barone, A. Palma and N. Sanna, *Chem. Phys. Lett.*, 2003, **381**, 451-457.
14. R. Gelabert, M. Moreno and J. M. Lluch, *ChemPhysChem*, 2004, **5**, 1372-1378.
15. F. V. R. Neuwahl, P. Foggi and R. G. Brown, *Chem. Phys. Lett.*, 2000, **319**, 157-163.
16. O. K. Abou-Zied, *J. Phys. Chem. B*, 2009, **114**, 1069-1076.
17. D. De and A. Datta, *J. Phys. Chem. B*, 2011, **115**, 1032-1037.
18. O. K. Abou-Zied, *J. Phys. Chem. B*, 2007, **111**, 9879-9885.
19. D. De, K. Santra and A. Datta, *J. Phys. Chem. B*, 2012, **116**, 11466-11472.
20. S. Mandal, S. Ghosh, H. H. K. Aggala, C. Banerjee, V. G. Rao and N. Sarkar, *Langmuir*, 2012, **29**, 133-143.
21. K. Rurack, K. Hoffmann, W. Al-Soufi and U. Resch-Genger, *J. Phys. Chem. B*, 2002, **106**, 9744-9752.
22. P. Prosposito, D. Marks, H. Zhang and M. Glasbeek, *J. Phys. Chem. A*, 1998, **102**, 8894-8902.
23. E. S. S. Iyer and A. Datta, *J. Phys. Chem. B*, 2012, **116**, 5302-5307.
24. S. Mandal, S. Ghosh, C. Banerjee, J. Kuchlyan and N. Sarkar, *J. Phys. Chem. B*, 2013, **117**, 12212-12223.
25. S. Mandal, S. Ghosh, C. Banerjee, J. Kuchlyan and N. Sarkar, *J. Phys. Chem. B*, 2013, **117**, 6789-6800.
26. H. A. Benesi and J. H. Hildebrand, *J. Am. Chem. Soc.*, 1949, **71**, 2703-2707.
27. O. K. Abou-Zied and A. T. Al-Hinai, *J. Phys. Chem. A*, 2006, **110**, 7835-7840.
28. D. Marks, H. Zhang, M. Glasbeek, P. Borowicz and A. Grabowska, *Chem. Phys. Lett.*, 1997, **275**, 370-376.
29. F. Biedermann, V. D. Uzunova, O. A. Scherman, W. M. Nau and A. De Simone, *J. Am. Chem. Soc.*, 2012, **134**, 15318-15323.
30. S. Vajda, R. Jimenez, S. J. Rosenthal, V. Fidler, G. R. Fleming and E. W. Castner, *J. Chem. Soc., Faraday Trans.*, 1995, **91**, 867-873.
31. F. Avila-Salas, C. Sandoval, J. Caballero, S. Guiñez-Molinos, L. S. Santos, R. E. Cachau and F. D. González-Nilo, *J. Phys. Chem. B*, 2012, **116**, 2031-2039.

4c. Excited State Proton Transfer Dynamics of an Eminent Anticancer Drug, Ellipticine in Octyl Glucoside Micelle

4c.1. Introduction and Motivation of the Work:

Alkyl glucosides are the class of non-ionic surfactants, widely used in food, cosmetic and pharmacy products. Alkyl glucosides contain a hydrophilic part comprised of glucose moiety, and a hydrophobic part consisting of hydrocarbon chain. These sugar surfactants are non-toxic and can be synthesized from renewable resources.[1,2] Another important aspect of these surfactants is their biodegradable nature. The main reason for the biodegradability is the presence of glucoside linkage, which widely occurs in nature, and its formation and breakage are controlled by different glucosidases.[3] These properties make them perfect substitutes of other surfactants, which are potentially dangerous to the environment. These biocompatible OBG surfactants are frequently used to study the dissolution and formation of biological membranes as well as the stabilization of proteins.[4-8] Considering the bio-compatible behavior of the alkyl glucoside, the micellar aggregate of these sugar based surfactants may be used as potential drug delivery carrier. It is important to understand the effect of the micellar confinement on solubility and stability of drug in order to use it in pharmaceutical field. Moreover, the dynamics study of drug molecules inside the glucoside micelle is very essential in order to get insight into the effect of confined environment on the stability of the drug molecules. In the present study, we have studied the modulation of proton transfer dynamics of a well known anticancer drug, ellipticine, when it is encapsulated inside one of the well studied glucoside micelle, namely, octyl-β-D-glucoside (OBG) micelle. We have chosen octyl-β-D-glucoside (OBG) because many properties such as phase diagram, structural behavior of the OBG have been extensively studied by various techniques.[9-21]

Ellipticine (5,11-dimethyl-6H-pyrido[4,3-b]carbazole), a pyridocarbazole alkaloid, a potential anticancer drug, was first isolated from the leaves of *Ochrosia elliptica* by Goodwin et al. in 1959.[22] Ellipticine (EPT) intercalates in DNA and inhibits the activity of DNA topoisomerase-II, which results inhibition of DNA replication and transcription process of RNA.[23-25] Due to the presence of basic pyridine nitrogen,[26] EPT exists in two prototropic forms depending on the pH as well as environmental polarity (**Scheme 4c.1**). It was found that EPT

exists as neutral form in non-polar and hydrophobic media, and exhibits emission peak in the range of 410-440 nm.[27] Ellipticine exists as protonated form in hydrophilic medium and emits at ~530 nm; whereas in methanol and ethylene glycol the drug exhibits concomitant dual emission at ~430 nm and ~510 nm.[27-29] Miskolczy *et al.* assigned the red edge emission of EPT to excited state proton transfer reaction by the solvent.[28] Recently, Samanta and coworkers reported solvent mediated excited state intramolecular proton transfer from the pyrrole nitrogen to pyridine nitrogen as origin of fluorescence from protonated EPT.[29]

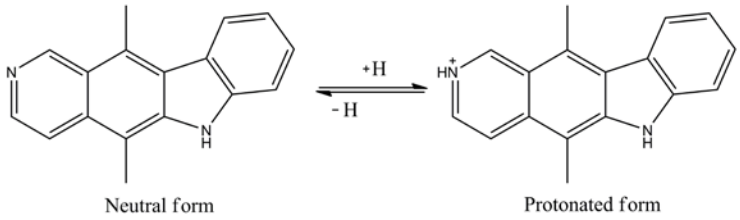

Scheme 4c.1. Different prototropic forms of ellipticine.

Previous studies have revealed that ellipticine exists as neutral form in cell cytoplasm and protonated form at nucleus.[26] Although ellipticine is considered as a potential anti-tumor drug, the major disadvantages in the usage of ellipticine in pharmaceutics are its toxicity and low solubility in aqueous solution. It is a big challenge for the researchers to improve the solubility and targeted delivery of the drug using biocompatible drug carriers. To understand how ellipticine is transported to its target, it is very important to establish a relationship between the environment and the photophysical properties of EPT. For that purpose the photophysical properties of the drug have been investigated in several confined and self-assembled systems such as cyclodextrins, cucurbiturils, micelles, reverse micelles, vesicles, bile salts and polymers.[30-35] Although several attempts have been made on photophysical properties of the drug in many biological and biomimicking media, to date excited state proton transfer dynamics of EPT has seldom been monitored in the aforementioned confined environments. Herein, we report the encapsulation of EPT drug in OBG micelles and the consequences of confinement on photophysical properties of EPT using steady state and time-resolved spectroscopic techniques. The focus of this work is to understand the effect of confinement on proton transfer dynamics of

ellipticine. Interestingly, we have observed that proton transfer is dramatically slowed down when the drug molecules are encapsulated in OBG micelles, which resulted emission from both the neutral and protonated forms of EPT. We have also constructed time resolved emission spectrum (TRES) and time resolved area normalized emission spectrum (TRANES), which provides information about the existence of multiple emissive species in the excited state. Finally, these results are compared with other conventional micelles such as CTAB, SDS and Triton-X, and we have observed that any such excited state proton transfer process is absent in the above mentioned three micelles.

4c.2. Results and Discussion:

4c.2a. Steady Sstate Measurements:

Absorption spectra of EPT in buffer and in presence of OBG are shown in **Figure 4c.1a**. The drug in buffer exhibits several peaks in 250-450 nm region with a peak maximum at 300 nm and two shoulders at 350 nm and 420 nm. Earlier reports divulge that these are the characteristic peaks of protonated form of EPT.[26] On gradual addition of OBG, absorption profile of EPT does not change significantly until certain concentration (≤ 25 mM). At higher concentration of OBG (≥ 26 mM), noteworthy changes are observed in absorption spectra (**Figure 4c.1a**). The peaks representing protonated form (300 nm and 425 nm) are almost vanished and two new peaks are appeared at ~280 nm and ~380 nm. These new peaks were previously observed in many instances, when EPT was incorporated in hydrophobic media.[35-37] Therefore, the above observations infer that EPT experiences hydrophobic environment above certain concentration of OBG (26 mM) and thereby, ground state neutral form generates at the cost of protonated form of EPT. Interestingly, the concentration of OBG (≥26 mM) after which the changes in absorption spectra of EPT observed is in good agreement with the previously reported critical micellar concentration (CMC) of OBG.[38]

Emission profiles of EPT in phosphate buffer and in presence of OBG are shown in **Figure 4c.1b**. EPT exhibits single emission maximum at 530 nm, which is believed to be originated from protonated form of the drug.[26] With the gradual addition of OBG to the buffer containing EPT solution, the fluorescence intensity at 530 nm slightly increases along with a small hump in the 420-450 nm region. However, at concentration ≥26 mM, the 530 nm peak

shoots up with a prominent new peak at 440 nm (**Figure 4c.1b**). The 440 nm peak also grows up and becomes comparable to the 530 nm peak at higher concentration of OBG. This kind of fluorescence switch of EPT from 530 nm in buffer to 440 nm in micelles is unique and can be visualized directly from the color change of solution from green to cyan (**Figure 4c.2**).

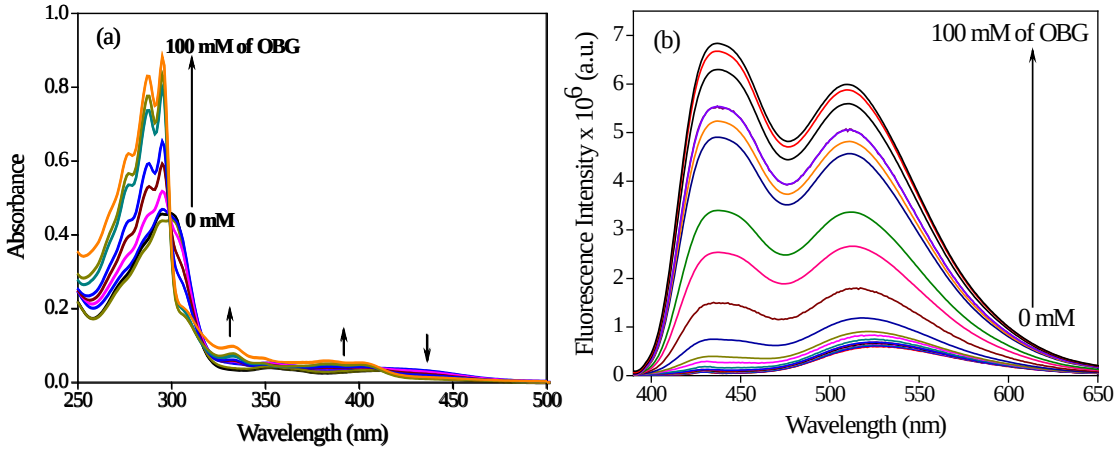

Figure 4c.1. Absorption (a) and Emission (λ_{ex} = 375 nm) (b) spectra of EPT in pH 7 buffer with increasing concentration of OBG (0 mM to 100 mM).

It is already well established that EPT residing in hydrophobic environment emits the blue region (420-440 nm),[36,37] and it is believed to be appeared from the neutral form of the drug. Thus, we believe that the newly appeared peak at 440 nm is coming from the neutral drug molecules. Hence, the appearance of blue emission at 440 nm demonstrates that conversion of the drug takes place from protonated to neutral form in presence of OBG micellar environment. However, if this switching of the form would be the case for the increment of neutral form peak intensity, then the intensity at 440 nm, which is signature peak of neutral form of EPT, should have been increased at the cost of protonated form peak intensity at 530 nm. Astonishingly, the intensity at 530 nm concomitantly increases along with 440 nm peak with the gradual hike in OBG concentration. Here it is necessary to mention that absorption results confirmed that transformation takes place from protonated to neutral form in OBG micelle (**Figure 4c.1a**).

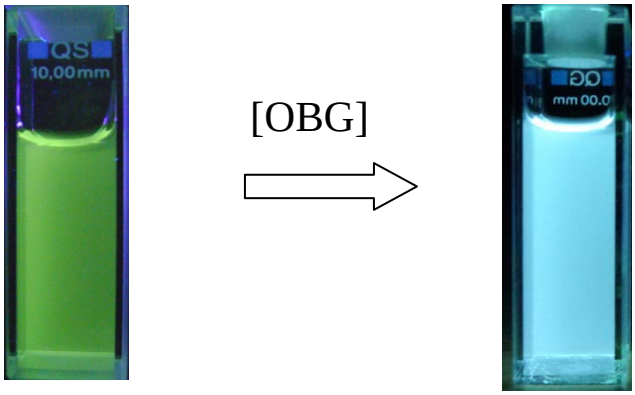

Figure 4c.2. Fluorescence switch of EPT in presence of OBG micelles (λ_{ex} = 360 nm).

Moreover, the excitation spectra monitored at 440 nm and 530 nm are very similar (**Figure 4c.3**). The excitation spectrum monitored at 530 nm, which is the characteristic emission maximum of protonated EPT, shows three bands at 300 nm, 355 nm and 420 nm in buffer (**Figure 4c.3**). In presence of OBG micelles these peaks are shifted to 280 nm, 335 nm and 400 nm, respectively. Moreover, these new peaks observed at 530 nm in OBG micelles are same as the bands observed in excitation spectrum collected at 440 nm which is attributed to neutral form. These results confirm that protonated form is generated in the excited state at the cost of neutral form via excited state proton transfer.

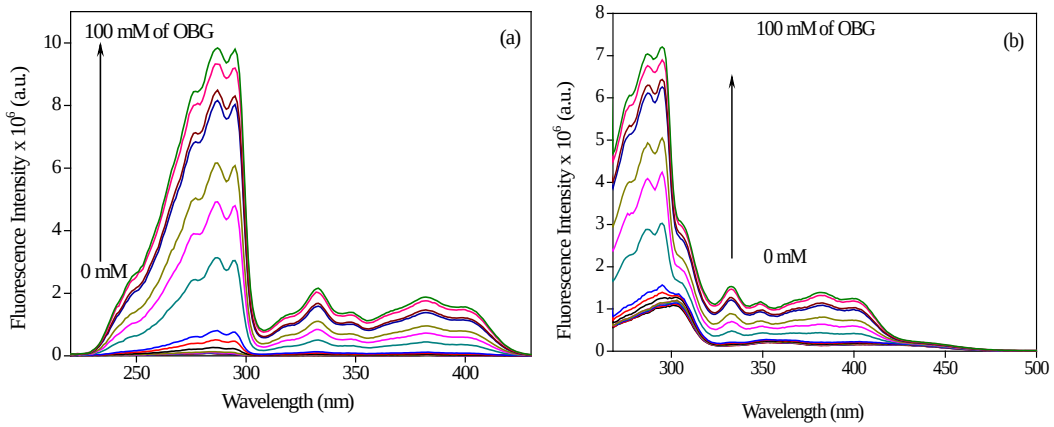

Figure 4c.3. Excitation spectra of EPT in buffer with increasing concentration of OBG (0 mM to 100 mM) collected at 440 nm (a) and 530 nm (b).

Based on above observations, we envisage that although in the ground state the population of neutral form of the drug increases in the micellar environment (probably due to

decrease surrounding polarity of the drug), in the excited state some of the neutral form of drug molecules are converted to the protonated form by excited state proton transfer process. As a result, the intensity of both the neutral as well as protonated form increases with OBG concentration.

The above results indicate that drug molecules are not buried completely inside the hydrophobic domain of the micelle, as protonated species in the excited state is not at all stable in the hydrophobic domain of the micelle. We guess the drug molecules reside near the palisade layer of the micelle, where hydrophilic sugar head groups of the surfactant are present. In order to confirm the effect of glucose moieties present in the micelle, the drug fluorescence was monitored with increasing concentration of glucose. Neither intensity enhancement nor new peak appearance was observed in emission spectrum of EPT up to 500 mM of glucose (**Figure 4c.4**) and it suggests that presence of sugar moieties are not solely responsible for the observed photophysics of the EPT.

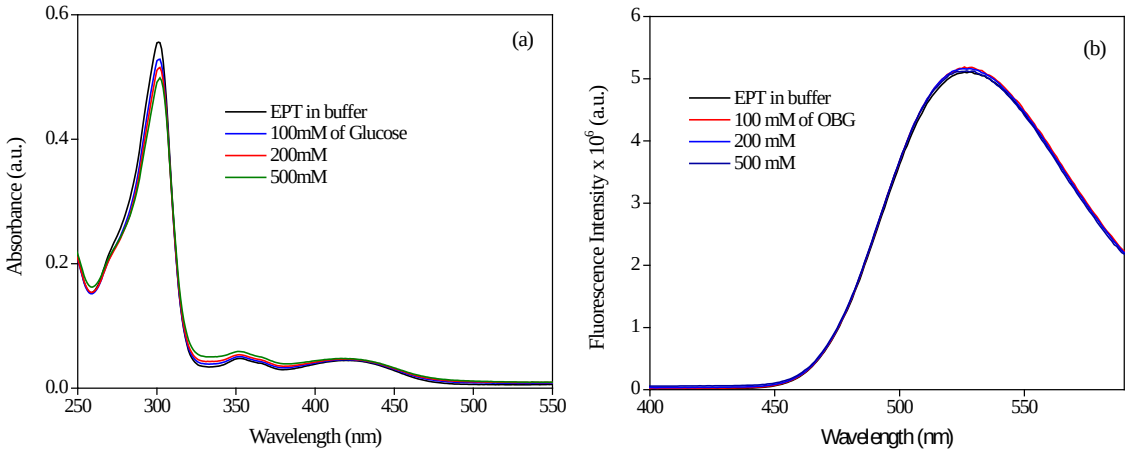

Figure 4c.4. Absorption (a) and Emission (b) spectra of EPT in pH 7 buffer with increasing concentration of glucose (0 mM to 500 mM).

To verify the effect of confined environment of the micelle, we have also collected the emission spectra of EPT in three different types of micelles, namely cationic, anionic and neutral micelles and the observed results are in good agreement with the literature reports.[31] In case of anionic SDS micelles, EPT exhibits protonated peak at 530 nm, whereas it shows peak at ~440

nm in CTAB micelle (**Figure 4c.5**). Notably, although TX-100 surfactant head group contains –OH group, the micellar environment of TX-100 does not exhibit any protonated peak of ellipticine at 530 nm (**Figure 4c.5**). Therefore, the appearance of both the peaks in case of OBG micelles is believed to be an outcome of confined as well as polarity of the surrounding environments. Although we have proposed that excited state proton transfer is the origin of green emission in OBG micellar environment, in order to gain deeper insight into the excited state proton transfer process we have performed time resolved measurements, which is discussed in the next section.

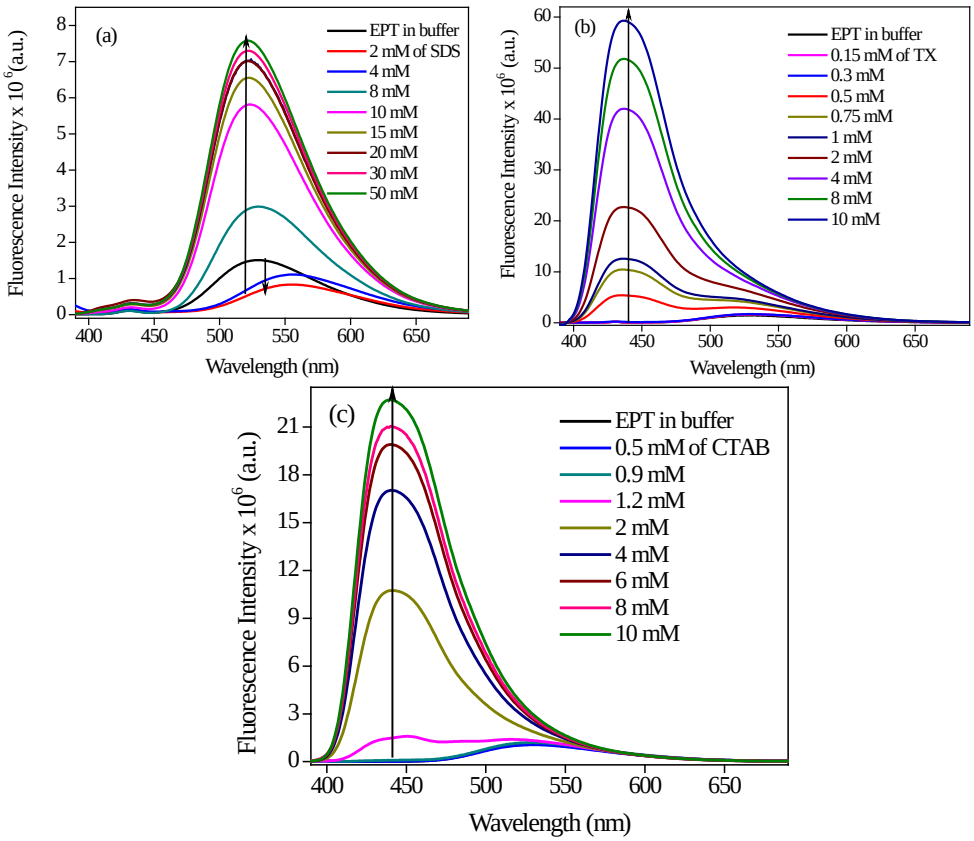

Figure 4c.5. Emission spectra of EPT in buffer with increasing concentration of (a) SDS (0 mM to 50 mM) (b) Triton-X (0 mM to 10 mM) and (c) CTAB (0 mM to 10 mM). (λ_{ex} = 375 nm).

4c.2b. Time Resolved Fluorescence Study:

Time-resolved fluorescence measurement is an excellent technique to monitor the excited state dynamics of molecules and is a unique method to identify multiple emissive species present in a given system.[39] Emission decay profiles of EPT in absence and in presence of OBG are collected at 440 nm and 530 nm in order to monitor the excited state dynamics of both neutral and protonated species, respectively (**Figure 4c.6**). As shown in **Table 4c.1**, protonated EPT (at 530 nm) exhibits bi-exponential decay profile in buffer having individual lifetime components of ~2 ns (87%) and ~6 ns (13%) with an average lifetime value of ~2.5 ns. In the present scenario, the assignment of individual component is complicated, as our lifetime profile consists of only decaying components. In case of methanol, where people observed dual emission, the decay profile at longer wavelength consists of a growth followed by decaying component. Moreover, the growth component lifetime was exactly matching with the decaying component of shorter wavelength. Therefore, it was easy to predict that the growth component to the excited state proton transfer process. As our decay profile in buffer is devoid of any growth component, it is difficult to assign individual components.

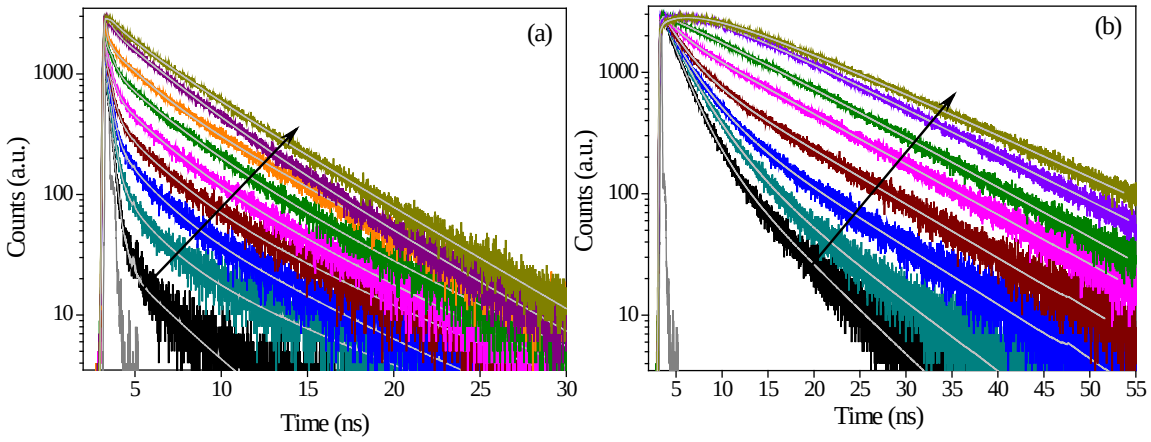

Figure 4c.6. Time resolved fluorescence decays of EPT in pH 7 buffer with increasing concentration of OBG (0 mM to 100 mM) collected at 440 nm (a) and 530 nm (b) (λ_{ex} = 375 nm).

Table 4c.1. Fluorescence decay parameters of ellipticine in presence of OBG (0 to 100 mM) (λ_{ex} = 375 nm) collected at

(a) 530 nm

Concentration of OBG	τ_1(ns)	τ_2(ns)	τ_3(ns)	a_1	a_2	a_3	χ^2	τ_{avg}[#](ns)
Buffer	1.93	5.93	-	0.87	0.13	-	1.02	2.45
10 mM	2.03	5.61	-	0.85	0.15	-	1.02	2.57
17 mM	2.08	5.32	-	0.81	0.19	-	1.06	2.70
19 mM	2.25	6.13	-	0.83	0.17	-	1.03	2.91
23 mM	2.29	6.85	-	0.82	0.18	-	1.08	3.11
25 mM	2.30	9.76	-	0.62	0.38	-	1.02	5.13
26 mM	1.88	10.47	-	0.31	0.69	-	1.03	7.80
27 mM	-	10.77	4.33	-	1.16	-0.16	1.05	11.80
30 mM	-	11.52	3.79	-	1.89	-0.89	1.05	18.40
50 mM	-	12.27	3.82	-	2.17	-1.17	1.10	21.63
100 mM	-	12.82	4.27	-	2.17	-1.17	1.05	22.82

(b) 440 nm

Buffer	0.04	0.29	2.27	0.61	0.38	0.01	1.11	0.16
10 mM	0.05	0.33	3.56	0.66	0.32	0.02	1.12	0.21
17 mM	0.05	0.36	3.80	0.68	0.30	0.02	1.08	0.22
19 mM	0.05	0.38	4.02	0.63	0.34	0.03	1.05	0.28
23 mM	0.09	0.62	4.33	0.52	0.29	0.19	1.03	1.05
25 mM	0.25	1.93	4.21	0.35	0.29	0.37	1.05	2.20
26 mM	-	1.46	4.39	-	0.35	0.65	1.07	3.36
27 mM	-	1.77	4.27	-	0.35	0.65	1.05	3.40
30 mM	-	2.02	4.37	-	0.34	0.66	1.06	3.57
50 mM	-	2.19	4.27	-	0.31	0.69	1.01	3.62
100 mM	-	2.01	4.23	-	0.30	0.70	1.04	3.56

[#] $\tau_{avg} = a_1\tau_1 + a_2\tau_2$

With the successive addition of OBG, the average fluorescence lifetime of EPT collected at 530 nm steadily increases until 26 mM of OBG. After 26 mM of OBG, the average lifetime shoots up to ~20 ns (**Figure 4c.6** and **Table 4c.1**). The increased average lifetime infers that the stability of protonated EPT is enhanced in presence of OBG micellar environment, as it is evident that OBG forms micellar assembly after 26 mM. The most intriguing observation is the appearance of ~4 ns growth component after 26 mM of OBG (τ_3 in **Table 4c.1a**). Moreover, the contribution of growth component increases with OBG concentration. Notably, this kind of long growth component of EPT was not observed in other confined environments, like reverse micelle, lipid bilayers, cyclodextrin/cucurbituril nano-cavity etc., and in that sense the growth feature observed in lifetime profile is unique. There are two possibilities for the appearance of growth component in the fluorescence transient; either due to the slow solvation dynamics or due to the excited state reaction, such as proton transfer process. In order to verify the first possibility, we have collected emission transients at longer wavelengths (red edge side) and the results depict no significant change in the growth component. This finding confirms the growth component appeared in the decay profile is not because of solvation, but may be due to the excited state proton transfer process. To unveil the proton transfer mechanism, we have further collected fluorescence transients at 440 nm, which is believed to be originated from neutral form of the drug. In buffer medium, EPT exhibits tri-exponential decay at 440 nm with individual lifetime components of ~40 ps, ~290 ps and ~2.3 ns exhibiting an average lifetime of ~160 ps. It is evident from **Figure 4c.1b** that the intensity of EPT at 440 nm is negligibly small in buffer medium. Moreover, protonated EPT also contributes significantly towards the intensity at 440 nm, and therefore, we believe the decay feature observed at 440 nm cannot be attributed solely to the neutral EPT molecules. However, we have collected the decay profile even at 440 nm in order to compare the dynamics of neutral EPT molecules generated in presence of OBG micellar environment. It is clear from the lifetime results that the average lifetime collected at 440 nm, which is believed to be originated from neutral drug, steadily increases with addition of OBG and jumps up to ~4 ns at ≥26 mM of OBG (CMC of OBG micelle). It is interesting to notice that the growth component (~4 ns) observed at 530 nm is in good agreement with one of the lifetime components collected at 440 nm (**Table 4c.1b**). This confirms that protonated form generates at the cost of neutral form, and the conversion of neutral to protonated form takes place through excited state proton transfer process. To confirm the presence of two different types of species in the excited state,

we have further constructed time resolved area normalized emission spectrum (TRANES), a recently developed technique to explore excited state components. TRANES method is a one-step extension of the commonly used time resolved emission spectrum (TRES) analysis.[40,41] TRES and TRANES of EPT between time 0.1 and 30 ns in presence of OBG micelles are shown in **Figure 4c.7**. A clear isoemissive point at 480 nm is noticeable in TRANES, indicating that the existence of equilibrium between neutral and protonated forms of the drug in the excited state. It is clear from TRANES that initial population is dominated by neutral species, however, at sufficiently longer time-scale the protonated species becomes dominated compared to the neutral one. This further supports our conjecture that protonated species generate at the cost of neutral one in the excited state. It is already discussed that the lifetime of protonated species consists of growth component (~4 ns), which is believed to be the formation time-scale of protonated form. In TRANES, we have also noticed that the reasonable intensity of protonated form is appearing after 4 ns. Therefore, these results confirm that proton transfer process takes place in OBG micelle in ~4 ns time scale. Earlier reports also elucidate that proton transfer dynamics can be slower in constrained environments.[42-46] No isoemissive point is observed below CMC of OBG micelle and in presence of glucose alone.

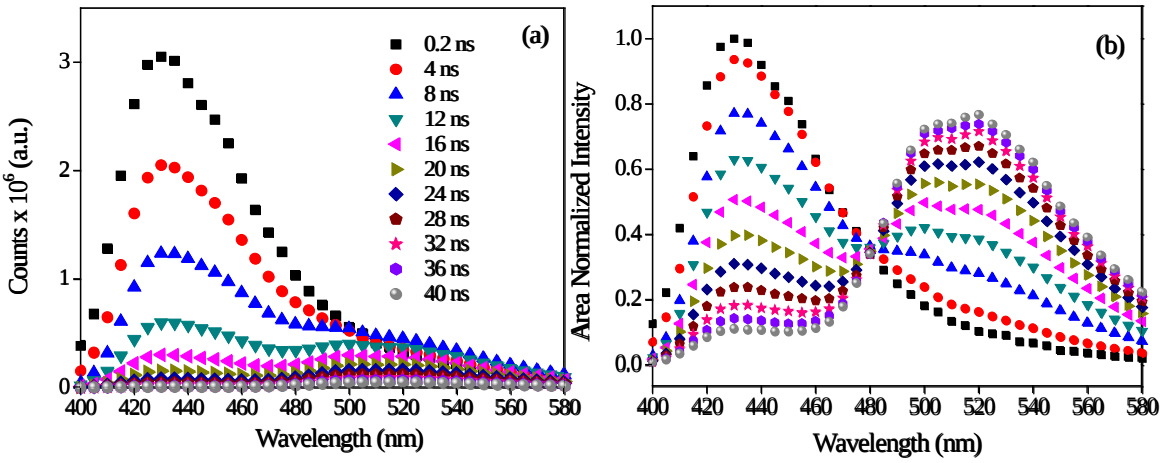

Figure 4c.7. (a) Time resolved emission spectra (TRES) and (b) time resolved area normalized emission spectra (TRANES) of EPT in presence of 100 mM of OBG.

We have also done lifetime measurements for other micelles, like SDS, CTAB and TX-100 micelles (**Figure 4c.8**). There is no growth observed in the decay profiles of EPT in any of SDS, CTAB and TX-100 micelles. Therefore, we believe that slowing down of ESPT process is not taking place in the above mentioned three conventional micellar environments, as we observed in case of OBG micelle. Therefore, based on the above observations, we anticipate that OBG micelle provides some appropriate environment for excited state proton transfer process, and we believe that glucose moiety of OBG has some definite role in this overall ESPT process.

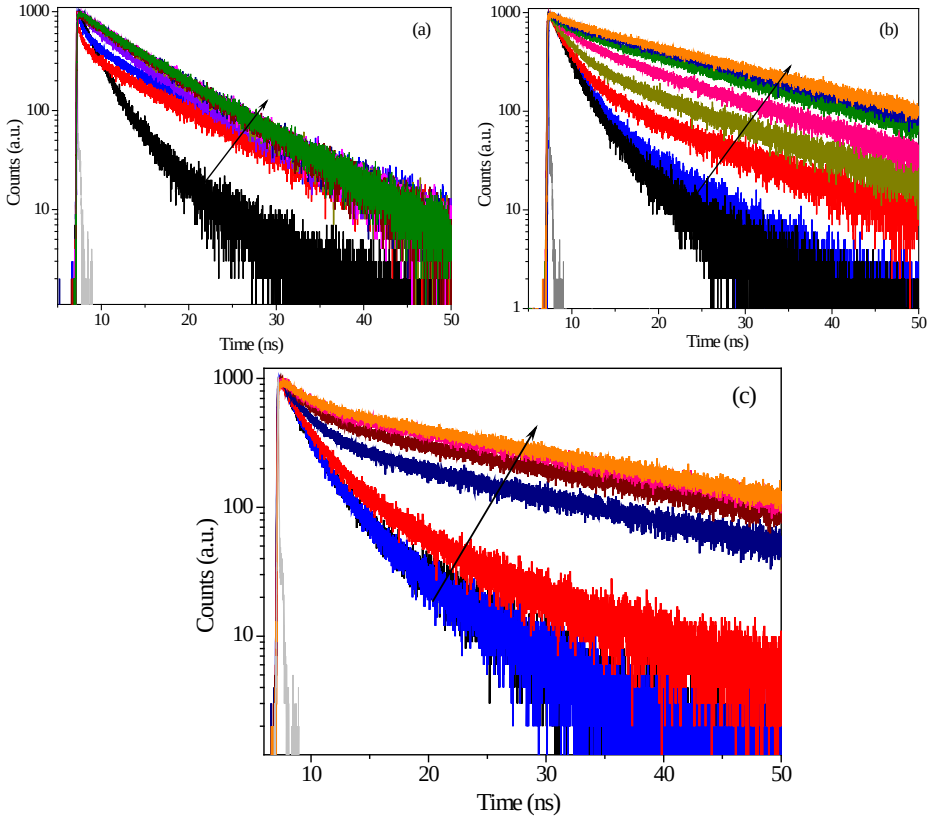

Figure 4c.8. Time resolved emission decays of EPT in buffer with increasing concentration of (a) SDS (0 mM to 50 mM) (b) Triton-X (0 mM to 10 mM) and (c) CTAB (0 mM to 10 mM) collected at 530 nm (λ_{ex} = 375 nm).

Furthermore time-resolved anisotropy measurements are performed to elucidate valuable information regarding the surrounding environment of the drug. The rotational relaxation of EPT in buffer takes place in 120 ps timescale. However, the anisotropy decay profile in presence of

micellar medium exhibits noteworthy changes in the rotational diffusion time (**Figure 4c.9**). The anisotropy decay of EPT in OBG micelles exhibits bi-exponential feature with correlation time constants of 120 ps and 2.6 ns with an average value of ~970 ps. The 120 ps component is believed to be originated from free EPT molecules, whereas 2.6 ns component can be assigned to the micelle encapsulated drug molecules. The increase in the relaxation time from 120 ps to 2.6 ns confirms the encapsulation of drug in OBG micelles, where EPT experiences more restricted environment compared to buffer medium. This further suggests that rigidity also have some role in the ESPT process of the drug in the excited state. The τ_r value is used to determine the hydrodynamic volumes from the Stokes–Einstein relationship. The evaluated effective hydrodynamic diameter of the micelle is 28.09 Å. This value is in good agreement with the reported hydrodynamic diameter.[47]

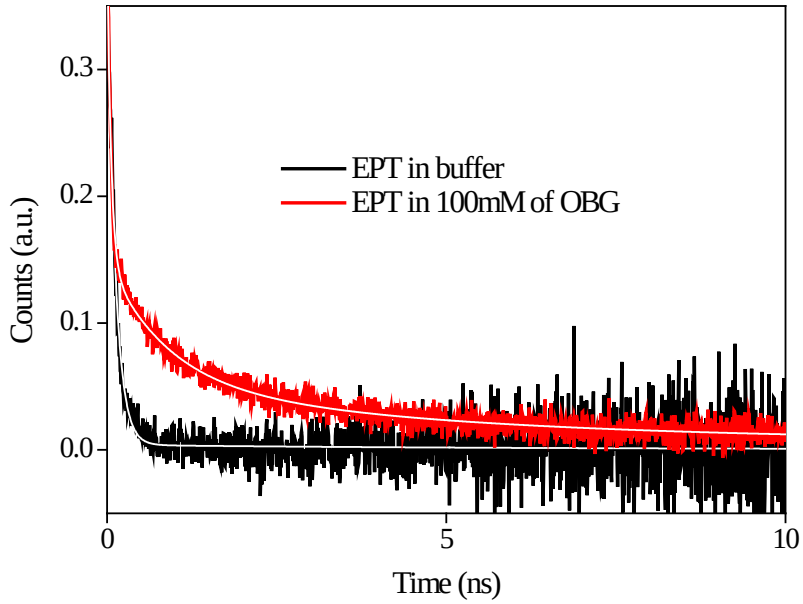

Figure 4c.9. Time resolved anisotropy decays of EPT in pH 7 buffer collected at 530 nm and in presence of 100 mM of OBG collected at 440 nm in emission spectrum (λ_{ex} = 375 nm).

Next we focus on the mechanism of excited state proton transfer in OBG micellar environment based on all the experimental evidences. Absorption data indicates the formation of ground state neutral EPT molecules after CMC of OBG, whereas steady state emission results

infer the presence of both neutral and protonated species in OBG micellar environment. Excitation spectra monitored at 440 nm and 530 nm confirm that protonated species are formed exclusively in the excited state due to excited state proton transfer (**Figure 4c.3**) process. Moreover, the lifetime results suggest the existence of both neutral and protonated species in the excited state, and the protonated species formed at the cost of neutral one in ~4 ns time-scale. Time-resolved anisotropy results depict that the drug experiences restricted environment in OBG micelle. Interestingly, this kind of excited state proton transfer dynamics is not observed in other conventional micellar environments like SDS, CTAB and TX-100. In case of anionic SDS micelles, EPT exhibits protonated peak at 530 nm, whereas in CTAB and TX-100 micelles it shows emission from neutral form at 440 nm. These results can be explained by the interplay of two effects. The first one is the local dielectric constant felt by the EPT, and the second is the local proton concentration at the micellar surface. It is known that the local dielectric constant for all these three micellar systems is around 35-40.[48] Certainly, this environment doesn't favor charged species such as protonated form of EPT, and therefore, neutral form of EPT should be the stable species in all these micellar systems. The absorption and fluorescence spectra of TPT in TX-100 and CTAB micelles support this conjecture. Contrastingly, in SDS system the emission is observed from protonated form instead of neutral form of the drug. This observation can be explained by the negative micellar surface attracting protons and making the local interfacial proton concentration much higher than the bulk solution of pH 7.[49,50] The presence of a higher proton concentration around SDS micelles appears to favor the protonation of the excited EPT under the local environment conditions and to compensate for the low polarity. Interestingly, unlike the other micellar systems, in excited state both neutral and protonated forms are observed in OBG micelles. Based on these observations we envisage that presence of glucose moiety and polarity of confined environment in OBG micelle take part major role for the conversion of neutral to protonated one in the excited state. It is already reported that the glucose molecules at first hydration shell of OBG micellar surface are projected inwards (away from bulk water) in the direction of the micellar hydrocarbon core, where the contact with water molecules is minimum.[51] Therefore, we anticipate that the drug molecules trapped in between the surfactants reside close to hydroxyl groups of glucose molecules, and thereby, excited state intermolecular proton transfer reaction takes place from glucose to drug molecules to yield excited state cationic form of the drug (**Scheme 4c.2**). Local dielectric constant experienced by

the drug molecule also contributes to the anomalous results obtained in OBG micelle. Though OBG micelles are neutral, the dielectric constant (~50)[52] at the palisade layer of OBG micelle is higher than that of above mentioned three micelles due to the presence of plenty of –OH groups at the interface of OBG micelle. Therefore, the higher local dielectric constant sensed by EPT molecule at the OBG micellar surface is also responsible for the stabilization charged species, such as protonated form of EPT in OBG micelle.

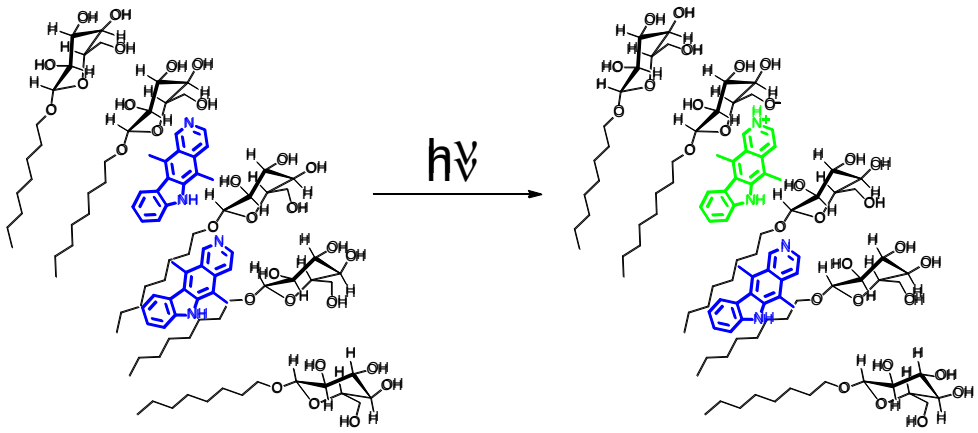

Scheme 4c.2. Excited state proton transfer process of EPT in octyl-β-D-glucoside micelle.

Our results suggest that EPT becomes less toxic in presence of OBG micellar environment, as absorption and emission results indicate the solubility of the drug increases in presence of OBG micellar environment. The drug loading to OBG micellar environment can be easily monitored with the help of fluorescence switching from green to cyan color. Thus, considering biocompatible nature of OBG and above mentioned points, we believe that OBG micelle may act as a suitable drug delivery carrier for EPT. Most importantly, for the first time we have shown that the ESPT dynamics of ellipticine depends on both the polarity as well as surrounding proton concentration. Another important implication of our work is that one can predict cellular environment with respect to polarity as well as proton concentration from the ESPT process of the drug.

4c.3. Conclusion:

In the present work, we have studied the photophysical and proton transfer dynamics of an eminent anticancer drug, ellipticine inside a biocompatible octyl-β-D-glucoside (OBG) micellar medium using steady state as well as time resolved spectroscopic techniques. UV-visible absorption study reveals the conversion of protonated to neutral form of EPT, when OBG concentration reaches above critical micellar concentration. Interestingly, the emission at 530 nm (attributed to the protonated form of the drug) is also observed along with neutral form (emits at 440 nm), even when we selectively excite the neutral molecules. The above observation clearly demonstrates that excited state proton transfer process inside the OBG micelle is responsible for the conversion of neutral to protonated form of the drug. Time resolved emission measurements depict a pronounced enhancement in the average lifetime of both neutral and protonated species collected at 440 nm and 530 nm, respectively, when EPT is encapsulated inside OBG micelles. Astonishingly, a rise component of ~4 ns is observed in the time-resolved emission decays collected at 530 nm above CMC of OBG, and it is attributed to the excited state proton transfer dynamics of EPT inside OBG micellar confinement. Time-resolved area normalized emission spectra confirm the existence of two species in the excited state, where neutral form transforms to the protonated form. This kind of proton transfer dynamics is absent in conventional micelles, like SDS, Triton X and CTAB, and therefore, indicates that the glucose molecules residing in the palisade layer of OBG micelle may have some role in the excited state proton transfer. Based on all the above observations, we conclude that the observed ESPT dynamics is a combined effect of local dielectric constant as well as presence of glucose moieties at the palisade layer of the OBG micelle.

4c.4. Reference:

1. H. Luders, *In Nonionic Surfactants: Alkylpolyglucosides*; D. Balzer, H. Luders, Eds.; Dekker: NewYork, **2000**.
2. K. Holmberg, B. Jönsson, B. Kronberg and B. Lindman, *Surfactants and Polymers in Aqueous Solution*, 2nd ed.; Wiley: NewYork, **2002**; Chapter1.
3. L. Stryer, Biochemistry, 3rd ed.; W. H. Freeman and Company: New York, **1988**.
4. M. Kasahara and P. C. Hinkle, *Proc. Natl. Acad. Sci. U.S.A.*, 1976, **73**, 396-400.
5. M. Ollivon, O. Eidelman, R. Blumenthal and A. Walter, *Biochemistry*, 1988, **27**, 1695-1703.
6. P. K. Vinson, Y. Talmon and A. Walter, *Biophys. j.*, 1989, **56**, 669-681.
7. N. A. Dencher and M. P. Heyn, *FEBS Lett.*, 1978, **96**, 322-326.
8. H. Michel and D. Oesterhelt, *Proc. Natl. Acad. Sci. U.S.A.*, 1980, **77**, 1283-1285.
9. E. Fischer, *Ber. Dtsch. Chem. Ges.*, 1893, **26**, 2400-2412.
10. B. J. Boyd, C. J. Drummond, I. Krodkiewska and F. Grieser, *Langmuir*, 2000, **16**, 7359-7367.
11. F. Nilsson, O. Söderman and I. Johansson, *Langmuir*, 1996, **12**, 902-908.
12. D. Hantzschel, J. Schulte, S. Enders and K. Quitzsch, *Phys. Chem. Chem. Phys.*, 1999, **1**, 895-904.
13. H. D. Dörfler and A. Göpfert, *J. Disper. Sci. Technol.*, 1999, **20**, 35-58.
14. M. G. Bonicelli, G. F. Ceccaroni and C. La Mesa, *Colloid Polym. Sci.*, 1998, **276**, 109-116.
15. P. Sakya, J. M. Seddon and R. H. Templer, *J. Phys. II*, 1994, **4**, 1311-1331.
16. A. Loewenstein and D. Igner, *Liq. Cryst.*, 1991, **10**, 457-466.
17. V. Kocherbitov, O. Söderman and L. Wadsö, *J. Phys. Chem. B*, 2002, **106**, 2910-2917.
18. S. Ogawa, K. Asakura and S. Osanai, *Carbohydr. Res.*, 2010, **345**, 2534-2541.
19. K. K. Karukstis, W. C. Duim, G. R. Van Hecke and N. Hara, *J. Phys. Chem. B*, 2012, **116**, 3816-3822.
20. S. Ogawa, K. Asakura and S. Osanai, *Phys. Chem. Chem. Phys.*, 2012, **14**, 16312-16320.
21. M. V. C. Cardoso and E. Sabadini, *Langmuir*, 2013, **29**, 15778-15786.
22. S. Goodwin, A. F. Smith and E. C. Horning, *J. Am. Chem. Soc.*, 1959, **81**, 1903-1908.

23. J.-B. Le Pecq, X. Nguyen Dat, C. Gosse and C. Paoletti, *Proc. Natl. Acad. Sci. U.S.A.*, 1974, **71**, 5078-5082.
24. M. Ohashi and T. Oki, *Expert Opin. Ther. Pat.*, 1996, **6**, 1285-1294.
25. C. L. Arteaga, D. L. Kisner, A. Goodman and D. D. Von Hoff, *Eur. J. Cancer Clin. Oncol.*, 1987, **23**, 1621-1626.
26. F. Sureau, F. Moreau, J. M. Millot, M. Manfait, B. Allard, J. Aubard and M. A. Schwaller, *Biophys. j.*, 1993, **65**, 1767-1774.
27. S. Y. Fung, J. Duhamel and P. Chen, *J. Phys. Chem. A*, 2006, **110**, 11446-11454.
28. Z. Miskolczy, L. Biczók and I. Jablonkai, *Chem. Phys. Lett.*, 2006, **427**, 76-81.
29. S. Banerjee, A. Pabbathi, M. C. Sekhar and A. Samanta, *J. Phys. Chem. A*, 2011, **115**, 9217-9225.
30. R. Thakur, A. Das, C. Adhikari and A. Chakraborty, *Phys. Chem. Chem. Phys.*, 2014, **16**, 15681-15691.
31. M. Sbai, S. Ait Lyazidi, D. A. Lerner, B. del Castillo and M. A. Martin, *J. Pharm. Biomed. Anal.*, 1996, **14**, 959-965.
32. R. Thakur, A. Das and A. Chakraborty, *Chem. Phys. Lett.*, 2013, **563**, 37-42.
33. R. Thakur, A. Das and A. Chakraborty, *Phys. Chem. Chem. Phys.*, 2012, **14**, 15369-15378.
34. S. Y. Fung, H. Yang and P. Chen, *Colloids Surf., B*, 2007, **55**, 200-211.
35. S. Y. Fung, H. Yang, P. T. Bhola, P. Sadatmousavi, E. Muzar, M. Liu and P. Chen, *Adv. Funct. Mater.*, 2009, **19**, 74-83.
36. A. Sengupta, R. K. Koninti, K. Gavvala, N. Ballav and P. Hazra, *Phys. Chem. Chem. Phys.*, 2014, **16**, 3914-3917.
37. R. K. Koninti, A. Sengupta, K. Gavvala, N. Ballav and P. Hazra, *Nanoscale*, 2014, **6**, 2937-2944.
38. D. Mańko, A. Zdziennicka and B. Jańczuk, *Colloids Surf., B*, 2014, **114**, 170-176.
39. J. R. Lakowicz, *Principles of Fluorescence Spectroscopy*, Springer, NewYork, 3rd edn, 2006.
40. A. S. R. Koti, M. M. G. Krishna and N. Periasamy, *J. Phys. Chem. A*, 2001, **105**, 1767-1771.
41. A. S. R. Koti and N. Periasamy, *J. Chem. Phys.*, 2001, **115**, 7094-7099.

42. N. Sarker, K. Das, S. Das, A. Datta, D. Nath and K. Bhattacharyya, *J. Phys. Chem.*, 1995, **99**, 17711-17714.

43. P. K. Chowdhury, K. Das, A. Datta, W. Z. Liu, H. Y. Zhang and J. W. Petrich, *J. Photochem. Photobiol. A*, 2002, **154**, 107-116.

44. B. Cohen, D. Huppert, K. M. Solntsev, Y. Tsfadia, E. Nachliel and M. Gutman, *J. Am. Chem. Soc.*, 2002, **124**, 7539-7547.

45. A. S. Klymchenko, G. Duportail, Y. Mély and A. P. Demchenko, *Proc. Natl. Acad. Sci. U.S.A.*, 2003, **100**, 11219-11224.

46. T. K. Mukherjee, P. Ahuja, A. L. Koner and A. Datta, *J. Phys. Chem. B*, 2005, **109**, 12567-12573.

47. B. Lorber, J. B. Bishop and L. J. DeLucas, *Biochim. Biophys. Acta, Biomembr.*, 1990, **1023**, 254-265.

48. F. Grieser and C. J. Drummond, *J. Phys. Chem.*, 1988, **92**, 5580-5593.

49. M. S. Fernandez and P. Fromherz, *J. Phys. Chem.*, 1977, **81**, 1755-1761.

50. B. Lovelock, F. Grieser and T. W. Healy, *J. Phys. Chem.*, 1985, **89**, 501-507.

51. P. Konidala, L. He and B. Niemeyer, *J. Mol. Graph. Model.*, 2006, **25**, 77-86.

52. C. J. Drummond, F. Grieser and T. W. Healy, *J. Chem. Soc., Faraday Trans. 1*, 1989, **85**, 551-560.

Chapter 5

Prototropical and Photophysical Properties of Ellipticine inside Molecular Containers and DNA

"In this chapter we interrogate the prototropical and photophysical properties of an important anticancer drug, ellipticine inside various molecular containers. When the drug is encapsulated in molecular containers the photophysics have been modulated depending over type and size of the nanocavity of molecular container. Using photophysical properties of the drug, it is released from the nanocavity to an important biomolecule DNA by altering pH of the medium as external stimuli. This chapter is divided in to two sections; in first section we explain the photophysical properties of ellipticine in molecular containers and in second section we cover the pH responsive release of the drug to DNA. These two sections are explained in detailed manner one by one as follows."

5a. Prototropical and Photophysical Properties of Ellipticine inside the Nano-cavities of Molecular Containers

5a.1. Introduction and Motivation of the Work:

Ellipticine is an important drug known to exhibit several antitumor and anti-HIV activities.[1-3] Although ellipticine is considered as one of the potential anti-tumor drugs, the major disadvantages in the usage of ellipticine in pharmaceutics are its toxicity and low solubility in aqueous solution. The problems have been circumvented by attaching the drug to polymer, micelle, vesicle, liposome and reverse micelle.[4-9] However, to get insight how ellipticine is transported to tumor cell, it is also necessary to establish a relationship between the environment and the photophysical properties of ellipticine. EPT (**Scheme 5a.1**) shows two interesting prototropic forms depending on the pH as well as environmental polarity as explained in the chapter 4c. For that macrocyclic hosts are excellent bio-mimetic systems to understand the effect of confinement on photophysical and protonation properties of the drug. Researchers have already tried to probe the complexation between EPT and cyclodextrins by steady state fluorescence, T-jump method. It was observed that β-CD forms 1:1 inclusion complex with EPT, whereas γ-CD forms 2:1 inclusion complex in a two-step process.[10, 11] Although kinetics and thermodynamics are well explored in the above mentioned studies, the photophysics are not well examined. Moreover, the dynamic aspect, which provides deep insight about the complex formation process, has not been addressed in their study.

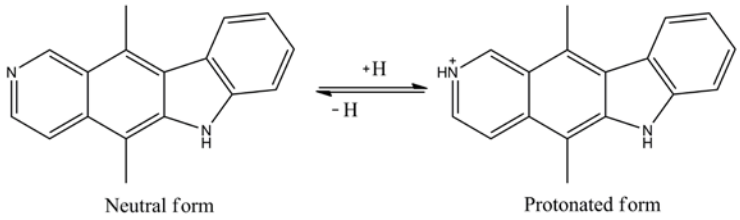

Scheme 5a.1. Different prototropic forms of ellipticine.

Here in this chapter, we have extensively studied the interaction behaviour between EPT and cucurbiturils with the help of steady state, time-resolved fluorescence techniques, and

compared the results with that of cyclodextrins. Finally, the docking and semi-empirical quantum chemical calculations have been employed in deciphering the molecular pictures of the interactions between EPT and macrocyclic hosts (CBn, CDs).

5a.2. Results and Discussion:

5a.2a. Steady State Measurements:

Absorption spectra of EPT in absence and presence of CBn are shown in **Figure 5a.1**. Drug in water (pH=6.5) exhibits absorbance in 250-450 nm region with the absorbance maximum at 300 nm, which is believed to be characteristic peak of protonated form of EPT.[11, 12] Upon addition of CB6, absorption profiles do not change significantly, except the absorbance at 300 nm slightly decreases. However, with gradual addition of CB7/CB8, the absorption peak shows a bathochromic shift from 300 nm to 308 nm along with decrement in absorbance. These noteworthy changes in absorption features suggest strong binding interactions between EPT and CBn in the ground state.

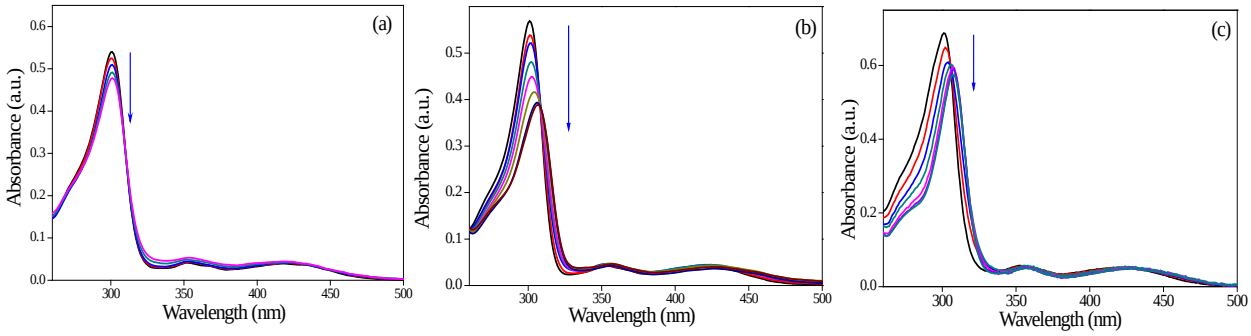

Figure 5a.1. Absorption spectra of EPT (15 μM) in presence of (a) CB6 (from 0 to 50 μM), (b) CB7 (from 0 to 700 μM) and (c) CB8 (from 0 to 100 μM).

To get clear insight about the complexation process, we have monitored emission profiles of EPT in presence of cucurbiturils having various cavity sizes (**Figure 5a.2**). EPT in aqueous solution exhibits a broad and unstructured peak at 530 nm, which is the signature peak of protonated EPT.[4] Upon addition of CB6, fluorescence intensity of EPT at 530 nm slightly increases, whereas huge intensity increment is observed along with hypsochromic shift (**Figure 5a.2**) upon addition of both CB7 and CB8. As the extent of peak enhancement in presence of

both CB7 and CB8 is more than that of CB6, it indicates that the interaction between drug and host is stronger in case of both CB7 and CB8. The blue shift in emission spectra further confirms the formation of inclusion complex between protonated EPT and CBn (CB7/CB8). It is also noticeable that the extent of blue shift in case of CB8 is lesser compared to CB7, which can be attributed to lower extent of hydrophobic interaction inside the CB8 cavity due to its larger cavity size than that of CB7. Here it is pertinent to mention that the average distance between 5-methyl and 11-methyl groups in EPT is 7 Å, while the inner diameters of the cavity of CB6, CB7 and CB8 are 5.8 Å, 7.3 Å, and 8.8 Å, respectively. CB6 cavity is too small to accommodate EPT from the pyridine ring side. However, it can encapsulate EPT from indole side, which would result a blue shift in fluorescence spectra, as it is known that polarity change affects indole emission.[13] As a result EPT cannot form inclusion complex with CB6.

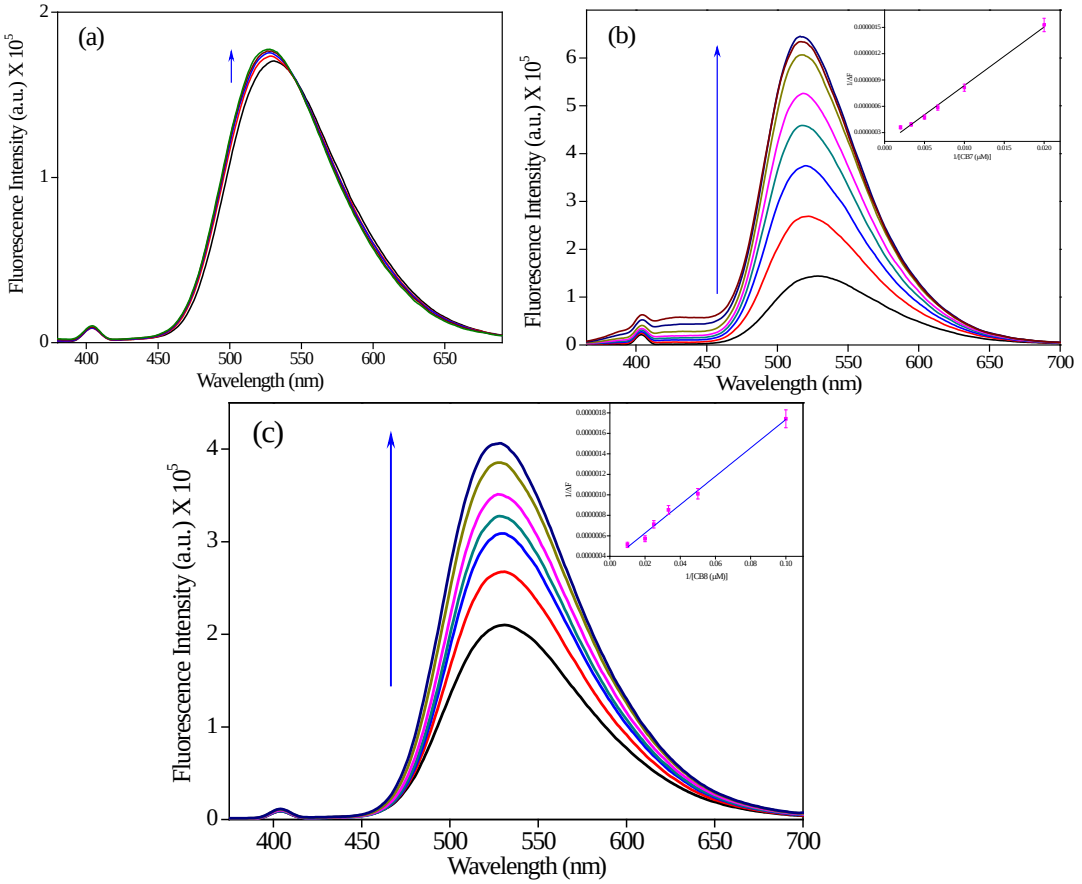

Figure 5a.2. Emission spectra of EPT (15 μM) in presence of (a) CB6 (from 0 to 50 μM), (b) CB7 (from 0 to 700 μM) and (c) CB8 (from 0 to 100 μM). Inset shows Benesi-Hildebrand plot.

Considering inner cavity sizes of both CB7 and CB8, it is possible that EPT can be encapsulated from the pyridine ring side. The increased intensity suggests that the non-radiative decay pathway, which arises due to free rotations of two methyl groups of drug, is reduced upon complexation with CB7/CB8. The intensity hike may also be attributed to the pK_a shift of pyridine nitrogen as an outcome of inclusion complexation, because there are reports about the pK_a shift of the drugs during inclusion complexation with cucurbituril.[14-16] In EPT-CB7/-CB8 complex, the pyridine nitrogen resides at the portal, and thereby, its pK_a value increases above 7.4. In order to verify whether excited state pK_a of ellipticine in presence of CBn is affected or not, we have determined the excited state pK_a with the help of Förster cycle.[17] We have verified that the excited state pK_a increases to 9.5 in presence of 500 μM of CB7. Therefore, we believe the pK_a shift of EPT also contributes towards the stability of drug in the inclusion complexes with CBn. It is also noticeable that a new peak at 440 nm appeared in addition to 530 nm peak, particularly at higher concentration of CB7. Note that neutral EPT exhibits emission peak in the range of 410-440 nm in non-polar solvents.[6] The appearance of 440 nm peak at higher CB7 concentration infers that few drug molecules are getting encapsulated in such a way that pyridine nitrogen stays inside hydrophobic cavity instead of staying at the portal.

The stoichiometry as well as binding constants of the inclusion complexes are determined from fluorescence intensity using Benesi-Hildebrand (BH) equation[18] The double reciprocal plot monitored at 530 nm is observed to be linear (R=0.997) for both CB7 (**Figue 5a.2b** inset) and CB8 (**Figue 5a.2c** inset), indicating formation of 1:1 inclusion complex between EPT and CBn, and the association constants (K_1) are estimated to be 2.9×10^4 M^{-1} and 2.1×10^5 M^{-1}, respectively.

5a.2b. Time Resolved Fluorescence Study:

Modulation in radiative properties of EPT upon interaction with CBn is clarified by fluorescence lifetime measurements. Fluorescence decays of EPT in absence and presence of CBn collected at corresponding emission maximum are shown in **Figure 5a.3** and fitting parameters are tabulated in **Table 5a.1**. At 530 nm, the drug exhibits bi-exponential decay in water having lifetime components of ~2 ns (84%) and ~6.5 ns (16%) with an average lifetime of ~2.7 ns. It is hard to assign each of the above mentioned lifetime components, hence, we will consider average lifetime instead of focusing individual components. The average lifetime of EPT in presence of CB6 increases from 2.7 ns to 3.21 ns. As we have already explained that CB6 cannot

accommodate the drug, the slight change in lifetime may be due to the ion-dipole/hydrogen bond interaction between EPT molecule (protonated) and carbonyl portals of CB6. This will be further verified by time resolved anisotropy measurement. In presence of CB7, average lifetime increases from 2.7 ns to 10.3 ns at maximum CB7 concentration (700 μM), whereas fluorescence lifetime of protonated EPT increases to 4.85 ns in presence of 100 μM CB8 (**Table 5a.1**). These noteworthy changes in lifetime further confirm the inclusion complex formation between EPT and CB7/CB8. The increase in lifetime of EPT on complexation with CBn (**Table 5a.1**) can be rationalized in terms of alterations in the radiative and non-radiative decay pathways (equation 2) of the drug due to their interaction with the macrocyclic host.

$$\frac{1}{\tau_f} = k_r + k_{nr} \qquad (5a.1)$$

Increased average lifetime (**Table 5a.1**) and enhancement in intensity of EPT in presence of CB7/CB8 (**Figure 3**) suggest the decrease in non-radiative decay rate of EPT inside the nano-cavity of CB7/CB8. We believe that the rotational motions of two methyl groups of EPT are restricted inside the nano-cavity of CBn; subsequently, fast non-radiative relaxation channel of the drug is arrested. A longer fluorescence lifetime component of 10-20 ns is appeared in presence of CBn hosts, indicating stability gained by the EPT upon encapsulation. The increased stability of protonated EPT inside the CBn nano-cavity may be attributed mainly to the ion-dipole interactions between protonated EPT and carbonyl portals of CBn.

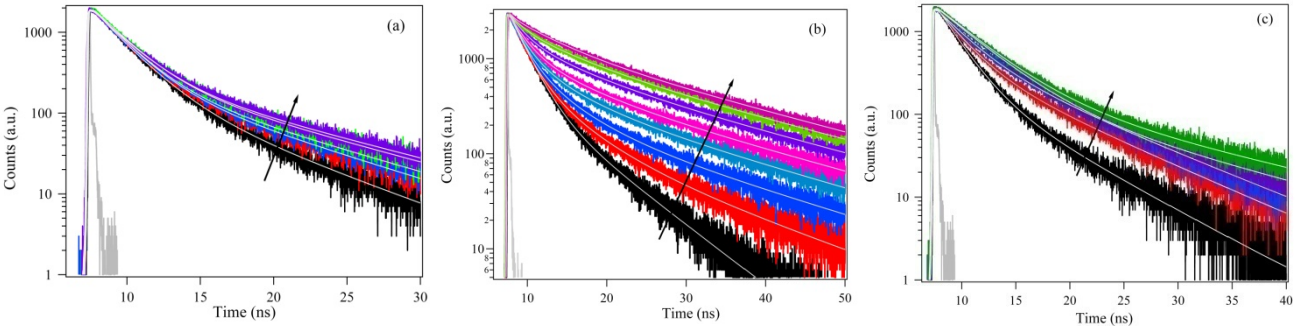

Figure 5a.3. Fluorescence decay overlays of EPT (15 μM) in presence of (a) CB6 (from 0 to 50 μM), (b) CB7 (from 0 to 700 μM) and (c) CB8 (from 0 to 100 μM) collected at 530 nm (λ_{ex}=375 nm).

Table 5a.1. Fluorescence decay transients of EPT in absence and presence of CBn collected at 530 nm (λ_{ex}=375 nm).

Sample	τ_1 (ns)	τ_2 (ns)	a_1	a_2	τ_{avg} [#]	χ^2
		Cucurbit[6]uril				
Ept in water	1.98	6.57	0.84	0.16	2.71	0.99
5 μM	1.98	7.46	0.86	0.14	2.73	1
10 μM	2.05	8.1	0.86	0.14	2.88	1.04
30 μM	2.12	8.82	0.86	0.14	3.06	1.05
50 μM	2.16	9.18	0.85	0.15	3.21	1.03
		Cucurbit[7]uril				
20 μM	2.1	8.77	0.86	0.14	3.01	1.05
40 μM	2.17	10.33	0.87	0.13	3.22	1.09
70 μM	2.19	11.45	0.85	0.15	3.56	1.09
100 μM	2.28	13.21	0.85	0.15	3.89	1.06
200 μM	2.35	14.93	0.79	0.21	4.96	1.14
300 μM	2.44	15.98	0.73	0.27	6.03	1.1
500 μM	2.75	17.05	0.63	0.37	8.07	1.1
700 μM	3.33	17.83	0.52	0.48	10.3	1.04
		Cucurbit[8]uril				
5 μM	2.12	7.15	0.76	0.24	3.35	0.99
10 μM	2.51	7.72	0.7	0.3	4.07	1.04
20 μM	3.42	9.28	0.81	0.19	4.52	1.04
50 μM	3.69	12.45	0.9	0.1	4.56	1.02
100 μM	3.75	14	0.89	0.11	4.84	0.99

[#] $\tau_{avg}=(a_1\tau_1 + a_2\tau_2)$

Time resolved anisotropy data provides information about the effect of microenvironment on rotational motions of the fluorophore, and hence, it can be used to probe the encapsulation process of EPT with cucurbituril. Anisotropy decay profiles of EPT in water and in presence of various host molecules are shown in **Figure 5a.4**. At 530 nm, EPT exhibits single exponential anisotropy decay in water with a rotational relaxation time of 120 ps. In presence of host, the rotational relaxation time (τ_r) of EPT increases owing to increased rigidity due to formation of inclusion complex with the host. In presence of CB6, the τ_r value is estimated to be 130 ps, which is almost equal to that of EPT in water (120 ps). Hence, anisotropy results support our conjecture that EPT doesn't form inclusion complex with CB6. In presence of CB7 and CB8 the τ_r values of EPT are found to be 565 ps and 355 ps, respectively, inferring that EPT gets encapsulated by the above mentioned macrocyclic hosts. The anisotropy results also suggest that EPT feels more restricted environment inside CB7 cavity compared to CB8, due to smaller cavity size of the former host. Thus, anisotropy results support our steady state observations, where we have observed more vivid changes for CB7 compared to CB8. The orientation of EPT in the inclusion complexes can be better understood from docking followed by quantum chemical calculations.

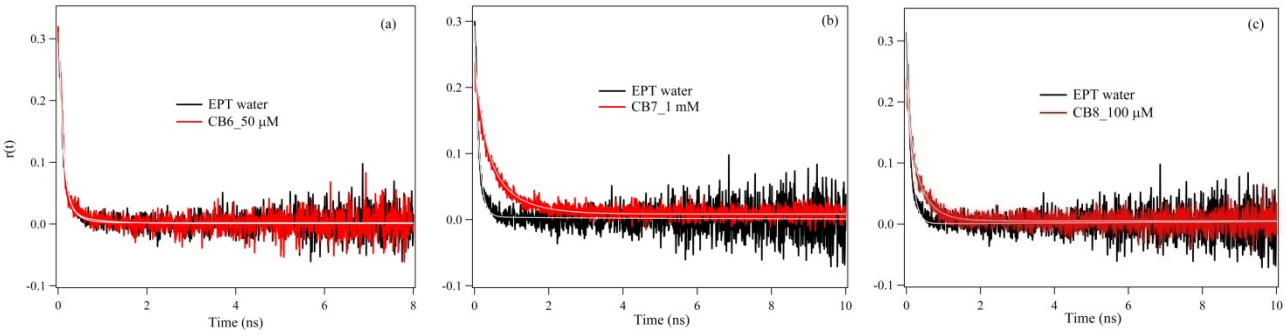

Figure 5a.4. Anisotropy decay overlays of EPT (15 µM) at 530 nm in presence of (a) CB6 (from 0 to 50 µM), (b) CB7 (from 0 to 0.7 mM) and (c) CB8 (from 0 to 100 µM) collected at emission maximum (λ_{ex}=375 nm).

5a.2c. Comparison of Photophysics of EPT between CD and CBn:

Significance of the CBn-EPT binding interaction is better understood when the above results are compared with that of cyclodextrins having similar cavity sizes. Although steady state results of EPT in CD are already reported,[10,11] the dynamic aspect, which provides deep perception to these binding processes, has not been addressed previously. Here, we mainly focus on the dynamics of EPT in presence of α-, β- and γ-CD with the help of time-resolved fluorescence measurements (**Table 5a.2**). It is already reported that EPT does not form inclusion complex with α-CD,[10] and we have also observed that average lifetime of protonated EPT slightly changes from 2.7 ns in water to 3.24 ns in presence of 20 mM of α-CD (**Table 5a.2**). Thus, lifetime results also support that EPT does not form inclusion complex with α-CD. Our studies showed that EPT also doesn't form any inclusion complex with CB6 which has comparable cavity size of α-CD. In presence of β-CD, the average lifetime of protonated EPT increases up to 3.6 ns, and is consistent with intensity hike in emission spectra. The lifetime data in presence of β-CD is devoid of ~10 ns component, which appears in presence of CB7 having similar cavity size. Moreover, the changes in lifetime as well as intensity are significantly higher in case of CB7, though the concentration of CB7 is few folds lower than that of β-CD. Hence, we believe the hydrophobic cavities of both CB7 and β-CD are not responsible for the modulation of photophysics of EPT, rather different topology of upper and lower rims of both the hosts is accountable for the modulation of photophysics of EPT in different extent. Cyclodextrins having hydrophobic cavity and hydroxyl groups in the rims encapsulate guest molecule mainly through hydrophobic as well as hydrogen bond interactions.[19, 20] On the other hand owing to carbonyl-lined portals, the binding interaction with CB7 takes place mainly through ion-dipole interaction, and it is quite likely that protonated form of EPT interacts with the electron rich carbonyl portal through the positive charge developed on the pyridine moiety. Therefore, EPT gains extra stability in the inclusion complex with CB7. As an outcome of the above mentioned effects, EPT exhibits more vivid changes in steady state as well lifetime profiles in presence of CB7 compared to β-CD.

Table 5a.2. Fluorescence decay transients of EPT in absence and presence of CD collected at 530 nm (λ_{ex}=375 nm).

Sample	τ_1 (ns)	τ_2 (ns)	a_1	a_2	τ_{avg} [#]	χ^2
			α-Cyclodextrin			
water	1.98	6.57	0.84	0.16	2.71	0.99
2 mM	2.02	6.55	0.83	0.17	2.8	0.99
4 mM	2.14	6.8	0.83	0.17	2.95	0.99
8 mM	2.22	6.87	0.82	0.18	3.04	1.03
12 mM	2.28	6.95	0.82	0.18	3.15	1.09
16 mM	2.38	7.16	0.82	0.18	3.24	1.07
			β- Cyclodextrin			
1.5 mM	2.1	6.34	0.82	0.18	2.86	1.01
3.5 mM	2.22	6.47	0.79	0.21	3.11	1.02
7 mM	2.25	6.27	0.77	0.23	3.195	1.03
14 mM	2.56	7.17	0.78	0.22	3.57	1.06
			γ- Cyclodextrin			
1.5 mM	2.2	12.07	0.93	0.07	2.89	1.04
3 mM	2.36	22.98	0.92	0.08	4.1	1.1
4.5 mM	2.4	25.67	0.88	0.12	5.23	1.1
6 mM	2.13	30.56	0.78	0.22	8.41	1.08
9 mM	1.935	31.51	0.68	0.32	11.33	1.1
12 mM	1.27	31.56	0.66	0.34	11.44	1.03
15 mM	1.25	31.55	0.65	0.35	11.82	1.13

[#] $\tau_{avg}=(a_1\tau_1 + a_2\tau_2)$

Interestingly, the emission profiles of the drug in presence of γ-CD are significantly different from other macrocyclic hosts. In presence of γ-CD, a marked increase in the emission intensity of EPT accompanied by a hypsochromic shift of ~50 nm is observed. Moreover, a peeping hump is generated at 475 nm around 300 μM of γ-CD (**Figure 5a.5a** inset), and the emission spectra become broad at higher concentration exhibiting an emission maximum at 480 nm (**Figure 5a.5a**). Although similar observation has been reported by other groups, the detailed interpretation of the spectra has not been addressed previously. In order to get clear perception about the spectral features, we have deconvoluted the emission spectra using Lorenzian fitting in presence of γ-CD (**Figure 5a.5b**). It is clearly seen from the deconvoluted spectra that a new peak appeared at ~480 nm along with main peak at ~530 nm at higher concentration of γ-CD. The peak position at 480 nm remains same although a huge increment in intensity is observed as γ-CD concentration increases, whereas the peak at 530 nm is gradually blue shifted along with the slight increase in intensity. The 530 nm peak definitely indicates the presence of protonated form of EPT, and the blue shift confirms the encapsulation of protonated EPT inside the γ-CD nano-cavity. The 480 nm peak may be ascribed to neutral form of EPT inside γ-CD nano-cavity as the neutral form generally exhibits emission maximum well before 450 nm.[6] The high bathochromic shift in presence of γ-CD may appear from the caging effect by the host. The binding interaction between the EPT and γ-CD is further examined by monitoring the fluorescence intensity of the drug with increasing concentration of the macrocyclic host. It is clearly noticeable that the titration curve (monitored at 530 nm) significantly deviates from linearity (**Figure 5a.5c**), pointing towards the formation of multiple inclusion complexes between host and guest. Moreover, a slope change is observed in the titration curve at around 300 μM. In fact there is report about the stepwise multiple inclusion complexation between EPT and γ-CD. Based on our titration curve as well as from literature report, it is reasonable to assume that 1:1 complexation equilibrium exists until 300 μM of γ-CD concentration , and thereafter 2:1 (γ-CD:EPT) inclusion complexation dominates. It is already reported that the interaction between EPT and γ-CD occurs in two steps, the first one involving the encapsulation pyridine residue of the drug and the second being the inclusion of 1:1 inclusion complex by another cyclodextrin from the indole side.[11] Therefore, based on our observation as well as literature reports, we envisage that pyridine ring resides at the rim in 1:1 inclusion complex, where it can access water. As a result, EPT prevails as protonated form in 1:1 inclusion complex.

On the other hand, pyridine nitrogen of EPT is prevented from exposure to water in 2:1 inclusion complex, as second cyclodextrin molecule acts as a cap for 1:1 inclusion complex.

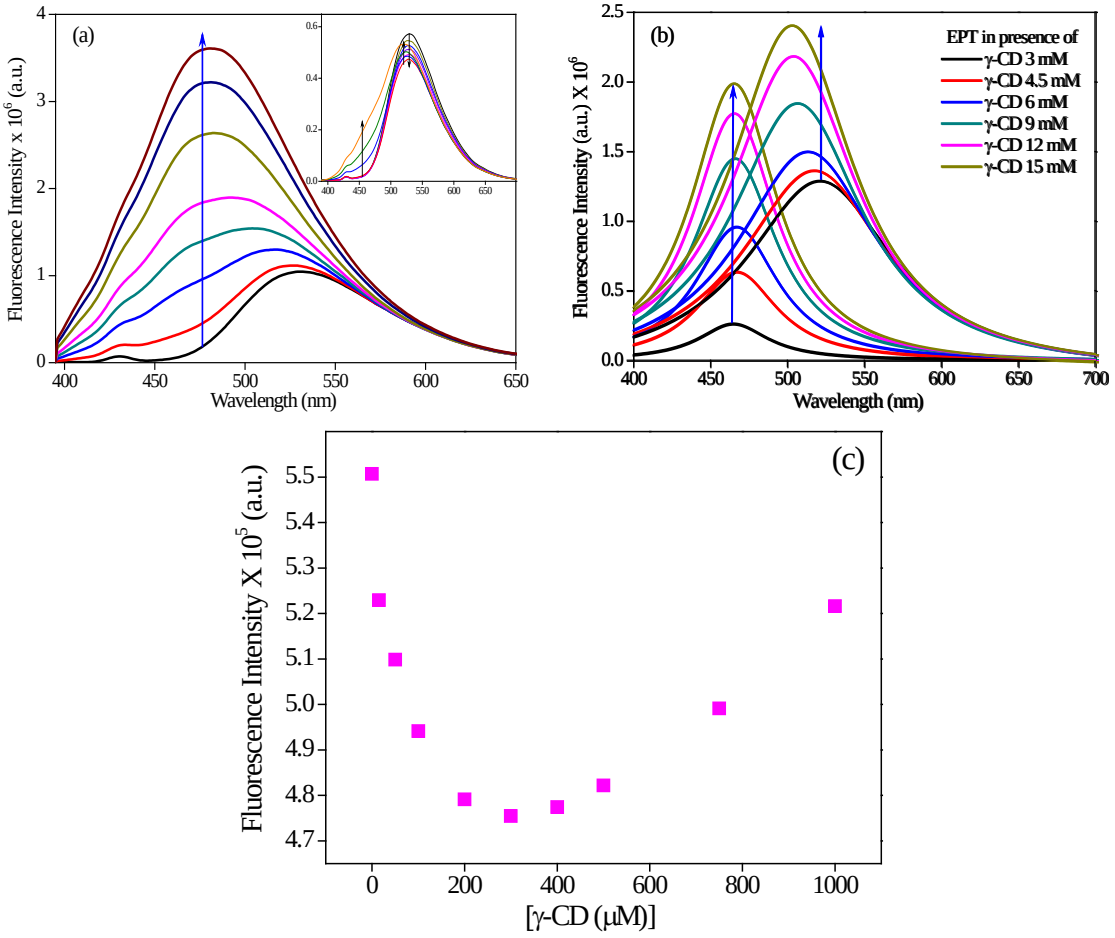

Figure 5a.5. Emission spectra of EPT (15 μM) in presence of γ-CD (0 to 15 mM); (a) original, (b) Lorenzian multipeak fits. (c) Fluorescence intensity of EPT at 530 nm with concentration of γ-CD.

The modulation in the radiative properties of EPT on interaction with γ-CD is also clarified by the fluorescence lifetime measurements (**Table 5a.2**). We have collected fluorescence lifetime of EPT in presence of γ-CD at the corresponding emission maximum. In presence of γ-CD, the fluorescence lifetime of EPT increases hugely from 2.7 to 10.36 ns (**Table 5a.2**). This four folds enhancement in fluorescence lifetime of EPT supports high binding affinity of γ-CD with EPT compared to other macrocyclic hosts (α-CD, β-CD). Moreover, with

the addition of γ-CD a new component with longer lifetime 25-35 ns arises at ≥300 μM and its contribution increases with gradual addition of γ-CD. Similar lifetime component for EPT was observed in non-polar solvents where neutral form predominantly exists in the solution. Therefore, we believe that the long component appeared in the decay profile is attributed to the neutral form of EPT, and is corroborative with steady state results where we have observed the formation of neutral of EPT in presence of γ-CD when 2:1 (γ-CD:EPT) inclusion complex is formed.

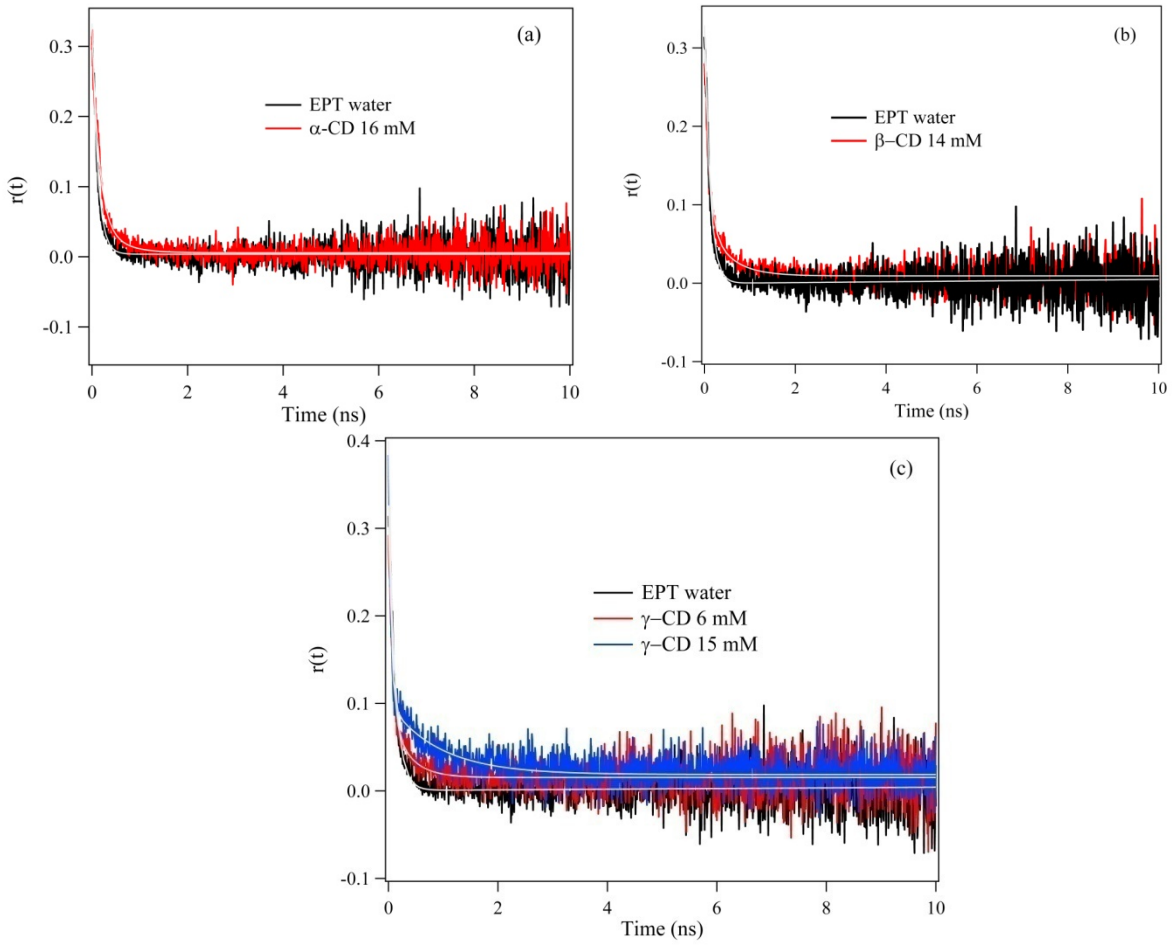

Figure 5a.6. Anisotropy decays of EPT (15 μM) in presence of (a) α-CD, (b) β-CD and (c) γ-CD collected at 530 nm (λ_{ex}=375 nm).

To further scrutinize the complexation processes with CDs, we have collected anisotropy decay profiles for EPT at emission maximum in presence of CDs (**Figure 5a.6**). As we have already stated, EPT exhibits single exponential anisotropy decay in water with a rotational correlation time of 120 ps. In presence of α-CD, the τ_r value is estimated to be 170 ps, which is not significantly higher than that of EPT in water (120 ps). Hence, anisotropy results support that EPT doesn't form inclusion complex with α-CD. However, in presence of β-CD and γ-CD the τ_r values of EPT are found to be 520 ps and 855 ps, respectively, affirming the formation of inclusion complexes between drug and above mentioned macrocyclic hosts. The longer rotational relaxation time-scale in presence of 15 mM of γ-CD further supports the formation of 2:1 inclusion complex (γ-CD:EPT), in which the drug molecule feels additional rigidity by second host molecule, which acts as a cap towards the 1:1 inclusion complex. To compare binding affinity of the drug between CDs and CBn, we have determined binding constants using BH plots, and the values are estimated to be 104 M^{-1}, 2.8×10^4 M^{-1} and 1.5×10^5 M^{-2} for β-CD:EPT, γ-CD:EPT and γ-CD:EPT:γ-CD inclusion complexes, respectively. On the other hand, the association constant between EPT and CBn is varied from 2.9×10^4 M^{-1} to 2.1×10^5 M^{-1}, indicating cucurbiturils have higher binding affinity towards EPT compared to CDs. This higher binding affinity may be attributed to the strong ion-dipole interactions of protonated EPT with carbonyl portals of CBn which are absent in CDs.

5a.2d. Docking and Quantum Chemical Calculations:

To obtain molecular picture of orientation of EPT in the inclusion complexes as well as to gain insight into the stabilization achieved due to encapsulation, we have docked the drug (EPT) into the host molecules (CDs and CBn), followed by a semi-empirical quantum chemical optimization. Following the experimental findings, we have taken protonated form of EPT for all the docking studies, except in the case of γ-CD, in which neutral form of the drug has also been considered during docking study. In case of γ-CD we have docked EPT (protonated form) and γ-CD to get 1:1 (γ-CD:EPT) inclusion complex. In order to get 2:1 (γ-CD:EPT) inclusion complex, we have docked 1:1 (γ-CD:EPT) inclusion complex with neutral EPT to another γ-CD. Since the docking and geometry optimization were done without consideration of any solvent and other parameters, these geometries provide only qualitative picture of the structures in the ground state. Optimized structures of the various inclusion complexes are shown in **Figure 5a.7**.

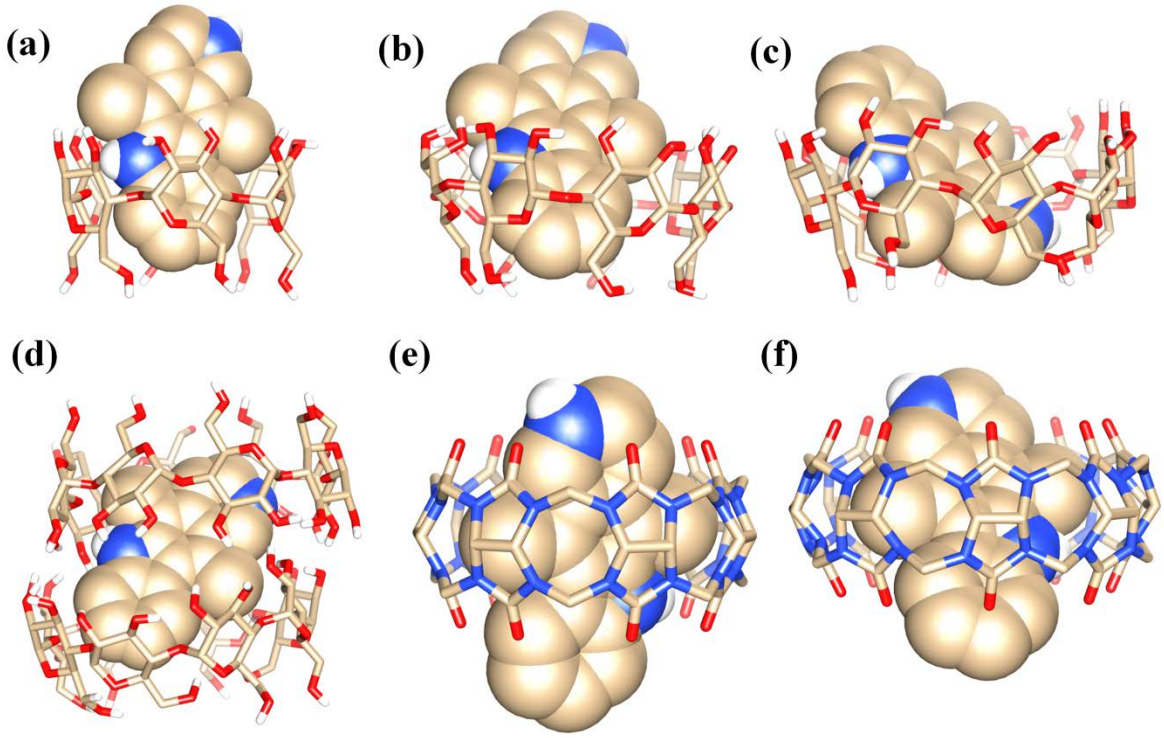

Figure 5a.7. Optimized structure of (a) docked α-CD:EPT complex (1:1), (b) docked β-CD:EPT complex (1:1) and (c) docked γ-CD:EPT complex (1:1), (d) docked γ-CD:EPT complex (2:1), (e) docked CB7:EPT complex (1:1) and (f) docked CB8:EPT complex (1:1).

Although the docking study indicates the formation of an inclusion complex between EPT and α-CD (**Figure 5a.7a**), the interaction energy obtained from quantum chemical optimization method is positive (5 kcal mol^{-1}), which indicates that energetically EPT does not prefer to be included inside the cavity of α-CD, probably due to the smaller size of the host cavity. Therefore, theoretical calculation supports our experimental findings that EPT does not form an inclusion complex with α-CD. In case of β-CD, the interaction energy is negative (-29 kcal mol^{-1}), suggesting that 1:1 inclusion complex formation between EPT and β-CD is energetically feasible. For γ-CD, both the 1:1 and 2:1 (γ-CD:EPT) inclusion complexes are energetically feasible by -23 kcal mol^{-1} and -35 kcal mol^{-1}, respectively. It is important to note that these two types of inclusion complexes in case of γ-CD were predicted previously by Chahine *et al.*,[11] and our experimental observation also infers the formation of stepwise multiple

inclusion complexation between EPT and γ-CD. It is clear from geometry optimized structure of 1:1 inclusion complex with γ-CD, entry of EPT takes place from pyridine side in such a way that pyridine rings of EPT are still accessible to water environment, which favors the existence of cationic form of EPT (**Figure 5a.7c**). But in case of 2:1 (γ-CD:EPT) inclusion complex, the EPT is completely buried inside the capsule formed by two γ-CD molecules and pyridine ring is totally protected from water (**Figure 5a.7d**). Hence, protonation is not feasible in this case, and as a result, EPT exists as neutral form in this 2:1 inclusion complex. The hydrophobic environment inside the capsule is believed to stabilize the neutral form of EPT. Theoretical studies fully support our conjecture drawn from experimental results that EPT exists as protonated form in 1:1(γ-CD:EPT) inclusion complex formed in lower concentration regime of host, whereas it subsists as neutral form in 2:1 inclusion complex at higher concentration regime of γ-CD.

If we compare the complexation of EPT with CDs and CBn, the orientation of EPT inside the nanocavity of CDs is different from that in CBn cavity. Heat of formations for inclusion complexes of EPT with CB7 and CB8 are -42 kcal mol^{-1} and -48 kcal mol^{-1}, respectively. From these energy values it is clear that the complex formation of EPT with CBn is energetically more favorable than with CDs. EPT orients inside CBn (7 and 8) in such a way that the pyridine moiety resides at the carbonyl portals of CBn, so that it is further stabilized through ion-dipole interaction (**Figure 5a.7e-f**). This additional binding interaction of EPT with CBn leads to the relatively higher interaction energies with CBn compared to CDs. Moreover, in this orientation there is a possibility for the increase in pK_a of pyridine nitrogen due to the surrounding electron rich carbonyl portals. Furthermore, in this orientation the EPT can access water environment, which causes protonation of EPT in the inclusion complexes formed by CBn.

5a.3. Conclusion:

In this work, the interaction behavior between an anticancer drug EPT and cucurbitruils has been demonstrated with the help of absorption, steady state fluorescence and time-resolved fluorescence techniques. For comparison, we have done similar experiments using conventional hosts, cyclodextrins. Our experimental results indicate the formation of 1:1 inclusion complexation of EPT with CB7 and CB8, and protonated form of EPT gets stabilized mainly through the ion-dipole interaction between host and positively charged drug. On the other hand,

drug does not from inclusion complex with CB6. Among cyclodextrins, α-CD does not form inclusion complex with the drug, whereas β-CD forms 1:1 inclusion complex with the protonated form of the drug. Notably, binding affinity for β-CD is less compared to CB7/CB8. Interestingly, in case of γ-CD, drug forms stable 1:1 inclusion complex in its protonated form at lower concentration of host, whereas drug is encapsulated by two γ-CD molecules at higher concentration of host, and thereby drug exists in neutral form at higher concentration of γ-CD. Molecular docking as well as quantum chemical calculations were employed to get insight into the orientation of EPT drug inside the nano-cavities of these macrocycles. The molecular pictures indicate that pyridine nitrogen of EPT is situated at the electron rich portal in the inclusion complexes with CBn, and as a result the basicity of quinoline nitrogen increases significantly. But in case of 2:1 inclusion complex (γ-CD:EPT) with γ-CD, the EPT is completely buried inside hydrophobic cavity of the capsule formed by two γ-CD molecules, and this hydrophobic environment stabilizes the neutral form of EPT which is not observed in other 1:1 inclusion complexes with CBn and β-CD.

5a.4. Reference:

1. L. M. Werbel, M. Angelo, D. W. Fry and D. F. Worth, *J. Med. Chem.*, 1986, **29**, 1321-1322.
2. G. Mathé, K. Triana, P. Pontiggia, D. Blanquet, M. Hallard and C. Morette, *Biomed. Pharmacother.*, 1998, **52**, 391-396.
3. L. Ding, J. Balzarini, D. Schols, B. Meunier and E. De Clercq, *Biochem. Pharmacol.*, 1992, **44**, 1675-1679.
4. S. Y. Fung, H. Yang, P. T. Bhola, P. Sadatmousavi, E. Muzar, M. Liu and P. Chen, *Adv. Funct. Mater.*, 2009, **19**, 74-83.
5. S. Y. Fung, H. Yang and P. Chen, *Colloids Surf., B*, 2007, **55**, 200-211.
6. S. Y. Fung, J. Duhamel and P. Chen, *J. Phys. Chem. A*, 2006, **110**, 11446-11454.
7. M. Sbai, S. Ait Lyazidi, D. A. Lerner, B. del Castillo and M. A. Martin, *J. Pharm. Biomed. Anal.*, 1996, **14**, 959-965.
8. R. Thakur, A. Das and A. Chakraborty, *Phys. Chem. Chem. Phys.*, 2012, **14**, 15369-15378.

9. R. Thakur, A. Das and A. Chakraborty, *Chem. Phys. Lett.*, 2013, **563**, 37-42.
10. M. Sbai, S. A. Lyazidi, D. A. Lerner, B. del Castillo and M. A. Martin, *Anal. Chim. Acta*, 1995, **303**, 47-55.
11. J. M. El Hage Chahine, J.-P. Bertigny and M.-A. Schwaller, *J. Chem. Soc., Perkin Trans. 2*, 1989, **0**, 629-633.
12. F. Sureau, F. Moreau, J. M. Millot, M. Manfait, B. Allard, J. Aubard and M. A. Schwaller, *Biophys. J.*, 1993, **65**, 1767-1774.
13. B. L. v. Duuren, *J. Org. Chem.*, 1961, **26**, 2954-2960.
14. N. Barooah, J. Mohanty, H. Pal and A. C. Bhasikuttan, *Phys. Chem. Chem. Phys.*, 2011, **13**, 13117-13126.
15. I. Ghosh and W. M. Nau, *Adv. Drug Deliv. Rev.*, 2012, **64**, 764-783.
16. Z. Miskolczy, L. Biczók and H. Görner, *J. Photochem. Photobiol. A*, 2009, **207**, 47-51.
17. J. R. Lakowicz.
18. H. A. Benesi and J. H. Hildebrand, *J. Am. Chem. Soc.*, 1949, **71**, 2703-2707.
19. M. V. Rekharsky, R. N. Goldberg, F. P. Schwarz, Y. B. Tewari, P. D. Ross, Y. Yamashoji and Y. Inoue, *J. Am. Chem. Soc.*, 1995, **117**, 8830-8840.
20. M. V. Rekharsky, M. P. Mayhew, R. N. Goldberg, P. D. Ross, Y. Yamashoji and Y. Inoue, *J. Phys. Chem. B*, 1997, **101**, 87-100.

5b. pH Induced Translocation of Ellipticine between Supramolecular Host and DNA

5b.1. Introduction and Motivation of the Work:

In recent years, development of stimuli responsive controlled release systems have become a prime focus in the scientific community due to their promising applications in biomedical fields. The control release of guest molecules can be achieved in response to various external stimuli such as temperature, pH, light, salt, enzymes, etc.[1-9] Among these, pH-responsive system has been extensively explored for target drug delivery in cancer therapy owing to the pH gradient between physiological environment (pH 7.4) and cell organelles such as endosome and cytolysosome (pH ~ 5.0).[10, 11] Till date versatile classes of macrocyclic hosts with excellent host-guest recognition properties and optimum biomedical applications have been synthesized.[3] Among them, cyclodextrins (CD) have received special interest because of their unique structure, with hydrophilic external surface and hydrophobic hollow cavity attracts wide variety of guest molecules.[12-14] As CDs are naturally available from starch, they are biocompatible, and exhibits less toxicity toward biological systems.[15] These beneficial properties have further fostered extensive studies on using CDs in several drug formulations and many biomedical applications.[3, 12-16] Not only drug encapsulation but release of the drug in presence of biopolymers (DNA, RNA etc.) is immensely important, as it is majorly associated with the therapeutic efficacy of the drug. In this context, few research works have also been devoted to understand the release of guest molecules from supramoleclar host in presence of several biomolecules.[7, 17-19] Owing to the physiological omnipresence in cells, we have chosen DNA as target molecule for releasing ellipticine from the nano-cavity of γ-CD. Not only drug release to biomolecule, but it will also be intriguing to study the reversible extraction of drug from DNA to supramolecular host using some external stimuli, so that the same DNA can be recovered and involved in other important cellular process. Here, we could able to achieve this reversible translocation of ellipticine between CD and DNA by simply varying the pH of the medium as an external stimulus (**Scheme 5b.1**). In non-polar and hydrophobic environments the drug exists in neutral form (N form), and exhibits an emission band in the range 430−470 nm.[20-24] In hydrophilic and polar media, EPT exists as a protonated/cationic form (C form), and emits at ~530 nm.[20-22, 25] In the previous

section of this chapter we have observed that the N form of EPT is encapsulated in γ-CD due to the hydrophobic environment of nano-cavity. But it is believed that the cationic form of the drug preferably intercalates in DNA,[26] which leads to fluorescence intensity enhancement of 530 nm band. Inspired by the well separated emission bands for EPT in γ-CD and DNA, herein this section; we explain the pH responsive translocation of EPT between these hosts by monitoring steady state, time-resolved fluorescence and circular dichroism spectroscopic tools.

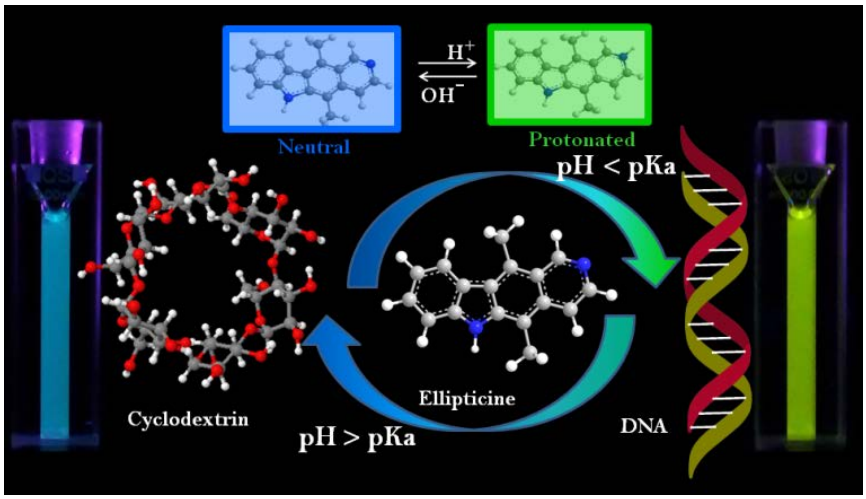

Scheme 5b.1. Different prototropic forms of ellipticine and its pH induced translocation between γ-CD and DNA.

5b.2. Results and Discussion:

5b.2a. Steady State Measurements:

Ellipticine shows three clear bands (~300 nm, 350 nm and 420 nm) in absorption spectrum at pH 7 (**Figure 5b.1a**). As the ground state pK_a of the drug is 7.4,[25] these bands can be assigned to cation (C) form of the drug. In presence of γ-CD, the characteristic three bands of C form are vanished and new bands at ~280 nm and 380 nm are observed. The new bands are previously ascribed to the neutral (N) form of EPT encapsulated in γ-CD.[25] When DNA is introduced into this system (EPT and γ-CD), an additional band is appeared at ~315 nm (**Figure 5b.1a**). Control experiment with DNA shows the similar band (~315 nm) in the absorption spectrum of EPT. Thus, the results indicate that EPT molecules might have been released to DNA from CD nano-

cavity. However, a small shoulder at 380 nm, which was assigned for γ-CD encapsulated EPT, still exists in the spectrum (**Figure 5b.1**). The existence of small hump at 380 nm indicates that minute population of EPT molecules still exist inside the CD nano-cavity. Next, to verify the effect of pH on release of the drug from γ-CD to DNA, we have changed the pH of the medium and the absorption spectra of EPT in presence of γ-CD and DNA collected at different pH conditions are shown in **Figure 5b.1b**. At lower pH (~5.0), the band at ~380 nm is vanished with an enhancement of shoulder peak at ~315 nm, and it matches exactly with the absorption spectrum of EPT in presence of DNA alone, suggesting only C form of might have been bound to DNA (**Figure 5b.1b**). On the hand, at higher pH (~8.5), the absorption band at ~380 nm is prevailed without any shoulder at ~315 nm, and, this spectral feature exactly matches with EPT:γ-CD spectrum (**Figure 5b.1**), indicating translocation of drug from DNA to γ-CD. In summary, absorption results provide hints about the pH responsive translocation of the drug in between CD and DNA. Further information about the translocation process of the drug in between CD and DNA can be obtained from fluorescence and circular dichroism measurements discussed in the subsequent sections of this article.

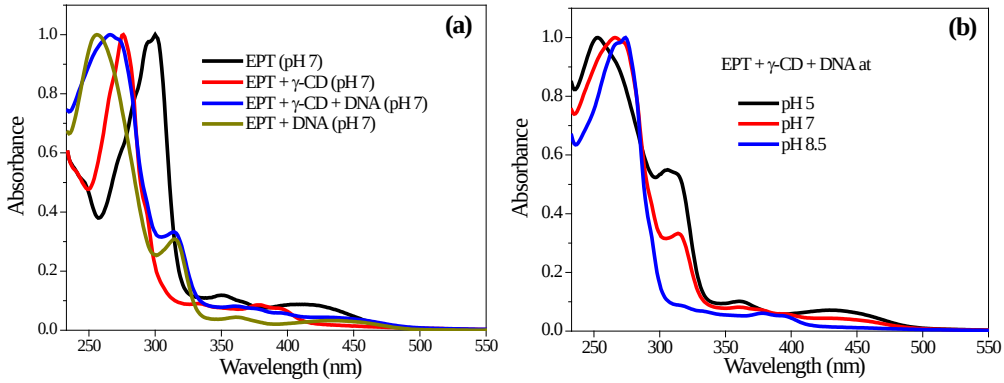

Figure 5b.1. (a) Absorption spectra of EPT (15 μM) in absence and presence of γ-CD (10 mM) and DNA (100 μM) at pH 7. (b) pH dependent emission spectra of EPT + γ-CD + DNA system.

Irrespective of the different excitation wavelengths of three absorption bands, the drug exhibits single emission band with maximum at 530 nm (**Figure 5b.2**) attributed to the excited C form of EPT.[25] In presence of γ-CD, this emission band undergoes a prominent blue shift (~470

nm) with a huge increment in fluorescence intensity due to the conversion of C to N form inside the hydrophobic nano-cavities of γ-CD.[25] To see whether the drug releases in presence of DNA or not, the γ-CD encapsulated EPT solution is titrated with ct-DNA. At pH 7, the addition of DNA to the γ-CD containing EPT solution, causes the appearance of new green fluorescence peak at ~520 nm along with concomitant decrement of 470 nm peak (**Figure 5b.2**). It is known that C form of the EPT intercalates in DNA[27] and results in vast increment of fluorescence intensity at 520 nm.[21, 22] Therefore, the appearance of green fluorescence peak for EPT in presence of γ-CD and DNA confirms that the drug is translocated from γ-CD to DNA. However, a small shoulder at 470 nm still exists even at higher concentration of DNA, (**Figure 5b.2**), inferring that complete translocation of EPT doesn't take place from γ-CD to DNA at this pH condition.

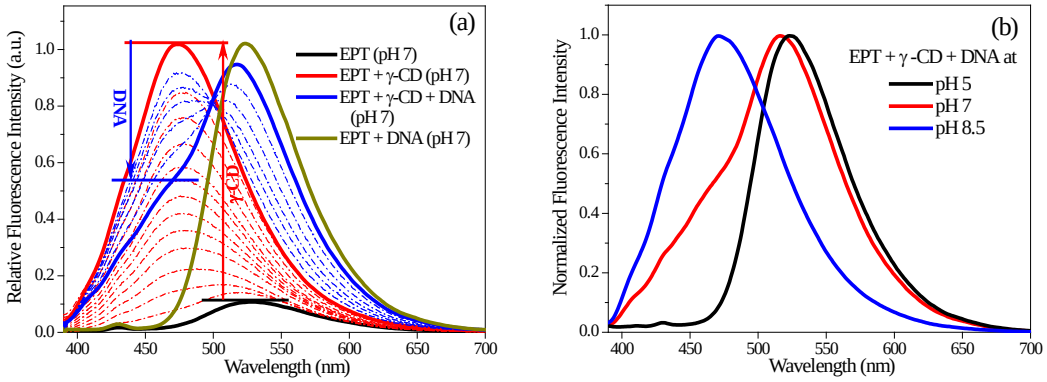

Figure 5b.2. (a) Emission spectrum of EPT (15 μM) in absence and presence of γ-CD (10 mM) and DNA (100 μM) at pH 7. The direction of arrow indicates increase in concentration. (b) pH dependent emission spectra of EPT + γ-CD + DNA system.

These results are further supported by association constants previously reported by our group.[22, 25] The binding constant for EPT with γ-CD ($1.5 \times 10^5\ M^{-2}$) is relatively lesser compared to the value with DNA ($5.04 \times 10^5\ M^{-1}$),[22, 25] which might cause the release of drug from CD to DNA. As both the association constants are not vastly different (as they are in the same order of magnitude), hence, it is expected that few population still exists inside the nano-cavity of γ-CD. Next, to verify the effect of pH on translocation of the drug between γ-CD and DNA, we have

changed the pH of the medium and the emission spectra of EPT in presence of γ-CD and DNA collected at different pH conditions are shown in **Figure 5b.3** and **Figure 5b.2b**. At lower pH (~5.0), a clear single band at 520 nm is observed in emission spectrum without exhibiting any shoulder at ~470 nm, and it matches exactly with the emission spectrum of EPT in presence of DNA, confirming that only C form bound to DNA exists in the medium (**Figure 5b.3a**). This suggests that the lowering of pH converts encapsulated N to C form which cannot be stabilized in hydrophobic cavity of γ-CD, and eventually comes out of the nano-cavity and binds with DNA. Astonishingly at higher pH (~8.5), we have noticed completely opposite trend i.e., the emission is completely switched to light blue color (at 470 nm). Notably, this emission spectral feature exactly matches with EPT:γ-CD case (**Figure 5b.3b**). As this blue color emission is attributed to N form, we believe that at higher pH (> pKa) the drug exclusively exists in N form; hence, it prefers to go to hydrophobic nano-cavity of γ-CD. In a nutshell, the steady state results suggest that the drug selectively stays at DNA at lower pH even in presence of γ-CD, and exhibits green color. Whereas at higher pH, it is preferentially located to γ-CD (**Figure 5b.2b**) even in presence of DNA, and emits blue color. In this way the pH controls the location of the drug, and this kind of pH driven translocation of drug confirmed from fluorescence switch might find possible applications in controlled drug delivery and release process.

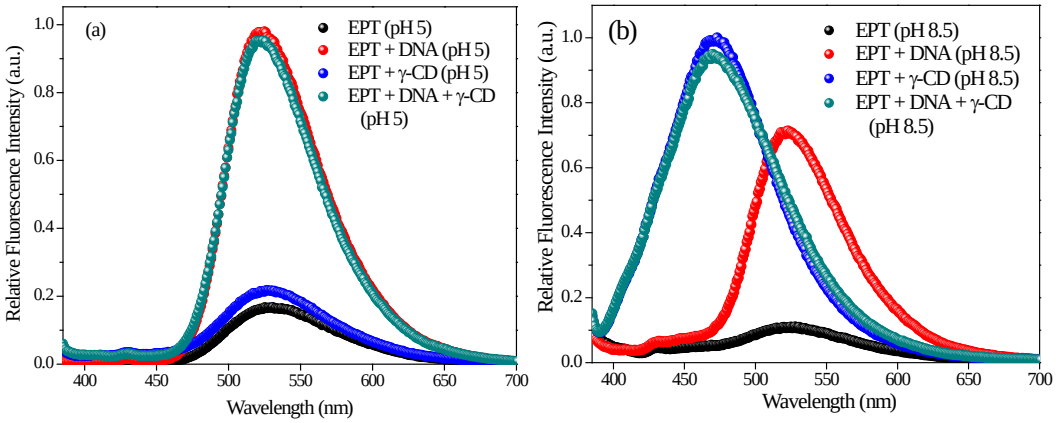

Figure 5b.3. Emission spectra of EPT (15 μM) in absence and presence of γ-CD (10 mM) and DNA (100 μM) at pH (a) 5, and (b) 8.5.

5b.2b. Time Resolved Fluorescence Study:

Time resolved fluorescence measurement is widely used technique to explore the excited state properties of the fluorophore. Thus fluorescence lifetime data can significantly contribute in realizing the translocation of EPT between γ-CD and DNA. The typical time-resolved fluorescence decay profiles are displayed in **Figure 5b.4** and the fitting parameters are summarized in **Table 5b.1**. The decay profile of free drug (PBS, pH 7) monitored at 530 nm exhibits biexponential feature with the lifetime components of 2 ns (90%) and 5.55 ns (10%) correspond to C form in accordance with the previous literature.[21, 25] In presence of γ-CD (10 mM) a new longer lifetime component ~32 ns is appeared (**Figure 5b.4** and **Table 5b.1**) and this lifetime is attributed to the N form of EPT generated inside the nano-cavity of γ-CD.[25] When DNA is introduced to this system, the longer lifetime component (32 ns) is decreased and converted to a new lifetime component with ~16 ns. A similar lifetime component of EPT is observed in DNA alone system, and attributed to the DNA bound EPT molecule (**Table 5b.1**). The change in environment around the drug can cause this significant change in fluorescence lifetime. The higher lifetime component (32 ns) in γ-CD compared to DNA case (16 ns) may be attributed to the hydrophobic environment inside the nano-cavity of γ-CD.

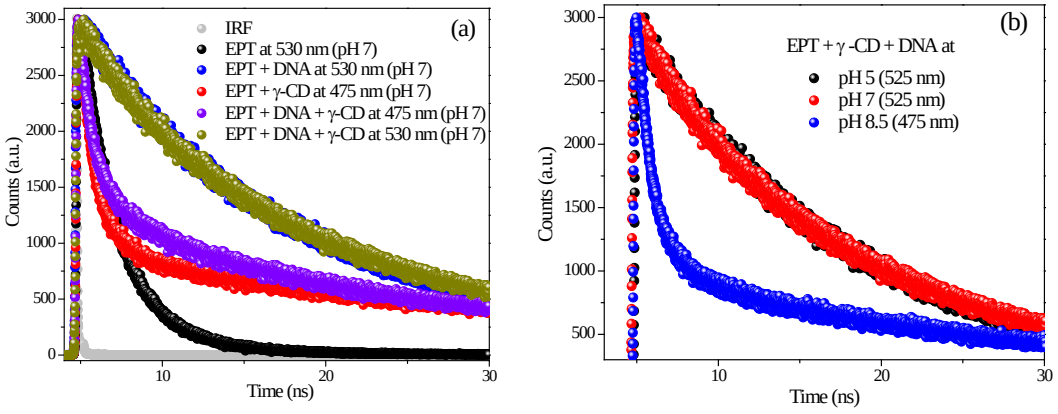

Figure 5b.4. (a) Fluorescence transients of EPT (15 μM) in absence and presence of γ-CD (10 mM) and DNA (100 μM) at pH 7, collected at respective emission maximum. (b) pH dependent fluorescence transients of EPT + γ-CD + DNA system.

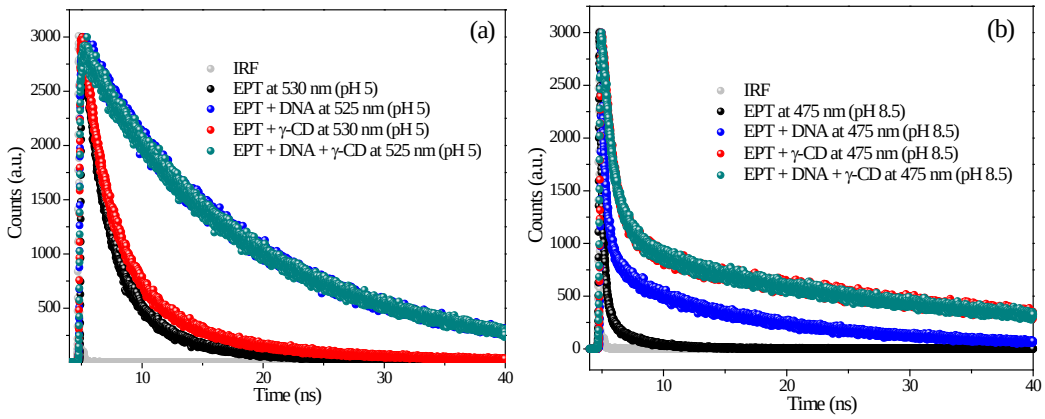

Figure 5b.5. Fluorescence transients of EPT (15 μM) in absence and presence of γ-CD (10 mM) and DNA (100 μM) at pH (a) 5 and (b) 8.5, collected at respective emission maximum.

Table 5b.1. Fluorescence transient fittings of EPT (15 μM) in absence and presence of γ-CD (10 mM) and DNA (100 μM) at different pH conditions, collected at respective emission maximum.

Sample	τ_1	a_1	τ_2	a_2	τ_3	a_3	$\langle\tau\rangle^{\#}$	χ^2
pH 7								
EPT at 530	1.99	0.9	5.55	0.1	-	-	2.34	1.1
EPT + γ-CD + DNA at 475	0.78	0.65	5.86	0.11	31.76	0.24	8.76	1
EPT + γ-CD + DNA at 525	-	-	5.47	0.31	19.2	0.69	14.96	1.15
EPT + DNA at 525	-	-	5.56	0.2	15.98	0.8	13.93	1.06
EPT + γ-CD at 475	0.82	0.71	5.74	0.07	36.78	0.22	9.22	1
pH 5								
EPT at 530	1.96	0.83	7.27	0.17	-	-	2.86	1.12
EPT + γ-CD + DNA at 525	-	-	5.93	0.18	16.18	0.82	14.34	1.04
EPT + DNA at 525	-	-	5.59	0.16	15.85	0.84	14.21	1.01
EPT + γ-CD at 475	0.95	0.43	3.46	0.49	22.58	0.08	3.92	1.09
pH 8.5								
EPT at 530	1.93	0.95	6.42	0.05	-	-	2.16	1.29
EPT + γ-CD + DNA at 475	0.8	0.67	5.35	0.09	35.3	0.23	9.27	1.03
EPT + DNA at 525	-	-	4.73	0.26	15.53	0.74	12.74	1.04
EPT + γ-CD at 475	0.83	0.69	6.24	0.08	38.11	0.23	9.79	1.01

$^{\#}\langle\tau\rangle = a_{1*}\,\tau_1 + a_{2*}\,\tau_2 + a_{3*}\,\tau_3$

To further verify this translocation process, we have changed the pH of the medium and the fluorescence decays of EPT in presence of γ-CD and DNA are collected at different pH conditions (**Figure 5b.5**). At lower pH (~5), almost similar observations are found as that of pH 7, confirming that C form prevails at lower pH and it favorably interacts with DNA. On the other hand at higher pH (8.5), the decay feature exactly matches with the fluorescence decay of EPT in γ-CD alone without DNA (**Figure 5b.5b**). These findings confirm that at higher pH the drug is translocated from DNA to γ-CD. Thus, the lifetime results are in accordance with the steady state findings, where we have observed pH dependent selective binding of EPT to either γ-CD or DNA even in presence of other biopolymer or macrocyclic host.

Further information about rotational relaxation of ellipticine in aforementioned systems can be obtained from time resolved anisotropy measurements. As shown in **Figure 5b.6** and **Table 5b.2,** EPT undergoes a fast rotational relaxation in aqueous buffer solution with a time scale of 130 ps. In presence of γ-CD, the rotational correlation time increases to 850 ps due to the encapsulation of EPT inside the γ-CD cavity.[25] When DNA is introduced in to this system (EPT + γ-CD), the rotational relaxation time shoots up to 11 ns (**Figure 5b.6** and **Table 5b.2)**. The anisotropy decay collected at 525 nm exactly matches with the DNA containing EPT spectrum (**Figure 5b.6**), which confirms the location of drug on DNA. As the steady state spectrum contains a shoulder at 475 nm, we have also probed the rotational relaxation of the drug in EPT containing γ-CD and DNA solution at 475 nm, and we have found slow rotational relaxation of the drug, which matches very closely to the γ-CD bound EPT molecules. This observation indicates that some population of EPT molecules involve inclusion complex formation even in presence of DNA at this pH condition, which results in slow relaxation of EPT in γ-CD nano-cavity. To probe the translocation of EPT between two host molecules, pH of the medium is varied (**Figure 5b.6b**). At lower pH (~5) anisotropy decay in γ-CD and DNA exhibits bi-exponential decay with an average correlation time of 10 ns (**Figure 5b.7a**). Here the anisotropy decay of EPT in presence of γ-CD and DNA overlays with the EPT:DNA system (**Figure 5b.7**). This indicates that at pH 5 the drug is translocated from γ-CD cavity to DNA. Whereas at higher pH (8.5), anisotropy decay of EPT in presence of γ-CD and DNA drastically decreases (**Figure 5b.6b**) and it matches with EPT:γ-CD decay (**Figure 5b.7b**), confirming that at higher pH the drug is displaced from DNA to the nano-cavity of γ-CD. Thus, the anisotropy decay results also

confirm that at lower pH (~5), the drug release takes place from γ-CD to DNA, whereas it retains inside the γ-CD cavity at higher pH (8.5).

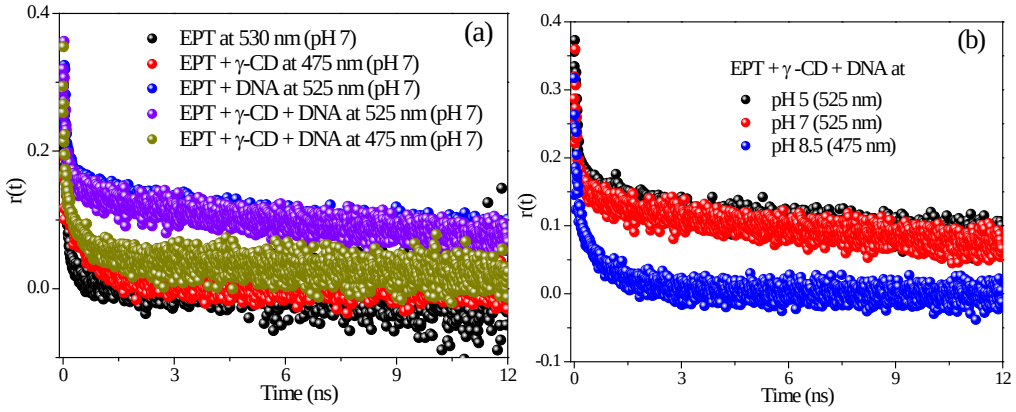

Figure 5b.6. (a) Anisotropy transients of EPT (15 μM) in absence and presence of γ-CD (10 mM) and DNA (100 μM) at pH 7, collected at respective emission maximum. (b) pH dependent anisotropy transients of EPT + γ-CD + DNA system.

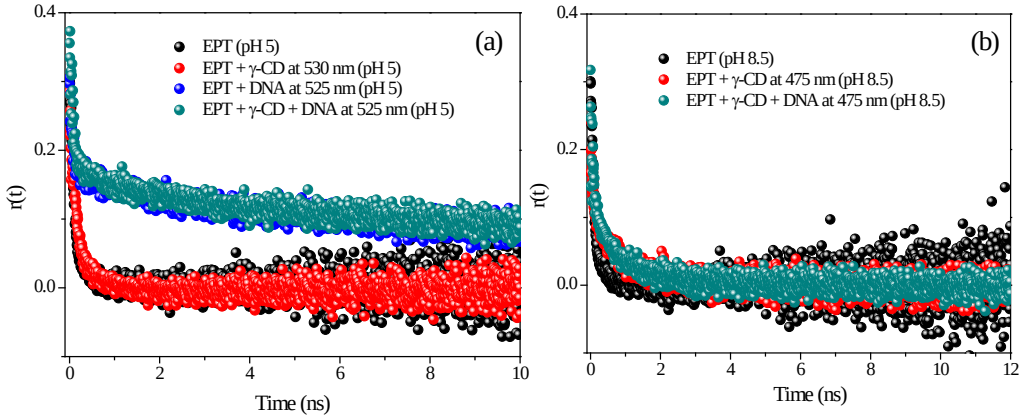

Figure 5b.7. Fluorescence anisotropy transients of EPT (15 μM) in absence and presence of γ-CD (10 mM) and DNA (100 μM) at pH (a) 5 and (b) 8.5, collected at respective emission maximum.

Table 5b.2. Anisotropy transient fittings of EPT (15 μM) in absence and presence of γ-CD (10 mM) and DNA (100 μM) at different pH conditions, collected at respective emission maximum.

Sample	τ_{1r}	a_1	τ_{2r}	a_2	χ^2
pH 7					
EPT at 530	0.12	-	-	-	1.03
EPT + γ-CD + DNA at 475	0.52	0.68	12.8	0.32	1.04
EPT + γ-CD + DNA at 525	0.5	0.41	18.48	0.59	1.07
EPT + DNA at 525	0.99	0.33	14.57	0.67	1.09
EPT + γ-CD at 475	0.85	-	-	-	1.02
pH 5					
EPT + γ-CD + DNA at 525	0.79	0.32	12.9	0.68	1.14
EPT + DNA at 525	1.15	0.31	13.73	0.69	1.11
EPT + γ-CD at 525	0.22	-	-	-	1.04
pH 8.5					
EPT + γ-CD + DNA at 475	0.96	-	-	-	1.04
EPT + DNA at 525	0.26	0.28	18.5	0.72	1.09
EPT + γ-CD at 475	0.86	-	-	-	1.04

5b.2c. Circular Dichroism Study:

Circular dichroism (CD) is utilized to further understand this pH responsive translocation phenomenon from DNA to cyclodextrin or vice versa. The CD spectrum of DNA at pH 7 buffer solution (**Figure 5b.8**) exhibits a positive peak at ~280 nm and a negative band at ~245 nm, which correspond to a typical right handed B-form of DNA.[28] In presence of EPT, the intensity of positive band (~280 nm) is reduced with an additional positive band appearing at ~320 nm in the CD spectrum. This band is exactly matching with the UV-visible absorption spectrum of EPT with DNA (**Figure 5b.1**). However, when we collected the CD spectrum for EPT alone in buffer, there is no peak observed in the spectrum. Thus, the 320 nm band in CD spectrum is assigned to induced CD signal, confirming the intercalation of drug in between the base pairs (**Figure 5b.8a**). With the addition of γ-CD to this solution, the ellipticity of the induced CD signal slightly reduces and a new shoulder at ~300 nm is appeared (**Figure 5b.8a**). To understand the origin of the shoulder at ~300 nm, we have collected CD profile in EPT containing γ-CD solution (in absence of DNA), and the system exhibits a positive CD signal at ~300 nm (**Figure**

5b.8a). Neither EPT nor γ-CD alone can give this kind of CD signal. Therefore, the appeared CD signal is attributed to the induced signal due to the formation of inclusion complex between EPT and γ-CD. Hence, the observed shoulder for EPT, DNA and γ-CD system at pH 7 (**Figure 5b.8a**) indicates the existence of slight population of EPT: γ-CD inclusion complex. Notably, in steady state results, we have also noticed the existence of slight population of EPT: γ-CD inclusion complex, even though major population of drug molecules bind to ct-DNA. The pH of the solution is varied to translocate the drug from DNA to γ-CD or vice-versa, and the results are shown in **Figure 5b.8b** and **Figure 5b.9**. At pH 5, the drug bound to DNA exhibits similar induced CD signal at 320 nm (**Figure 5b.9a**) as that of pH 7. However, with the addition of γ-CD to this solution, no significant change is observed in CD spectra (**Figure 5b.9**). The absence of any shoulder at ~300 nm confirms that the drug is not encapsulated in the nano-cavity of γ-CD at pH 5. Interestingly, when the pH of the solution is increased to pH ~8.5, addition of γ-CD to EPT + DNA causes an appearance of structured bands in between 290-310 nm **(Figure 5b.9b)**. Moreover, the induced CD signal band at ~320 nm responsible for DNA intercalation is vanished in presence of γ-CD (**Figure 5b.9b**), inferring that the drug is translocated completely from DNA to the nano-cavity of γ-CD. Hence, the circular dichroism results once again validate and confirm the pH induced reversible translocation of EPT in between DNA and γ-CD.

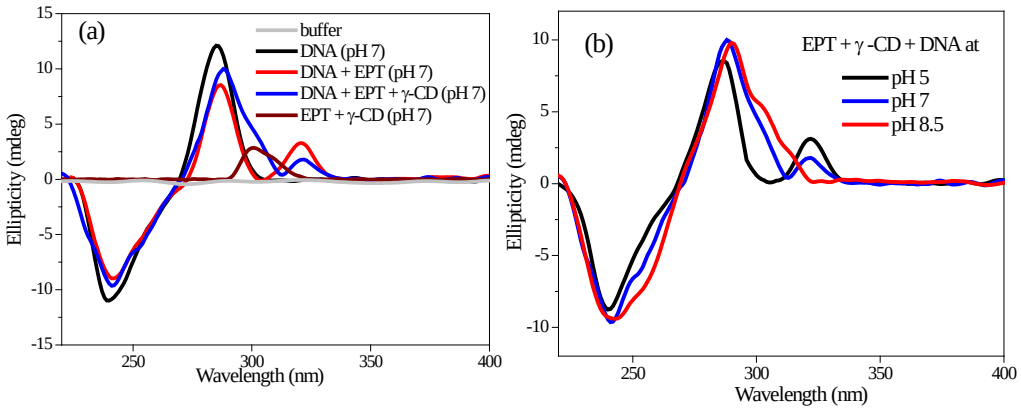

Figure 5b.8. (a) Circular dichroism (CD) spectra of DNA (200 μM) in absence and presence of γ-CD (10 mM) and EPT (30 μM) at pH 7. (b) pH dependent CD spectra of EPT + γ-CD + DNA system.

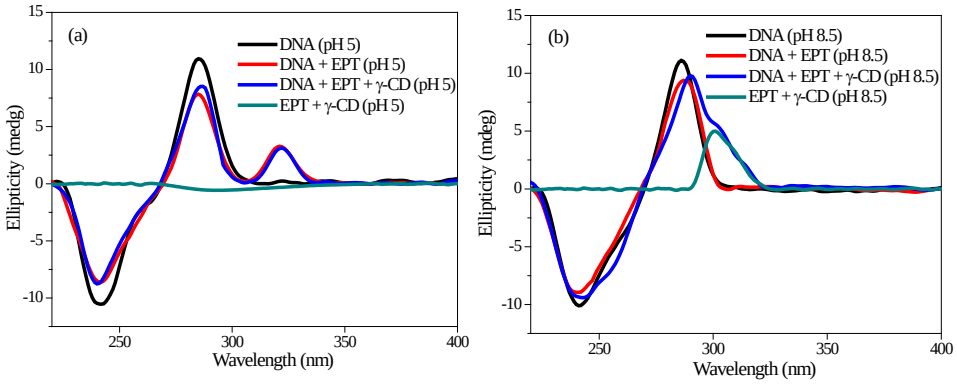

Figure 5b.9. Circular dichroism spectra of DNA (200 μM) in absence and presence of γ-CD (10 mM) and EPT (30 μM) at (a) pH 5 and (b) pH 8.5.

The novelty of the present work is environmental pH responsive drug release. If the cyclodextrin encapsulated EPT enters to cell by endocytosis process, and home into lysosomal compartment (where the pH is ~5.0),[29] then, the drug can be easily released from CD nano-cavity and interact with nuclear DNA, as we have shown that the drug is easily translocated from CD to DNA at lower pH. On the other hand, by chance, the CD encapsulated drug reaches to mitochondrial matrix (where the pH is ~8.0),[29] in that case, the drug will not release to interact with mitochondrial DNA, since the drug will not come out from CD matrix at higher pH. At neutral pH (pH 7.0), CD encapsulated drug will partially release to nuclear DNA. In this way, the pH of the surrounding environments will govern the efficacy of the drug release.

5b.3. Conclusion:

In summary, we have investigated the pH triggered interplay of EPT inside the nano-cavities of a supramolecular host γ-cyclodextrin and DNA using photophysical properties of the drug by means of steady-state and picosecond time-resolved fluorescence techniques. When EPT resides in γ-CD nano-cavity its fluorescence increases with a large hypsochromic shift whereas the fluorescence is enhanced several folds without such blue shift in presence of DNA. Based on these fluorescence changes, the transportation of drug between γ-CD and DNA is successfully monitored by simple change of pH of the medium. Steady state and time resolved studies confirm that at higher pH (~8.5) the drug stays inside the nano-cavity of γ-CD and at lower pH (~5.0) it resides in DNA. Circular dichroism results further confirm the translocation of EPT

between above mentioned host molecules. Hence, by using the simple fluorescence switch one can monitor the location of drug, and this kind of pH driven translocation of drug might find possible applications in emergent controlled drug delivery process.

5b.4. Reference:

1. R. Liu, Y. Zhang, X. Zhao, A. Agarwal, L. J. Mueller and P. Feng, *J. Am. Chem. Soc*., 2010, **132**, 1500-1501.
2. H. P. Rim, K. H. Min, H. J. Lee, S. Y. Jeong and S. C. Lee, *Angew. Chem. Int. Ed.*, 2011, **50**, 8853-8857.
3. X. Ma and Y. Zhao, *Chem. Rev.*, 2015, **115**, 7794-7839.
4. S. Mura, J. Nicolas and P. Couvreur, *Nat. Mater*., 2013, **12**, 991-1003.
5. Y. Cao, X.-Y. Hu, Y. Li, X. Zou, S. Xiong, C. Lin, Y.-Z. Shen and L. Wang, *J. Am. Chem. Soc.*, 2014, **136**, 10762-10769.
6. I. Hwang, W. S. Jeon, H.-J. Kim, D. Kim, H. Kim, N. Selvapalam, N. Fujita, S. Shinkai and K. Kim, *Angew. Chem. Int. Ed.*, 2007, **46**, 210-213.
7. M. Sayed and H. Pal, *Phys. Chem. Chem. Phys.*, 2015, **17**, 9519-9532.
8. Z. Qi and C. A. Schalley, *Acc. Chem. Res.*, 2014, **47**, 2222-2233.
9. Q. Hu, P. S. Katti and Z. Gu, *Nanoscale*, 2014, **6**, 12273-12286.
10. J. Su, F. Chen, V. L. Cryns and P. B. Messersmith, *J. Am. Chem. Soc.*, 2011, **133**, 11850-11853.
11. K. Engin, D. B. Leeper, J. R. Cater, A. J. Thistlethwaite, L. Tupchong and J. D. McFarlane, *Int. J. Hypertherm.*, 1995, **11**, 211-216.
12. R. N. Dsouza, U. Pischel and W. M. Nau, *Chem. Rev.*, 2011, **111**, 7941-7980.
13. J. Zhang and P. X. Ma, *Adv. Drug Deliv. Rev.*, 2013, **65**, 1215-1233.
14. M. V. Rekharsky and Y. Inoue, *Chem. Rev.*, 1998, **98**, 1875-1918.
15. T. Irie and K. Uekama, *J. Pharm. Sci.*, 1997, **86**, 147-162.
16. M. E. Brewster and T. Loftsson, *Adv. Drug Deliv. Rev.*, 2007, **59**, 645-666.
17. M. Shaikh, J. Mohanty, A. C. Bhasikuttan, V. D. Uzunova, W. M. Nau and H. Pal, *Chem. Commun.*, 2008, 3681-3683.
18. K. Uekama, F. Hirayama and T. Irie, *Chem. Rev.*, 1998, **98**, 2045-2076.

19. A. C. Bhasikuttan, J. Mohanty, W. M. Nau and H. Pal, *Angew. Chem. Int. Ed.*, 2007, **46**, 4120-4122.
20. S. Y. Fung, J. Duhamel and P. Chen, *J. Phys. Chem. A*, 2006, **110**, 11446-11454.
21. R. K. Koninti, A. Sengupta, K. Gavvala, N. Ballav and P. Hazra, *Nanoscale*, 2014, **6**, 2937-2944.
22. A. Sengupta, R. K. Koninti, K. Gavvala, N. Ballav and P. Hazra, *Phys. Chem. Chem. Phys.*, 2014, **16**, 3914-3917.
23. R. Thakur, A. Das, V. Sharma, C. Adhikari, K. S. Ghosh and A. Chakraborty, *Phys. Chem. Chem. Phys.*, 2015, **17**, 16937-16946.
24. R. Thakur, A. Das and A. Chakraborty, *Phys. Chem. Chem. Phys.*, 2012, **14**, 15369-15378.
25. A. Das, R. Thakur and A. Chakraborty, *RSC Adv.*, 2013, **3**, 19572-19581.
26. F. Sureau, F. Moreau, J. M. Millot, M. Manfait, B. Allard, J. Aubard and M. A. Schwaller, *Biophys. J.*, 1993, **65**, 1767-1774.
27. A. Canals, M. Purciolas, J. Aymami and M. Coll, *Acta Crystallogr., Sect. D: Biol. Crystallogr.*, 2005, **61**, 1009-1012.
28. J. Kypr, I. Kejnovská, D. Renčiuk and M. Vorlíčková, *Nucleic Acids Res.*, 2009, **37**, 1713-1725.
29. J. R. Casey, S. Grinstein and J. Orlowski, *Nat. Rev. Mol. Cell Biol.*, 2010, **11**, 50-61.

******** THE END ********